HYPERPOLARIZATION USING PARAHYDROGEN

Majid Khan

Doctor of Philosophy

University of York

Chemistry

September 2013

ABSTRACT

Work presented in the thesis encompasses the hyperpolarization techniques, SABRE and PHIP, within the context of nuclear magnetic resonance spectroscopy. In the first instance, pyridine derivatives have been hyperpolarized using [Ir(COD)(IMe)Cl]. The effect of solvent, magnetic field, concentration, temperature, shake time, position of pyridyl ring and sterics were examined in order to optimize the hyperpolarization process for SABRE. The horizon of this study was further broadened to hyperpolarize biologically relevant molecules. The hyperpolarization studies carried out on the biological molecules ultimately provided us with an insight into the conditions necessary to optimize the hyperpolarization phenomena. Factors such as temperature shake time, pKa, concentration, exchange rate, steric hindrance around binding site were observed to contribute to the polarization transfer process and a fine interplay between these factors leads to an effective and efficient polarization transfer to the substrate under observation. Reaction of $[IrCl(DMSO)_3]$ with PPh_3 in the presence of *p*-H_2 at 298 K, yielded long-lived *p*-H_2 enhanced hydride resonances for two new complexes. These complexes were identified as the trisubstituted triphenylphosphine product $[IrCl(H)_2(PPh_3)_3]$ and the disubstituted product, $[IrCl(H)_2PPh_3)_2(DMSO)]$ and these products were characterized by NMR spectroscopy. Furthermore, the reaction of $[IrCl(DMSO)_3]$ with pyridine led to the formation of monosubstituted complex $[IrCl(H)_2(py)(DMSO)_2]$ and the SABRE effect was observed in the resonances of the free pyridine. The reaction of complex, $[IrCl(DMSO)_3]$, with amino acids yielded new dihydrido amino acid complexes.

Nomenclature

"For labelling of H positions in compounds please refer to Appendixes since a non-standard methodology has been used, although all compounds have been named according to IUPAC conventions"

CONTENTS

LIST OF FIGURES

LIST OF TABLES

Acknowledgements

First and foremost I would like to express my gratitude to Prof. Simon Duckett for allowing me to do this project and the great guidance and encouragement that he gave me throughout the project. Special thanks go to Adrian Charlton, my industrial supervisor from food and environment agency, for his support.

My intimate gratitude goes to Department of Chemistry University of York, including academic and technical staff for the pleasant and valuable time I had during the studies. I wish to thank the University of York, FERA and Wild fund scholarship for their financial support.

I would also like to thank past and present members of the SBD group. Last but not least, I am thankful to my family and friends for their support during the hard times of this project.

Declaration

The work presented in this thesis is exclusively the work of the author and contains no work that is the result of collaboration, except where specified to the contrary, either directly or by reference. This thesis has not been submitted for any other degree.

Majid Khan

"Champions aren't made in gyms. Champions are made from something they have deep inside them – a desire, a dream, a vision**."**

Muhammad Ali

CHAPTER ONE

INTRODUCTION

1.1 Nuclear magnetic resonance spectroscopy

The revolutionary work of Edward Purcell and Felix Bloch in the laboratories of the physics department at Harvard and Stanford led to the discovery of nuclear magnetic resonance effect in 1945. Nuclear magnetic resonance is the absorption of energy by a proton to induce spin flipping when the frequency of electromagnetic radiation is exactly equal to the precessional frequency of the spinning proton, i.e.; the two frequencies are in resonance, hence the term nuclear magnetic resonance (NMR). For their pioneering work Edward Purcell and Felix Bloch were awarded a Nobel prize in 1952. Since then, this physics experiment has become a focal point for many scientists and eventually, nuclear magnetic resonance (NMR) spectroscopy has been transformed into a powerful tool that is used in most of the natural and medical sciences.[1, 2]

Nuclear magnetic resonance spectroscopy,[3] as the name implies, is the form of spectroscopy that depends upon the magnetic property of an element, thus it deals with transitions between the magnetic energy levels of nuclei of a molecule. Like UV-Vis and IR spectroscopy, nuclear magnetic resonance also depends upon the absorption of certain wavelengths of radiation. The radiation is in the radio frequency range. A radio frequency has a rate of oscillation in

the range of around 3 kHz to 300 GHz, and the alternating currents which carry radio signals. NMR spectroscopy is a widely used analytical technique in chemistry, physics, biology and medicine, one shortcoming of NMR spectroscopy is that it suffers from inherently low sensitivity.

1.1.1 Principle and theory of NMR

Nuclear magnetic resonance (NMR) spectroscopy[4] is undertaken in a strong magnetic field. Zeeman first observed the strange behaviour of certain nuclei subjected to a strong magnetic field at the end of the last century, but practical use of nuclear magnetic resonance was made only in the 1950s when NMR spectrometers became commercially available. Certain nuclei, such as ^{1}H, ^{13}C, ^{19}F, ^{2}H and ^{15}N possess a spin angular momentum and hence a corresponding magnetic moment μ (Equation 1.1):

$$\mu = \gamma h[I(I+1)]^{1/2}/\ 2\pi \qquad \textit{Equation 1.1}$$

where h is planck's constant and γ is the magnetogyric ratio. When such nuclei are placed in a magnetic field B_0 applied along the z-axis, they can adopt one of $(2I+I)$ quantized orientations, where I is the spin quantum number of the nucleus. Each of these orientations corresponds to a certain energy level as shown in Figure 1.1. The relationship of energy with magnetic moment and magnetic field is given in equation 1.2.

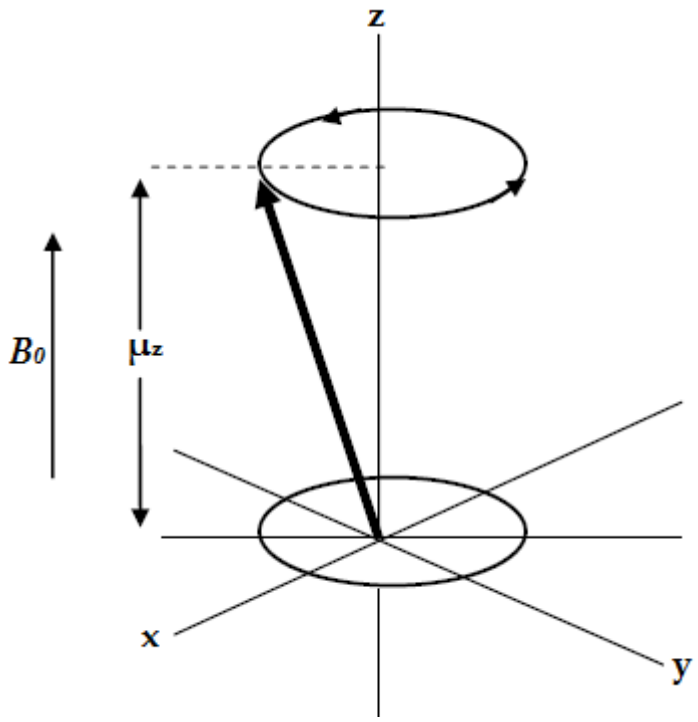

Figure 1.1: ***Representation of the precession of the magnetic moment about the axis of the applied magnetic field, B_0. The magnitude μ_z of the vector corresponds to the Boltzmann excess in the lower energy (α) state.***

$$E = -\mu_z B_0 = -m_1 \gamma B_0/2\pi \quad \text{.....Equation 1.2}$$

where m_1 is the magnetic quantum number of the nucleus. In the lowest energy orientation, the magnetic moment of the nucleus is most closely aligned with the external magnetic field (B_0), while in the highest energy orientation it is least closely aligned with the external field. Transitions from the lower energy to the higher energy level can occur by absorption of radiofrequency radiation of the correct frequency. The energy difference ΔE between these energy levels is proportional to the external magnetic field (Figure 1.2) as defined by the

equation $\Delta E = \gamma h B_0/2\pi$. In frequency terms, this energy difference corresponds to (Equation 1.3):

$$\nu_0 = \gamma B_0 / 2\pi \quad \text{.....Equation1.3}$$

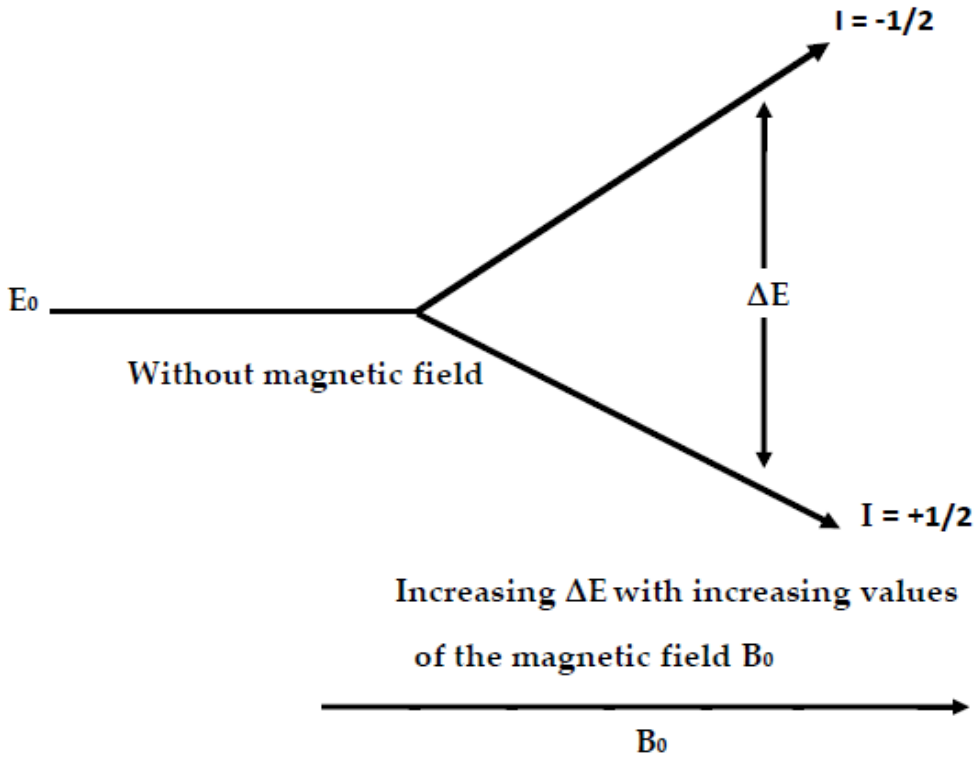

Figure 1.2: The energy difference between two energy states ΔE increases with increasing value of the applied magnetic field B_0, with a corresponding increase in sensitivity.

Before being placed in a magnetic field,[5] the nucleus is spinning on its axis, which is stationary. The external magnetic field (the NMR magnet) causes the spinning nucleus to exhibit a characteristic wobbling motion (precession) often compared to the movement of a gyroscopic before it topples, when the two ends of its axis no longer remain stationary but trace circular paths in opposite direction (Figure 1.3). If a radiofrequency field is now applied in a direction

perpendicular to the external magnetic field and at a frequency that exactly matches the processional frequency ("Larmor" frequency) of the nucleus, absorption of energy will occur and the nucleus will suddenly "flip" from its lower energy orientation to the higher energy orientation, in which it is aligned in the opposite direction. It can relax back to the lower energy state through spin-lattice relaxation T_1 by transfer of energy to the assembly of surrounding molecules ("lattice") and spin-spin relaxation (T_2) involving transfer of energy to a neighbouring nucleus. The change in the impedance of the oscillator coils caused by the relaxation is measured by the detector as a signal in the form of a decaying beat pattern, known as a free induction decay (FID), which is stored in the computer memory and converted from a time-domain data to the frequency-domain spectrum by a mathematical operation known as Fourier transformation.

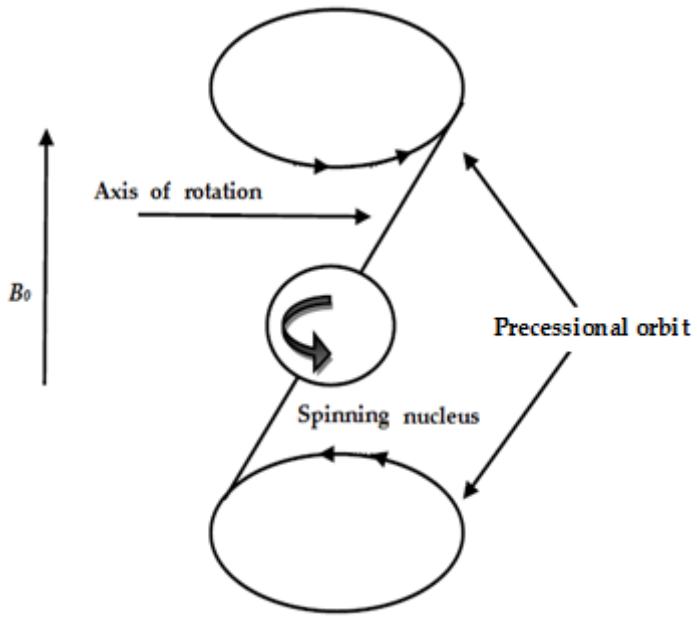

Figure 1.3: ***Precessional motion of an NMR active nucleus in magnetic field B_0.***

Thus, excitations caused by absorption of radiofrequency energy cause nuclei to migrate to a new energy level,[6] and an equilibrium state is soon established. In nuclei with positive magnetogyric ratios, such as ^{1}H and ^{13}C, the lower energy state will correspond to the +½ state, and the higher energy -½ state; but in nuclei with negative magnetogyric states, e.g., ^{29}Si and ^{15}N, the opposite will be true. If the populations of the upper and lower energy states were equal, then no energy difference between the two states of the nuclei in its parallel and anti parallel orientations would exist and no NMR signal would be observed. However, at equilibrium there is a slight excess ("Boltzmann excess") of nuclei in the lower energy (α) state as compared to the upper energy (β) state, and it is this difference in the populations of the two energy levels that is responsible for the NMR signal (Figure 1.4).

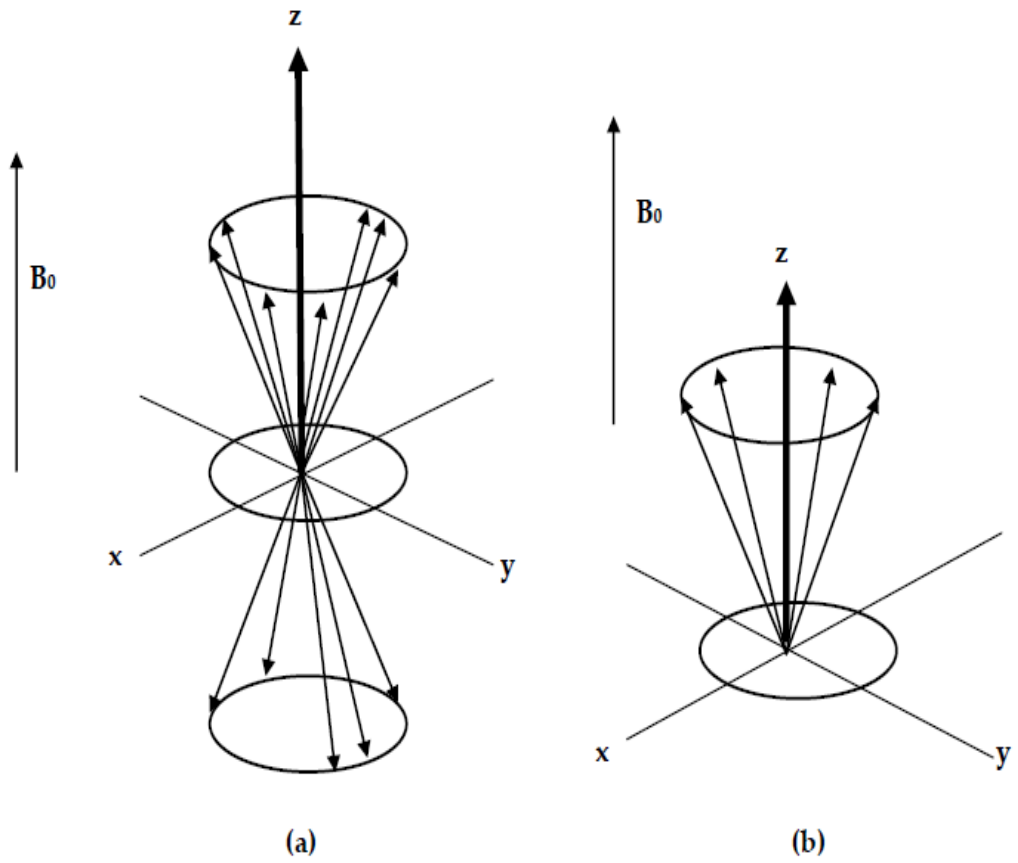

Figure 1.4: ***(a) Vector representation displaying a greater number of nuclei aligned with the magnetic field B_0; (b) Excess spin population (Boltzmann distribution excess) aligned with B_0 results in an bulk magnetization vector in the +z direction.***

Since signal intensity is dependent on the population difference between the nuclei in the upper and lower energy states, and since the population difference depends on the strength of the applied magnetic field, the signal intensities will be significantly higher on instruments with more powerful magnets. As the population difference between the spin states is inherently very small in case of NMR spectroscopy a weak signal is detected. The Boltzmann distribution gives the ratio of the spin population N_α and N_β in these energy levels as equation 1.4.

$$N_\beta / N_\alpha = e^{-\Delta E / kT} \approx 1 - \gamma h B_0 / 2\pi kT \quad \textit{Equation 1.4}$$

Where N_α is the population of the lower energy state and N_β is the population of the upper energy state. *h* is the planck's constant, γ is the gyromagnetic ratio, B_0 is the strength of an applied magnetic field, k is the Boltzmann constant. At 298 K, the population difference for a proton with a Lamour frequency of 300 MHz in a magnetic field of 7 T (70,500 G) can be calculated as:

$$N_\beta / N_\alpha = 1-[(6.63\times10^{-34})\ (26753)\ (70{,}500)/2\times3.14)/\ (1.38\times10^{-23}\times298)]$$
$$= 0.999952$$

In the similar way, at 298 K, the population difference for a proton with Lamour frequency of 500 MHz in a magnetic field of 11.5 T (117,500 G) is as follows:

$$N_\beta / N_\alpha = 1-[(6.63\times10^{-34})\ (26753)\ (117{,}500)/2\times3.14)/\ (1.38\times10^{-23}\times298)]$$
$$= 0.999919$$

The relative spin population detected in at a 300 MHz magnet is so small that there are only 48 protons out of 2,000,000 are available in a magnetic field of 7 T (70,500 G) to observe an NMR signal. Similarly, at a magnetic field of 11.5 T (117, 500 G), the relative spin population difference is still only 81 protons out of 2,000,000.

At room temperature, the energy difference between theses aforementioned states is so diminutive that the Boltzmann distribution of chemically identical nuclei is such that the populations of nuclear spin states

which are in dynamic equilibrium are almost indistinguishable. Since the strength of the detected signal in magnetic resonance spectroscopy experiments is proportional to the population difference between the energy levels, the NMR signals acquired are characteristically weak. In other words, the NMR transitions that take place between the energy levels are closely spaced giving rise to a situation where almost equal populations of spins are aligned parallel or antiparallel to the external magnetic field B_0. For example, the population difference between higher and lower energy levels at room temperature for ^{13}C nuclei at a magnetic field of 4.7 T, which corresponds to a resonance frequency of 50.2 MHz, is only 1.000008.

The magnitude of NMR signal can be enhanced by a process called hyperpolarization, in which a significant excess of magnetic nuclei are induced into an identical spin state. This results in a large increase in available signal strength due to the much larger inequality of populations across the energy levels probed by NMR.

There are several techniques available which can be used to surmount the issue of sensitivity in conjunction with nuclear magnetic resonance spectroscopy (NMR) that are collectively known as hyperpolarization techniques. These hyperpolarization techniques include optical pumping,[7] in which hyperpolarization of noble gases is achieved by the optical pumping of a specific electronic transition of an alkali vapour, and the relaxation of this excited state is coupled to a nearby nuclear spin and hence causes a spin flip. Eventually, this builds up a large net population difference and leads to large nuclear spin polarization in case of ^{129}Xe.

One of the most often used methods of enhancing the NMR signal strengths was proposed by Bowers and Weitekamp in 1986. They proposed that the addition of molecular H_2 enriched in the *para* state could result in the enhancement of NMR signals. This method was initially called *para*hydrogen and synthesis allows dramatically enhanced nuclear alignment (PASADENA), and later named *para*hydrogen induced polarization (PHIP). *Para*hydrogen induced polarization (PHIP) produces hyperpolarization that exceeds the normal level by using a suitable catalyst, which transfers the nuclear alignment of *p*-H_2 (where the two nuclear spins are in antiparallel configurations) to a substrate by way of a hydrogenation reaction.[8] It is the two nuclei that were in *p*-H_2 which are hyperpolarized. Another hyperpolarization technique called signal amplification by reversible exchange, which has been developed recently is considered to be a significant extension of PHIP.

Levitt *et al*.[9] demonstrated the existence of exceptionally long-lived nuclear spin states in solution-state nuclear magnetic resonance. The lifetime of nuclear spin singlet states in systems containing coupled pairs of spins-1/2 may exceed the conventional relaxation time constant T1 by more than an order of magnitude. These long lifetimes may be observed using *p*-H_2, if the long-lived singlet states are prevented from mixing with rapidly relaxing triplet states. The potential of the singlet state for long-term storage of nuclear spin order in ordinary NMR was concealed for many years for several reasons: 1. The singlet state is antisymmetric with respect to nuclear spin exchange and therefore gives rise to no direct macroscopic observables, since these are inherently symmetric; 2. Access to the singlet state from the macroscopic world requires the existence of symmetry-breaking nuclear spin interactions; 3. Any symmetry-breaking interactions conceal the relaxation behaviour of the singlet state by converting it

rapidly into the rapidly-relaxing triplet state. In SABRE the metal template, usually a metal carbene complex, facilitates the transfer of polarization to the substrate that can again be detected after the application of an RF pulse.[10, 11] Dynamic nuclear polarization (DNP) is a well established hyperpolarization technique, which makes use of the large Zeeman splitting of electrons and exercise dipolar couplings to transfer the polarization to nuclei in the vicinity of a radical.[12] The hyperpolarization phenomenon is illustrated in Figure 1.5.

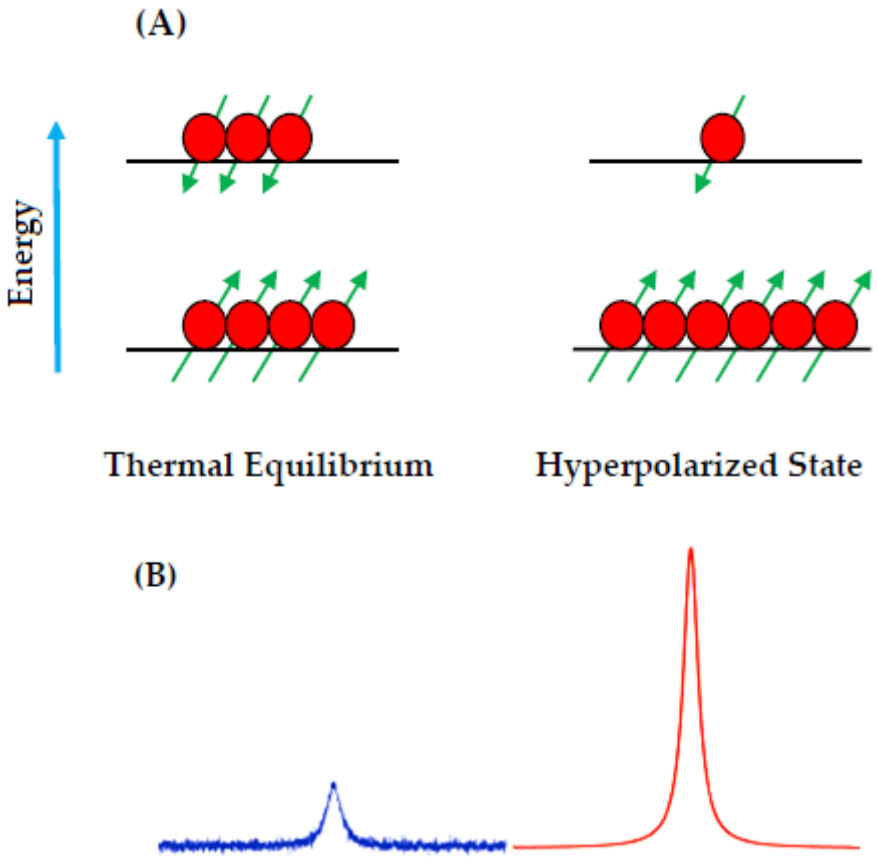

Figure 1.5: ***(A) NMR Spin populations at thermal equilibrium and in the hyperpolarized state; (B) The NMR spectra indicating the spin populations in a sample with thermal polarization is shown on the left while those in a hyperpolarized sample is on the right.***

Hyperpolarization techniques such as PHIP and SABRE are relatively quick, cheap and effective and can be successfully used to achieve the non-Boltzmann state necessary to improve the NMR signal strength. The following sections mainly focus on the PHIP, SABRE, DNP and their applications.

1.2 *Ortho*hydrogen (*o*-H_2) *and para*hydrogen (*p*-H_2)

Dihydrogen possesses two isomers namely: *Ortho*hydrogen (*o*-H_2) and *para*hydrogen (*p*-H_2). In case of *o*-H_2, the spins of individual nuclei are aligned parallel (higher energy state), or while the *para* state occurs with antiparallel nuclear spins (lower energy state) as illustrated in Figure 1.6.

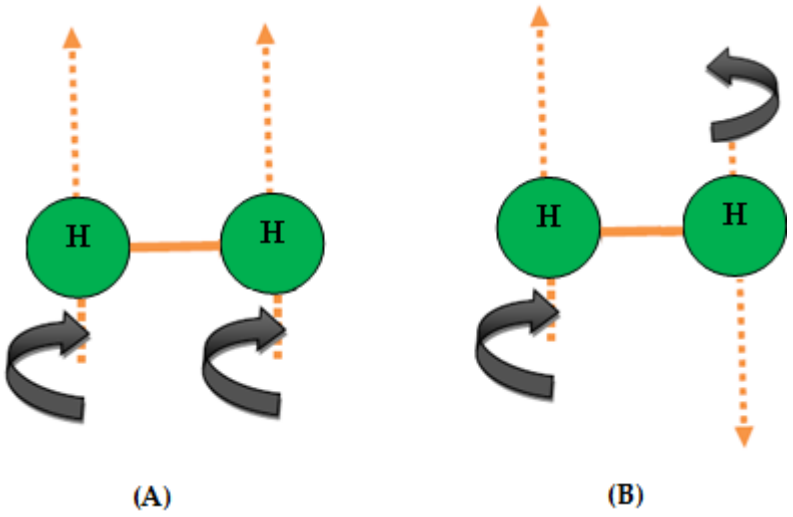

Figure 1.6: ***The spin isomers of dihydrogen: (A) ortho; (B) para.***

*Ortho*hydrogen (*o*-H_2) and *para*hydrogen (*p*-H_2) resemble each other in their chemical characteristics, disparities exist in their heat capacities, electrical conductivities, and adsorption properties.[8, 9] At low temperatures, the adsorption and conversion of *o*-H_2 and *p*-H_2 using TiO_2 (rutile) and charcoal of

high surface area is observed. In this study, two types of experiments have been carried out: (a) kinetic experiments to establish whether the adsorption-desorption equilibrium is fast enough to vary a gas phase composition after immediately contacting the gas with the surface. (b) Equilibrium experiments were undertaken in which the gas was allowed to come to a complete *o*-H_2 and *p*-H_2 equilibrium on the catalytic surfaces. It has been shown experimentally that *o*-H_2 has more adsorption affinity for charcoal or TiO_2 than *p*-H_2. The preferential adsorption of *o*-H_2 is mainly due to hindered rotation of the adsorbed *ortho* hydrogen. It has been suggested there may be other contributory factors such as greater polarizability of the rotating molecule (*o*-H_2) in comparison to the non-rotating molecule (*p*-H_2 in the lowest rotational state).

P-H_2 is more stable than *o*-H_2, as it can access a lower rotational energy state. It possesses no magnetic moment and is therefore undetectable in NMR. The *ortho* isomer of dihydrogen retains magnetic resonance activity. At room temperature, the statistical ratio between the *ortho* and *para* isomers of dihydrogen was found to be 3:1. The 3:1 ratio between *ortho* and *para* isomers of dihydrogen were first validated by Raman spectroscopy.[15, 16] The existence of *ortho* and *para* isomers of H_2 derives from the Pauli principle, which requires that the overall wave functions of fermions (protons) must be antisymmetric with respect to the exchange of nuclei.

According to the Born-Oppenheimer approximation, the overall wave function of a particle can be divided into nuclear and electronic components. The nuclear wave function can be further divided into translational, vibrational, rotational and spin components as given in Equation 1.5.

$\Psi = \Psi_{electronic}\Psi_{nuclear} = \Psi_{electronic}\ \Psi_{translational}\Psi_{\ vibrational}\Psi_{\ rotational}\Psi_{\ spin}$ ***Equation.1.5***

In the ground state, the translational, electronic, vibrational wave functions are constantly symmetric for a homonuclear diatomic molecule. Therefore, the product of rotational and nuclear wave functions has to be antisymmetric. In order to fulfil the requirement of antisymmetric rotational states, J = 1, 3, 5 etc (odd values), are restricted to symmetric nuclear spin wave functions, and the symmetric rotational states, J = 2, 4, 6 (even values), are limited to antisymmetric nuclear spin wave functions. This is summarised in Table 1.1. H_2 molecules with symmetric nuclear spin configurations are called *o*-H_2 and those with antisymmetric nuclear spin configurations are called *p*-H_2.

Table 1.1 ***Spin states of dihydrogen molecule in relation to their rotational energy levels.***

Label	***Spin state***	***J***	***Rotational state***
Ortho	Symmetric	3	Antisymmetric
Para	Antisymmetric	2	Symmetric
Ortho	Symmetric	1	Antisymmetric
Para	Antisymmetric	0	Symmetric

The nuclear spin wave function is characterised by magnetic quantum number, $m_I = \pm½$, and it can be represented by the labels α or β, for values of m_I = +½ or -½ respectively that a particular nucleus may take. Molecular H_2 consists of two protons (x and y in this example); therefore four combinations of nuclear spin wave functions are possible, as shown:

$\Psi = \alpha_x\alpha_y$

$\Psi = \beta_x\alpha_y$

$\Psi = \alpha_x\beta_y$

$\Psi = \beta_x\beta_y$

The exchange of two identical particles cannot be detected experimentally (according to quantum mechanics). Such a process can be represented by the interchange of labels in the above example. Because altering the labels has no physical significance, the resulting states must be indistinguishable from the initial state. Therefore, βα and αβ wave functions are not allowed since the interchange of labels would result in a product that is different from the initial state. Consequently, linear combinations of the two states must be used, termed αβ + βα and αβ − βα. This is allowed by quantum mechanics, and the states are isoenergetic outside a magnetic field.

The αα, ββ and αβ+βα wave functions are symmetric (corresponding to *o*-H_2) with respect to exchange of nuclei, whilst the αβ − βα state is antisymmetric (corresponding to *p*-H_2). This antisymmetric property can be explained as follows:

$\Psi_{spin} = \alpha\beta - \beta\alpha$

Exchange the nuclei x and y

$\Psi_{spin} = \beta\alpha - \alpha\beta$

$= -\alpha\beta + \beta\alpha$

$= -(\alpha\beta - \beta\alpha)$

$= -\Psi_{spin}$

It can therefore be concluded that *o*-H_2 is nuclear triplet and *p*-H_2 is the nuclear singlet. This is depicted simply in Figure 1.6.

According to Boltzmann distribution, at room temperature the energy difference between the triply degenerate state and the singlet state is negligible conferring *o*-H_2 and *p*-H_2 with natural abundance of 75% and 25%. It has been observed that there is also strong temperature dependence and lowering the temperature supports the lowest energy state. At a temperature of 0 K, all the H_2 molecules exist in the *p*-H_2 form but experimentally H_2 is completely converted to *p*-H_2 (99.8%) at a temperature of 20 K. In the same manner 50% enrichment can be achieved at a temperature of 77 K.

An *ortho* isomer can be converted to low energy *para* state by simply cooling at low temperature in the presence of a suitable catalyst such as charcoal or iron trioxide, the role of the catalyst is just to perturb the dihydrogen molecule and thereby reduce its symmetry. However, isomer interconversion requires changing a *J* value, and at least one value of m_I. The process is therefore forbidden. According to literature[17-19] the interconversion between the these two isomers (*ortho* and *para*) requires of the order of a year at ambient temperature and a pressure of 1 atm. Table 1.2 demonstrates that the lowest rotational energy state corresponds to the *para* isomer and therefore the population of the *p*-H_2 increases as the temperature decreased.

Table 1.2 ***Effect of temperature on the relative populations of o-H_2 and p-H_2.***

Temperature (K)	*% o-H_2*	*% p-H_2*
0	0	100
20	0.18	99.82
75	48.14	51.86
150	71.46	28.54
273	74.87	25.13
>273	75.00	25.00

A study by Chapovsky *et al*.[20] described that the room temperature interconversion between *o*-H_2 and *p*-H_2 takes about a year to complete at a pressure of 1 atm. Isomer relaxation happens to be slow due to intermolecular forces, or to small intermolecular cross-sections. Studies into spin isomers were initiated as early as 1929 but there are few molecules for which isomer separation was achieved such as H_2, CH_3F, H_2O, CH_2O, Li_2 and H_3^+. Apart from hydrogen molecules, the isomer separation is a big challenge because most of the molecular species possess similar physical and chemical characteristics.

Bonhoeffer and Hartect,[21] carried out the conversion of *o*-H_2 and *p*-H_2 by passing the H_2 gas over a *para*magnetic catalyst (charcoal) at a temperature of 78 K and this method demonstrated to give equilibrium amounts of *o*-H_2 and *p*-H_2. Duckett and co workers[22] experimentally proved that >99.8% *p*-H_2 can be produced by cooling H_2 gas in the presence of a *para*magnetic catalyst using a closed cycle helium cooler. A point worth noting is that if H_2 gas is enriched with a *para* isomer, it is possible to bring it back up to the room temperature and

it retains the *para* state as long as the catalyst has not been removed. The rationale behind this, is that interconversion of *o*-H_2 to *p*-H_2 cannot take place without the catalyst.

1.3 *Para*hydrogen induced polarization (PHIP)

Bowers and Weitekamp[23] in 1986 demonstrated that *para*-H_2 can be used to increase the sensitivity of NMR spectroscopy shortly after their initial predictions that symmetry breakdown of *para*-H_2 on addition to metals or unsaturated organic substrates should lead to large absorption and emission spectra in ^1H. In their study, Wilkinson's catalyst, $RhCl(PPh_3)_3$,[24] was used to convert acrylonitrile ($H_2C{=}CHCN$) to propionitrile (CH_3CH_2CN) under 1 atmosphere of *p*-H_2. PHIP was only evident during *p*-H_2 addition to acrylonitrile, with enhancements of approximately 100-fold. Weak resonances assigned to the dihydride species $Rh(H)_2Cl(PPh_3)_3$ were also observed, indicating a potential intermediate. An interesting feature of this investigation was the use of the phase profile of the enhanced hydride resonances to assign an absolute sign to the coupling constants. Since the emission component of the hydride resonance appeared at a lower field than the absorption component, $^2J_{HH}$ had to be negative.

*Para*hydrogen induced polarization (PHIP) can be used to hyperpolarize NMR active nuclei. PHIP has proved to be a very efficient and effective technique. PHIP is generally the result of a chemical reaction called hydrogenation in which *p*-H_2 nuclei are transferred into another molecule usually a substrate possessing certain symmetry properties. Under the right conditions, the spin state of *p*-H_2 is preserved in the spins of the hydrogen

nuclei which become part of a newly formed hyperpolarized molecule and ultimately the polarization can be transferred from the *p*-H_2 molecule to the other nuclei. In this fashion, the magnitude of NMR resonances of heteronuclei such as ^{1}H, ^{13}C, ^{15}N and ^{31}P can be enhanced.

1.3.1 PHIP in NMR spectroscopy

The *p*-H_2 molecule does not possess any magnetic moment and so it is NMR silent. As a consequence, all H_2 present in a system must correspond to *ortho*hydrogen and can be observed at δ 4.55 in a ^{1}H NMR spectrum. This means that that the symmetry of *p*-H_2 to be broken in order to observe an NMR signal, i.e. the two ^{1}H nuclei must become magnetically distinct. In this way PHIP can be achieved. PHIP is of two types namely: *para*hydrogen and synthesis allow dramatically enhanced nuclear alignment (PASADENA)[23] and adiabatic longitudinal transport after dissociation engenders net alignment (ALTADENA).[25]

1.3.2 The PASADENA effect

To understand the effect that *p*-H_2 plays on the ^{1}H NMR spectrum of a metal dihydride, the origin of the resonances needs to be considered first. The AX spin system can be achieved in a simple dihydride complex with two chemically distinct but weakly coupled nuclei (i.e. an AX is such a spin system in which the coupling constants between nuclei are small compared to the differences in chemical shift). The protons of MH_2 type complex can take up four spin state configurations in the energy levels and all the spins have to be taken into account mutually as the nuclei are coupled. The spin states can be

characterized by labels αα,ββ, αβ and βα. When a MH_2 spin system is placed in the magnetic field, the four transitions (αα → αβ, αα → βα, αβ → ββ, βα → ββ) occur that can be detected by NMR spectroscopy and the resultant ^1H NMR spectrum observed to be consisting of a pair of doublets.

The addition of *o*-H_2 to the MH_2 type complex gives rise to a condition where the energy levels will be occupied according to the Boltzmann distribution, resulting in an equilibrium population of nuclear spins across the energy levels. The MH_2 product is formed by the addition of *p*-H_2, (αβ–βα spin state) the product hydrides populate the αβ and βα states of the product, resulting in a non-Boltzmann spin distribution. Although the exact mechanism by which this spin transfer occurs is unknown, it is known that *p*-H_2 corresponds to an entangled state, so the two protons of the molecule share a link. This means that the population difference, and hence the intensity of the NMR signal, is much higher than the Boltzmann distribution would predict as there is potentially no population in the αα and ββ spin states. It is worth noting that two of the transitions now occur in the opposite direction (sense), resulting in an emission absorption doublet in the ^1H NMR spectrum (the two components are antiphase to each other). This effect was observed for a reaction occurring in a strong magnetic field and named as PASADENA.[26] The whole process of polarization transfer via PASADENA is illustrated in Figure 1.7.

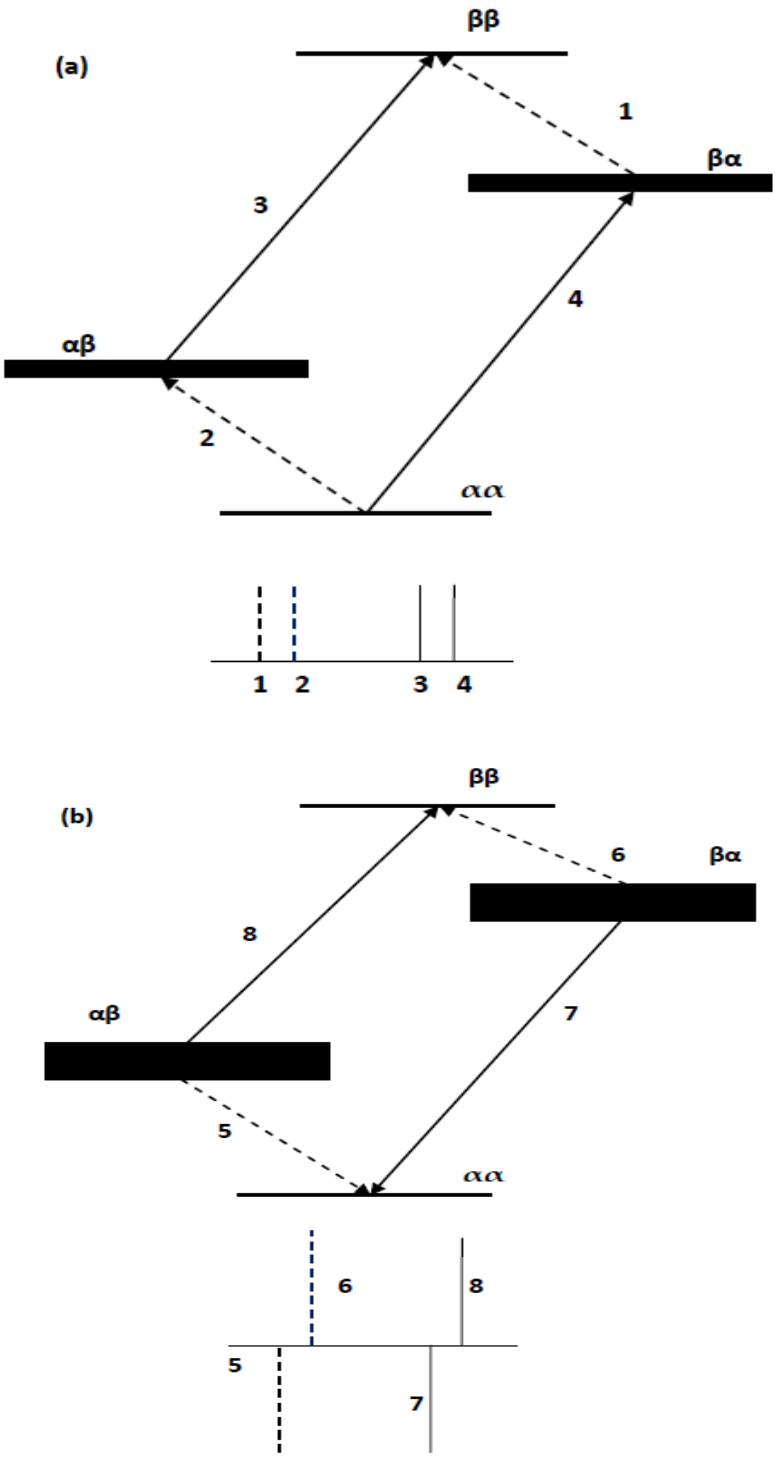

Figure 1.7: Spin state populations (represented by lines thickness) and corresponding NMR signal patterns for an AX spin system: (a) Boltzmann conditions; (b) A schematic representation of a ^1H NMR spectrum in case of a PASADENA experiment.

If we take into account the Figure 1.7, it is clear that when normal-H_2 is added to a metal complex the resulting spin states have similar populations (Boltzmann distribution); however, if *p*-H_2 is added two of the spin states of the complex are selectively populated, resulting in a non-Boltzmann distribution and thus enhanced signal. This sensitivity gain can then be used to record information about the ligand sphere of the metal. The preservation of non-Boltzmann distribution of spins is important in order to observe the effect of *p*-H_2 in the acquired NMR spectra. It can be achieved by pairwise addition, which acts to preserve the spin properties of *p*-H_2 comparative to ^1H relaxation. In pairwise addition mechanism, the two H_2 atoms enriched in *para* spin state simultaneously bind to the metal in a manner such that spin correlation is maintained between the two protons. Moreover, during the aforementioned pairwise addition, the symmetry of *p*-H_2 is broken, and hydride ligands acquire inequivalent positions around the metal centre. In such a case where the hydride ligands are equivalent, it is anticipated that a $\alpha\beta-\beta\alpha$ spin states in the A_2 type spin system would be populated and as the spin state does not interact with a magnetic field so no NMR resonance can be observed.[26]

A study by Aime and co workers[27] demonstrated polarization transfer from the *p*-H_2 can be achieved into the A_2 spin system, if a product is formed instantly on exposure to *p*-H_2 with magnetically inequivalent hydride ligands arranged around the metal centre. The magnetic inequivalency can be achieved by breaking the symmetry as *p*-H_2 refers to an unobservable singlet state, highly polarized which requires to be converted into an observable magnetization so as to be detected. A convenient way is to transform the relevant state of an A_2 spin system; the so-called longitudinal spin order denoted by the spin function $(1/\sqrt{2})$ $(\alpha\beta - \beta\alpha)$ into states of the same zero quantum number leading to

observable transitions (namely the $\alpha\beta$ and $\beta\alpha$ states of an AX spin system). These aforementioned states are highly polarized leading to transitions from $\alpha\beta$ to $\beta\beta$ resulting in an enhanced NMR signals arising from the overpopulated $\alpha\beta$ and $\beta\alpha$ energy levels.

1.3.3 The ALTADENA effect

A different reaction is observed if the reaction involving *p*-H_2 takes place outside the NMR spectrometer,[28] in the Earth's weak magnetic field, and the sample is subsequently transferred into the spectrometer for analysis. In a weak magnetic field, the spin system is strongly coupled, so the coupling between nuclei is large relative to the frequency difference between them. Under such conditions, the added *p*-H_2 protons remain in their initial eigenstate, so they are still characterised by the spin function of *p*-H_2, $\alpha\beta - \beta\alpha$. The same is true for *o*-H_2 protons. If the transfer into the magnet takes place adiabatically in the quantum mechanical sense (i.e. if the spin populations remain unaltered), the system will adapt itself at all times to the new conditions, so the spin functions are retained. This means that the population of each spin state of the initial hydrogen molecule ($\alpha\alpha$, $\beta\beta$, $\alpha\beta + \beta\alpha$, $\alpha\beta - \beta\alpha$) is transferred into one spin state of the MH_2 product ($\alpha\alpha$, $\beta\beta$, $\alpha\beta$, $\beta\alpha$). As explained in section 1.3.2, *p*-H_2 is an entangled state and may only transfer to the $\alpha\beta$ or $\beta\alpha$ spin states. Former *p*-H_2 protons will therefore selectively populate the lower-energy of those two states, since *p*-H_2 itself corresponds to the low energy isomer. As a result, only two observable transitions are possible, as shown in Figure 1.8, and only two resonances are observed, an enhanced emission and an enhanced absorption. This effect is called ALTADENA (adiabatic longitudinal transport after dissociation engenders net alignment).

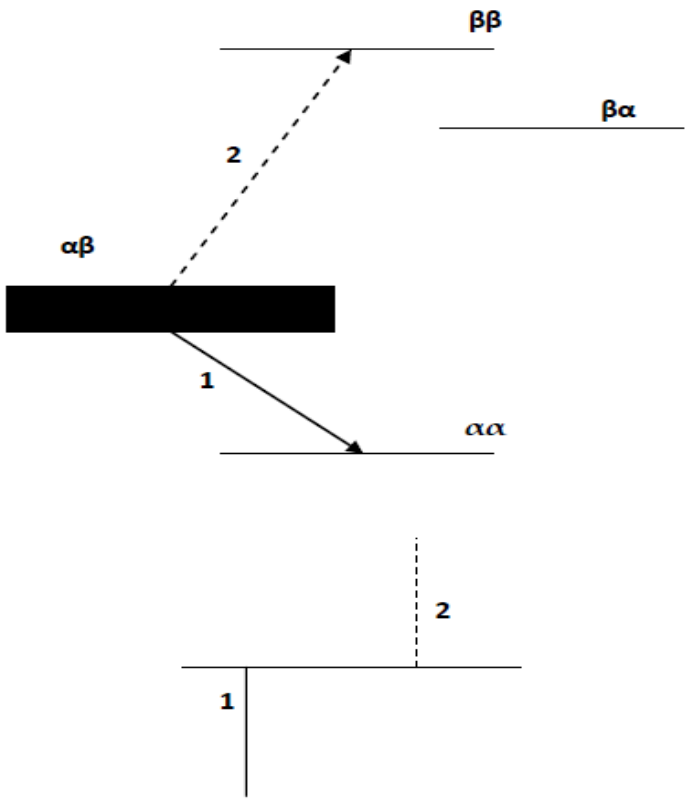

Figure 1.8: ***Spin state populations (represented by line thickness) and corresponding NMR signal patterns for an AX spin system under parahydrogen-derived ALTADENA conditions.***

In order to observe the ALTADENA effect, sample transfer into the probe must be rapid relative to proton spin-lattice relaxation, so the phenomenon is generally easier to observe with organic products due to their longer T_1 values. The ALTADENA effect is transitory in nature. Once the sample has been inserted into the magnet and the initial *p*-H_2 spin population is depleted, ALTADENA signal enhancements will either turn into PASADENA in the presence of rapid exchange with free *p*-H_2, or will be lost completely if the exchange is too slow.[28]

1.4 Product operator formalism

In product operator formalism,[29] the density operator of the spin system is expressed as a linear combination of base operator products. Cartesian base operators have found widespread use because they are very well suited for the description of pulse effects and time evolution. When multiple quantum coherence is involved, shift base operators prove to be more efficient. The Cartesian base operators are I_x, I_y, I_z, and E=2 (E is the unit operator). For a weakly coupled two-spin system (I = 1/2), there are 16 product operators. These operators are: (1) zero-spin operator E=2; (2) one spin operators $I1_x$, $I1_y$, $I1_z$, $I2_x$, $I2_y$, and $I2_z$; (3) two-spin operators $2I1_xI2_x$, $2I1_xI2_y$, $2I1_xI2_z$, $2I1_yI2_x$, $2I1_yI2_y$, $2I1_yI2_z$, $2I1_zI2_x$, $2I1_zI2_y$, and $2I1_zI2_z$. The following section encompasses the product formalism of p-H_2.

1.4.1 Product formalism of p-H_2

In order to understand the only $p$ara-hydrogen spectroscopy approach,[30] the spin dynamics of the *para*-hydrogen derived systems need to be further considered. The initial two spin order term $2I_zS_z$ yields $2I_yS_y$ after a $\pi/2(x)$ r.f. pulse which is a mixture of zero and double quantum coherences that are not directly observable. These terms evolve further during a finite delay, τ, according to their frequency shifts, ω_I and ω_S, into those detailed in Equation 1.6:

$$\begin{aligned}
&2I_xS_x\{1/2\cos[\tau(\omega_I - \omega_s)] - 1/2\cos[\tau(\omega_I + \omega_s)]\}\\
&\quad + 2I_yS_x\{1/2\sin[\tau(\omega_I - \omega_s)] - 1/2\sin[\tau(\omega_I + \omega_s)]\}\\
&\quad - 2I_xS_y\{1/2\sin[\tau(\omega_I - \omega_s)] + 1/2\sin[\tau(\omega_I + \omega_s)]\}\\
&\quad - 2I_yS_y\{1/2\cos[\tau(\omega_I - \omega_s)] + 1/2\cos[\tau(\omega_I + \omega_s)]\}\ldots\ldots\ldots\ldots\ldots\ldots\textit{Equation.1.6}
\end{aligned}$$

These terms are subsequently converted by a $\pi/2(y)$ pulse into those shown in Equation 1.7:

$$2I_zS_z\{1/2\cos[\tau(\omega_I - \omega_s)] - 1/2\cos[\tau(\omega_I + \omega_s)]\}$$
$$+ 2I_yS_z\{1/2\sin[\tau(\omega_I - \omega_s)] - 1/2\sin[\tau(\omega_I + \omega_s)]\}$$
$$- 2I_zS_y\{1/2\sin[\tau(\omega_I - \omega_s)] + 1/2\sin[\tau(\omega_I + \omega_s)]\}$$
$$- 2I_yS_y\{1/2\cos[\tau(\omega_I - \omega_s)] + 1/2\sin[\tau(\omega_I + \omega_s)]\} \quad \textit{Equation.1.7}$$

Some of these terms then continue to evolve with time such that detectable coherences are created during acquisition of the FID. Pulsed field gradients (PFGs) are used to select either the ZQ or DQ coherence pathways to produce observable magnetization that originates from the $2I_zS_z$ spin order of the *para*-hydrogen. The pulse sequences used experimentally to implement OPSY as illustrated in Figure 1.9. When the second $\pi/2$ r.f. pulse is flanked by two PFGs of ratio of 1:2, several coherences are retained at end of the second gradient, ignoring evolution during the second gradient pulse, as shown in Equation 1.8:

$$1/2\ 2I_zS_z\pi\cos[\tau(\omega_I - \omega_s)] + 1/4\ 2I_xS_x\pi\cos[\tau(\omega_I - \omega_s)]\}$$
$$+ 1/4\ 2I_yS_y\cos[\tau(\omega_I - \omega_s)] - 1/4\ 2I_zS_x\pi\cos[\tau(\omega_I + \omega_s)]\}$$
$$- 1/4\ 2I_xS_z\cos[\tau(\omega_I + \omega_s)] - 1/4\ 2I_yS_z\pi\cos[\tau(\omega_I + \omega_s)]\}$$
$$- 1/4\ 2I_zS_y\cos[\tau(\omega_I + \omega_s)]\} \quad \textit{Equation.1.8}$$

During the acquisition I_x, I_y, S_x, S_y, I_zS_x, I_zS_y, I_xS_z, and I_yS_z are generated in differing proportions depending on the chemical shift and scalar coupling for I and S. Non-observable coherences and magnetization are also generated. This situation corresponds to the double quantum coherence selected variant and is referred to as OPSY-d.

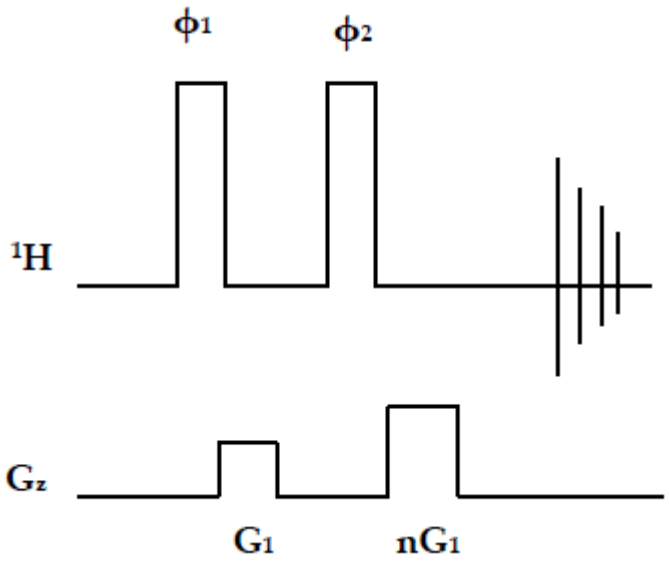

Figure 1.9: ***Quantum coherence selection based OPSY sequences. Gradient strength (G): 53 G cm^{-1}, first gradient duration for the experiment was 1 ms using a half sine gradient with 0.5 ms stabilization delay. For the case: n = 2, giving a double quantum coherence selection (OPSY-d) the second gradient pulse duration was 2 ms; for n = 0, no second gradient pulse is employed.***

Experimentally, the use of PFGs with opposite polarity produced the clearest spectra and the pulse sequence for this is depicted in 1.9. In contrast, when the second $\pi/2$ r.f. pulse is preceded by a single PFG (i.e. gradient ratio 1:0) different coherences are retained after the second r.f. pulse, these are shown in Equation 1.9, and a zero quantum coherence selection form of the experiment, OPSY-z, is implemented. Observable magnetization is then generated during the acquisition and the coefficients for the coherences and magnetization are different to those in the OPSY-d.

$$1/2\ 2I_zS_z\cos[\tau(\omega_I - \omega_s)] - 1/2\ 2I_zS_z\cos[\tau(\omega_I + \omega_s$$

$$+ 1/2\ 2I_zS_x\{\cos[\tau(\omega_I - \omega_s)] + 1/2\ 2I_zS_z\pi\{\cos[\tau(\omega_I + \omega_s)]\} \quad \text{Equation 1.9}$$

The pulse sequence for OPSY-z is depicted in Figure 1.9. These two coherence pathways can be selected without retaining any signal from thermally polarized magnetization (derived from $I_z + S_z$) in a single observation. Thermal magnetization of the type $I_z + S_z$ is converted into $I_y + S_y$ by the initial $\pi/2(x)$ r.f. pulse which is then dephased by the gradients. The efficiency of the sequence can further be increased by phase cycling.[31, 32]

1.5 The use of *p*-H_2 in NMR experiments

The *p*-H_2 can be used in the conventional NMR experiments with some modifications in describing the initial magnetization of a metal dihydride complex containing chemically distinct hydride ligands. Most of the active complexes containing hydride ligands formed by the addition of *p*-H_2 correspond to AX spin system. The product operator formulism is used to depict the initial magnetization of the AX spin system, which is given by product operator representation $I_z^AI_z^X$, where Z indicates the direction of magnetization in a Cartesian coordinate system, while A and X represent the labels for the two nuclei in the aforementioned spin system. The following section describes the 1D and 2D NMR experiments in relation to *p*-H_2.

1.5.1 ^{1}H NMR experiment

After the metal complex is formed, the most important experiment to do is the 1D NMR experiment to characterize the complex derived from *p*-H_2. The

product operator with a single transverse component, (I_X or I_Y), results in an observable magnetization.

$$I_z^A I_z^X \longrightarrow I_z^A I_z^X \cos^2(\alpha) + I_x^A I_z^X \cos(\alpha)\sin(\alpha) + I_z^A I_x^X \cos(\alpha)\sin(\alpha) + I_x^A I_x^X \sin^2(\alpha)$$

The application of an RF pulse results in the generation of terms as mentioned above in the product operator formalism, only the second and third terms give rise to antiphase A and X magnetization that can be directly observed. The first and last terms are responsible for zero and double quantum coherences and cannot be observed directly in NMR spectroscopy. The application of an RF pulse with a flip angle of 90^o, the resultant magnetization is generated with cos 90^o, which is equal to zero so, no magnetization is observed. In case of a conventional 1D NMR experiment, the maximum signal can be achieved by the application of a 90^o pulse and maximum transverse magnetization is achieved by the application of a 45^o excitation pulse. Bargon and co workers made use of selective pulses to engender pure antiphase magnetization A and X terms directly form ($I_x^A I_z^X$).[33]

1.5.2 Only *para*hydrogen induced polarization (OPSY)

Only *para*hydrogen induced polarization (OPSY)[34, 35] is a technique used to observe the NMR resonances derived from *p*-H_2. Pulsed field gradient encoded pulses sequences have been used in OPSY. In OPSY, the double quantum (DQ) coherent terms ($2I_{1x}I_{2x}$) and single quantum (SQ) I_x terms generated for the thermal magnetization by the first $\pi/2$ pulse. Their precession during a gradient pulse produces a distribution of terms $I_{1x}I_{2y}$ and $I_{1y}I_{2x}$. The second 90° pulse and

subsequent gradient pulse with an area twice the first one, convert the aforementioned terms into observable $I_{1y}I_{2z}$ and $I_{1z}I_{2y}$ terms. Because the *p*-H_2 derived signals dephased during the first gradient at twice the rate of the thermally based SQ terms, only this magnetisation is refocused by the second gradient and therefore only *p*-H_2 derived signals are observed. The ^{1}H OPSY sequence is shown in Figure 1.10.

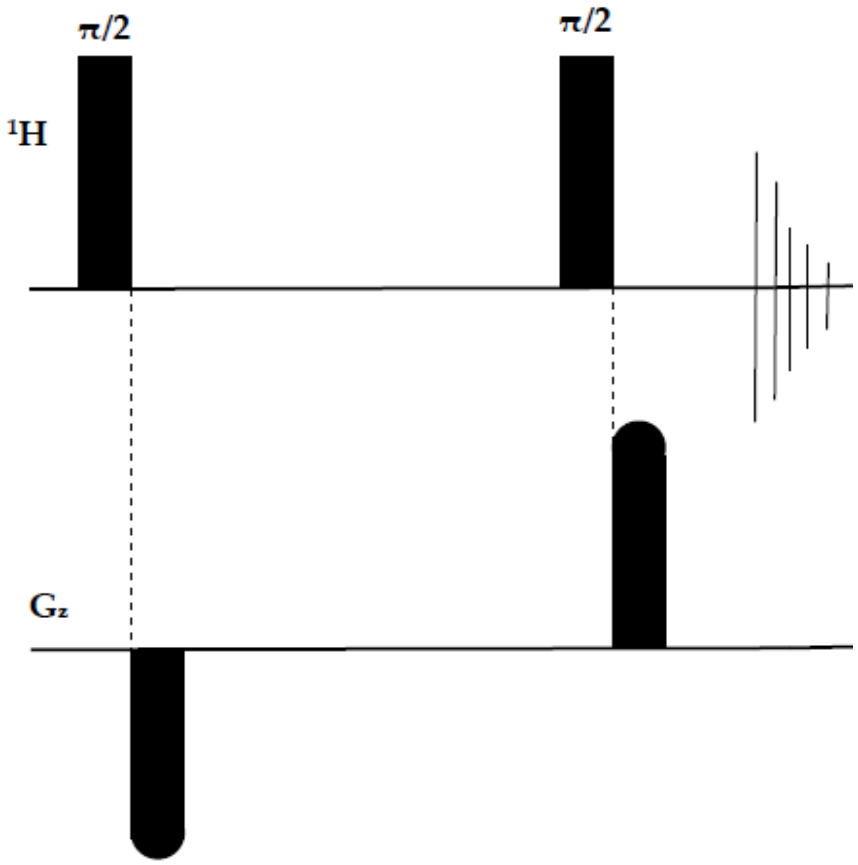

Figure 1.10: ***Field gradient encoded pulse sequence for ^{1}H OPSY.***

1.5.3 1D EXSY/nOe experiment

The nuclear Overhauser effect (nOe) is a net change of the signal intensity from one spin due to the relaxation of a saturated spin that is dipole-dipole coupled to the first spin. nOe's develop due to through-space rather than through-bond interactions, and so contain information on the distances between spins. The rate at which the nOe builds up is entirely dependent on the dipole-dipole relaxation of the spins involved, and also on the strength and frequency of the fluctuating magnetic field, which in turn depends on the distance between the nuclei involved in the spin system and the rate of tumbling of the molecules. The nOe experiment cannot be completed efficiently if there is a presence of *para*magnetic impurities such as metal ions, dissolved oxygen and rust within the sample, because they dominate the T_1 relaxation processes, resulting in the distortion of any nOe experiment.

The pulse sequence to carry out nOe/exsy experiments consists of shaped pulses and field gradients to selectively irradiate the signal of interest and suppresses spectral artefacts.[33, 35] Selective pulses are important because they allow one to reduce the number of dimensions from three to two or less. It is therefore not surprising that there is an increasing need for selective pulses which are able to excite, de-excite, invert, or refocus coherences.

The effect of pulses can be seen in the finally acquired NMR spectrum, which shows the magnetization transfer excited by the selective pulses or transferred from the nOe effect or by a chemical exchange within the specified mixing time.[34] The pulse sequence used is called the Double Pulsed Field Gradient Spin Echo (DPFGSE) after the first 90° excitation pulse, which

comprises two selective 180° pulses, each of them sandwiched between two gradient pulses. The purpose of using the DPFGSE is to invert the desired signal and to destroy all other magnetization. The pulse sequence makes the exchange between the two spins observable because it generates nOe effects that are transient rather the steady state. In the mixing delay or period, another 180° gradient pulse is applied to suppress the effect of T_1 relaxation on the acquisition of an NMR spectrum prior to the final 90° pulse.[34] The pulse sequence of the PHIP-modified selective 1D NOESY is depicted in Figure 1.11.

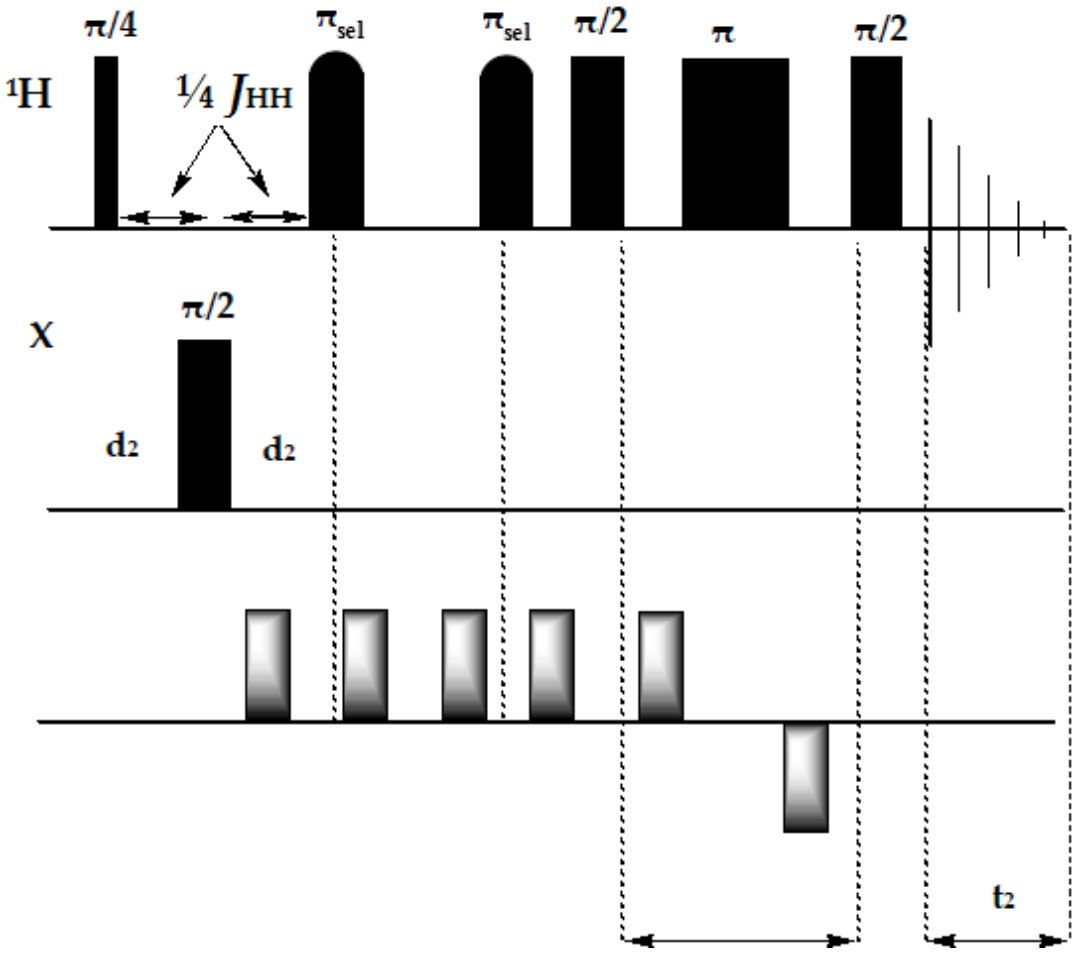

Figure 1.11: PHIP-modified selective 1D NOESY pulse sequence.

In the modified pulse sequence for 1D nOe as demonstrated in Figure 1.5, the initial 90° pulse is replaced by a 45° pulse to generate antiphase magnetization, which is then refocused by a composite pulse, where $d_2 = ¼ J_{HH}$. The rest of the pulse sequence is identical as observed in the conventional NMR pulse sequence after the application of a first 90° pulse.

1.6 2D NMR experiments and *p*-H_2

In the literature, it has been cited that the conventional two-dimensional NMR techniques such as ^{1}H-X HMQC, ^{1}H-^{1}H COSY and ^{1}H OPSY-COSY can be used to study systems consisting of *p*-H_2 derived hydride ligands.[33, 34] The Heteronuclear Multiple Quantum Correlation (HMQC) experiment provides correlation between protons and their attached heteronuclei through the heteronuclear scalar coupling. In the HMQC experiment, the coherence is transferred from sensitive nucleus such as ^{1}H to insensitive nucleus (^{13}C). On the other hand, the Correlation Spectroscopy (COSY) is a homonuclear chemical shift correlation experiment based on the transfer of polarization by a mixing pulse between directly *J*-coupled spins. While ^{1}H OPSY-COSY is also a type of homonuclear chemical shift correlation experiment that is used in conjunction with OPSY to reveal the resonances derived from *p*-H_2.

1.6.1 ^{1}H-X HMQC NMR experiment

The HMQC is a type of heteronuclear shift correlation experiment. As the name implies it is used to detect the chemical shifts of heteronuclei via scalar couplings between them and the proton nuclei. In case of a HMQC experiment, there are two frequency axis, one of the axis F_2 is used to detect the ^{1}H chemical

shifts, while the heteronuclear chemical shifts are on the F_1 axis. In HMQC experiment, the resonances correspond to the two nuclei that connect through a scalar coupling as also observed in case of a COSY experiment.

In a HMQC experiment, the magnetization transfer takes place from ^1H nucleus to the X nucleus and then back to proton in the detection period.[36] The HMQC experiment takes advantage of the greater proton sensitivity over most heteronuclei and removes resonances that do not couple to heteronuclei, such as solvent signals. The HMQC experiment resembles a COSY experiment except a slight modification is required in the pulse sequence, which is the replacement of the first 90° pulse by a 45° pulse to generate antiphase magnetization. The pulse sequence used for HMQC in PHIP experiments is given in Figure 1.12.

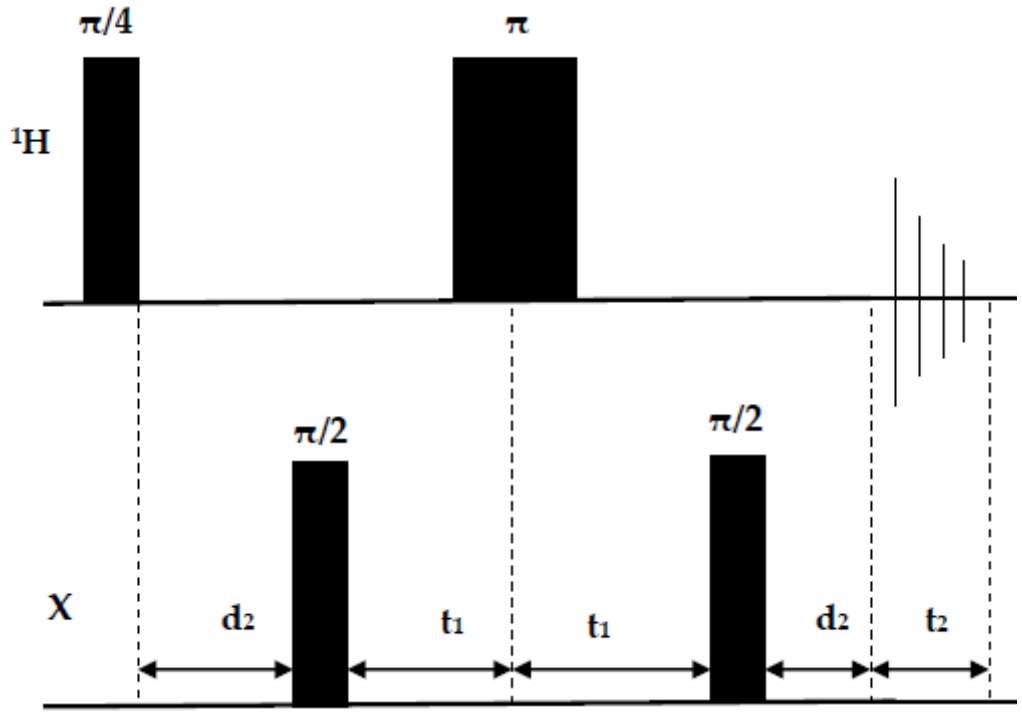

Figure 1.12: ***PHIP modified pulse sequence for the ^1H-X HMQC experiment.***

1.6.2 COSY experiment

The correlation spectroscopy (COSY) is a type of homonuclear NMR experiment used to detect nuclei which exhibit mutual scalar couplings. The 2D COSY experiment has a clear advantage over the 1D experiment since a wide range of chemical shifts and correlations can be monitored simultaneously. The COSY spectrum exhibits two types of peaks. Diagonal peaks show the same chemical shift on both the axis, whereas the cross-peaks demonstrate different chemical shifts on the both axis. The observation of a cross-peak linking two diagonal peaks signifies that the two nuclei in question exhibit a scalar coupling.

The conventional COSY experiment comprises of two 90^{o} pulses, separated by initial delay t_1, which is responsible for the generation of the second frequency dimension. It has been shown that a slight modification is necessary in the conventional COSY pulse sequence for use in the PHIP experiments. This is the replacement of the first 90^{o} pulse with a 45^{o} pulse to yield antiphase ^{1}H magnetization.[35-38] The aforementioned pulse sequence can also be used for heteronuclear decoupling during the t_2 period, with an effect of re-focussing the ^{1}H magnetization.[33, 39, 40] The COSY pulse sequence is shown in Figure 1.13.

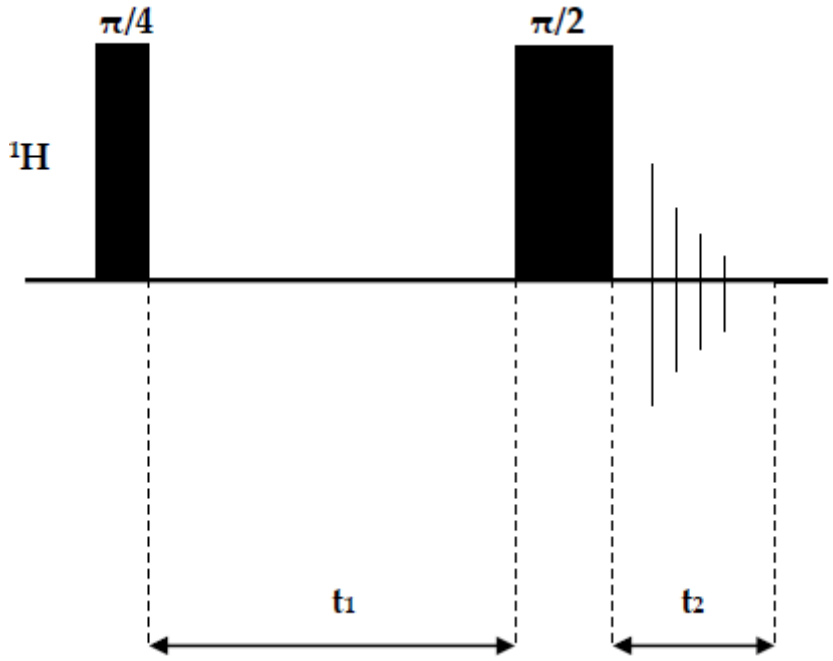

Figure 1.13: Pulse sequence for the PHIP- modified COSY experiment.

1.6.3 ^{1}H OPSY-COSY

The OPSY sequence can also be applied to two dimensional experiments.[34] The pulse sequence for OPSY adapted COSY is shown in Figure 1.14, where the initial 90° pulse of the standard COSY sequence has been replaced with a 45° pulse in the case of the *p*-H_2 adapted experiment by the OPSY sequence.

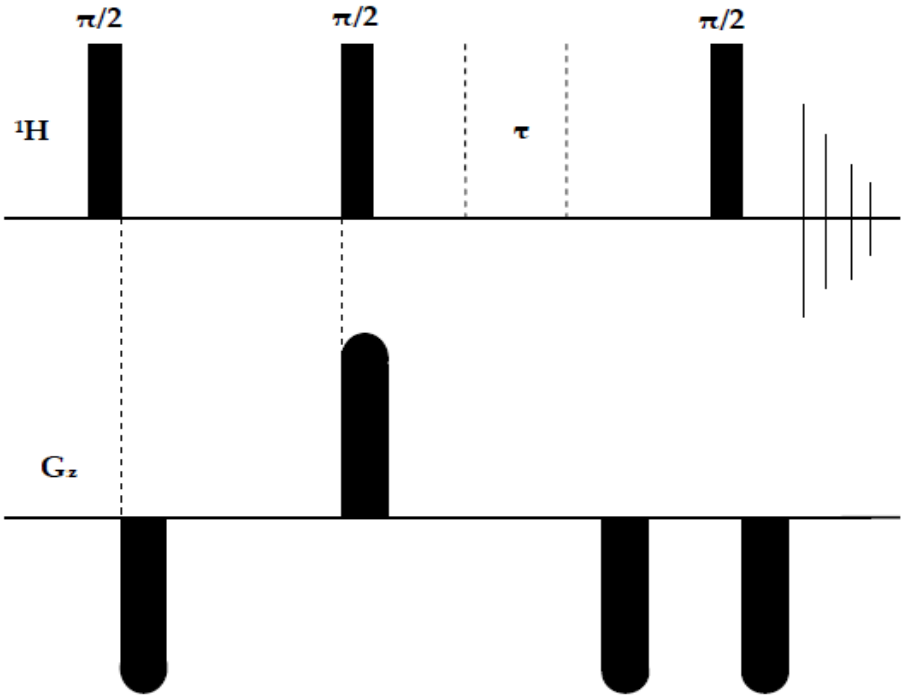

Figure 1.14: Pulse sequence for ^{1}H-^{1}H OPSY-COSY

A sample containing 4-vinylcyclohexene and [Rh(COD)(dppb)]BF_4 (where dppb is bis(diphenylphosphino)butane) in CD_3OD was examined under 3 bar of *p*-H_2 (Figure 1.15). Figure 1.16a shows a typical ^{1}H NMR spectrum produced during this reaction.[34]

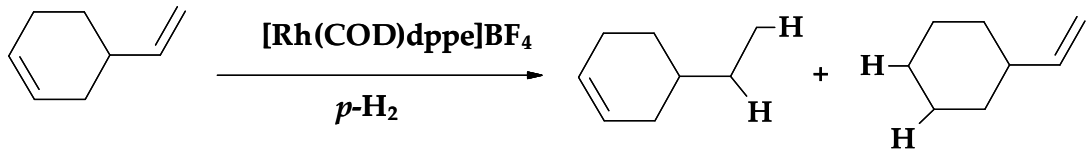

Figure 1.15: Reaction of 4-vinylcyclohexene and [Rh(COD)(dppb)]BF_4 in CD_3OD leads to the formation of 4-ethylcyclohexene and vinylcyclohexane.

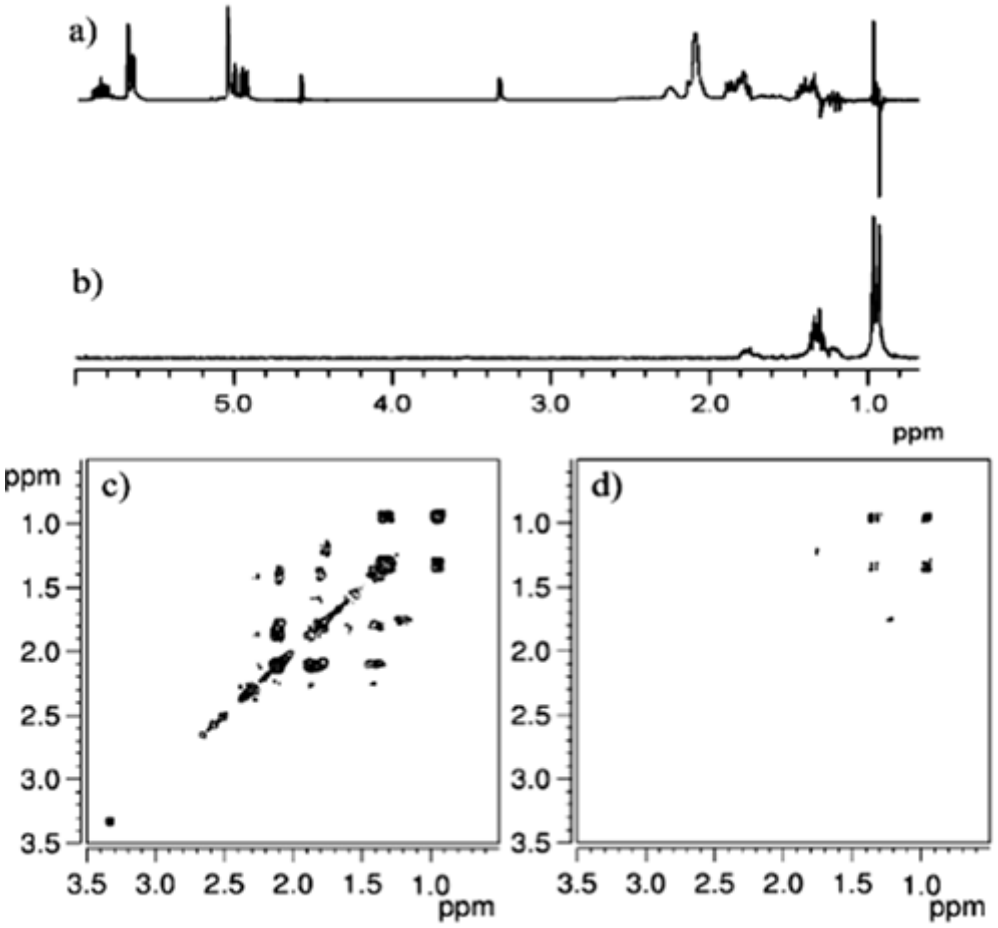

Figure 1.16: ***^{1}H NMR spectra for a sample containing [Rh(COD)(dppb)BF$_4$] (1 mg) and 4-vinylcyclohexene (10 µL) in CD$_3$OD (500 µL) under 3 bar p-H$_2$: (a) ^{1}H PHIP; (b) ^{1}H OPSY; (c) p-H$_2$ COSY; (d) OPSY-COSY. (Reproduced with permission from reference 34).***

A PHIP enhanced signal is observable for the methyl group of the hydrogenation product 4-ethylcyclohexene at δ 0.95 ppm, along with a smaller PHIP enhanced resonance at δ 1.21 ppm. Upon application of the OPSY filter (Figure 1.16b) these peaks appear very easily, and two further resonances are observed at δ 1.76 ppm and 1.32 ppm, which were previously obscured by thermal signals. The larger of these signals, at δ 1.32 ppm, corresponds to the

methylene resonance of 4-ethylcyclohexene and the weaker PHIP signals, at δ 1.76 ppm and 1.21 ppm; arise from the *p*-H_2 derived ring protons of the alternative hydrogenation product vinylcyclohexane. GC-MS data show no evidence for the double hydrogenation to ethylcyclohexane on the time scales of these experiments. These data therefore reflect the kinetic selectivity of the initial hydrogenation step. Figure 1.16c shows a COSY spectrum that was also recorded during this reaction. In contrast, Figure 1.16d shows the corresponding OPSY-COSY spectrum where the thermally derived signals have been removed. The peaks that arise from the major hydrogenation product 4-ethylcyclohexene are now visible, in addition to weaker cross peaks for the minor hydrogenation product vinylcyclohexane.

1.7 Applications of PHIP

The PHIP method is a well established technique in the field of NMR spectroscopy which finds numerous applications in wide areas ranging from chemistry, biosciences and in the field of medical diagnostics. Some of the selected applications of NMR-PHIP are described in the following section.

1.7.1 Selected applications of NMR-PHIP

The PHIP phenomenon was first experimentally demonstrated by Bowers and Weitekamp.[8] They used Wilkinson's catalyst [$RhCl(PPh_3)_3$] to convert acrylonitrile (H_2C=CHCN) into propionitrile (CH_3CH_2CN) in the presence of *p*-H_2 at a pressure of 1 atmosphere. Figure l.17a shows the proton NMR spectrum (υ_0 = 200 MHz) of a deutrobenzene (C_6D_6) solution 0.76 M in acrylonitrile and

0.035 M in [RhC1(PPh3)3] obtained by Fourier transformation of the free-induction decay after a 6 μs π/2 pulse. Figure 1.17b shows the ^{1}H NMR acquired after the sample was enriched with 50% *p*-H_2. Figure 1.17c demonstrates an NMR spectrum obtained with a delay of 200 s with no further addition of H_2 and shows the antiphase multiplets of Figure 1.17b are transient in nature. As the propionitrile is the product of the reaction, the transient nature of the enhanced NMR resonances must be due to the spin-lattice relaxation process, which produces signals greater in magnitude than the signal obtained at thermal equilibrium for the propionitrile.[8]

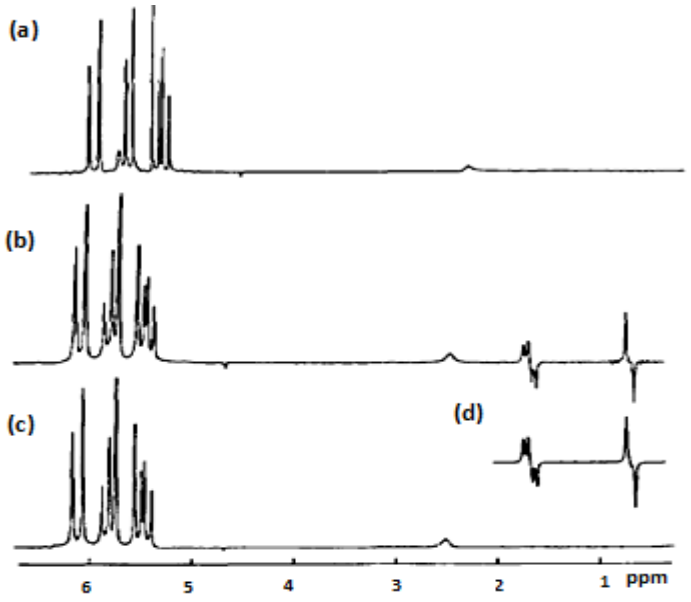

Figure 1.17: ***(a) shows the thermal ^{1}H NMR spectrum prior to the reaction. The intense resonances are due to acrylonitrile substrate; (b) ^{1}H NMR spectrum was acquired subsequent to hydrogenation to propionitrile; (c) an NMR spectrum of the equilibrated sample demonstrates that the resonance of b was a large transient enhancement; (d) a line simulation of enhanced signals. (Reproduced with permission from reference 8).***

In the aforementioned study,[8] it has been concluded that the *ortho-para* population differences are converted to nuclear magnetism, which is then measured. The inverse of this phenomenon would be to deduce the nuclear spin order of an ensemble of molecules by measuring the *ortho-para* population differences of the H_2 formed by their dehydrogenation. Since the spin state is modified by the dynamics under rf pulses and internal couplings, the branching ratio to *ortho* and *para* products would depend on the NMR of the dihydrogen precursor.

The detection of intermediates is necessary in order to understand the steps involved in a catalytic process. The *p*-H_2 can be used to detect intermediates particularly in case of transition metal complexes containing mono-, bi-, or multidentate ligands coordinated to the metal centre. The use of *p*-H_2 in the 2D NMR techniques was first illustrated by Messerle and co-workers,[37] in which they used *p*-H_2 to detect the ^{103}Ru and ^{31}P chemical shifts and eventually from the magnitude and relative size of heteronuclear coupling constants, they were able to determine the exact structures of $[Rh(H)_2(Cl)(PMe_3)_3]$ and $[Rh(H)_2(PMe_3)_4Cl]$ complexes. The magnitude of the heteronuclear couplings were measured by acquiring the decoupled heteronuclear correlation spectra of the compounds i.e. the active anti-phase coupling $J_{(XH)}$, where X= ^{31}P or ^{103}Rh, has been removed. This means from the ^{1}H-^{31}P correlation, the two couplings $J_{(^{1}H,\ ^{103}Rh)}$ and $J_{(^{31}P\text{-}^{103}Rh)}$ can be measured from the splittings in the ^{1}H and ^{31}P (F2 and F1) dimensions respectively. From the ^{1}H-^{103}Rh correlation, the two couplings $J_{(^{1}H,\ ^{31}P)}$ and $J_{(^{31}P\text{-}^{103}Rh)}$ can be measured from the splittings in the F2 and F1 dimensions respectively. The HMQC spectra acquired are shown in Figure 1.18.

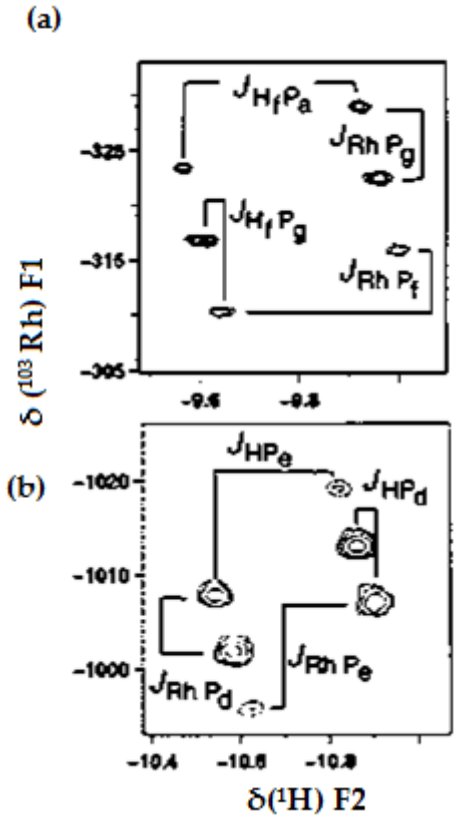

Figure 1.18: ***(a) ^{1}H-^{103}Rh correlation spectrum (HMQC), ^{103}Rh decoupled in F2, showing correlated transition between H_f and ^{103}Rh; (b) ^{1}H-^{103}Rh correlation spectrum (HMQC), ^{103}Rh decoupled in F2, showing correlation between resonances due to ^{1}H and ^{1}H-^{103}Rh.(Reproduced with permission from reference 37).***

Duckett *et al.*[41] demonstrated that when a solution containing [Ir(BPM)(CO)$_2$][BPh$_4$] (BPM = bis(pyrazole-1-yl)methane) in 0.1mM, thf-d_8 was charged with 3 atm *p*-H$_2$ in a sealable 5 mm NMR tube, and examined by ^{1}H NMR spectroscopy at 323 K over a period of 2 h, a product containing metal–hydride ligands was observed as a consequence of the signal enhancement available through *p*-H$_2$. The first formed, kinetically preferred, reaction product was the iridium (III) product formed by direct H$_2$ addition over one of the CO–

Ir–N axes: *cis*-[Ir(H)$_2$(BPM)(CO)$_2$](Figure 1.19). The two inequivalent metal–hydrides, H$_a$ and H$_b$, of complex, *cis*-[Ir(H)$_2$(BPM)(CO)$_2$], are mutually coupled (J = 4 Hz) and resonate at δ -7.80 and δ -16.13, which indicates that H$_a$ is *trans* to a CO and H$_b$ is *trans* to the N-donor.

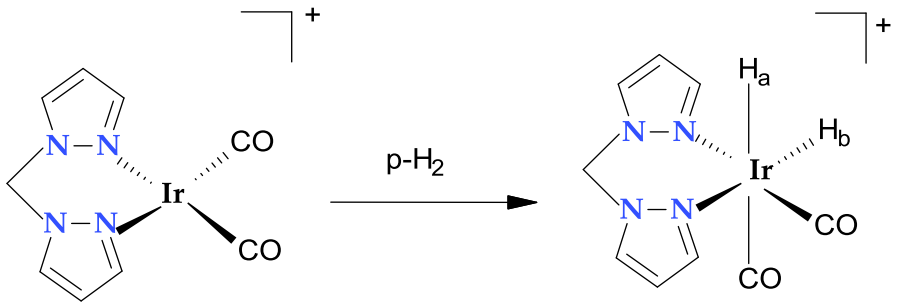

Figure 1.19: ***Formation of a complex, cis-[Ir(H)$_2$(BPM)(CO)]$^+$ in a reaction of [Ir(BPM)(CO)$_2$][BPh$_4$] with p-H$_2$.***

In an affiliate study by Permin and co workers,[42] in which they demonstrated that the addition of 0.5 equiv of SnBr$_2$ to an acetone solution of IrBr$_2$(CO)$_2$- leads to the in situ generation of mixed bromo tribromostannyl complexes. The major polarization was seen for bromo tribromostannyl complex (Figure 1.20).

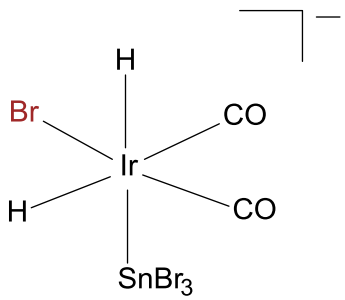

Figure 1.20: ***The Structure of complex, [IrBr(H)$_2$(CO)$_2$]$^-$SnBr$_3$.***

The ^{1}H-^{117,119}Sn couplings (7.6% and 8.6% natural abundances, respectively) allow for unambiguous structural assignment. Specifically, the resonance at δ-11.91 exhibits ^{117,119}Sn satellites indicative of the stannyl ligand being *trans* to the hydride, while the resonance at δ -8.67 shows *cis* ^{117,119}Sn couplings and a chemical shift characteristic of the hydride being *trans* to CO (Figure 1.21).

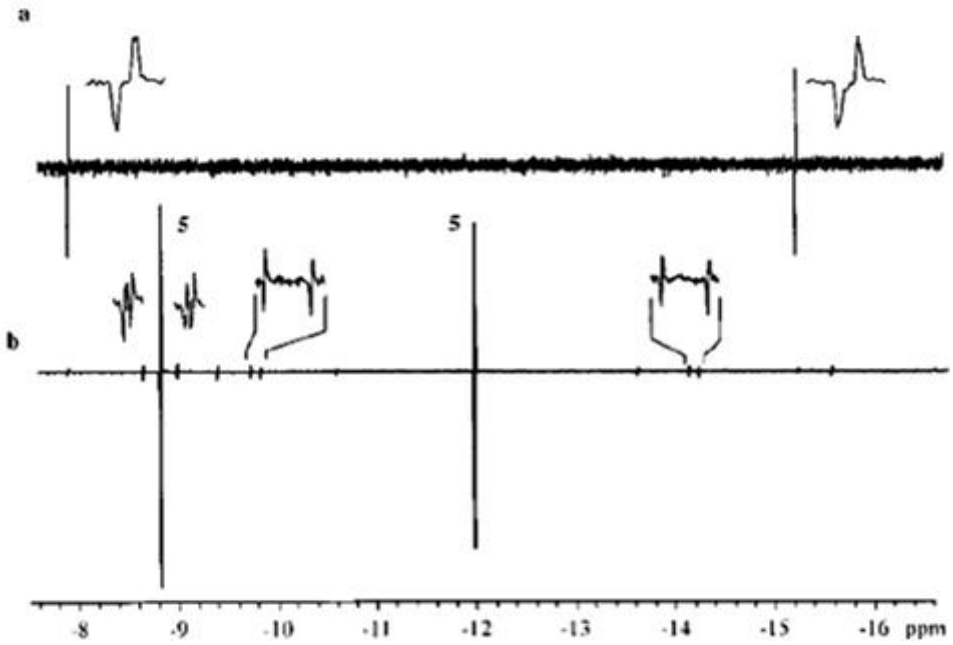

Figure 1.21: ***PHIP ^{1}H spectra of the [IrBr$_2$(CO)$_2$]-SnBr$_2$ system in acetone-d$_6$ at room temperature and short reaction time: (a) no SnBr$_2$ added; (b) 0.5 mol equiv of SnBr$_2$.(Reproduced with permission from reference 42).***

In a separate study by Eisenberg *et al*.[28] they carried out the hydrogenation of a 1 mM solution of RhCl(CO)(PPh$_3$)$_2$ in benzene-d$_6$ warmed with ca. 3 atm *p*-H$_2$. When monitored by ^{1}H NMR spectroscopy two sets of hydride resonances were observed, as shown in Figure 1.22a. Figure 1.22b simplifies the original spectrum to the extent that the two hydride resonances appear as doublets of antiphase doublets with J_{RhHa} = 24.6 Hz and J_{HH} = -11 Hz.

The hydride resonances were observed to be showing emission-absorption profile with $^{2}J_{HH}$. The hydrogenation product in an NMR spectrum was demonstrated by the absorption-emission signal with $^{2}J_{HH}$. The HMQC experiment revealed two rhodium coupled hydride resonances that are connected to a single type ^{31}P nucleus (Figure 1.22c). Another HMQC experiment was acquired to observe ^{103}Rh as it is 32,000 times less sensitive to direct observation than ^{1}H. In this experiment, both of the hydride resonances were observed to connect to a rhodium (III) centre that resonates at δ 925 and couples to ^{31}P (Figure 1.22d).

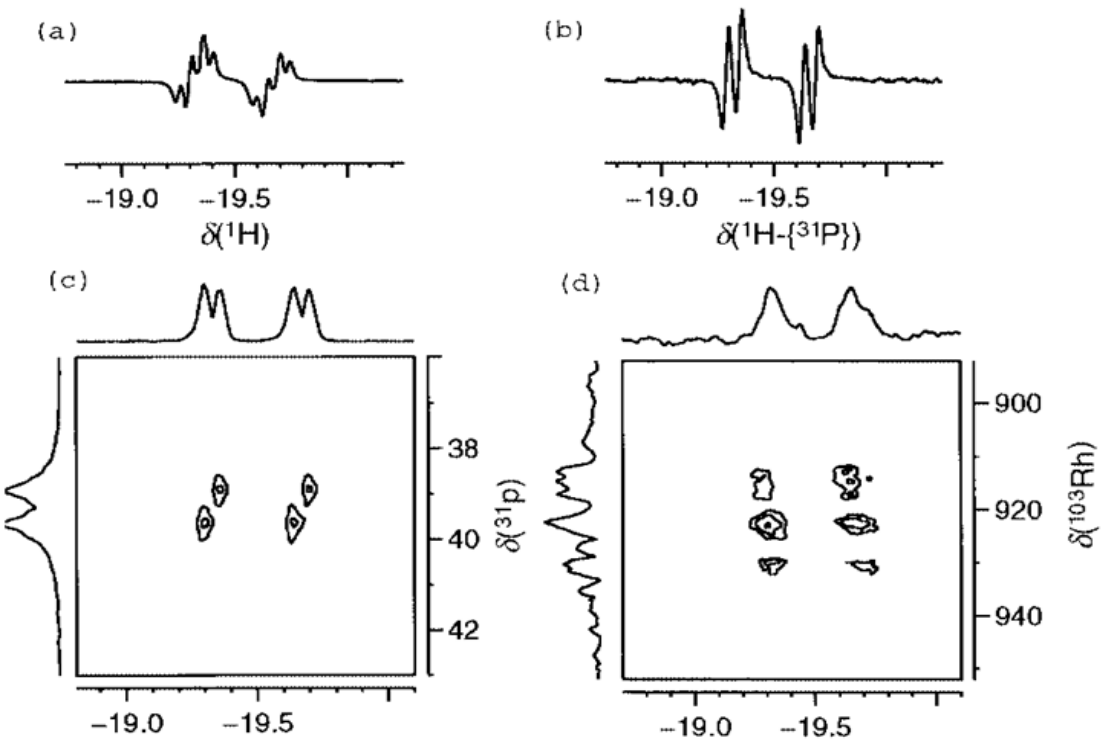

Figure 1.22: ***NMR spectra obtained by warming $RhCl(CO)(PPh_3)_2$ in benzene-d_6 at 348 K: (a) ^{1}H spectrum indicating the two hydride resonances; (b) ^{1}H-{^{31}P} spectrum; (c) ^{1}H-^{31}P HMQC spectrum (^{31}P decoupled); (d) ^{1}H-^{103}Rh HMQC spectrum.(Reproduced with permission from reference 28).***

Another PHIP study by Colebrook and co workers on the reaction of Rh(1) complex, [RhX(CO)(PR_3)$_2$], (Figure 1.23a) (where X= Cl, Br, I and R= Me, Ph) in the presence of *p*-H_2 led to the formation of halide-bridged binuclear hydride complexes.[43, 44] There was a variation in the formation of isomers within the solution as the iodide leads to the formation of multiple isomers. On the other hand, all the other halides resulted in the formation of a monohydride species. In a similar study by Koch *et al*.[45] demonstrated that the reaction of [RhCl(NBD)$_2$]$_2$ (Figure 1.23b) with phosphines in the presence of *p*-H_2 led to the formation of mononuclear complexes.

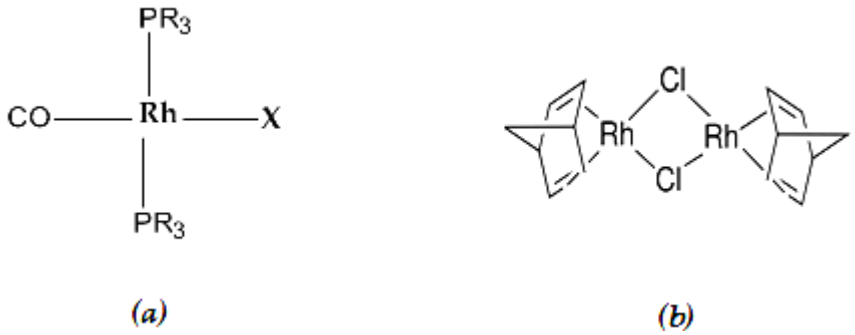

(a) *(b)*

Figures 1.23: ***Structures of complexes: (a) [RhX(CO)(PR_3)$_2$]; (b) [RhCl(NBD)$_2$]$_2$.***

The method to quantify the rate of hydrogenation by *p*-H_2 was developed by Eisenberg *et al*.[46] and called ROCHESTER (rates of catalytic hydrogenation estimated spectroscopy through enhanced resonances) in which the rhodium catalyst, [Rh(NBD)(chiraphos)]$^+$ was used to hydrogenate acetamidocinnamate (Figure 1.24).

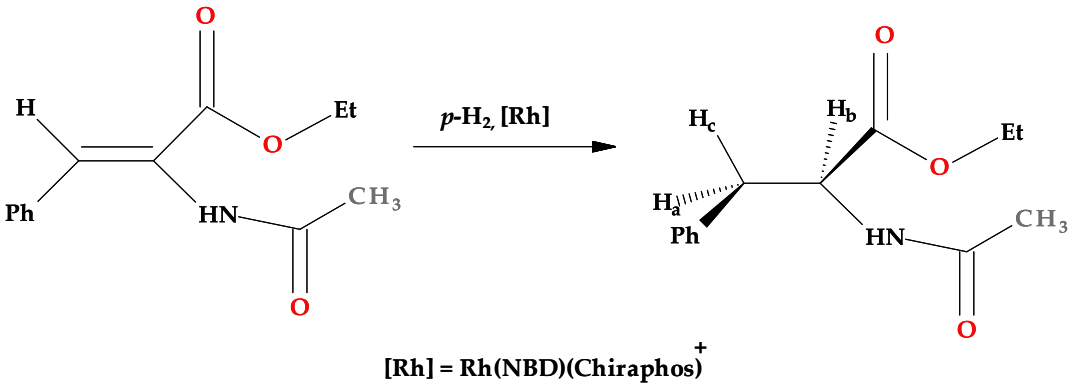

Figure 1.24: System used in the development of the ROCHESTER method.

The polarization intensities of the hydride ligands and the methyl protons revealed that the rate of polarization decay is equal to the rate of hydrogenation. Both rates here found to be proportional to each other even after the catalyst concentration has varied. They suggested an equal rate of polarization decay and rate of hydrogenation is because of the substrate is present in the solution in excess and the H_2 dissolved in solution acts as a limiting reagent.

The *para*hydrogenation studies involving alkene by Aime *et al*. led to the polarization transfer to alkene protons,[47] thought due to be an exchange between alkene protons and the hydrides.[48, 49] Isotopic labelling later confirmed that the polarization transfer from the hydrides to the alkene protons took place through nOe effect. These studies can be used to detect unsaturated molecules bound to the metal complex even if there is no hint of hydride exchange or hydrogenation. The aforementioned studies suggest the PHIP could assist in detecting the intermediates or products of side reactions, which are not involved in the main catalytic cycle.

Bargon *et al.*[50] developed a method known as DYPAS (dynamic PASDENA), found to be very useful in measuring the rate of decay of a process involving *p*-H_2. As illustrated in Figure 1.25, the pulse sequence of DYPAS is based on a variable delay between the *p*-H_2 addition followed by a 45° excitation pulse and finally plots a spectrum of intensity versus time. If the mechanistic scheme for the process is known, the intensity decay can be described by a series of differential equations, which can be solved to yield rate constants.

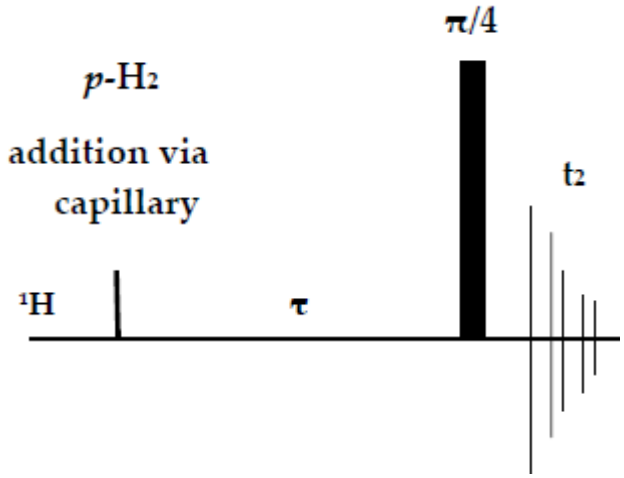

Figure 1.25: Pulse sequence for the DYPAS experiment.

Another method that can be used to directly probe the dynamic process is EXSY,[51] in which the integration values of a signal in the spectrum can be used to calculate the rate constant for that process at a specific temperature. In case of two-site exchange, the calculation is trivial; however, in the case of exchange involving multiple sites, simulations via a linear-least square analysis are required. A study by Schott and co workers[52] on a complex $Ru(CO)_2(H)_2(PPh_3)_3$, a highly fluxional system in which they analyzed the exchange between the hydride ligands and the phenyl ring protons by using EXSY (Figure 1.26).

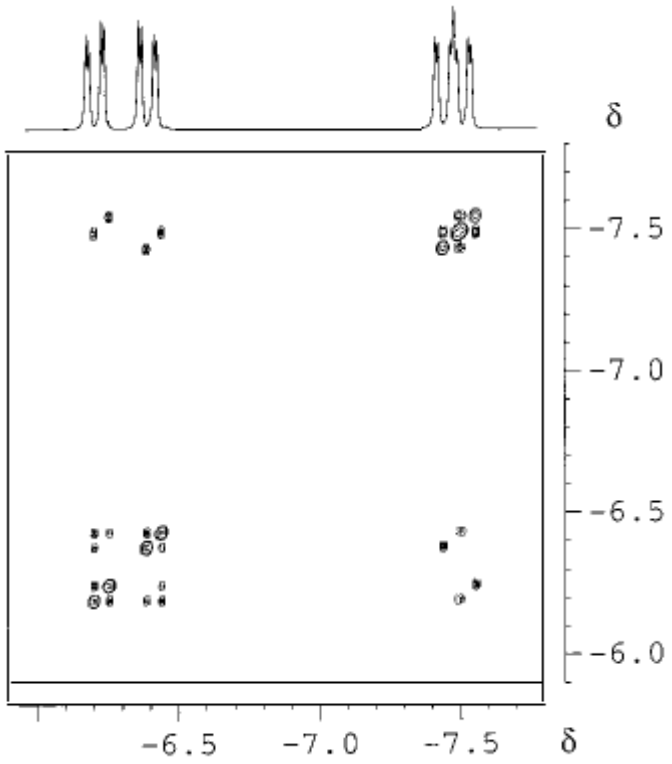

Figure 1.26: ***$^{1}H\{^{31}P\}$-EXSY spectrum of $Ru(CO)_2(H)_2(PPh_3)_3$ in $C_6H_5CD_3$ at 305 K with a mixing time of 0.5 s.(Reproduced with permission from reference 52).***

Ulrich *et al*.[53] have recently reported PHIP hydrogenation experiments in the presence of NMR shift reagents including lanthanide shift reagents (See Figure 1.27) and it was considered to be the first application of PHIP to *f*-block elements. The addition of lanthanide shift reagents resulted in a shift in the position of NMR resonance caused by their paramagnetic nature. The quenching of *p*-H_2 enhancement can be prevented by the addition of a small amount of racemic shift reagent. The benefit of using chiral shift reagents results in the differentiation between the enantiomers leading to diminutive chemical shift.

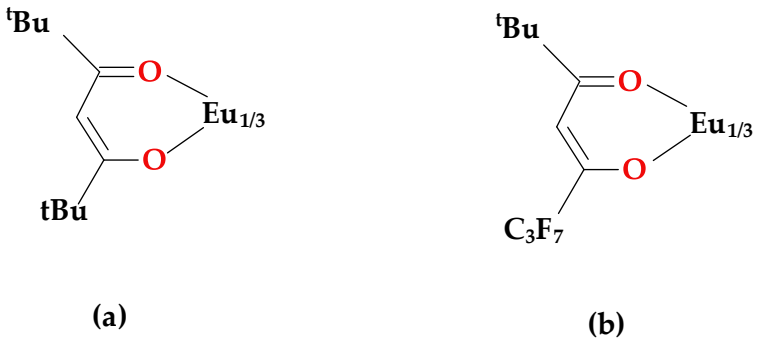

Figure 1.27: *Structures of: (a) Eu(dpm)$_3$; (b) Eu(fod)$_3$*

The first PHIP studies on biologically relevant molecules were conducted by Bargon *et al*.[54, 55] in which they reported the homogenous *para*hydrogenation reaction using dehydroamino acid. Dehydroamino acid is an amino acid that has lost two hydrogen atoms in order to form a double bond. In a similar PHIP study, the complex $[Ir(CO)_2(H)_2(I)_2]^-$ shown to react with histidine in D_2O.[56] PHIP has also been applied to magnetic resonance imaging experiments in *vivo* for polarization transfer to ^{13}C. These studies suggested that the PHIP can be successfully applied to the biomolecules and such a study will help us to understand the biological systems.[57]

Very recent research by Aime *et al*.[58] studied the NMR of ^{15}N-properglycholine with *p*-H_2. Properglycholine is an unsaturated derivative of choline (Figure 1.28). A magnetic field cycling procedure between earth and zero magnetic field was used to transfer the spin order of *p*-H_2 to the ^{15}N resonance of properglycholine.

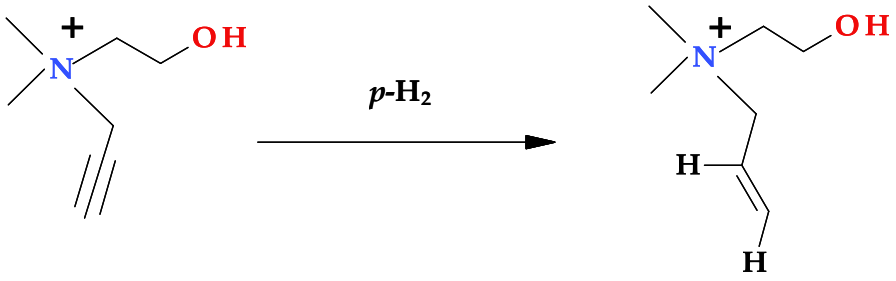

Figure 1.28: The reaction of proparglycholine with p-H₂.

The reaction of proparglycholine with *p*-H₂ (Figure 1.28) resulted in the formation of different isomeric products but only the nontransposed isomer demonstrated the ^{15}N signal enhancement with value of 3000 by exhibiting an emission charterer as demonstrated in Figure 1.29. The isomer which polarized successfully was identified by using a retro INEPT experiment that allowed the transfer of polarization from the ^{15}N to ^{1}H signal.

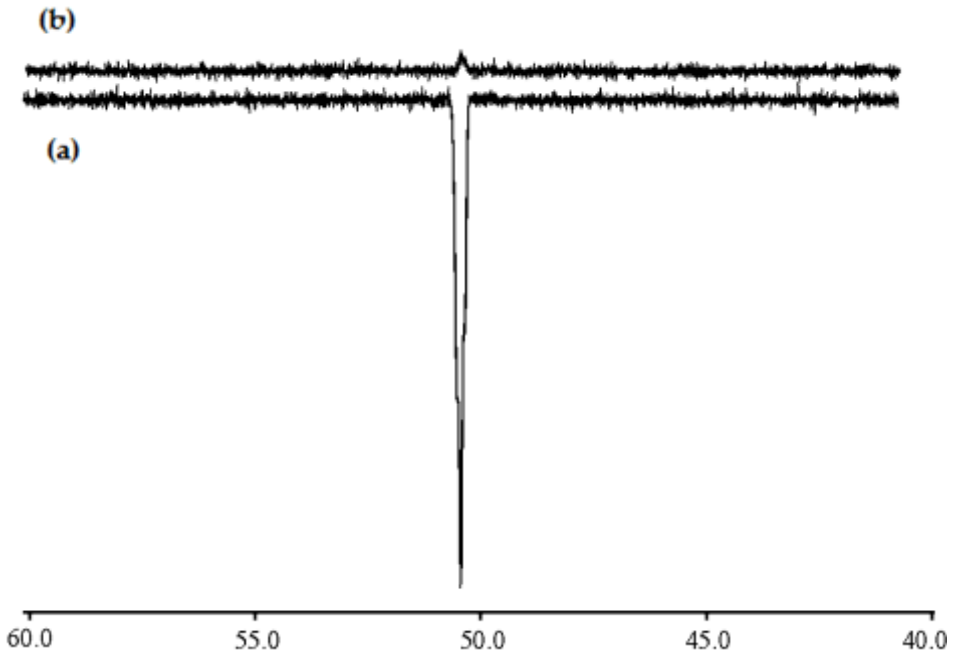

Figure 1.29: ***^{15}N spectrum of parahydrogenated ^{15}N-propargylcholine: (a) single-scan spectrum recorded immediately after parahydrogenation and field cycling and (b) 80-scan spectrum recorded after relaxation (acetone-d_6/CD_3OD 4:1, RT, 9.4 T). The signal enhancement is about 3000 times. As the magnetic field profile is not exactly known inside the cylinder, polarization may be further increased by using an electromagnetic field shield. (Reproduced with permission from reference 58).***

1.8 Signal Amplification by Reversible (SABRE)

It has recently been shown that the enhancement of an NMR signal by *p*-H_2 can be achieved through an interaction with a suitable inorganic template that contains H_2. The role of the template is simply to establish equilibrium between bound substrate and free substrate. Upon dissociation, the substrate

retains the polarization that was originally located on *p*-H_2 and its NMR signal strengths are noticeably amplified. This technique has been termed 'Signal Amplification by Reversible Exchange'. The schematic representation of polarization transfer process in SABRE is shown in Figure 1.30.[5]

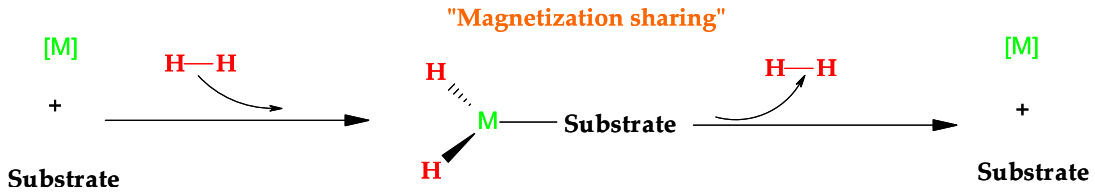

Figure 1.30: ***Schematic representation of the magnetization transfer using SABRE.***

The SABRE experiment completes in three intervals, E_1, E_2 and E_3 as shown in Figure 1.31.[59] The starting point, t_0, for time evolution is defined as the instant that the complex forms. The first interval, E_1, runs from t_0 to t_d, the time at which the substrate dissociates from the complex. The second interval, E_2, runs from t_d until the time, t_f, at which the sample is inserted into the magnet. The third interval, E_3, which may be termed the dynamic field period referred to as field cycling is defined from the time at which the sample is inserted into the magnet until it finally rests in the static measurement field at time, t_m. During this latter period, the sample experiences a rapid increase in the magnitude of the magnetic field until the measurement field is attained. This field increase is dealt with as adiabatic process. Once at the measurement field, the spin states of the substrate are interrogated.[59]

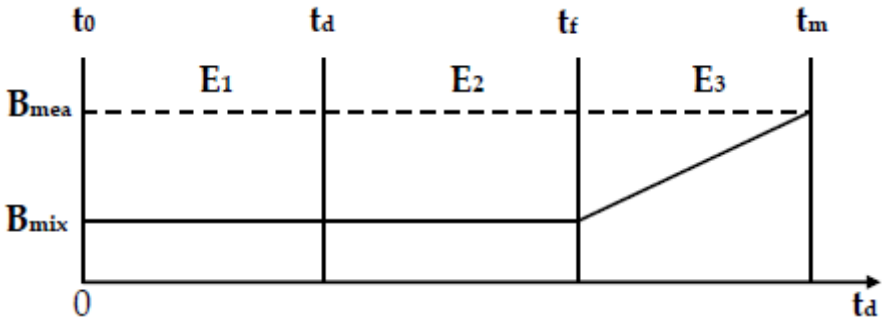

Figure 1.31: ***The variation of magnetic field strength (B_{mea}, B_{mix}) in the SABRE experiment as a function of time, (t_0–t_d interval E_1, t_d–t_f interval E_2 and t_f–t_m interval E_3).***

After the polarization transfer to the substrate is completed, the substrate is separated from the metal complex. The ligand is chemically or physically labile and in a case where the ligand is labile, the dissociation from the metal complex is achieved by contacting the complex with a solution containing a ligand in free form. Equilibrium is usually established between the bound and unbound (free) ligand resulting in disassociation of the hyperpolarized substrate from the metal complex.[5]

1.8.1 Selected applications of NMR-SABRE

Rosales *et al.*[60] carried out a reaction using the complex $[Ir(COD)(PPh_3)_2]^+$, (COD = cyclooctadiene -, 1, 5-diene) dissolved in dichloromethane by bubbling *p*-H_2 through a solution in the presence of excess pyridine. The final the product was isolated in the solid state as $[Ir(COD)(PPh_3)_2]^+$ (Figure 1.32a). The aforementioned reaction was carried out using ^{15}N-labelled pyridine in the presence of *p*-H_2. The reaction led to the formation of $[Ir(H)_2(PPh_3)_2(pyridine)_2]^+$ and $[Ir(H)_2(PPh_3)(pyridine)_3]^+$ products (Figures 1.32a and 1.32b), which were

substantially enhanced in the subsequent NMR spectrum. The hydride ligands arranged around the metal complex were magnetically inequivalent and attributable to a second order spin system. The enhancement of hydride resonance in the complex $[Ir(H)_2(PPh_3)(pyridine)_3]^+$ was much larger in comparison to that of $[Ir(H)_2(PPh_3)_2(pyridine)_2]^+$. This study led to the conclusion that *p*-H_2 exchanges at a faster rate in case of $[Ir(H)_2(PPh_3)(pyridine)_3]^+$ than that of $[Ir(H)_2(PPh_3)_2(pyridine)_2]^+$.

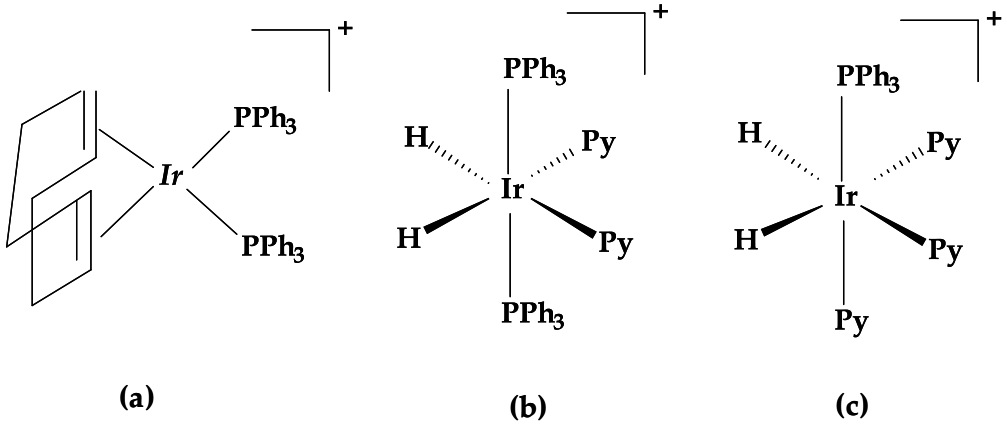

Figure 1.32: Structures of complexes: (a) $[Ir(COD)(PPh_3)_2]^+$; (b) $[Ir(H)_2(PPh_3)_2(pyridine)_2]^+$; (c) $[Ir(H)_2(PPh_3)(pyridine)_3]^+$.

Haake *et al.*[60, 61] devised a series of heteronuclear experiments to transfer the polarization from the hydride resonances to the ^{15}N pyridine using PHIP adapted experiments. The acquired NMR spectra revealed that the most efficient polarization transfer was observed by using the PH-INEPT experiment. The refocused PHIP-INEPT only resulted in weak ^{15}N signal enhancement due to the transverse relaxation of ^{15}N resonance during the refocusing echo. The complex, $[Ir(H)_2(py)(PPh_3)_2Cl]$, was used to transfer *p*-H_2 derived polarization to the ^{15}N pyridine. An EXSY pulse sequence was applied to the aforementioned experiment and a refocused sequence was necessary to generate an observable

in-phase ^{15}N resonance and hence the PH-INEPT experiment was used as a founding block for a new PH-INEPT$_+$ experiment (Figure 1.33). In PH-INEPT+ sequence, the first proton $\pi/2$ pulse was replaced by $\pi/4$ pulse with the same phase as the final proton $\pi/2$ pulse compared to a conventional INEPT experiment. The PH-INEPT+ sequence yields antiphase signals of the heteronuclei. If in-phase signals of the heteronuclei are required, the coupling to the heteronuclei can be refocused during one additional delay (τ) which can be incorporated into the pulse sequence. The PH-INEPT+ pulse sequence contains exactly these additional steps to refocus the antiphase heteronuclear couplings which subsequently enable a decoupling of the proton. The preparative sequence was followed by a 90°$_{-y}$ pulse to store the ^{15}N polarization as +Z-magnetization, a delay for ligand dissociation followed by a further 90° read pulse. There was a significant enhancement of free ^{15}N-pyridine signal by using such an approach.

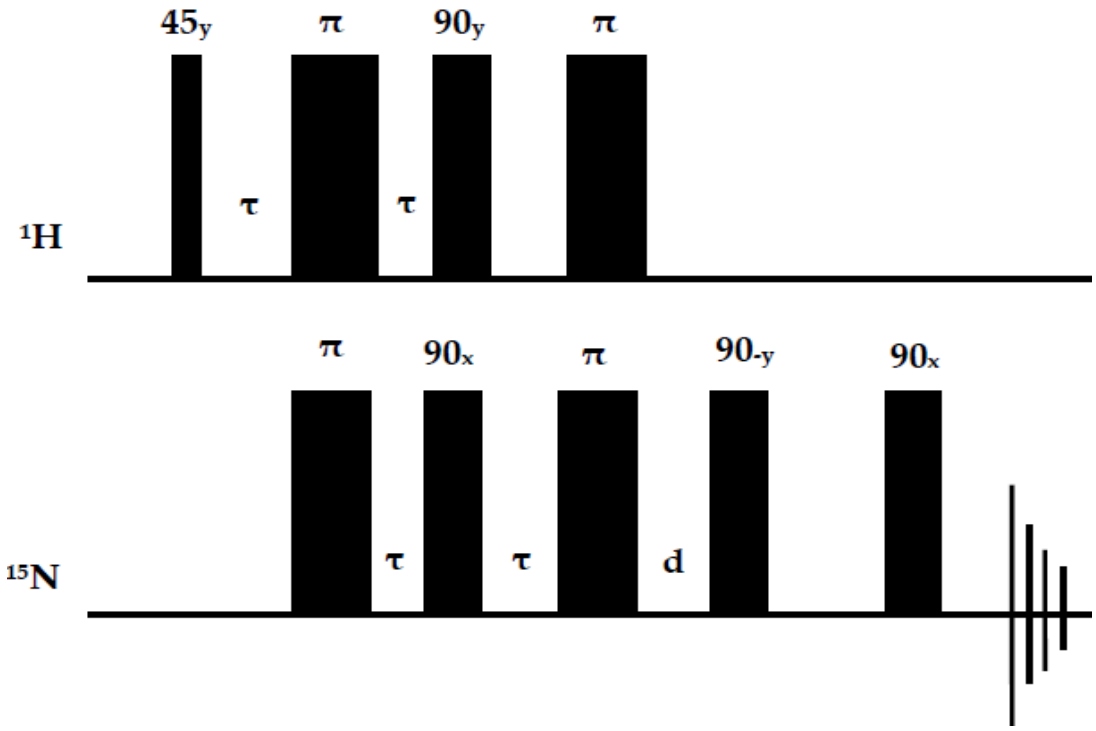

Figure 1.33: PH-INEPT$_+$ pulse sequence

In a separate study,[60, 62] Ir(COD)(PCy$_3$)][BF4] (where Cy is cyclohexyl and COD is cyclooctadiene) were used in place of PPh$_3$ ligands. The complex, [Ir(COD)(pcy$_3$)BF$_4$], undergoes an oxidative addition reaction with hydrogen, during which the COD is hydrogenated, and it yields a new octahedral complex of chemical composition [Ir(H)$_2$(pcy$_3$)(py)$_3$]$^+$BF$_4^-$. This reaction sequence is shown in Figure 1.34. The pyridine ligands *trans* to the hydrides are labile and exchange with free pyridine molecules in solution, acting as substrates in the polarization transfer process. This resulted in a substantial level of signal enhancement because of rapid exchange rates of *p*-H$_2$ and that of pyridine. A ^{1}H NMR was acquired which showed a large emission signal for the free ^{15}N resonances in the spectrum. These observations led to the following deductions: (a) The PHIP experiment under low field conditions results in the spontaneous polarization transfer to the protons of pyridine when the pyridine is temporarily ligated to the iridium hydride complex; (b) an exchange between the free and the ligated (bound) pyridine results in the polarization transfer to the free pyridine resonances without having the proton derived from *p*-H$_2$ chemically incorporated into the molecule. When a similar experiment was repeated by changing the substrate to pyridine, an analogous trend in the level of signal enhancement was observed.

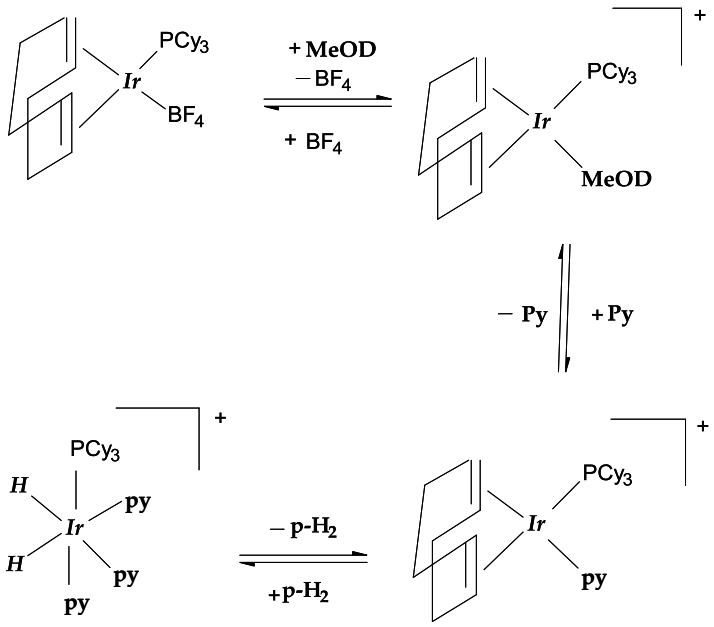

Figure 1.34: ***The steps involved in the reaction of complex, [Ir(COD)(PCy$_3$)BF$_4$], with pyridine in the presence of p-H$_2$ to form [Ir(H)$_2$(PCy$_3$)(py)$_3$]$^+$.***

In the most recent study on SABRE by Duckett *et al.*[63] it has been demonstrated that SABRE can be used to analyze materials at low concentration by using a range of NMR techniques in conjunction with SABRE such as ^{13}C, ^{13}C{^{1}H}, and NOE in addition to complex NMR techniques for instance 2D COSY, ultra fast 2D COSY and 2D HMBC. In this study, quinoline was polarized using a complex, [Ir(COD)(IMes)(Cl], as a polarization transfer catalyst. All these experiments have been carried out using a flow probe, on which the hyperpolarization studies can be completed at a variable magnetic field. From the observations made in this study, it has been established that the SABRE experiment can be effectively applied to any system containing a low concentration of the substrate.

Pines *et al*.[64] demonstrated that it is possible to acquire an NMR spectrum at zero field using PHIP, and detection can be made by using an optical atomic magnetometer. They also showed that SABRE can be employed in the hyperpolarization studies at zero field, which was exhibited by carrying out the hyperpolarization experiments using pyridine (6 mM) in a sample of volume 250 μL. The acquisition of ^{1}H NMR spectrum exhibited the enhanced resonances with sufficient sensitivity to resolve all the peaks in the NMR spectrum. The non-PHIP operates in situ, nonreactive and does not require a prepolarizing magnet and it has been illustrated that non-PHIP can be used in conjunction with an optical atomic magnetometry to carry out hyperpolarization studies at zero- and low-field NMR spectroscopy.

1.9 Dynamic nuclear polarization (DNP)

Dynamic nuclear polarization (DNP) is a technique, which offers the potential for dramatic improvements in NMR sensitivity by transferring polarization from unpaired electron spins, (which are intrinsically more highly polarized than nuclear spins due to their larger magnetic moment) to coupled nuclear spins.

The DNP phenomenon was first observed in 1953 by Carver and Slichter,[65] and then later individually observed by Jeffries,[66] Erb *et al*.[67] and also by Abragam and Proctor.[68] It was not until the mid 1980s that the DNP technique was used for NMR signal enhancement in a range of chemical and biochemical systems, with enhancements of 10 or more regularly observed at room temperature. These applications have been extensively reviewed.[69-71]

1.10 Selected Applications of DNP- NMR

Some of the selected applications of DNP-NMR techniques are as follows.

1.10.1 Applications of Solid State DNP/Solid State NMR

The DNP process involves the transfer of electron polarization to nuclear polarization in the solid state. DNP is one of the best hyperpolarization method used today. It is widely used in solid state NMR and in recent studies,[72] it has been found to be extremely useful in liquid state NMR. DNP requires the presence of unpaired electrons, which are well-distributed (homogeneously) within the sample, for the process to be effective. To distribute the sample homogeneously within an aqueous sample, a glass-former (e.g. glycerol or glycol or DMSO) is added. This prevents crystallisation and results in the production of an amorphous solid when the sample is frozen. In the solid state, microwave irradiation is used to transfer the high electron spin polarization to the nuclear spin states. It has been shown[72, 73] that by using DNP at low temperatures the nuclear polarization of ^{1}H can be increased to 100% and for ^{13}C can be increased to 50%. The DNP method has been shown to be more than capable of improving the sensitivity of ^{1}H, ^{13}C and ^{15}N NMR in the solid state.[74-76]

Griffin and co-workers[77-79] have developed a technique for measuring high resolution solid state NMR spectra at low temperature from frozen solutions. They employed a high magnetic field (5 T, which corresponds to a ^{1}H frequency ca. 211 MHz), with a microwave frequency ca. 140 GHz, with the entire

experiment conducted at or below 90 K. The compound of interest is dissolved in a glass forming solvent mixture, together with the stable free radical. In most studies, they employed the free radical TEMPO (2, 2, 6, 6-tetramethyl-piperidine-1-oxyl) or simple TEMPO derivatives (Figure 1.35). The sample is contained in a low temperature CP/MAS probe. In the DNP experiment, polarization is primarily transferred to proton.

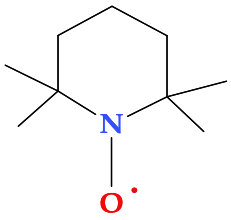

TEMPO

Figure 1.35: ***Molecular structure of TEMPO (2, 2, 6, 6-tetramethyl-piperidine-1-oxyl) free radical used in the DNP studies.***

Reynhardt and co-workers reported[80-82] a series of studies of DNP on natural diamond. In natural diamond *para*magnetic centres occur due to the presence of a nitrogen impurity. The normal carbon lattice is a three dimensional array of covalently bound sp^3 hybridized carbon. If nitrogen is substituted for carbon, the sp^3 hybridized nitrogen forms covalent bonds to three carbons and its remaining two electrons are a lone pair. The fourth neighbouring carbon is not bonded to the nitrogen and has an unpaired electron in a sp^3 hybrid orbital.

Zhou *et al*.[83] investigated a charred polynaphthalene sample at room temperature in a 1.88 T magnetic field, at room temperature. The ^{13}C, ^{1}H and

electron frequencies were 20.2 MHz, 80.8 MHz and 53.0 MHz respectively. The solid state ^{13}C spectrum was measured with magic angle spinning (MAS) and gave a single line in the aromatic region with a polarization enhancement *ca*. 100. When the ^{13}C spectrum was measured using ^{13}C-{^{1}H} cross-polarization (CP) and MAS, the polarization enhancement of the aromatic signal was weaker (*ca*. 12). In the CP/MAS spectrum, the polarization at ^{13}C arises indirectly from the unpaired electrons *via* ^{1}H. The unpaired electrons are located on the aromatic rings, and therefore the direct polarization transfer is to the aromatic carbons and not the aliphatic carbons. However, for ^{1}H very efficient spin diffusion results in aromatic proton polarization being transferred to aliphatic protons. In the same report, the intensity of direct ^{13}C polarization with variation of the microwave frequency was studied. The maximum and the minimum polarization observed were antisymmetric about the electron frequency, and separated by almost exactly twice the ^{13}C resonance frequency. This was strong evidence that the principal mechanism for the DNP enhancement was the solid state effect. The time constant for build-up of the polarization was measured as 19 s and the spin-lattice relaxation time after the microwaves were switched off was 38 s.

In a study aimed at the development of polarized targets for low energy neutron reactions Hautle and Iinuma[84] used $LaAlO_3$ crystals, doped with Nd^{3+} to provide the *para*magnetic centres. The magnetic field applied was 2.35 T and the DNP was performed at a temperature below 0.3 K. For the DNP process a tuneable 70 GHz impact diode was used. In order to measure the polarization of the ^{139}La and ^{27}Al nuclei a Q-meter NMR system was used. The results showed an increase in polarization for ^{139}La of +47 % for 21 positive polarization and -56.5% for negative polarization and an increase in polarization for ^{27}Al of

+62% and -71%. It was shown that substantially higher ^{139}La and ^{27}Al polarization could be reached at lower temperatures.

In efforts to improve the efficiency of the polarization transfer Griffin and co-workers[85-91] used biradicals as the polarization source, in which two TEMPO units were linked together. Most recently a mixture of TEMPO and TAM free radicals was used as the polarization source. This gave a ^{1}H polarization enhancement factor ca. 50 times greater than when TEMPO was used alone. The effect was assigned to the difference in the EPR frequencies being close to the ^{1}H nuclear resonance frequency. In exploring DNP at even higher magnetic fields Bajaj *et al*.[77] reported DNP at 9 T (250 GHz for the EPR) for both ^{13}C and ^{15}N in biomolecules, using 4-aminoTEMPO as the polarization source.

1.10.2 Applications of Solid State DNP/Liquid State NMR

DNP effects can occur in heterogeneous systems as illustrated in the following examples. Odintsov *et al*.[92] studied molecular diffusion in aqueous (paramagnetic) char suspensions. The DNP enhancement measurements of the water protons in the char suspensions were made in a magnetic field B_0 = 117.5 G, with the ^{1}H resonance frequency of 0.5 MHz and an electron resonance frequency of 328.8 MHz. It was concluded that the main DNP processes in char suspensions occurred in pores, and the short-range nuclear electronic interactions in pores had a dominant effect on DNP enhancement. Differences in porosity played an important role in determining the efficiency of the DNP.

Wind *et al*.[93] measured ^{1}H DNP on supercritical ethylene in the pressure range 60-300 bar, with suspended powdered 1, 3-bisdiphenylene-2-phenylallyl (BDPA) free radicals. The measurements were made in a magnetic field of 1.4 T,

with the electron resonance frequency ca. 40 GHz. At all pressures the DNP was a positive effect with enhancement factors between 12 and 17. They pointed out that in liquids molecular motions render the electron-nuclear interactions time-dependent, and the polarization transfer is then governed by the Overhauser effect. The ^{1}H DNP enhancement as a function of microwave frequency was dominated by a single feature at the electron frequency, indicative of the Overhauser effect. Weaker antisymmetric wings were indicative of a degree of solid state effect or thermal mixing, and this was interpreted as part of the ethylene being adsorbed at the surface for a long time compared with the inverse of the electron-nuclear dipolar coupling strength.

The results for solid-state ^{13}C polarization for [^{13}C]-urea with a trityl radical in frozen solution (1.2 K) in a 3.35 T magnetic field (ω_e *ca.* 94 GHz) showed[94,95] that the build-up time constant was 4900 s (see Figure 1.36). Once the microwaves were turned off the spin-lattice relaxation time, T_1 was found to be 28,200 s. It was shown that for 15 mM radical concentration, the maximum ^{13}C polarization obtained in the solid state was 42%. The microwave frequency used was 93.952 GHz, the microwave power was of 100 mW (source output level) and the temperature was 1.1 K.

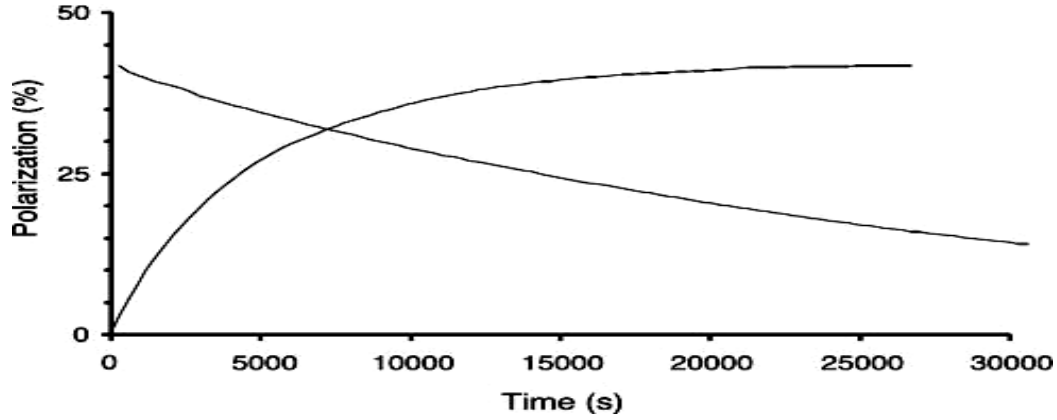

Figure 1.36: ***[^{13}C] urea ^{13}C polarization build up in the solid with 15 mM radical concentration. (Reproduced with permission from reference 94).***

The increasing curve shows the incrase in polarization with microwaves on (93.952 GHz, 100 mW output) (Figure 1.37). The decreasing curve shows the loss of polarization once the microwaves are turned off. When the radical concentration was increased to 20 mM then the maximum polarization went down to 26%. The build-up time constant and T_1 shortened to 2,755 and 15,800 s respectively.

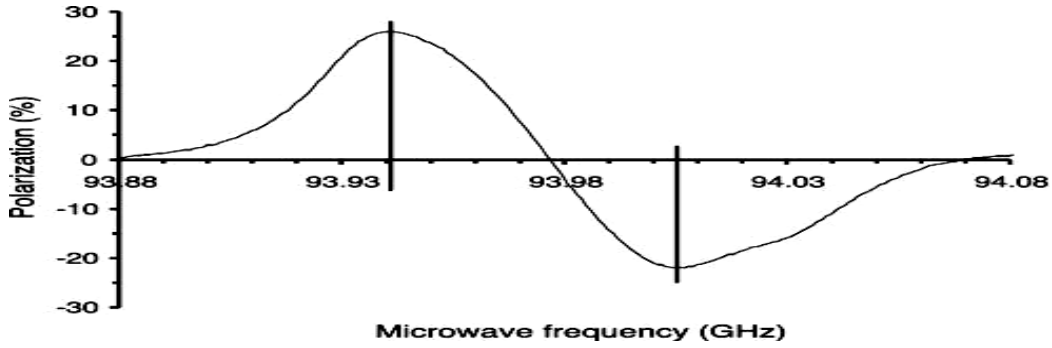

Figure 1.37: ***^{13}C polarization against microwave frequency when the radical concentration is 20 mM. The output power is 100 mW and the temperature is 1.1 K. (Reproduced with permission from reference 95).***

Figure 1.25 shows the dependence of ^{13}C polarization on the microwave frequency. The DNP spectrum showed a positive enhancement peak of 26% at 93.942 GHz and a negative enhancement peak of 22% at 94.005 GHz. The separation between the two peaks was found to be 63 MHz. Both mechanisms of DNP, the solid state effect and thermal mixing are expected to produce a similar polarization profile with a maximum and a minimum symmetrically spaced about the electron Larmor frequency. For the solid state effect the frequency separation between the maximum and the minimum should be about 72 MHz (twice the ^{13}C resonance frequency, 39.9 MHz), whereas for the thermal mixing mechanism the separation is ca. at the nuclear resonance frequency.

For the liquid state DNP to work, after dissolving the solid sample it was transferred to the 9.4 T magnet within 6 s to measure the NMR signal intensity. The results showed that the ^{13}C polarization of the sample was 20%. The signal to noise ratio of the hyperpolarized spectrum and thermally polarized sample were 4592 and 7 respectively (Figure 1.38).

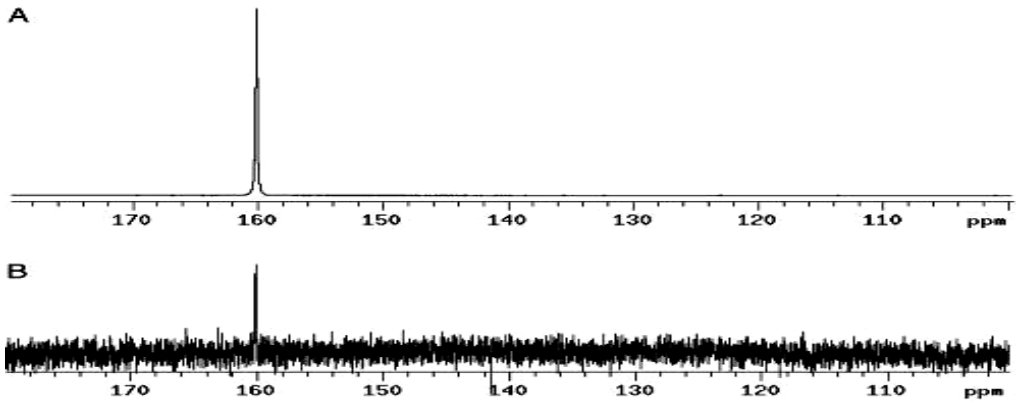

Figure 1.38: ***(A) ^{13}C spectrum of the hyperpolarized sample. The concentration of urea was 59.6 mM and the polarization was 20%. (B) ^{13}C spectrum of the same sample at thermal equilibrium. (Reproduced with permission from reference 94).***

Figure 1.26 shows the ^{13}C spectrum of the unlabelled urea sample, which was hyperpolarized using the DNP-NMR method, compared with the spectrum obtained at thermal equilibrium. The latter spectrum was obtained after 65 hrs of averaging at Ernst-angle conditions, which corresponds to a pulse angle of 13.5^{o} and repetition time of 1s.

The spectrum in Figure 1.39 was used to measure the ^{13}C polarization. This was done by polarizing ^{13}C and measuring the ^{15}N spectrum of [^{13}C]-urea and comparing the integrals of the doublet peak, which was *J*-coupled to the ^{13}C enriched carbon. The ^{13}C polarization was the normalized difference between both integrals. The polarization of 37% was obtained for ^{13}C. Similarly, a polarization of 7.8% was found for ^{15}N.

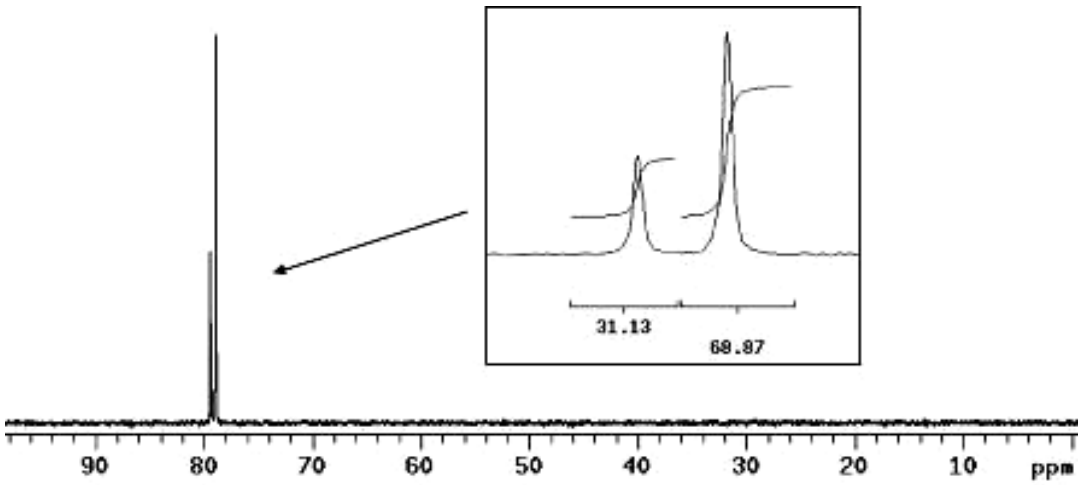

Figure 1.39: ***Natural abundance ^{15}N spectrum of ^{13}C-labelled urea. (Reproduced with permission from reference 95).***

Further development of the Malmő group's experiment has been undertaken by Oxford Instruments Molecular Biotools Ltd. (OIMBL) who has produced a commercial system called *HyperSense*™ by that it is possible to monitor spin-lattice relaxation of the hyperpolarized sample in the NMR magnet, measuring the decay of polarization by use of small flip-angle measuring pulses. In this way,[96] they measured ^{13}C T_1 values for ^{13}C-labelled acetate and at the natural abundance level for ^{13}C in acetaminophen, and ^{15}N in nicotinamide.

In a collaborative effort between the OIMBL applications laboratory and the Weizmann Institute (Israel), Frydman and Blazina[97] have applied ultra-fast (one shot) methods to obtain a hyperpolarized two-dimensional ^{13}C-^{1}H chemical shift correlation (HSQC) for pyridine (0.47 mM, ^{13}C natural abundance), and a ^{15}N-^{1}H HSQC spectrum from 200 nM $^{15}N_2$-urea.

In this chapter, I have described some of the most significant approaches available to achieve hyperpolarization to date. In this thesis, I describe a series of studies based on the exploration of the SABRE effect. I have employed the catalyst, [Ir(COD)(IMe)Cl], for the first time and extended these studies to include complex, [Ir(Cl)$(DMSO)_3$], to explore the potential to hyperpolarize amino acids.

CHAPTER TWO

Hyperpolarization studies of pyridine derivatives using SABRE

2.1 Introduction

The non-hydrogenative *para*hydrogen induced polarization (NH-PHIP) technique, which is also known as signal amplification by reversible exchange (SABRE), has been reported in various publications and demonstrated to be applicable to a wide range of substrates and catalysts.[59] In this chapter, hyperpolarization studies involving pyridine derivatives based on the SABRE technique are described using the complex, [Ir(COD)(IMe)Cl], ***1***, (where, IMe is 1, 3 -dimethylimidazole-2-ylidene and COD is cyclooctadiene) an *N*-heterocyclic carbene complex. The structure of complex, [Ir(COD)(IMe)Cl], ***1***, is shown in Figure 2.1.

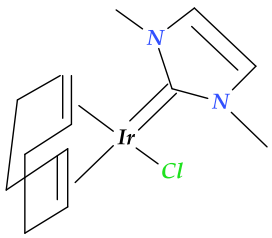

Figure 2.1: ***The structure of complex, [Ir(COD)(IMe)Cl], 1.***

Utilisation of polarization transfer from *p*-H_2 without the need for a chemical reaction was first described by Duckett and co-workers in the *Journal of Inorganic Chemistry* in 2009.[62] In this particular paper, they reported the *para*hydrogenation reactions of the phosphine based catalyst $[Ir(COD)(PR_3)_2]BF_4$ (where R = Ph, *p*-tolyl or *p*-C_6H_4-OMe) with pyridine which resulted in the formation of *fac, cis*-$[Ir(PR_3)_2(py)_2(H)_2]BF_4$ (Figure 2.2a) and *fac, cis*-$[Ir(PR_3)(py)_3(H)_2]BF_4$ (Figure 2.2b). Polarized hydride resonances were observed for these products. It was found that the electronic properties of phosphines such as *p*-methoxyphenyl phosphine, when in their bis formation affect the rate of loss of the pyridine in combination with a radio frequency based magnetization transfer step. An enhancement level of 120-fold was achievable in ^{15}N labelled pyridine when transferred from the *p*-H_2 derived hydride protons.

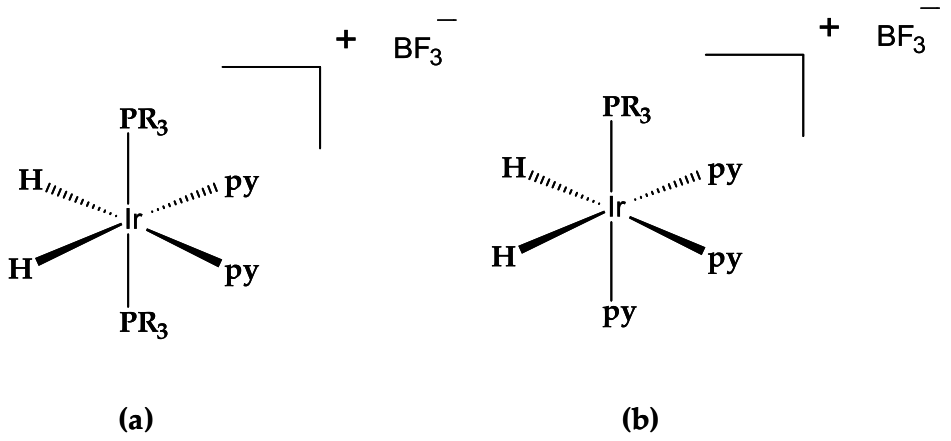

Figure 2.2: ***Structure of complexes: (a) fac, cis-$[Ir(PR_3)_2(py)_2(H)_2]BF_4$, (b) fac, cis -$[Ir(PR_3)(py)_3(H)_2]BF_4$.***

2.2 Phosphines ligands

Phosphines have a lone pair on the P atom that is appreciably basic and nucleophilic, and can serve as an σ donor.[98] Phosphines also have empty orbitals on the P atom that can overlap with filled d orbitals on 3d-metal ions and behave as π acceptors. The empty P–R σ* orbital plays the role of acceptor in metal complexes of PR_3. As the atoms attached to the P atom become more electronegative, the empty P–R σ* orbitals become more stable (lower in energy) making the ligand a better acceptor of electron density from the metal centre (Figure 2.3).

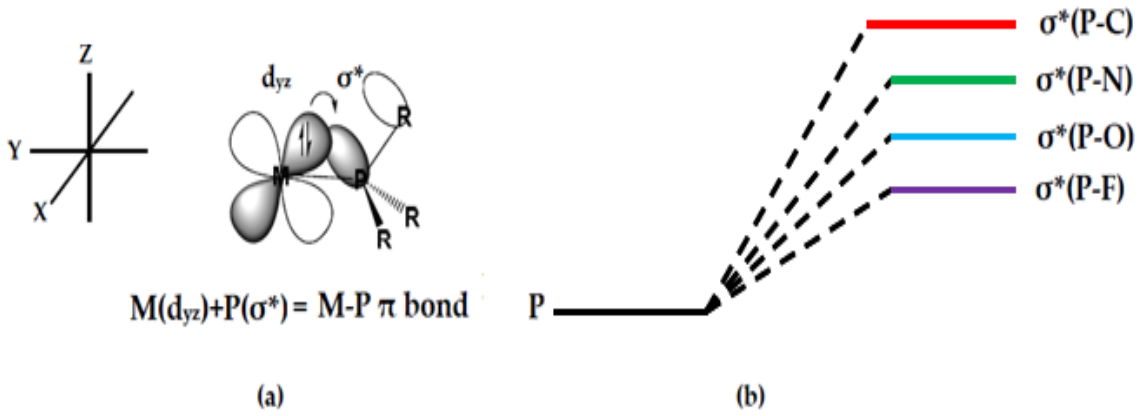

Figure 2.3: ***(a) Formation of a metal phosphorus π bond; (b) as the phosphorus atom becomes more electronegative, the empty P–R σ* orbital becomes more stable.***

The bonding of phosphines[99] to a d-metal atom, made up of a σ bond from the ligand to the metal and a π bond from the metal back to the ligand, is completely analogous to the bonding of CO to a d-metal atom. Quite which orbitals on the P atom behave as π acceptors has been the subject of

considerable debate in the past with some groups claiming a role for unoccupied 3d orbitals on P, and some claiming a role for the P-R σ* orbitals; current consensus favours the σ* orbitals. In any case, each phosphine provides an additional two electrons to the valence electron count. The bonding of phosphines to d-metal atoms is a composite of σ bonding from the ligand to the metal atom, and π back-bonding from the metal atom to the ligand (Figure 2.4).

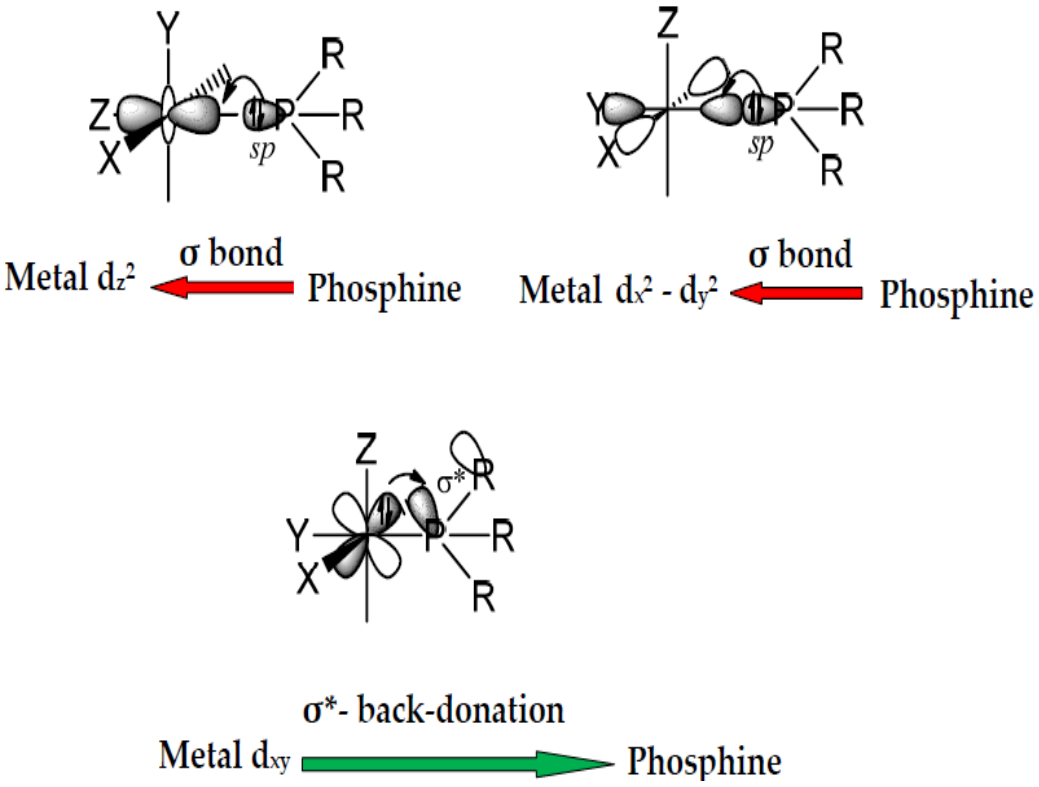

Figure 2.4: ***An σ bonding from the phosphine ligand to the metal atom, and π back-bonding from the metal atom to the phosphine ligand.***

Generally there are two properties of phosphine ligands that are considered important in discussions of the reactivity of their complexes: their steric bulk and their electron donating (and accepting) ability. The steric bulk of phosphines can be expressed in terms of the notional cone occupied by the

bonded ligand (Figure 2.5). An important feature of PR_3 as a ligand is the variable steric size, which can be adjusted by changing R. The σ-donating ability and π-acceptor ability of phosphines are inversely correlated in the sense that electron-rich phosphines, such as PMe_3, are good σ donors and poor π acceptors. Electron-poor phosphines, such as PF_3, are poor σ donors and good π acceptors. Thus Lewis basicity can normally be used as a single scale to indicate their donor/acceptor ability. The generally accepted order of basicity of phosphines is: $PCy_3 > PEt_3 > PMe_3 > PPh_3 > P(OMe)_3 > P(OPh)_3 > PCl_3 > PF_3$ and is easily understood in terms of the electronegativity of the substituents on the P atom.[98]

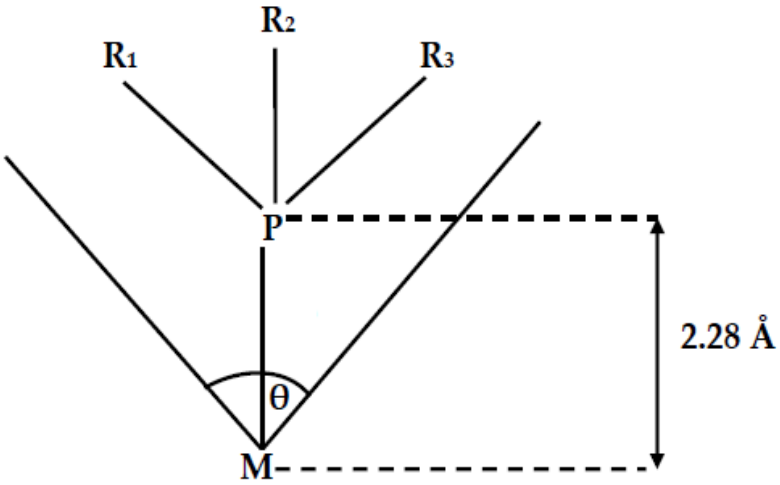

Figure 2.5: ***Tolman's cone angle diagram of PR_3.***

The basicity of a phosphine is not simply related to the strength of the M-P bond in a complex, for instance an electron-poor metal atom forms a stronger bond with an electron-rich (basic) phosphine, whereas an electron-rich metal atom will form a stronger bond with an electron-poor phosphine. If there are carbonyl ligands present in a metal-phosphine complex, then the carbonyl

stretching frequency can be used to assess the basicity of the phosphine ligand: this method allows us to conclude that PF_3 is a π acceptor comparable to CO.

When the phosphines were changed to better donors such as *N*-heterocyclic carbenes, the SABRE effect was seen. In order to explore this process, a variety of phosphines including (PCy_3, $PPhCy_2$, PPh_2Cy, PEt_3, P^iPr_3, P^nBu_3, P^tBu_3 and P(1-naphthyl)$_3$ were tested.[100, 101] Polarization experiments were conducted by using 2 mg of [Ir(COD) (PCy_3)(py)]BF_4 with two equivalents of PR_3 and pyridine. The sample was degassed, exposed to *p*-H_2 and shaken in the earth's magnetic field (50 μT) before the sample was placed into the NMR magnet for ^{1}H NMR spectrum acquisition. The results obtained from these phosphine based iridium catalysts showed a marked difference in the levels of polarization on the pyridine. The highest degree of enhancement was demonstrated by the complex [Ir(COD)(PCy_2Ph)(py)]BF_4 in a reaction with pyridine. The results obtained suggested that the differences in the enhancement levels were due to a variation in the exchange rate of the hydride and the pyridine ligands and hence this might be expected due to an electron donating and steric characteristics of phosphines.[102]

The SABRE phenomenon has been studied by a number of workers within the Duckett group. They have demonstrated that the lifetime of the metal complex and the strength of the magnetic field experienced by the sample during magnetization transfer are important.[103] It is possible to control these effects through: (i) ligand design; (ii) substrate selection and; (iii) experimental hardware. This chapter describes the work on extending this approach by preparing a new SABRE catalyst [Ir(COD)(IMe)Cl], ***1***. The SABRE catalyst, [Ir(COD)(IMe)Cl], ***1***, contains a ligand 1, 3-dimethylimidazole-2-ylidene (IMe),

which is an example of an *N*-heterocyclic carbene (NHC). The structure of a typical *N*-heterocyclic carbene is shown in Figure 2.6.

Figure 2.6: ***Structure of a typical N-heterocyclic carbene ligand.***

2.3 Carbene chemistry

Carbene, CH_2, possesses only six electrons around its carbon atom. Substituted carbenes are less reactive and can behave as ligands towards metals.[98] Principally, carbenes can exist in one of two electronic configurations: with a linear arrangement of the two groups bound to the carbon atom and the two remaining electrons unpaired in two p orbital's, or with the two groups bent, the two remaining electrons paired, and an empty p orbital.[98, 104] Carbenes with a linear arrangement of groups are referred to as 'triplet carbenes' (because the two electrons are unpaired). The structure of a triplet carbene is shown in Figure 2.7.

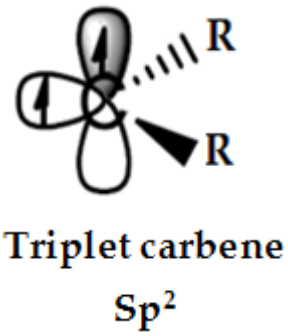

Figure 2.7: ***Structure of a triplet carbene.***

Carbenes possessing the bent arrangement are known as singlet carbenes and these are the normal form for carbenes.[98] The electron pair on the carbon atom of a singlet carbene is suitable to form a bond with the metal atom, resulting in a ligand-to-metal bond. The empty p orbital on the C atom can then accept electron density from the metal atom, thus stabilizing the electron-poor carbon atom. The structure of a singlet carbene is shown in Figure 2.8.

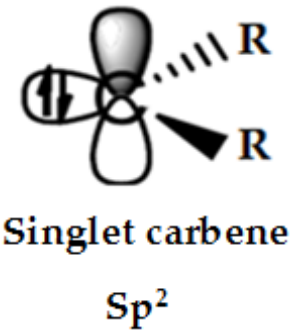

Figure 2.8: ***Structure of a singlet carbene.***

Carbenes bonded to metal atoms by a metal-carbon double bond are known as Fischer carbenes (Figure 2.9a).[98, 105] Fischer carbenes are electron deficient at the C atom and consequently are easily attacked by nucleophiles. When the back-bonding to the C atom is very strong, the carbene can become electron rich and is thus prone to attack by electrophiles. Carbenes of this type are known as Schrock carbenes (Figure 2.9b).

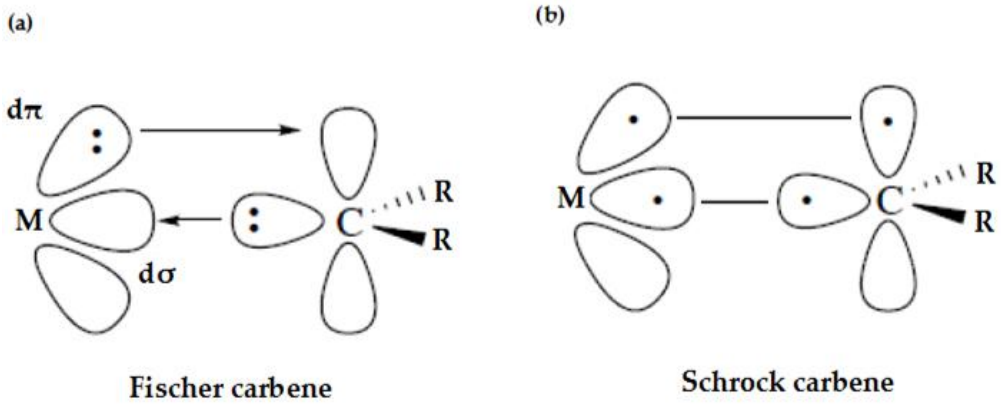

Figure 2.9: ***Structures of: (a) Fischer carbene; (b) Schrock carbene.***

More recently,[98] a large number of derivatives of what are known as *N*-heterocyclic carbenes (NHCs) have been used as ligands. In most NHCs, two nitrogen atoms are adjacent to the carbene carbon atom, and if the lone pair on the nitrogen is considered to be largely p-orbital based, then strong π-donor interactions from the two nitrogen atoms can help to stabilize the carbene. Tying the carbene C atom and the two N atoms into a ring helps to stabilize the carbene, and five-membered rings are common (Figure 2.6). Additional stability can be achieved by placing a double bond in the ring, which provides two additional electrons that may then become part of a six-electron aromatic structure.

2.4 *N*-heterocyclic carbene complexes

N-heterocyclic carbene ligands were first reported by Öfele,[106] Wanzlick and Schonher,[107] but later their isolation by Arduengo and co-workers has revolutionised their contribution to catalysis.[108] NHCs are analogous to phosphines which are widely utilized as ligands for catalysis.[109] The first catalytic applications of NHC complexes were described by Hermann in 1995.[110]

Hermann and co-workers prepared the carbene-palladium complexes from [Pd(OAc)$_2$] and 1, 3-dimethylimidazolium iodide in more than 70% and 40% yields respectively (Figure 2.10) . After their studies on the turnover frequency of these catalysts, they concluded that the factors which give NHCs superiority over phosphines are: (a) NHCs are easier to synthesize on the large scale; (b) the salts of NHCs are stable without decomposition in air; (c) a strong metal-carbene bond provides high thermal and electrolytic durability, which in turn leads to the long shelf life and resistance to oxidation.[110] A search of the literature in 2013 revealed more than 720 papers in the field of *N*-heterocyclic carbene chemistry, which reflects the growing importance of this group of ligands.

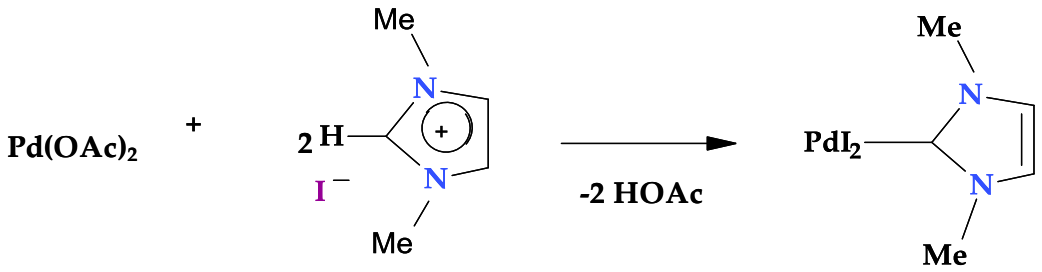

Figure 2.10: ***Formation of diiodobis {1, 3-dimethylimidazoline-2-ylidine} palladium (II) in the reaction of [Pd(OAc)$_2$] with 1, 3-dimethylimidazolium iodide.***

N-heterocyclic carbenes (NHCs) occupy a pivotal position in inorganic coordination chemistry because they not only bind to transition metals but also to the main group elements such as beryllium, sulphur, and iodine.[111] Spectroscopic analysis[112] has demonstrated that a close relationship exists between NHCs and alkyl phosphines. They are both pronounced σ-donors and only poor π-acceptors with very little back bonding character. This has led to

correlations being made between two ligand classes.[113] In the case of *N*-heterocyclic carbenes (NHCs), it has also been observed that they are stronger donors in comparison to even basic phosphines. Until now as far as their steric profile is concerned, the NHCs are fan-shaped in comparison to PR_3 being cone shaped.[114, 115]

The NHCs ligands occupy a pivotal position in transition metal catalysis due to the stability of the complexes formed and their electronic and steric effects.

2.4.1 Stability of *N*-heterocyclic carbene complexes

The stability of an NHC is often described in terms of the singlet – triplet gap which is the energy difference between the singlet ground state and the triplet excited state (see Figure 2.11).[116] When this difference is small, then there is a strong tendency for the NHC to dimerize forming tetraaminoethylenes. The stable NHC*'s* have typically singlet – triplet gaps above 65 kcal mol^{-1}.[116-119]

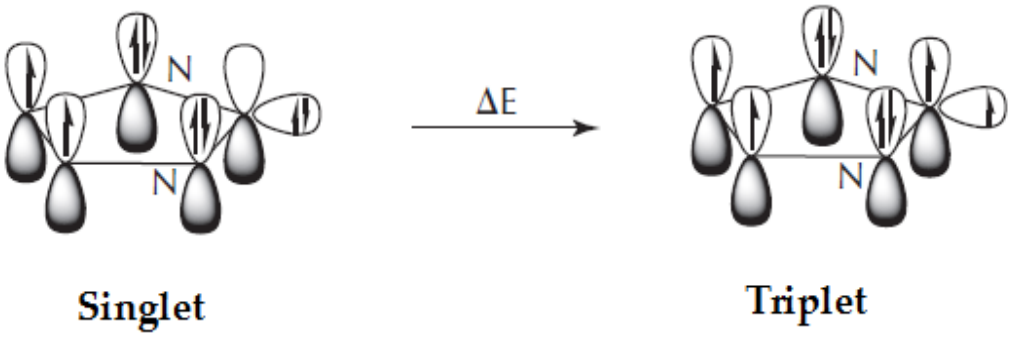

Figure 2.11: ***Energy difference between the singlet ground state and the triplet excited state.***

The first stable NHC that was isolated corresponded to 1,3 - diadamantyl - 1 *H* - imidazol - 2 - ylidene, an unsaturated carbene with bulky substituents on the nitrogen atoms (see Figure 2.12).[116, 120] It was thought that steric and electronic factors contributed to its stability and its reluctance to dimerize. It is easy to imagine that the bulky adamantyl substituents would prevent the two carbene carbon atoms from approaching each other and forming a C=C double bond. It is equally easy to count the 6 π - electrons (two from the C=C double bond and four from the two nitrogen lone pairs) and assume that there is aromaticity due to a delocalized 6 π - electron system.[116, 121]

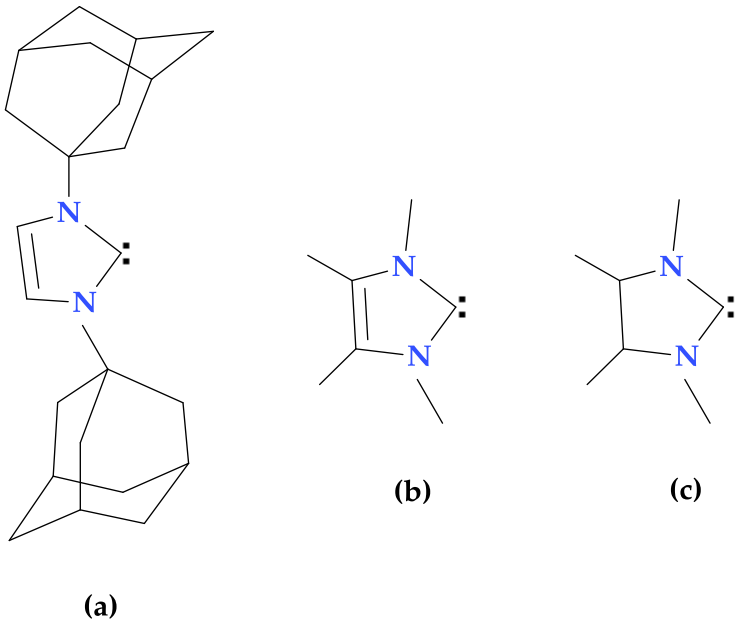

Figure 2.12: ***A series of the first three frameworks of free carbenes: (a, b) sterically unprotected unsaturated NHC; (c) sterically unprotected, saturated NHC.***

From thermodynamic considerations, the main contribution to the stability of the NHC comes from a combination of the large electron -

withdrawing effect of the electronegative nitrogen atom on the σ - electrons of the C - N single bond, paired with π_N - π_C back-donation via the p orbitals (see Figure 2.13).[97] The presence of a C=C double bond in the backbone provides additional thermodynamic stabilization of at least 20 kcal mol^{-1}.[121]

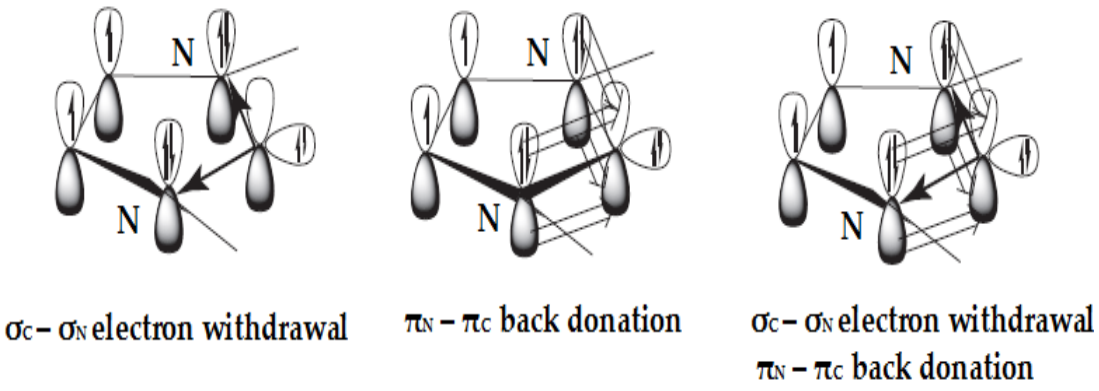

Figure 2.13: Electronic stabilization of NHC

Structural analysis shows that in the unsaturated NHC, the C_4 - C_5 and N_3 - C_4 bonds are shorter but the C_2 - N bonds longer than in the unsaturated NHC, as is expected in a delocalized 6 π - electron system. The N_1 - C_2 - N_3 bond angle at the carbene carbon atom is larger in the saturated than unsaturated NHC. This corresponds to a higher percentage of s character for the C_2 - N bonds of the saturated form compared with the unsaturated NHC.[116] Of course, the differences in the C_4 - C_5 and N_3 - C_4 bond lengths are as expected based on the introduction of a formal C=C double bond, but the relative lengths of the C_2 - N bonds need further explanation. The difference does not lie in a stronger p_π - p_π contribution for the saturated carbene, but in fact the larger s character in the hybrid orbitals of the carbene carbon atom of the saturated NHC results in a larger Coulombic attraction between N and C_2.[116-119]

NHCs have been reported to make stable bonds with a number of transition metals such as Ir, Ru, W, Pd, and Pt.[122, 123] In general; they form weak bonds as demonstrated by the NHCs bond dissociation energies (BDE). BDE is the amount of energy required to homolytically cleaves a chemical bond. The BDE data of selected NHC ligands are given in Table 2.1.

Table 2.1: Data indicating the bond strength of NHC ligands.[122]

Ligand	***BDE [Kcal/mol] (theoretical) For L in $Ni(CO)_3L$***
IAd	20.4
I^{t}Bu	24.0
PPh_3	26.7
IMes	41.1

The equilibrium constant for ligand dissociation observed for the *N*-heterocyclic carbene complex is less than that for the related phosphine ligands. This implies that there is a smaller amount of the free NHCs present in solution, which will act to increase the lifetime of the complex along with its robustness to moisture, heat and air. In spite of the fact that NHCs can be isolated and stored they are still very sensitive and are very reactive towards many electrophilic compounds.[123] A number of publications have been reported that describe the inertness of metal-carbene bonds,[124-126] but examples of their reactivity include the migratory insertion of an NHC into a ruthenium-carbon

double bond[125] and the reductive elimination of alkylimmidazolium salts from NHC alkyl complexes.[124]

2.4.2 Electronic properties of *N*-heterocyclic carbene complexes

N-heterocyclic carbenes are therefore considered to be electron rich, neutral σ-donor ligands. Studies encompassing the theoretical and experimental aspects suggest in case of the *N*-heterocyclic carbene complexes overall interaction energies are the result of π-back bonding.[122] The explicit results are weighed down by the dependency on the metal, and the co-ligands.[122, 127-130] The electron-donating characteristics can be semi-quantified by evaluating the stretching frequencies of the CO ligands of the complexes such as $[LRh(CO)_2Cl]$,[131] $[LIr(CO)_2Cl]$[131] or $[LNi(CO)_3]$[132] with L = NHC or PR_3. The data collected illustrate (Table 2.2) that NHCs are comparatively better σ-donor ligands than the most basic trialkyl phosphines.

Table 2.2: ***IR spectroscopic data for the carbonyl stretching frequencies of [LNi (CO)$_3$] observed in CH_2Cl_2.***[132, 133]

Ligand	νCO ***(A_1)[cm^{-1}]***	νCO ***(E)[cm^{-1}]***
IMes	2050.7	1969
SIMes	2051.5	1968
IPr	2051.5	1970
IMe	2054.1	1970
SIPr	2052.2	1971
ICy	2049.6	1964
PPh_3	2068.9	1990
PCy_3	2056.4	1973
P^tBu_3	2056.1	1971

From the IR spectroscopic data given in Table 2.2, it can be concluded that the electron donating abilities of ligands is inversely proportional to the reported IR values. All the reported NHCs exhibit variable levels of electron-donation properties while the phosphines cover a much broader electronic range on going from alkyl to aryl phosphines. As far as the exchange of substituents is concerned, the substituents are located on the edges of the ligands that are replaced in NHCs, in comparison to the phosphines where the substituents directly attached to the donor atoms participate in bonding to the metal. Furthermore, *N*- heterocyclic carbenes are referred to as higher field as well as higher-trans effect ligands because of their electron-donor characteristics.[134]

2.4.3 Steric effects of *N*-heterocyclic carbene complexes

The steric properties of *N*-heterocyclic carbenes as defined by Tolman's cone angle descriptors proved to be a poor tool to illustrate their steric demand. *N*-heterocyclic carbenes are not cone shaped but instead are described as wedges or fences (Figure 2.14). Indeed *N*-heterocyclic carbenes usually posses a flat centre and spreading wings - often the *N*-substituents are referred to as wingtips.[135, 136] An *N*-heterocyclic carbene has two relevant angles in the coordination sphere of a metal, one connected with the wingspan and one attached with the effective height of the carbene, a parameter largely determined by the wings as the N - substituents protrude beyond the flatness of the imidazole centre. The anisotropic nature of the *N*-heterocyclic carbenes and their property of rotation around the metal carbene bond can be significant in determining their electronic and steric interactions.[137-139]

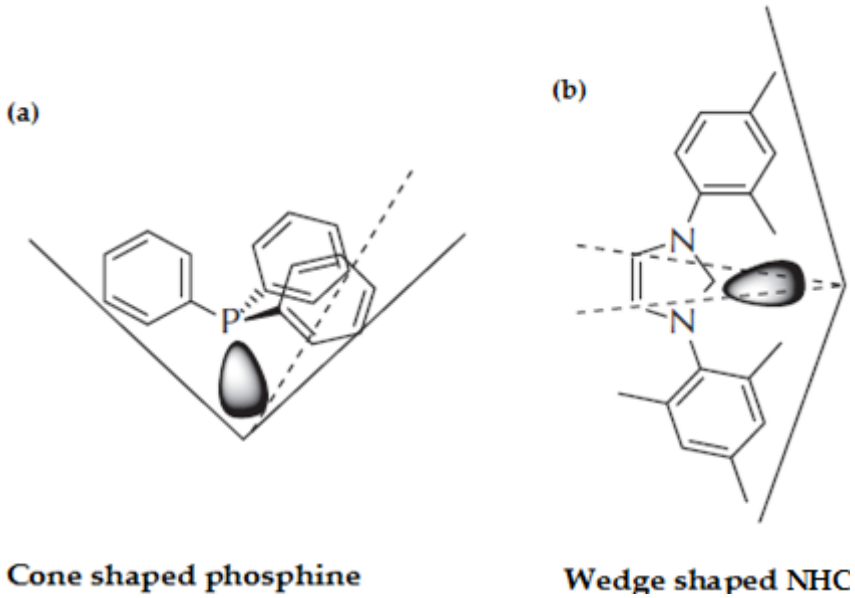

Figure 2.14: *The angular dependence of the steric effect: (a) a cone shaped phosphine; (b) a wedge shaped NHC*

2.5 pKa

pKa is the negative logarithm of Ka which is a measure of the dissociation or ionization of an acid (Equation 2.1). pKa is therefore a measure of the strength of an acid. The larger the value of Ka, the stronger the acid. The lower the value of pka, the stronger the acid. pKa is therefore a characteristic of a compound which undergoes acid-base reactions and is an indication of the substrates ability to give up or accept a hydrogen ion.[142]

$pKa = -\log_{10} Ka$……Equation 2.1

The pKa of a compound is related to pH and indicates how likely, at a given pH, the compound will be ionized. pH is the negative logarithm of the hydrogen ion concentration in a solution (Equation 2.2). There are two possibilities; that a compound is either negatively charged because it gives up a hydrogen ion, or positively charged because it picks up an extra hydrogen ion. This is an important function for the functional groups of many organic and biologically relevant compounds, as the presence of a charge on a functional group affects solubility and can also have an impact on reactivity due to charge based interactions.

$pH = -\log_{10} [H^+]$……...Equation 2.2

The pKa of a compound is dependent on how the substrate molecule can stablize charge.[143] Where a compound has to stablize a negative charge near the hydrogen atom, it will retain that hydrogen ion, and thus it's pKa will be low. Moreover, if a compound can stabilize a positive charge, it will be more likely

to accept a hydrogen ion, and thus acts as a base. A characteristic of a molecule that stabilizes charges, either because of an intrinsic electronegativity (ability to pull electrons close) of atoms in the molecule (known as inductive effect) or due to the ability to spread the charge around the molecule, is delocalization (resonance effects).

2.5.1 Electronic effects

A molecule is neutral as the positive charge of the nulceus of each atom is evenly balanced by the negative charge of outer electrons. The movement of the electrons from one part of the molcule to another will result in the separations of positive and negative charges. The substrate molecule is thus activated for interaction with an electrophile or nucleophile. Such an effect produced by the movement of electrons is called an electronic effect. There are two important electronic effects, (a) the Inductive effect; (b) the Resonance effect.[142]

2.5.1.1 Inductive effect

The displacement of an electron pair in a covelant bond due to an electronegativity difference between joined atoms is associated with polarization of the bond. For example, the inductive effect in an alkyl halide may be depicted as shown in Figure 2.15. The inductive effect is represented by symbol I. An arrow head placed along the bond indicates the direction of the displacement of the electron pair.

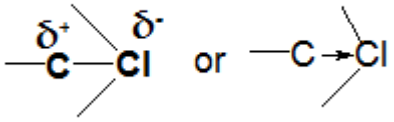

Figure 2.15: An inductive effect in the alkyl halides.

When the group bonded to a carbon atom is less electronegative than carbon, the inductive effect involves the displacement of electron pair towards the carbon atom. This is called +ive inductive effect or +I effect. The group causing +I effect by releasing electrons to the carbon atom is called an electron donating group. Examples are: CH_3-, CH_3CH_2-. When the group bonded to a carbon is more electronegative, then the inductive effect involves the displacement of the electron pair away from the carbon atom. This is called negative effect or –I effect. Groups causing an –I effect by withdrawing electrons from the carbon atom are: -NO_2, -NH_2, -X(Cl, Br, I) and –OH.

2.5.1.2 Resonance effect

An electronic effect caused by the displacement of electrons in a double bond is referred to as a resonance or mesomeric effect. The resonance effect is a permanent effect which involves the delocalization of π electrons from a multiple bond to an atom or from a multiple bond to a single bond or from an atom with lone pair of electrons to a single covalent bond. A mesomeric effect is denoted by M. Like the indictive effect, when –M, when the delocalization of electrons is towards an atom or group, and +M, when the electrons are delocalized away from an atom or group (Figure 2.16).

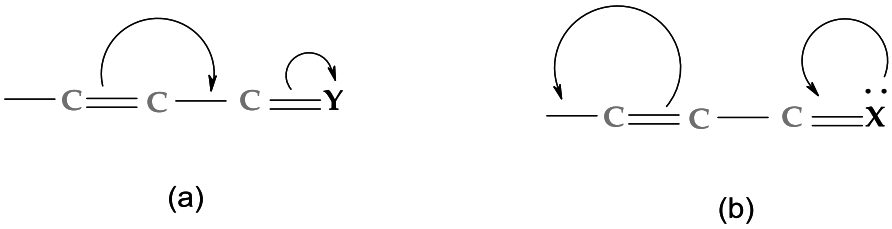

Figure 2.16: Resonance effect: (a) -M effect; (b) +M effect.

2.6 Steric effect of a substituent

Following experimental studies initiated by A. W. Hofmann in 1872,[140] the term "steric hindrance" was adopted to describe an effect, whereby in certain structural circumstances the particular location and the spatial dispositions of atoms or groups appeared to exert an inhibitory influence on the rates of reactions at neighbouring centres. In the first investigations leading to the concept of steric hindrance it was found that the presence of a substituent X in positions *ortho* to a reacting group YZ, and especially two such substituents, e.g., in the compound (Figure 2.17), had a retarding influence on the rates of the reactions of YZ (involving directly the atom Y adjacent to the aromatic nucleus) which was quite unequalled by effects exhibited when the substituent was other than in the *ortho*-positions. Furthermore, it was observed that an influence of this kind was exerted by atoms and groups of diverse character (e.g., by both " positive " and "negative" types), and it was concluded that the chemical nature of the substituents was less important in these circumstances than their location in the *ortho*-positions with respect to the reaction centre.

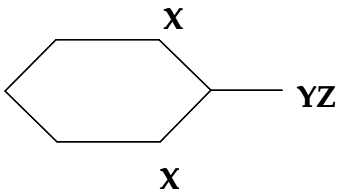

Figure 2.17: Structure of a compound with X_2YZ Substituents

Meyer *et al.*[140] observed that the atoms or groups which prevented esterification in hot alcoholic solutions were larger than those which produced the same effect when cold, and they concluded that the influence of an *ortho* substituent appeared to depend on its size, measured, as he supposed, by the sum of the atomic weights of the atoms present. They considered that vicinal substituents occupy space near the carboxylic group and, depending on the extent of the shielding effect produced, prevent in various degrees the formation of the ester.

Recently,[141] a quantitative analysis of the steric effect of aliphatic groups was carried out. It was proposed that there are two contributors to the steric effect: steric strain and steric shielding (hindrance). When a sterically demanding group is introduced near a reactive center, deformation of its reactive zone will occur. By quantifying this deformation, a convincing correlation was established with Taft's steric parameters for groups of typical size, supporting the intuitive image of steric shielding; bulky groups slow down the reaction by limiting the accessibility of the reactive centre. Steric effects operate almost alone in acid catalysed hydrolysis of substituted esters and led Taft to define the total steric effect, ES, of a substituent according to Equation 2.3:

$E_S = \log (k/k_0)_A$ **……Equation 2.3**

where k and k_0 are the rate constants for the hydrolysis of the substituted and the reference esters, respectively. The average values of log (k/k_0)A for five related reactions (vide infra) were used to reduce small specific effects and experimental errors in evaluating E_S.

On the other hand, the strong initial repulsion between the reactant and the substrate by means of filled–filled orbital interaction results in the deformation of the substrate as well as creating a less stabilizing reaction zone, which is the manifestation of steric strain. Taft also played a pioneering role in understanding how the steric effect operates.[141] His statements that ''it is meaningless and deceptive to say that a molecule is ''sterically hindered'' from a general reactivity point of view'' and ''changes in steric interactions between reactant and transition states are the only factors that affect rates'' clearly highlight his interpretation of the steric effect within the framework of transition state theory.[141]

2.7 Catalyst selection

The first carbene catalyst prepared by Duckett *et al*. and used for SABRE experiments was the complex, [Ir(IMes)(COD)Cl], **2**. It was demonstrated to be a much more effective polarization transfer catalyst than its predecessor phosphine catalysts. The complex, [Ir(IMes)(COD)Cl], **2**, contains the mesityl groups which offers more steric hindrance to the substrate binding. It was consequently decided to investigate if the polarization of the substrate could be improved by altering the carbene ligand. The selection of a carbene ligand was

based on the following factors; which include a degree of control over the flexibility, electronic and steric properties. Therefore, [Ir(IMe)(COD)Cl], ***1*** was prepared. Hermann *et al*.[144] reported the X-ray crystal structure of complex, [Ir(IMe)(COD)Cl], ***1***, and it is displayed in Figure 2.18 while the X-ray crystal structure of complex, [Ir(IMes)(COD)Cl], **2**, is given in Figure 2.19.[145]

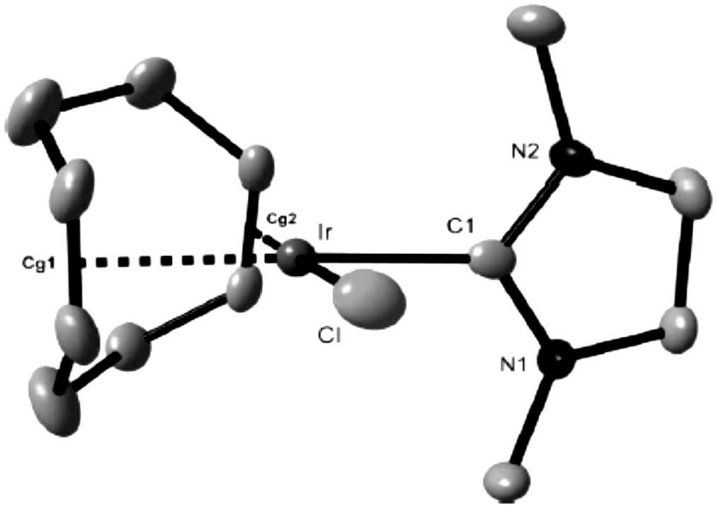

Figure 2.18: ***Diamond plot of [Ir(IMe)(COD)Cl], 1, in the solid state. Thermal ellipsoids are drawn at the 50% probability level. Hydrogen atoms are omitted for clarity.[144]***

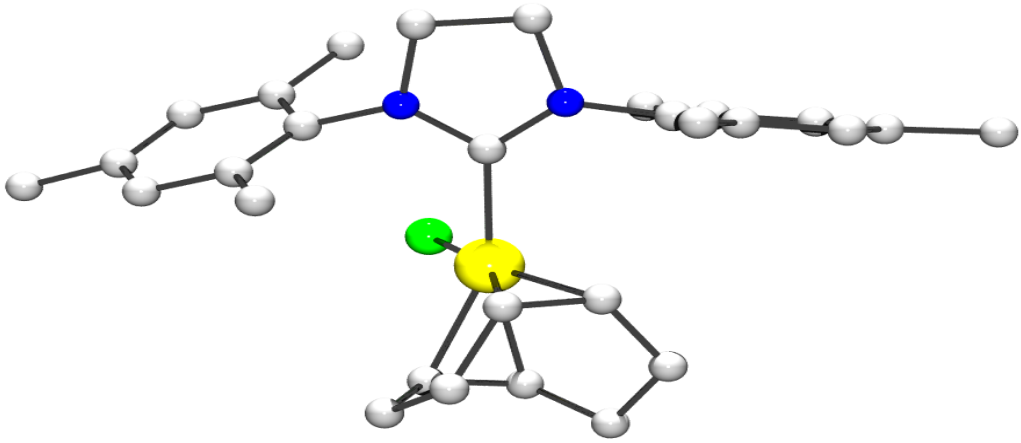

Figure 2.19: Ball and stick representation of complex, [Ir(IMes)(COD)Cl], 2.[144]

The major difference between [Ir(IMe)(COD)Cl], ***1,*** (Figure 2.20a)and [Ir(IMes)(COD)Cl], ***2,*** (2.20b) lies in the greater steric congestion offered by the mesityl groups in case of [Ir(IMes)(COD)Cl], ***2*** as opposed to the methyl groups present in [Ir(IMe)(COD)Cl], ***1,*** as shown in Figure 2.20.

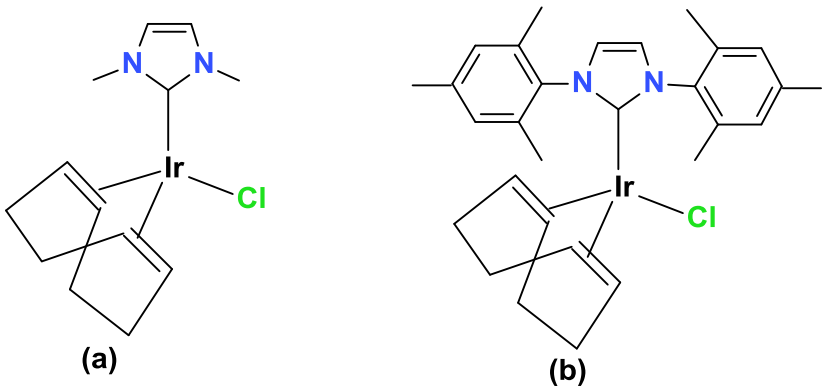

Figure 2.20: Structures of: (a) [Ir(IMe)(COD)Cl], 1; (b) [Ir(IMes)(COD)Cl], 2.

In this particular study, ***1*** has been used as a SABRE catalyst to polarize a range of selected substrates comprising of pyridine derivatives. The characterization of ***1*** and the effect of various factors on the polarization

transfer process were explored and will be discussed in the following sections. The molecular structures of the substrates examined in this chapter are shown in Figure 2.21.

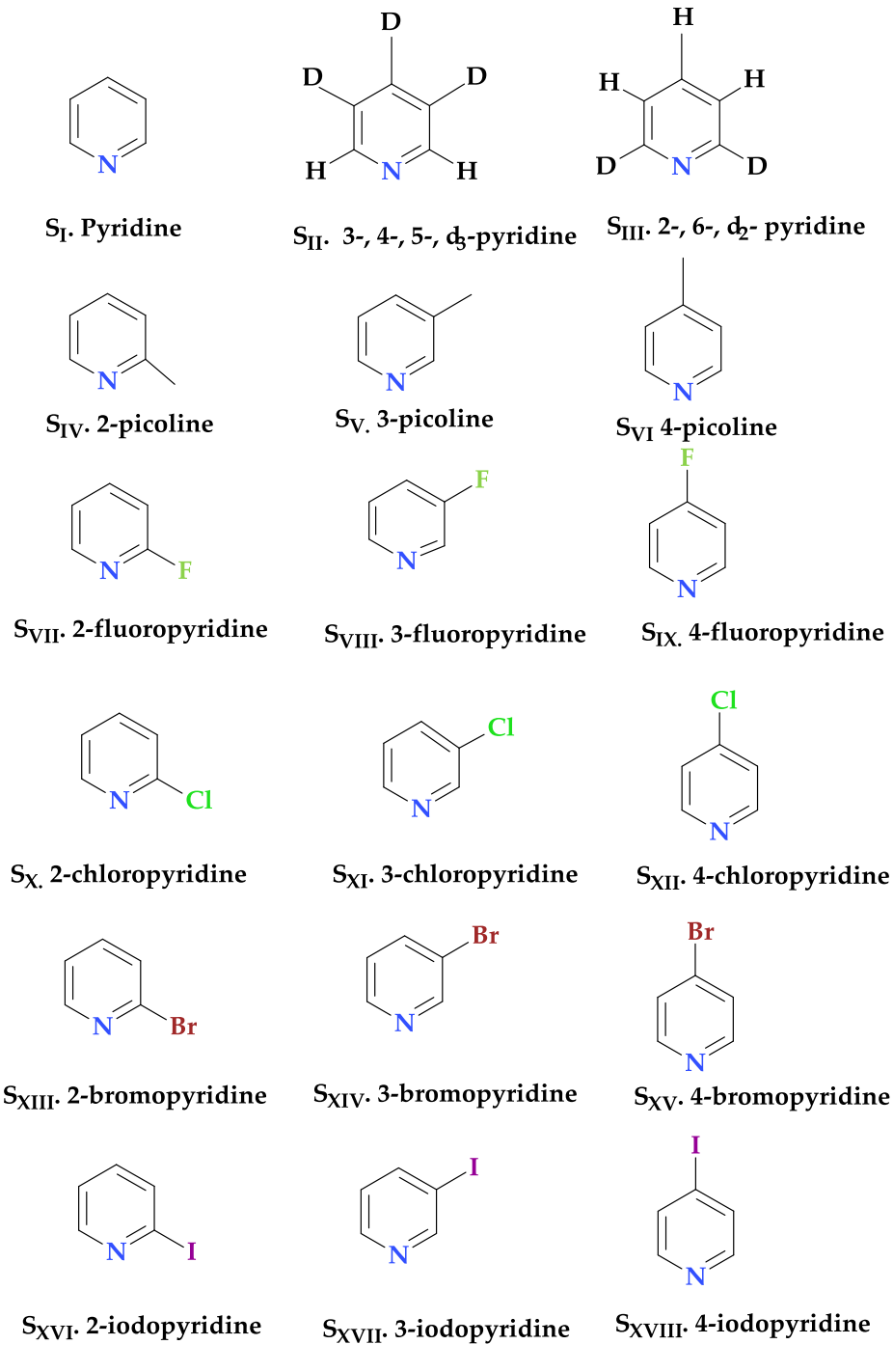

Figure 2.21: Molecular structures of the substrates examined in this chapter.

2.8 Characterization of [Ir(COD)(IMe)Cl], *1*

[Ir(COD)(IMe)Cl], ***1,*** proved to be soluble in both polar and non-polar solvents, it is air stable and reacts with *p*-H_2. The two H_2 atoms enriched in *para* spin state simultaneously bind to the metal in a manner such that spin correlation is maintained between the two protons as explained in section 1.3.2 of chapter 1. It was prepared according to the literature method,[146] and the synthesis is fully described in the experimental section of the thesis. Most significantly, the ^{1}H NMR signal for the methyl groups of the IMe ligand appear at δ 3.89 ppm, and a change in the chemical shift of this resonance can be used to confirm evidence for a reaction. The full NMR characterization data for this species is given in Table A1, Appendix A.

2.9 Reactions of *1* with pyridine in the presence of *p*-H_2

Pyridine (S_I in Figure 2.21) has been used as a substrate in most of the previous studies reported on SABRE.[100-104] and therefore was selected as a reference substance. The pKa of pyridine is 5.17 which suggests that it will bind weakly to a metal centre though the lone pair of electrons associated with the nitrogen. In this case, the reaction discussed in section 2.9.1 suggests that the subsequent intermediate $[Ir(H)_2(COD)(IMe)]^+Cl^-$ should be formed so that the COD ligand can undergo hydrogenation. The ^{1}H and ^{13}C NMR data for pyridine is given in Table A2, Appendix A.

2.9.1 Catalyst activation

1 was tested as a potential SABRE based polarization transfer catalyst for pyridine. In order to achieve this, a sample solution containing pyridine (0.005 mmol) and ***1*** (0.0031 mmol) in 0.6 cm^3 of d_4-methanol was prepared. The sample was then degassed using a mixture of dry ice and acetone and activated with *p*-H_2, and the resultant reaction was monitored by ^1H NMR spectroscopy.

During the activation process, pyridine replaces the iridium bound chloride ligand which becomes a counter ion. The catalyst then undergoes an oxidative addition reaction with hydrogen, during which the COD is hydrogenated, and it yields a new octahedral complex of the general chemical composition $[Ir(carbene)(sub)_3(H)_2]^+Cl^-$. This reaction sequence is shown in Figure 2.22. The addition of H_2 without pyridine being present leads to the slow formation of metallic iridium. It is therefore impossible in this case to characterize the proposed intermediate.

The formation of the metallo-organic complex, an iridium complex, $[Ir(IMe)(py)_3(H_2)]^+$, ***3***, derived from carbene catalyst, ***1***, is shown in Figure 2.22. The pyridine ligands *trans* to the hydrides are labile and exchange with free pyridine molecules in solution, acting as substrates in the polarization transfer process.[2] During the lifetime of the complex, the polarization transfer takes place via isotropic mixing, which allows the transfer of magnetization component of one nucleus to the corresponding component of its scalar coupled partner. After ligand exchange, the former pyridine ligands remain in solution exhibiting strongly enhanced signals in the respective NMR spectra.[100-103]

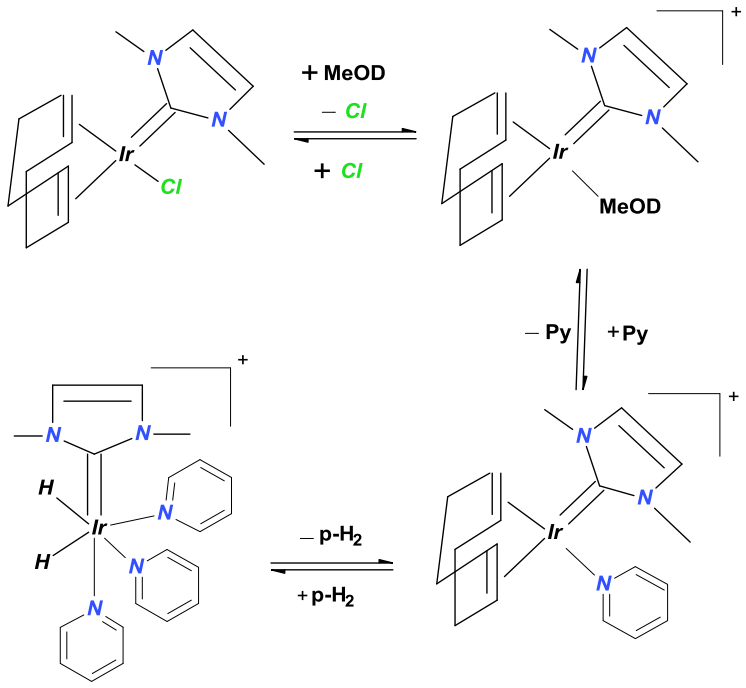

Figure 2.22: The steps involved in the reaction of [Ir(COD)(IMe)Cl], 1, with pyridine in the presence of p-H_2 to form $[Ir(IMe)(py)_3(H_2)]^+$, 3.

The most notable changes in the associated NMR spectra correspond to the detection of a hydride resonance at δ -22.31 and a new NMe signal at δ 3.17 for ***3***. Full NMR data for this complex, ***3***, is given in Table A3, Appendix A.

When the aforementioned reaction was completed with *p*-H_2, hyperpolarization was evident in the resulting ^{1}H NMR spectrum. This observation was made by adding by *p*-H_2 and shaking the NMR tube at a magnetic field of 65 G prior to recording the NMR spectrum. Typical ^{1}H NMR spectrum obtained in this way is shown in Figure A4, Appendix A.

The hyperpolarized ^{1}H NMR spectrum showed strongly enhanced signals for the free pyridine at δ 8.59, δ 7.78 and δ 7.42 respectively (Figure A4, Appendix A). Previous work in the research group using the related complex [Ir(COD)(IMes)Cl], ***2,*** produces comparatively improved signal enhancement for the ^{1}H NMR signals of pyridine at 298 K. This may be reflected in ligand exchange rates which have been proposed to be important in bringing the *p*-H_2 into contact with the substrate.

2.10 Pyridine: Ligand exchange with *1*

A series of ^{1}H EXSY experiments were conducted in order to establish whether ***3*** undergoes hydride and pyridine ligand exchange. The rates of dissociation of the pyridine and H_2 from ***3*** were therefore determined. This approach works by selectively exciting the magnetization within one site of the molecule that is to be probed. A small delay is then allowed to develop before the signal is measured. During this delay chemical reactions become evident through the observation of secondary peaks in the new NMR spectra. If this delay is increased and the process repeated, we can build up curve that is suitable for kinetic analysis. The associated rate constants and activation parameters for hydride and pyridine exchange processes are listed in Tables A5, A7, A8 and A10, Appendix A. An Eyring plot for hydride and pyridine exchange processes are shown in Figures A6 and A9, Appendix A.

The data collected from EXSY measurements, suggested that when a ligated pyridine signal at δ 8.67 ppm was excited, magnetization transfer into the analogous free pyridine resonance at δ 8.59 ppm was seen. The kinetic data

based on variable temperature studies allowed us to determine the activation parameters $\Delta H^{\ddagger}$ = 91.4 ±29 kJ mol^{-1}, $\Delta S^{\ddagger}$ = 40.7 ±12 kJ mol^{-1}, $\Delta G^{\ddagger}$ $^{-1}$ = 75.5 ±0.3 kJ mol^{-1} for the pyridine exchange in ***3*** from the site *trans* to the hydride ligand. The hydride exchange rates were determined to be $\Delta H^{\ddagger}$ = 83.2 ±7 kJ mol^{-1}, $\Delta S^{\ddagger}$ = 41.5 ±10.2 kJ mol^{-1}, $\Delta G^{\ddagger}$ = 78.9±0.2 kJ mol^{-1}. The related rate constant for pyridine exchange is 0.32 s $^{-1}$ at 303 K. The values of $\Delta S^{\ddagger}$ are consistent for a process involving ligand loss.

2.11 Pyridine: effect of *p*-H_2 contact time

The hyperpolarization of pyridine was now achieved by activating the sample in a mixture of dry ice and acetone for ca. 15 minutes and then bringing the *p*-H_2 into contact with pyridine through shaking the sample at a magnetic field of 65 G. The sample is then monitored by ^{1}H NMR spectroscopy. The enhancement and polarization levels achieved with variable contact times are given in Table A11, Appendix A. The effect of shake time on the magnitude of ^{1}H signal enhancement is graphically shown in Figure 2.23.

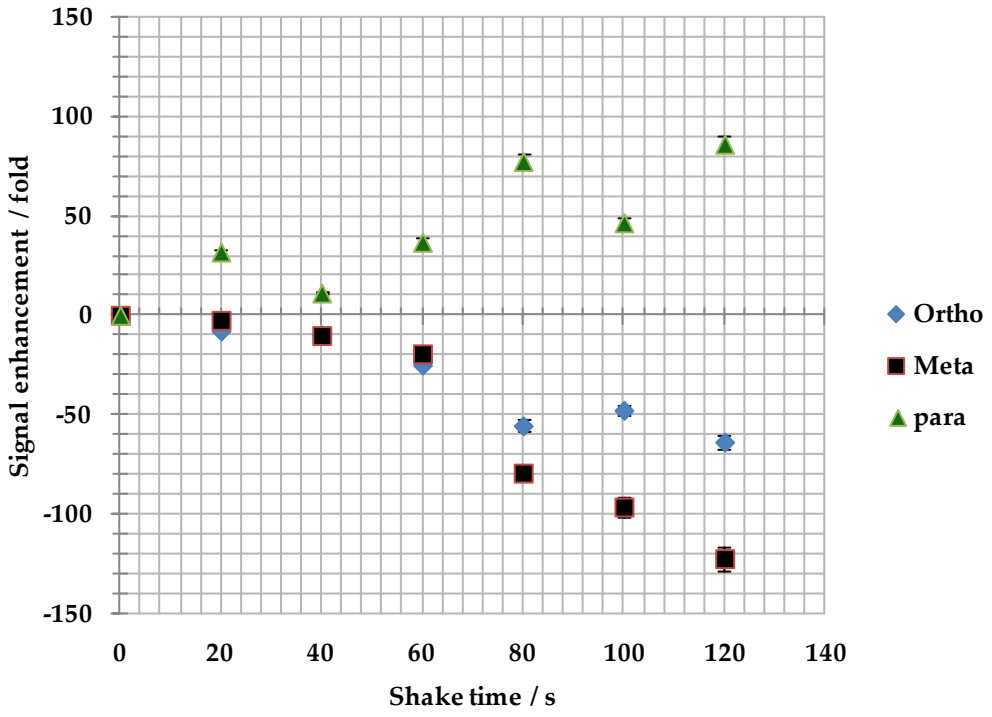

Figure 2.23: ***Graph showing the levels of signal enhancement at the ortho, meta and para positions of pyridine as a function of the shake time.***

Figure 2.23 demonstrates that for a shake time of 20 s, the signals for the *ortho*, *meta* and *para* pyridine resonances were -9.8, -10.2 and 11.2 times larger than the corresponding Boltzmann controlled signals. The enhancement levels for a 60 s shake were determined to be -9.1, -19.4 and 26.8 fold while those for a 120 s shake were -63.9, -122.6 and 86.2 fold respectively. The degree of signal enhancement was therefore found to increase with the length of time spent in contact with *p*-H_2. The *meta* protons of pyridine retain their ability to be hyperpolarized for a longer period of time and thereby achieve far greater levels of signal enhancement.

2.12 Pyridine: effect of temperature

To explore the effect of temperature, a sample containing pyridine and ***1*** in 0.07 and 0.0031 mmol concentrations was placed in an NMR tube that was fitted with a Young's tap to allow the *p*-H_2 introduction. The solution was cooled in a mixture of liquid nitrogen and dry ice (-78°C) for ca. 30 minutes before exposing it to *p*-H_2. When the resulting hyperpolarized ^{1}H NMR spectrum was acquired, there was a substantial increase in the level of ^{1}H signal enhancement levels over those observed at room temperature. The average ^{1}H signal enhancement levels under these conditions were: *ortho* (256.95), *meta* (415) and *para* (175.23) fold for a shake time of 120 s. Since the signal to noise ratio scales with the square of the number of scans, comparable results would require 172,225 scans if a thermally polarized sample was employed. This measurement would take 6 days, rather than the 3 seconds used here. It is suggested that at the aforementioned temperature (-78°C) an efficient exchange between the substrate and the catalyst resulted in is optimal polarization transfer taking place.

2.13 Pyridine: effect of concentration

In order to investigate the lower concentration limit for substrate detection, several experiments were devised. The standard concentrations employed for the hyperpolarization experiments were 0.0031 mmol of ***1*** with pyridine at 0.063 mmol, in 0.6 cm^3 of d_4-methanol. The sample was then activated by keeping it in dry ice and acetone mixture for *ca*. 6 min. The catalyst loading is kept constant while the substrate loading was varied from 0.05 mmol to 1.3×10^{-3} mmol and all the experiments were conducted with a contact time

of 120 s under identical conditions. Enhancement and polarization levels as a function of substrate loading are given in Table A12, Appendix A. The results obtained are graphically depicted in Figure 2.24.

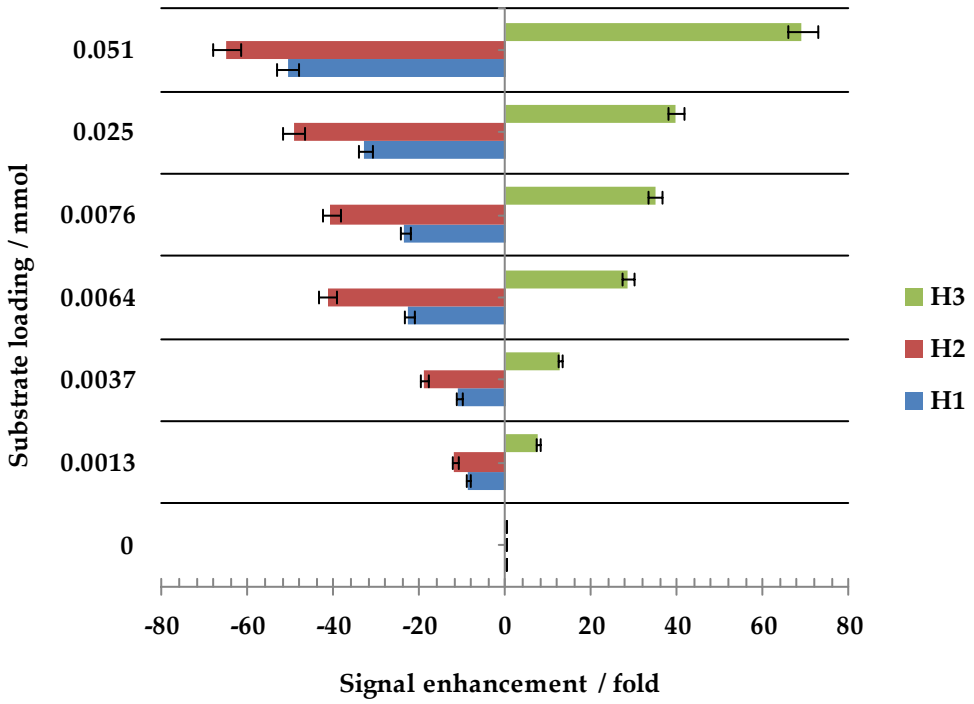

Figure 2.24: Effect of substrate loading on the extent of the ^{1}H NMR spectral signal enhancement for the three proton sites of pyridine when the polarization step is completed in a magnetic field of 65 G.

From the Figure 2.24, it is obvious that higher levels of enhancement can be observed even if the substrate is present in at low concentrations. In concentration studies, the pyridine has been shown to stabilize the active iridium catalyst resulting in efficient polarization transfer.

2.14 Pyridine: effect of solvent

So far, methanol proved to be an excellent solvent for hyperpolarization studies using SABRE. In order to expand our solvent studies and to find a suitable solvent with a wider applicability and solubility, it was decided to carry out the hyperpolarization experiments in a variety of solvents using ***1*** with pyridine as the substrate. The first experiment was carried out by using DMSO as a solvent, but it did not show any polarization transferring activity on exposure to *p*-H_2. When the same sample was reanalysed after an interval of 12 hrs, hyperpolarization was evident but it was not substantial which suggested the sample in DMSO requires a long time to activate. It also appears that no stable active iridium complex is formed. Acetone proved to be the worst solvent because it promoted the rapid degradation of the sample upon exposure to *p*-H_2, and this study was not pursued any further.

Water was also tested because of having an environmentally friendly and it's solubility in biologically relevant molecules. Unfortunately, it did not show any effect on the polarization transfer process. The carbine complex is only partially soluble in water, which limits the formation of an active iridium complex and ultimately demonstrated very little polarization transfer in water. When the same experiment was conducted by changing the solvent from DMSO to chloroform, it took about a day to fully activate, so it proved that chloroform is not a good choice for hyperpolarization studies. When methanol was used as a solvent, it proved to be the most efficient solvent in activating ***1*** and yielding polarization transfer activity. The results obtained from the solvent studies are summarized in Table A13, Appendix A.

There are two likely rationalizations that can be given for the observation of the enhanced resonances in the NMR spectra of the substrate in methanol. One is that the solvent molecules can act as a substrate and bind directly to the active polarization transfer catalyst, thereby aiding in providing stability to an active iridium complex. A structure of an active catalyst formed in case of pyridine is shown in Figure 2.25. The second is that the enhancements are negatively correlated with the viscosity of the solvents (methanol < acetone < D_2O < DMSO). In the extreme narrowing limit, proton spin relaxation rates are faster for the substrate-metal complex in more viscous solvents, causing polarization loss and a concomitant lower level of signal enhancement. By replacing the protons with deuterons, the spin relaxation reduces and methanol-d_4 showed the substantial levels of signal enhancement as demonstrated in section 2.15.

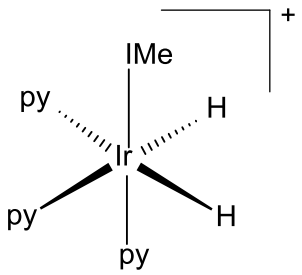

Figure 2.25: ***Structure of the active catalyst 3 formed in case of pyridine.***

2.15 Effect of deutration on the hyperpolarization process

To explore the effect of deutration on the magnetization transfer process more closely, two deutrated pyridines: 2-, 6-, d_2-pyridine and 3-, 4-, 5-, d_3-pyridine (S_{II} and S_{III} in Figure 2.21) were tested using [Ir(COD)(IMe)Cl], ***1***, as the

SABRE catalyst. Deutration or isotopic labelling is a phenomenon in which isotopes are used as tracers, i.e., the starting material is labelled at some particular position and after reaction the labelled atom is then located in the product. In recent years, the use of isotopes has been extremely helpful in the study of reaction mechanisms and rearrangements.

The mechanism of polarization transfer is via the J_{HH} coupling framework.[4] There are two distinct types of magnetic interactions (couplings) between nuclei with a non-zero spin, the direct interaction (dipole-dipole interaction: D) and the indirect or spin-spin splitting or scalar coupling; J). The direct coupling (dipole-dipole interaction: D) is about 1000 times as large as the scalar couplings (at 2 Å distance dipolar coupling is about 30,000 Hz). The dipolar couplings are distance and orientation dependant. In mobile isotropic liquids, the random motion of molecules completely averages the dipolar couplings, so direct effect can be observed.

The scalar coupling J is a through bond coupling interaction,[4-6] in which the spin of the neighbouring proton affects the net field felt by a proton generally through the bonding electrons, and causes the proton to experience different net field. So this interaction between neighbouring protons to cause the spin-spin splitting is known as spin-spin coupling. The spin-spin coupling or J coupling (always reported in Hz) is field independent (i.e., the J is constant at different magnetic field strengths) and is mutual ($J_{AB} = J_{BA}$). As the effect is transmitted through the bonding electrons, the magnitude of J falls off rapidly as the number of intervening bonds increases. Coupling over one (^{1}J), two (^{2}J) and three (^{3}J) bonds usually dominate the fine structure of NMR spectra, but

coupling across four (^{4}J) and five (^{5}J) bonds is often seen, especially through π bonds (double and triple bonds).

The number of bonds in the molecule that lie between the hydride ligand and the group to be polarized might therefore be expected to affect the polarization transfer process. The purpose of using the deutrated pyridine (2-, 6-, d_2-pyridine and 3-, 4-, 5-, d_3-pyridine) in this particular study was to investigate the route of polarization transfer to various functionalities within the molecule.

The 2-, 6-, d_2-pyridine and 3-, 4-, 5-, d_3-pyridine were investigated using the SABRE. ^{1}H and ^{13}C NMR data and enhancement and polarization data for 2-, 6-, d_2-pyridine and 3-, 4-, 5-, d_3-pyridine are given in Tables A14-A19, Appendix A. The hyperpolarized ^{1}H spectra for 2-, 6-, d_2-pyridine and 3-, 4-, 5-, d_3-pyridine are shown in Figures A20 and A21, Appendix A.

The best enhancement levels observed as a function of shake time at each proton site in 2-, 6-, d_2-pyridine were found to be H_1 (-185.8), H_2 (92.3) fold, while the best enhancement levels observed as a function of temperature at each site in 2-, 6-, d_2-pyridine were found to be H_1 (-210.4), H_2 (82.2) fold. In contrast, the best enhancement levels achieved for 3-, 4-, 5-, d_3-pyridine as a functions of shake time and temperature were H_1 (-936.6) and H_1 (-1022.2) fold respectively. The effect of shake time and temperature on the enhancement levels achieved for 2-, 6-, d_2-pyridine and 3-, 4-, 5-, d_3-pyridine are shown graphically in Figures 2.26 and 2.27.

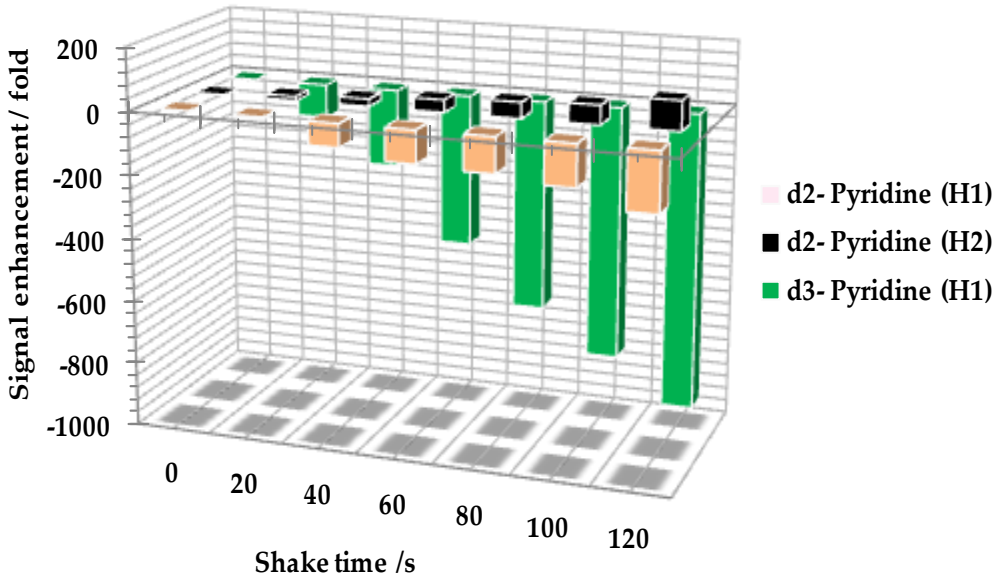

Figure 2.26: Effect of shake time on the magnitude of the ^1H NMR signal enhancement for the indicated proton resonances of 2-, 6-, d_2-pyridine and 3-, 4-, 5-, d_3-pyridine when the polarization step is completed in a magnetic field of 65 G.

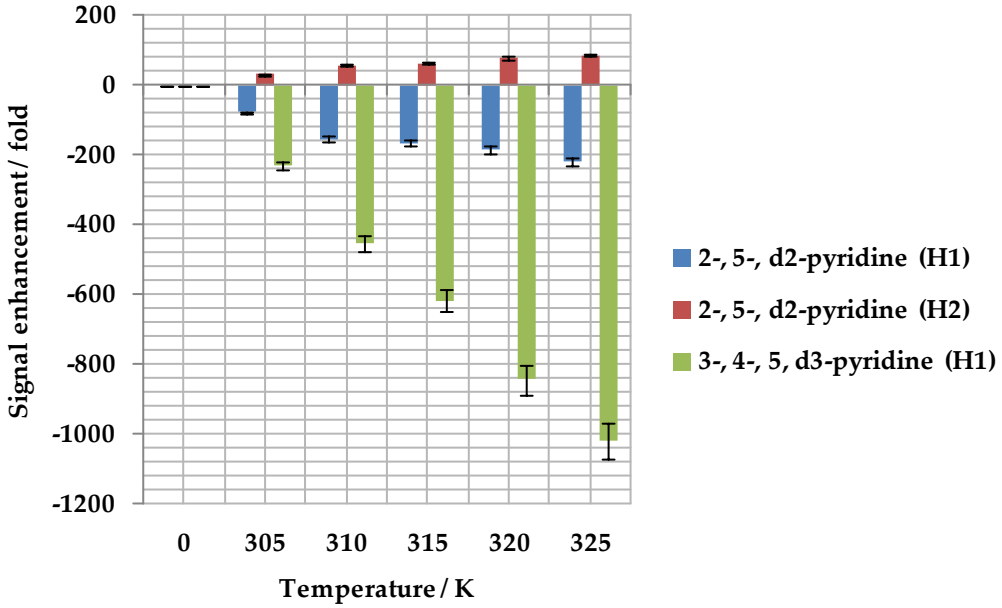

Figure 2.27: ***Effect of temperature on the magnitude of the ^{1}H NMR spectral signal enhancement at the indicated proton resonances of 2-, 6-, d_2-pyridine and 3-, 4-, 5-d_3-pyridine when the magnetization transfer step is conducted in a magnetic field of 65 G.***

The results obtained from the 2-, 6-, d_2-pyridine and 3-, 4-, 5-, d_3-pyridine studies are compared in Figures 2.26 and 2.27. These results confirm that the polarization transfer can be successful via hydride-substrate couplings associated with both *ortho* and *meta* groups. It appears that the *ortho* and *meta* couplings provide the best route to signal enhancement. It is also very interesting to note that shake times of 120 s and a temperature of 325 K proved optimal. Beyond this point, the *p*-H_2 reservoir has been observed to deplete and at longer shake times no further signal enhancement was observed.

The observations made by using deutrated pyridines with ***1*** gives us an insight into how the polarization transfer takes place to a substrate under observation. From an experimental point of view, it was established that an

ortho proton signal gave a stronger enhancement as in the case of 3-, 4-, 5-, d_3-pyridine in comparison to those obtained for 2-, 6-, d_2-pyridine when the results were achieved in the magnetic field of 65 G. However, when 2-, 6-, d_2-pyridine was polarized using **2** as a polarization transfer catalyst, no polarization transfer was observed. It is therefore also inferred that both the *meta* and *para* protons couple to the hydride and can provide an efficient route for polarization transfer process as was observed in case of 2-, 5-, d_2-pyridine. As already observed in case of pyridine, three molecules are bound to the active complex and will most probably have to share the coherence transferred from the *p*-H_2. Due to lower number of spins receiving the *p*-H_2 polarization in case of 3-, 4-, 5-, d_3-pyridine, the signal enhancement rose to 1022 fold, a significant increase when compared to pyridine using SABRE.

2.16 Effect of magnetic field variation on the enhancement levels

In order to observe the effect of magnetic field on the enhancement levels, an automated system was used called a flow probe. This system consists of sample compartment and the mixing chamber, which contains the substrate along with the catalyst and the solvent. A copper coil is wrapped around the mixing chamber to generate a magnetic field in the vertical direction with a range between -150 to 150 G. The compartment and the mixing chamber are joined together with the flow probe that is present in the observation magnet. The sample is injected into a mixing chamber via a syringe and *p*-H_2 is then bubbled through the sample via the six inlets that are located below the sample reservoir for uniform distribution of *p*-H_2 in the sample solution. The *p*-H_2 for

the polarizer is provided by a generator located a few meters away and the nitrogen gas is used to transfer the sample solution from and to the probe head for spectral acquisition by NMR spectroscopy. The schematic of the flow probe built by Bruker is shown in Figure 2.28.

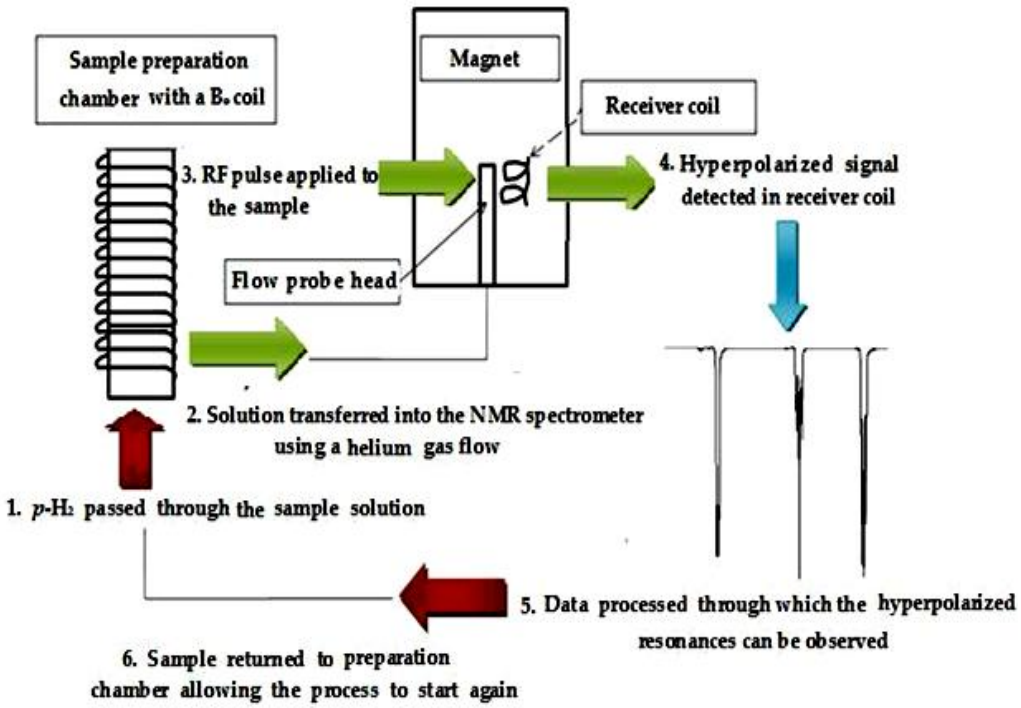

Figure 2.28: Schematic depicting the flow probe and sequence involved in the sample hyperpolarization.

As described in section 2.2, the level of polarization is predicted to vary with the strength of the magnetic field experienced by the sample during the polarization transfer process. 3-, 4-, 5-, d_3-pyridine was examined on the flow probe and the resulting enhancement levels were determined as a function of the magnetic field experienced during the polarization transfer process. The enhancement and polarization levels achieved as a function of magnetic field are given in Table A22, Appendix A.

Previously,[59] the level of signal enchantment demonstrated an intricate dependence on the magnitude of the magnetic field experienced by the sample during the polarization step. The Duckett group conducted a number of experiments in which the effect of varying the mixing field for the polarization of pyridine with ***2*** was explored by using the flow probe. In case of ***1,*** the temperature is the limiting factor which prevented more explicit investigations. However, in case of 3-, 4-, 5-, d_3-pyridine, it showed good level of enhancement and system was tested in the range 0 to-150 G, incremented in steps of 10 G, recording a ^{1}H NMR spectrum and ^{1}H OPSY NMR spectrum at each field. The OPSY method is used to probe the magnetic states being created after polarization transfer to the substrate. OPSY was performed using either a zero, double, triple or quadruple filter to detect the magnetic states produced at variable magnetic field (0-150 G) as illustrated in Figure A23, Appendix A.

Figure A23a, Appendix A illustrates how the relative amounts of I_z magnetization, as determined through ^{1}H NMR spectroscopy with a 90° read pulse, present in the hyperpolarized 3-, 4-, 5-, d_3-pyridine sample varies with the strength of the polarization transfer field for the proton environment. Figure A23b, Appendix A demonstrates the corresponding data for the relative amounts of I_zS_z magnetization that was selected using the double quantum filtered OPSY sequence as a function of the strength of the polarization transfer field. In this case the data is presented as a stacked chemical shift plot where the abscissa corresponds to the strength of the polarization transfer field (65 G).

The observations from these experiments reveal that no triple or quadruple coherences are observed in case of 3-, 4-, 5-, d_3-pyridine, however, we do observe zero, single and double quantum coherences. The zero and

single quantum coherences are observed to decay linearly with increment delay but the enhancement levels observed for the hyperpolarized sample in relation to thermal I_z magnetization in the non-hyperpolarized sample was found to be field dependant and observed to be highest at magnetic field of 65 G. Double quantum coherence levels were found to increase after 50 G but the signal enhancement levels observed in case of double quantum coherences were lower than those observed for zero and single quantum coherences.

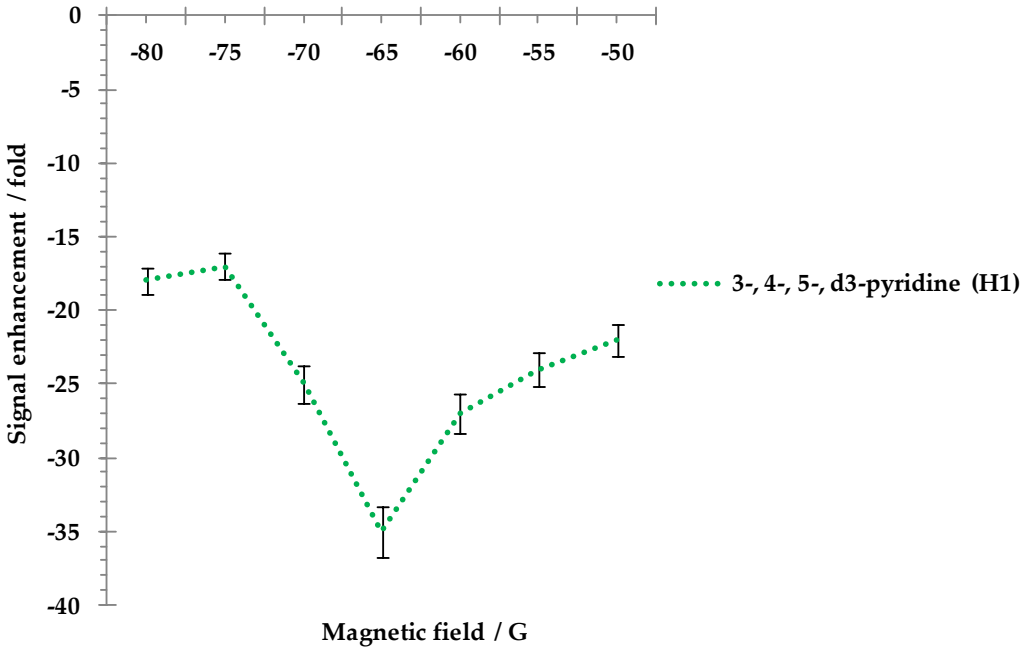

Figure 2.29: ***Enhancement levels achieved for 3-, 4-, 5-, d_3-pyridine as a function of magnetic field.***

So, it is inferred from the results obtained in the hyperpolarization study involving 3-, 4-, 5-, d_3-pyridine using ***1*** that the polarization transfer process is dependent on the magnetic field experienced by the sample during the magnetization transfer process. Ultimately the level of signal enhancement can

be optimised through varying the mixing field. It can also be seen that in the hyperpolarization studies involving ***1*** and 3-, 4-, 5-, d_3-pyridine, the maximum ^{1}H enhancement is observed at a magnetic field of 65 G (Figure 2.29).

2.17 Effect of a substituent's position within a pyridyl ring on the signal enhancement

Pyridine is referred to as a 'model substrate' when compared to related materials such as picolines that contain a single substituent. In order to study the effect of the substituent's position within the pyridyl ring on the enhancement levels, 2- picoline, 3- picoline and 4-picoline (S_{Iv}, S_v and S_{vI} in Figure 2.21) were examined. ^{1}H and ^{13}C NMR data, enhancement and polarization data for 2-picoline, 3-picoline and 2-picoline are given in Tables A24-A32, Appendix A. The hyperpolarized ^{1}H NMR spectra for 2-picoline, 3-picoline and 2-picoline are shown in Figures A33-A35, Appendix A.

A comparison of the signal enhancement levels achieved as a function of shake time and temperature for 2-picoline, 3-picoline and 4-picoline are shown graphically in Figures 2.30 and 2.31.

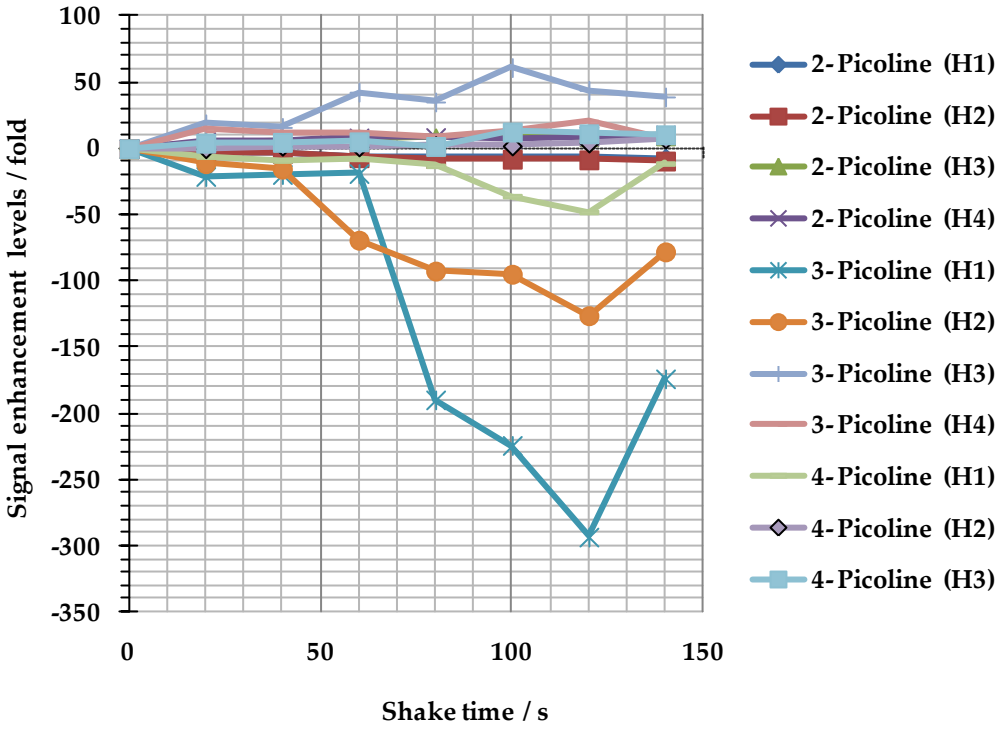

Figure 2.30: Effect of shake time on the extent of the ^{1}H NMR spectral signal enhancement for the indicated proton sites of 2-, 3-, 4-picoline when the polarization step is completed in a magnetic field of 65 G.

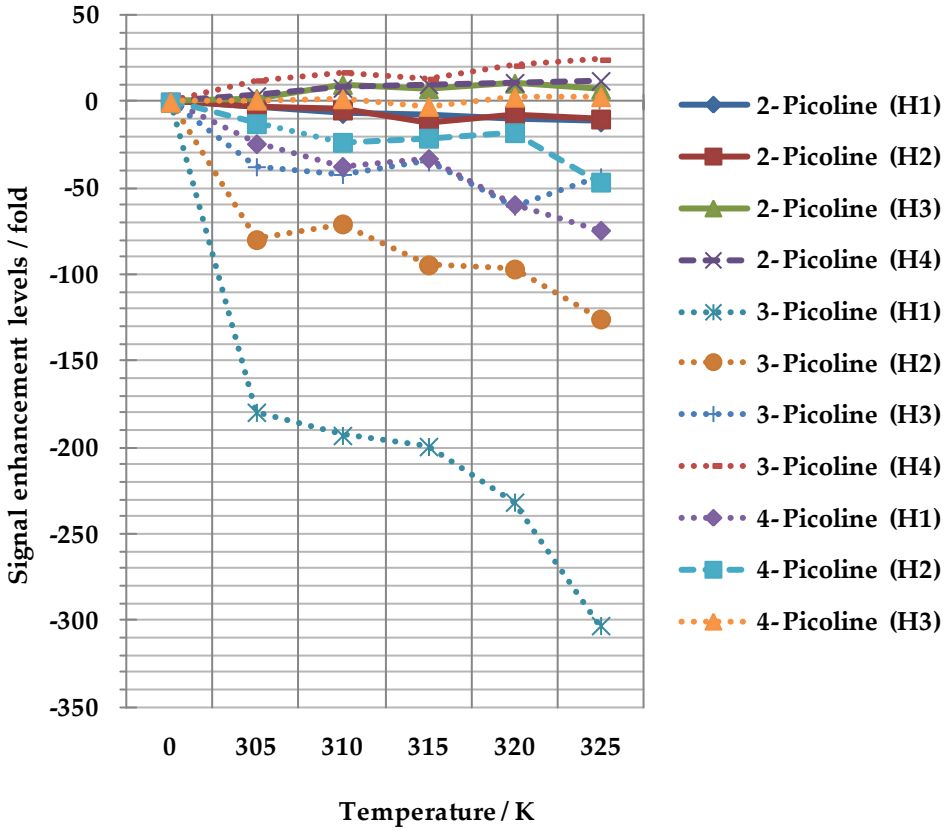

Figure 2.31: Effect of temperature on the magnitude of the ^{1}H NMR spectral signal enhancement at the indicated proton resonances of 2-, 3-, 4-substituents of picoline when the magnetization transfer step is conducted in a magnetic field of 65 G.

Comparison of ^{1}H signal enhancement for 2- picoline, 3- picoline and 4-picoline as illustrated in Figures 2.30 and 2.31, reveals that 3-picoline exhibits comparatively better enhancement levels for all the proton sites. From a basicity point of view, the order is 4-picoline>2-picoline>3-picoline while the order of steric hindrance among three picolines is 2-picoline>3-picoline>4-picoline. From a theoretical perspective it is thought that polarization transfer process is dependent on the interplay between the lifetime of the complex, the scalar couplings, chemical shift of the hydride and protons of the substrate. In the case

of 3-picoline, the polarization transfer catalyst would be expected to have a lifetime that is intermediate between that of 2-picoline and 4-picoline. In the case of the methyl groups present in the picolines, the much reduced signal enhancement could partially be attributed to larger relaxation rates compared to the spins directly attached to the heterocyclic ring. In methyl group carrying derivatives, the couplings from the ring protons to the CH_3 groups occurs across a quaternary carbon resulting in a ^4J coupling with a smaller magnitude. The efficiency of the polarization transfer might be limited by the size of this coupling resulting in a significantly lower level of signal enhancement observed for the substrates possessing the methyl groups.

2.18 Effect of sterics on the hyperpolarization

To explore how the steric congestion affects the polarization transfer pathway, a series of mono substituted pyridines were selected as substrates. These do not prove to polarize well with the carbene complexes, [Ir(IMes)(COD)Cl] (Figure 2.32a). and [Ir(SIMes)(COD)Cl] (Figure 2.32b). Both the complexes differ from each other in a sense that in a complex, [Ir(SIMes)(COD)Cl], the imidazolium substructure is fully saturated compared to complex, [Ir(IMes)(COD)Cl].

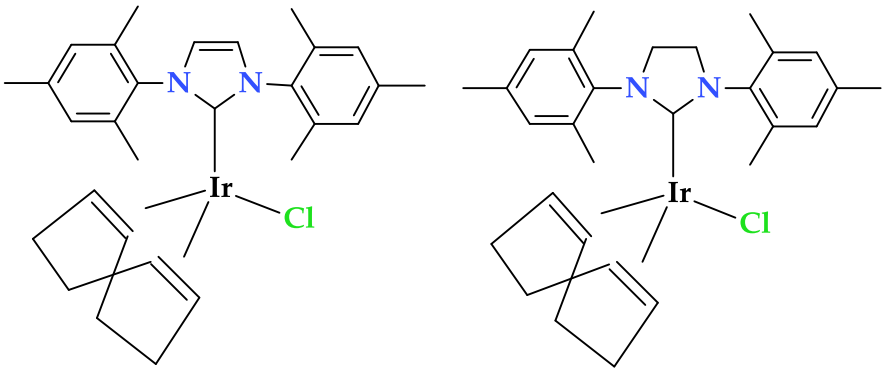

(a) (b)

Figure 2.32: Carbene complexes: (a) [Ir(IMes)(COD)Cl]; (b) [Ir(SIMes)(COD)Cl].

2.18.1 Hyperpolarization of 2- fluoropyridine, 3- fluoropyridine and 4- fluoropyridine

The effect of sterics on the hyperpolarization was investigated using 2-fluoropyridine, 3-fluoropyridine and 4-fluoropyridine (S_{VII}, S_{VII} and S_{IX} in Figure 2.21). ^{1}H and ^{13}C NMR data, enhancement and polarization data for 2-fluoropyridine, 3-fluoropyridine and 4-fluoropyridine are given in Tables A36-A44, Appendix A. The hyperpolarized ^{1}H NMR spectra for 2-fluoropyridine, 3-fluoropyridine and 4-fluoropyridine are shown in Figures A45-A47, Appendix A. A comparison of levels of signal enhancement as function of shake time and temperature achieved for 2-fluoropyridine, 3-fluoropyridine and 4-fluoropyridine is shown graphically in Figures 2.33 and 2.34.

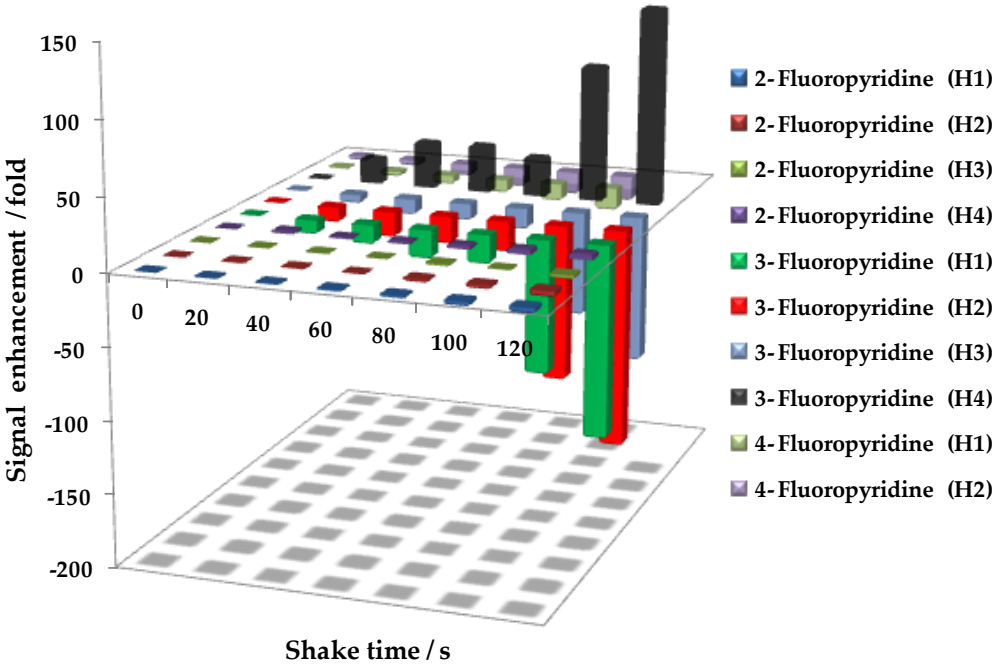

Figure 2.33: Effect of shake time on the magnitude of the ^{1}H NMR spectral signal enhancement for the indicated proton resonances of 2-fluoropyridine, 3- fluoropyridine and 4-fluoropyridine when the polarization step is carried out in a magnetic field of 65 G.

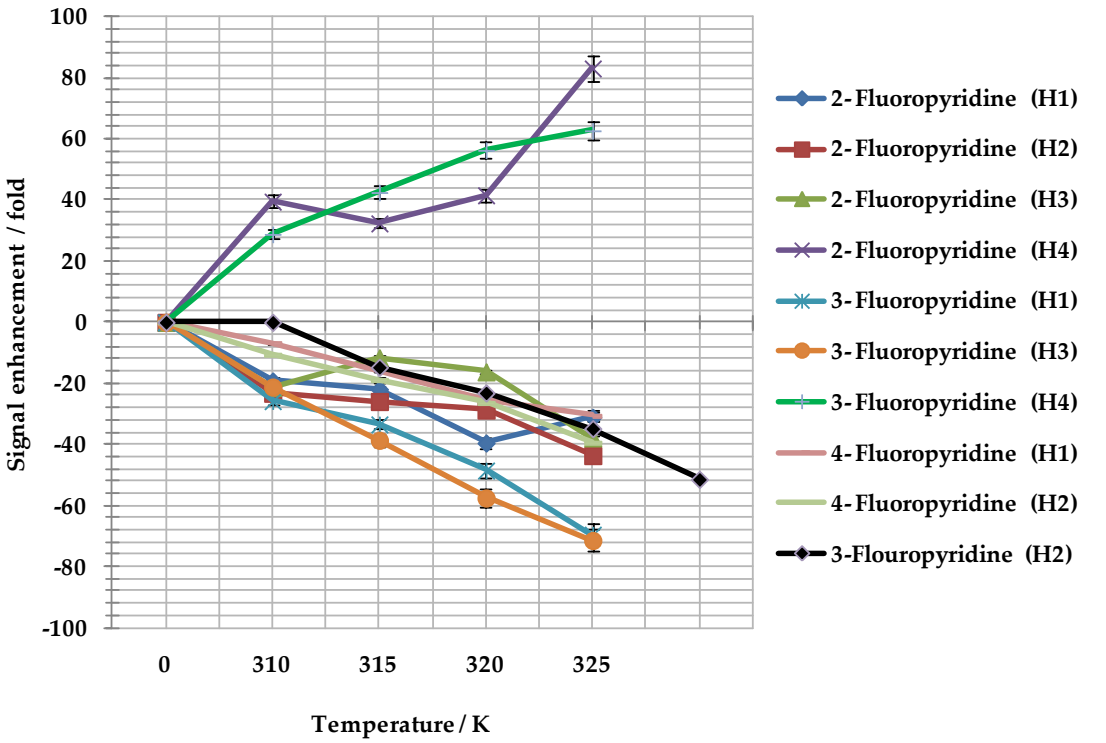

Figure 2.34: Effect of temperature on the magnitude of the ^1H NMR signal enhancement at the indicated proton resonances of 2-, 3-, 4-fluoro pyridine when the magnetization transfer step is carried out in a magnetic field of 65 G.

From Figures 2.33 and 2.34, it is clear that in terms of enhancement the 3-fluoropyridine outperforms 2-fluoropyridine and 4-fluoropyridine. 3-fluoropyridine achieved an enhancement of 83 fold at 325 K. 2-fluoropyridine, 3-fluoropyridine and 4-fluoropyridine were found to deliver optimum hyperpolarization at 325 K. This is due to the fact as SABRE is dependent on the temperature according to exchange rate. The ligand exchange rates are directly proportional to temperature (Equation 2.4); this ultimately favours achieving the optimum state of hyperpolarization. pKa is also thought to govern the polarization process. The pKa of 3-fluoropyridine is intermediate between 2-fluoropyridine and 4-fluoropyridine.

$$k = \frac{KT}{h}.e^{\frac{-\Delta G}{RT}}$$ ……Equation 2.4

Where k is the rate constant, K is the Boltzmann constant, 1.38×10^{-23} JK^{-1}, h is the Planck constant, ΔG is the Gibbs energy of activation, R is the gas constant, T is temperature.

The comparison of the structures of substrates in Figure 2.21 (S_{VII}, S_{VIII} and S_{IX}) indicate that steric hindrance of the F substituent at the *ortho* position prevents the effective transfer of polarization to other sites within the substrate. In case of 3-flouropyridine, it implies that less steric hindrance around the binding site allows the substrate to stay at the metal centre for a sufficient period of time necessary for an effective polarization transfer process. In the case of 3-fluoropyridine, the formation of a weak M-N bond eventually aids in successful polarization transfer using SABRE. The atomic radius of fluorine is only 42 pm. Even though the atomic radius of fluorine is smaller than that of the other substituents used in this chapter it clearly allows binding with the metal. It is clear from Figures 2.33 and 2.34 that hyperpolarization studies involving the fluoro pyridines reveal that if a substituent is located on the *meta* or *para* positions, then the enhancement levels are far greater than those present when on the *ortho* position. In order to test these effects more widely, the Cl, Br and I pyridine derivatives have also been screened.

2.18.2 Hyperpolarization of 2-chloropyridine, 3- chloropyridine and 4-chloropyridine

The effect of sterics on the hyperpolarization was further investigated using 2-chloropyridine, 3-chloropyridine and 4-chloropyridine. ^{1}H and ^{13}C NMR data, enhancement and polarization data for 2-chloropyridine, 3-chloropyridine and 4-chloropyridine (S_X, S_{XI} and S_{XII} in Figure 2.21) are given in Tables A48-A56, Appendix A. The hyperpolarized ^{1}H NMR spectra for 2-chloropyridine, 3-chloropyridine and 4-chloropyridine are shown in Figures A57-A59, Appendix A. A comparison of levels of signal enhancement as function of shake time and temperature achieved for 2-chloropyridine, 3-chloropyridine and 4-chloropyridine are shown graphically in Figures 2.35 and 2.36.

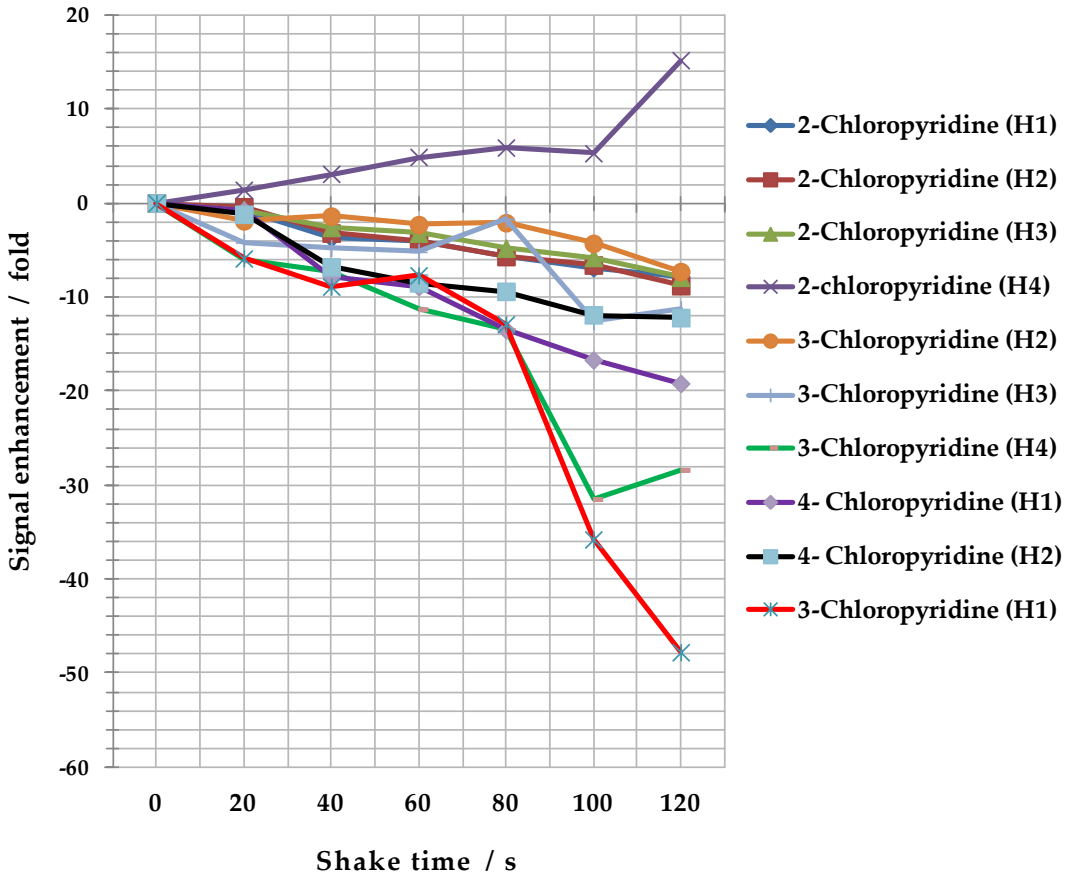

Figure 2.35: Effect of shake time on the magnitude of the ^{1}H NMR spectral signal enhancement for the indicated proton resonances of 2-, 3-, 4-chloro pyridine when the magnetization transfer step is conducted in a magnetic field of 65 G.

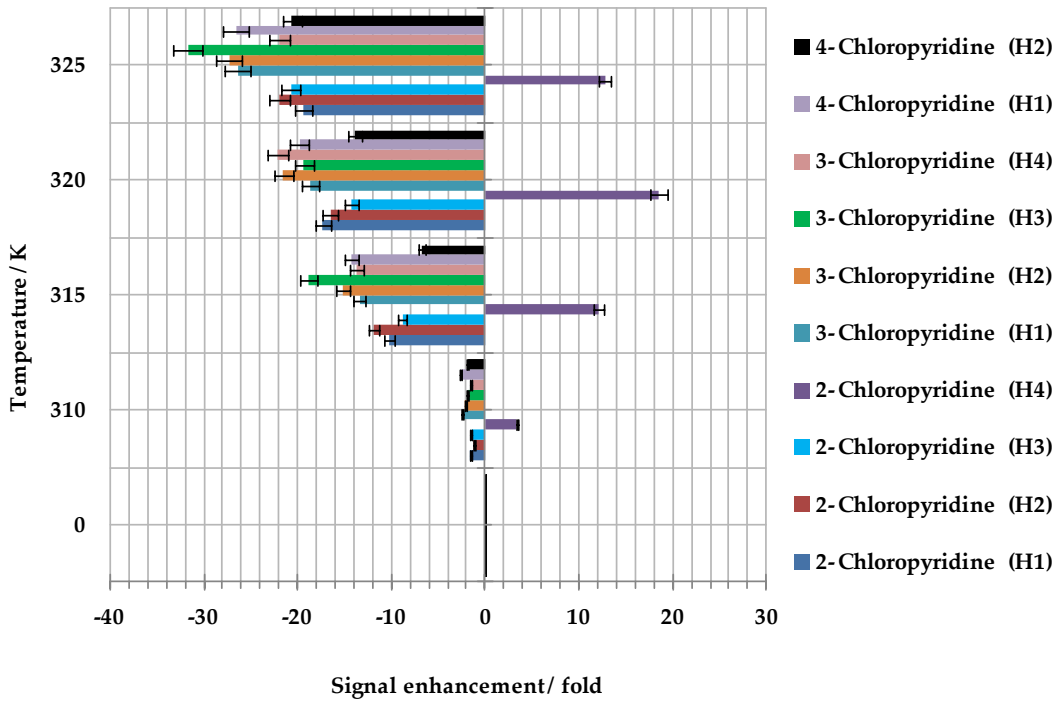

Figure 2.36: Effect of temperature on the magnitude of the ^{1}H NMR spectral signal enhancement at the indicated proton resonances of 2-, 3-, 4-chloro pyridine when the magnetization transfer step is conducted in a magnetic field of 65 G.

By taking into account the enhancement levels achieved as a function of shake time and temperature for 2-chloropyridine, 3-chloropyridine and 4-chloropyridine, it is clear that 3-chloropyridine is most enhanced as demonstrated in Figures 2.35 and 2.36. The pKa of 3-chloropyridine is in between 2-chloropyridine and 4-chloropyridine and this suggests that the pKa might be one of the factors that contributes to the substrate metal binding. Steric hindrance is thought to be another important factor which suppresses the optimal polarization transfer process in the case of 2-chloropyridine which is sterically more hindered than either 3- or 4-chloropyridine. The atomic radius of chlorine is 79 pm in comparison to 42 pm of fluorine thereby suggesting that

weaker binding to the metal centre will result if steric effects are important. Because the enhancement levels observed for the two chloro substituted pyridines are far lower than those observed in case of fluoro-derivatives, it would therefore seem that pKa is the dominant factor.

2.18.3 Hyperpolarization of 2-bromopyridine, 3- bromopyridine and 4-bromopyridine

The effect of sterics on the hyperpolarization process was explored using 2-bromopyridine, 3-bromopyridine and 4-bromopyridine. ^{1}H and ^{13}C NMR data, enhancement and polarization data for 2-bromopyridine, 3-bromopyridine and 4-bromopyridine (S_{XIII}, S_{XIV} and S_{XV} in Figure 2.21) are given in Tables A60-A68, Appendix A. The hyperpolarized ^{1}H NMR spectra for 2-bromopyridine, 3-bromopyridine and 4-bromopyridine are shown in Figures A69-A71, Appendix A. A comparison of the levels of signal enhancement as function of shake time and temperature achieved for 2-bromopyridine, 3-bromopyridine and 4-bromopyridine are shown graphically in Figures 2.37 and 2.38.

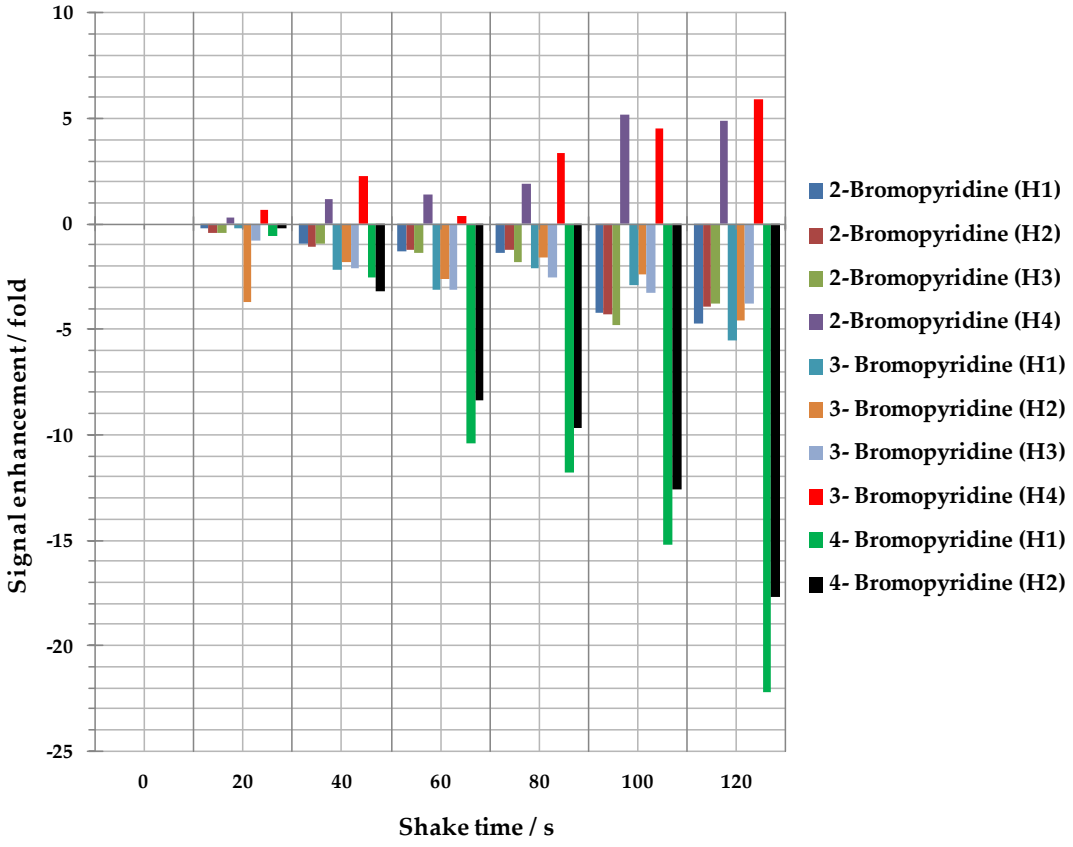

Figure 2.37: Effect of shake time on the magnitude of the ^{1}H NMR spectral signal enhancement at the indicated proton resonances of 2-, 3-, 4-bromo pyridine when the magnetization transfer step is performed in a magnetic field of 65 G.

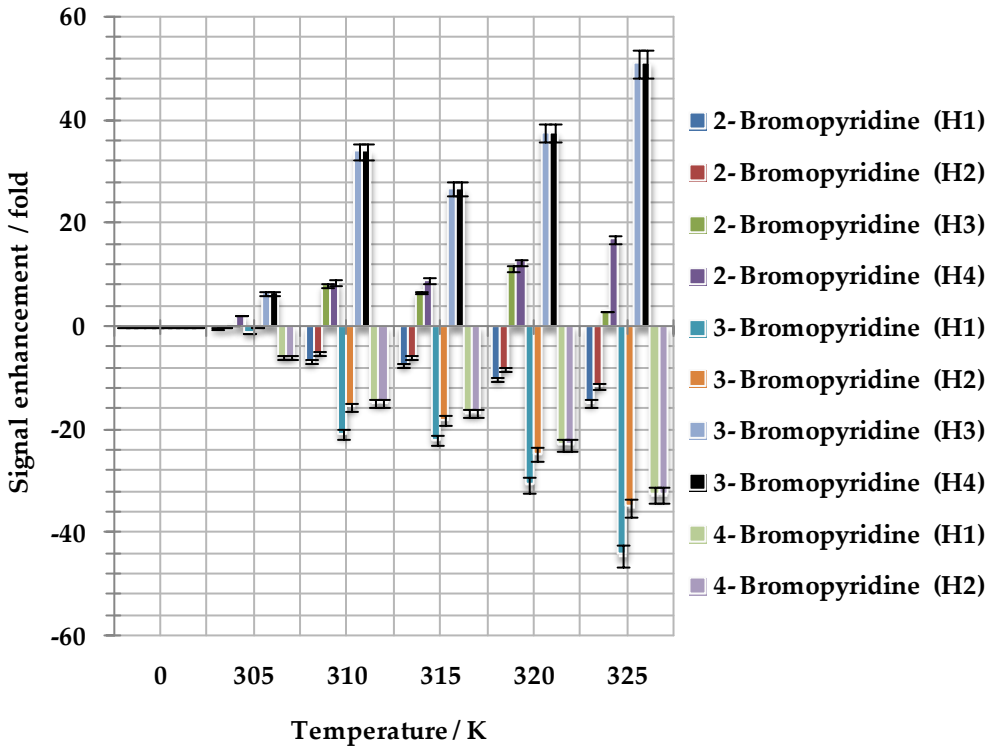

Figure 2.38: ***Effect of temperature on the magnitude of the ^{1}H NMR spectral signal enhancement at the indicated proton resonances of 2-, 3-, 4-bromo pyridine when the magnetization transfer step is accomplished in a magnetic field of 65 G.***

Figures 2.37 and 2.38 reveal that out of 2-bromopyridine, 3-bromopyridine and 4-bromopyridine, 3-bromopyridine is comparatively more enhanced. From the structures (SXIII, SXIV and SXV) shown in Figure 2.21, it is clear that the presence of a bromo substituent at the *ortho* position may lead to steric problems, particularly when two such molecules bind *cis* to one another at the metal centre. In the case of 2-bromopyridine and 4-bromopyridine, less stable complexes form that reduce the likelihood to achieve hyperpolarization. Out of the three bromo substituted pyridines, the 2-bromopyridine showed the lowest enhancement. The atomic radius of bromine is 114 pm and it is about three

times larger than that of fluorine and therefore the observed enhancement levels for the bromo derivatives of pyridine are far less than those of the fluoro substituted systems.

2.18.4 Hyperpolarization of 2- iodopyridine, 3- iodopyridine and 4-iodopyridine

The 2-iodopyridine, 3-iodopyridine and 4-iodopyridine were investigated using the SABRE. ^{1}H and ^{13}C NMR, enhancement and polarization data for 2-iodopyridine, 3-iodopyridine and 4-iodopyridine (S_{XVI}, S_{XVII} and S_{XVIII} in Figure 2.21) are given in Tables A72-A80, Appendix A. The hyperpolarized ^{1}H NMR spectra for 2-iodopyridine, 3-iodopyridine and 4-iodopyridine are shown in Figures A81-A83, Appendix A. A comparison of the levels of signal enhancement as function of shake time and temperature achieved for 2-iodopyridine, 3-iodopyridine and 4-iodopyridine are shown graphically in Figures 2.39 and 2.40.

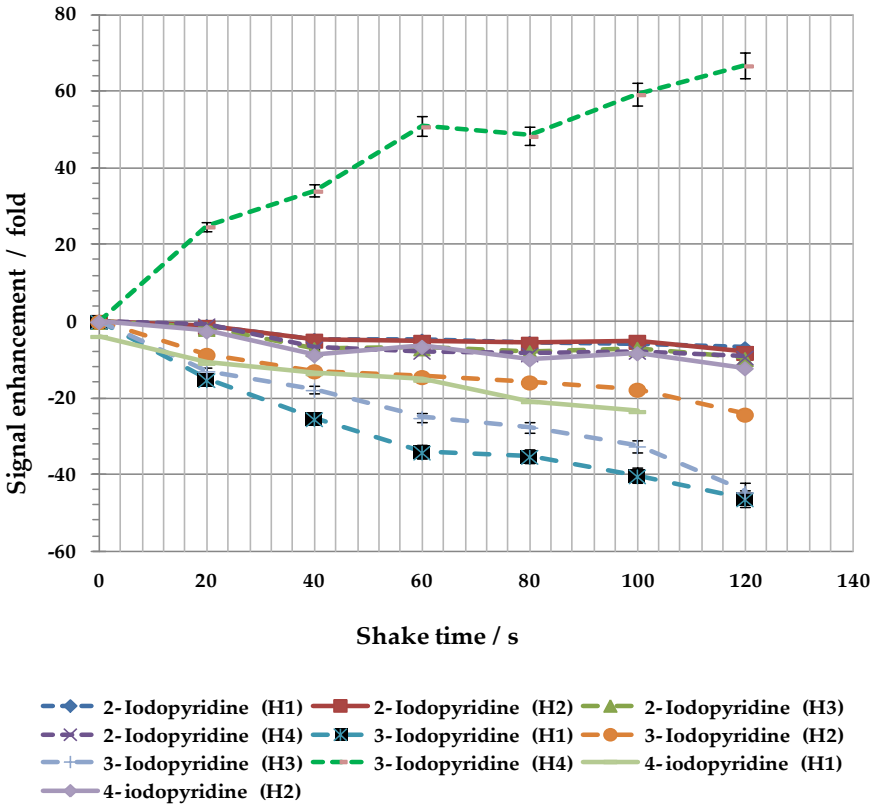

Figure 2.39: Effect of shake time on the magnitude of the ^{1}H NMR spectral signal enhancement for the indicated proton resonances of 2-, 3-, 4-iodo substituents pyridine when the polarization transfer step is carried out in a magnetic field of 65 G.

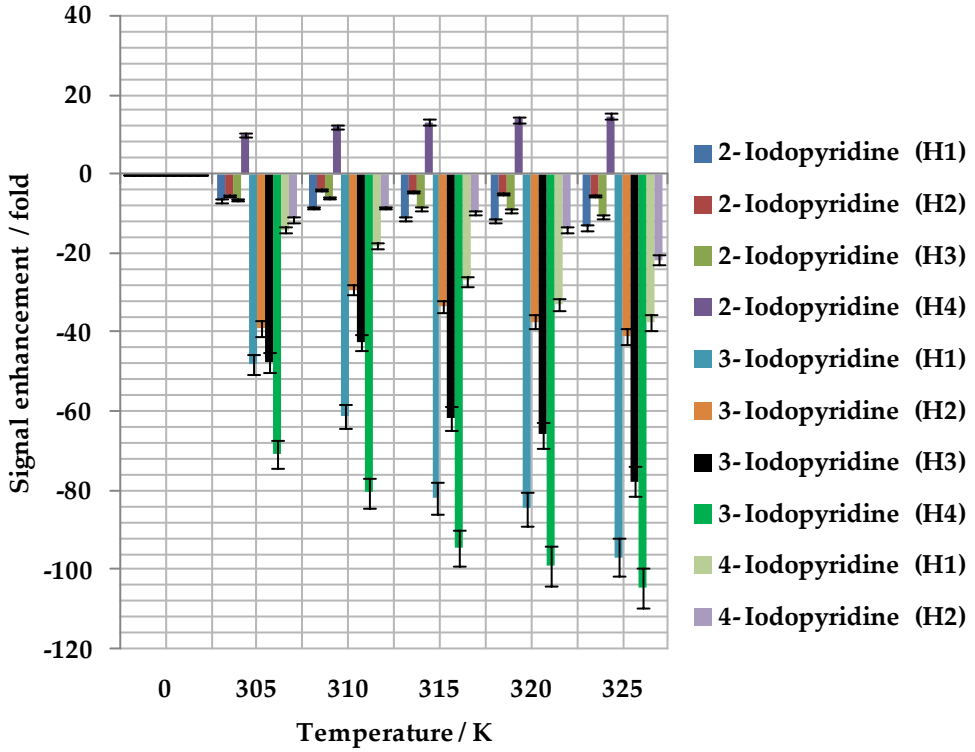

Figure 2.40: ***Effect of temperature on the magnitude of the ^{1}H NMR spectral signal enhancement at the indicated proton resonances of 2-, 3-, 4-iodo pyridine when the magnetization transfer step is carried out in a magnetic field of 65 G.***

Figures 2.39 and 2.40 demonstrate ^{1}H spectra acquired under non-Boltzmann conditions as functions of shake time and temperature exhibiting signal enhancement levels for 2-iodopyridine, 3-iodopyridine and 4-iodopyridine. The hyperpolarization studies involving 2-, 3-, 4-iodo substituent's of pyridine show that 3-iodopyridine is better enhanced than its counterparts 2-, 4-iodopyridine. From the structures (S_{XVI}, S_{XVII} and S_{XVIII}) shown in Figure 2.21, the presence of iodo substituent's on the *ortho* position gives rise to more steric hindrance in polarization transfer than if it is present on the *meta* position. 3-iodopyridine has a pKa value of 3.25, 2-iodopyridine 0.90 and

4-iodopyridine 1.82. The sterically cumbersome 2-iodo substituent does not allow the substrate to bind effectively to the metal centre which ultimately hinders the polarization transfer necessary to achieve a hyperpolarized state and leads to weaker polarization transfer than its counterparts 2-, 4-iodo substituent's of pyridine.

2.19 Conclusions

In most of the hyperpolarization studies which have used SABRE, the IMes ligand has been used.[100-104] In this project, an iridium complex, [Ir(IMe)(COD)Cl], ***1***, was prepared and its applicability as a SABRE catalyst was investigated in hyperpolarization studies which analyzed the interaction with a variety of substrates in the presence of *p*-H_2. In case of ***1***, the aromatic group of IMes is replaced by a methyl group, resulting in a much smaller and sterically less bulky ligand (Figure 2.41). It has been demonstrated by others that the IMes system exhibits an array of limitations based on its large steric bulk, which makes it unsuitable for the polarization of relatively large substrates.[102]

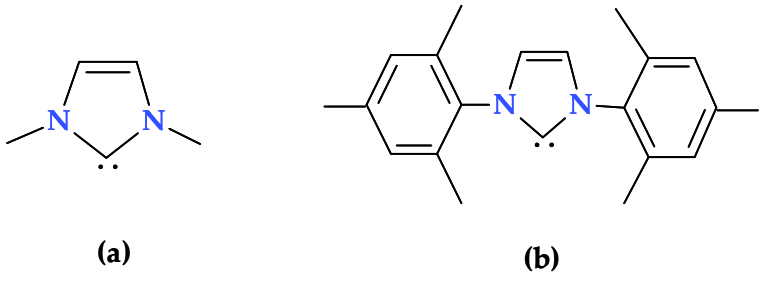

(a) **(b)**

Figure 2.41: ***Structures of: (a) IMe ligand; (b) IMes ligand.***

The hyperpolarization studies with ***1*** highlighted the beneficial function of a carbene complex in polarization transfer, through which the substrate

molecules become hyperpolarized from *p*-H_2. The exchange rates of both the substrate and hydride ligands are also of prime importance to the magnetization transfer process. It is due to the fact that ***1*** has less steric hindrance due to methyl group attached to both nitrogen of imidazole ring and therefore expected to form a relatively stable hyperpolarizing species. Furthermore, ***1*** also proved to bind strongly to substrates such as 2-fluoropyridine, where the steric effects should be small as compared to **2**. The level of signal enhancement is observed to be ligand dependent, with pyridine being significantly more polarizable than the picolines and the monosubstituted pyridines studied.

The effect of shake time on the signal enhancement was investigated. The shake time was changed from 0 to 120 s for each of the substrate examined in this chapter. The signal intensity was observed to increase as a function of shake time up to 120 s. However, after 120 s, the sample relaxes and weaker hyperpolarization is observed. This data collected for the substrates given in Figure 2.18 suggests that a correct shake time is essential for achieving optimum levels of signal enhancement. This reflects the fact that the amount of *p*-H_2 in the NMR tube is finite and when consumed, relaxation acts to remove the hyperpolarization.

For 2-, 6-, d_2-pyridine after 120 s shake time there is typically a 50% increase in the level of signal enhancement when compared to a 60 s shake time. However, at shake times of above 140 s, there is a significant reduction in the signal enhancement level. It should be noted that these measurements were completed for a 65 G polarization transfer field.

The effect of magnetic field on the polarization transfer process was further monitored by using 3-, 4-, 5-, d_3-pyridine. During polarization transfer, the magnetic field experienced by the sample, the lifetime and couplings within the complex affect the process. When they match, as revealed in the theoretical description of Green *et al.*, optimum transfer is likely.[59] This process can be thought of as similar to that of an INEPT experiment where the value of the evolution delay is set to $\frac{1}{2}J$ for polarization transfer from ^{1}H to ^{13}C. To explore the effect of magnetic field on the flow probe, NMR spectra were acquired using a 10 s bubble time with a delay of 1 s before transferring to the NMR probe. The maximum enhancement is observed at a magnetic field of 65 G, therefore all the hyperpolarization studies as functions of shake time and temperature have been conducted at a magnetic field of 65 G, which is consistent in enhancing the signal intensity for all the substrates examined in this chapter using SABRE.

The effect of electron donating and bulky substituents on the polarization transfer process was further explored by comparing 2- picoline, 3- picoline and 4-picoline. In the case of 2-picoline, steric hindrance of the bulky CH_3 group at the 2-position inhibits polarization from the metal to the substrate. The positive electron donating inductive effect of the CH_3 group therefore has little effect on stabilising the complex. In the case of 3-picoline, the steric factor is substantially reduced and resonance effects become dominant. These effects mean that from a basicity point of view, the order is 4-picoline>2-picoline>3-picoline while the order of steric hindrance among three picolines is 2-picoline>3-picoline>4-picoline. The sum of the enhancement levels for all the protons sites observed in as a function of: (a) shake time; (b) temperature are shown in Figures 2.42 and 2.43. It is clear that 3-picoline works best, and consequently 4-picoline must

bind too strongly. This is supported by the temperature dependence which demonstrates that the polarization of 4-picoline can be improved very dramatically by warming as its exchange rate increases.

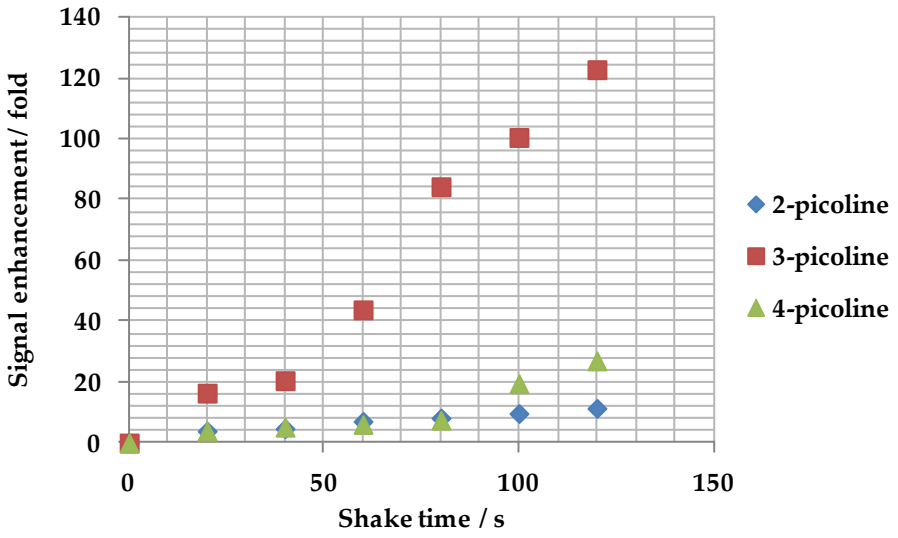

Figure 2.42: Sum of the enhancement levels for all the ^{1}H hyperpolarized sites observed in case of 2- picoline, 3- picoline and 4-picoline as a function of shake time.

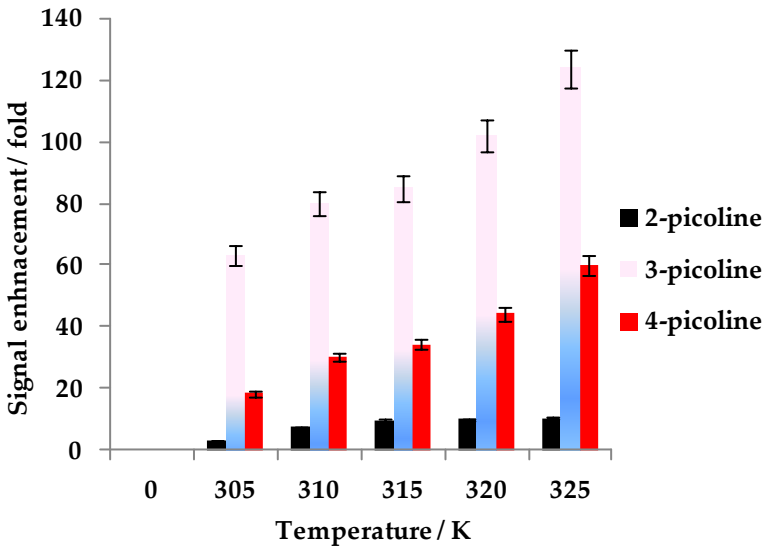

Figure 2.43: ***Sum of enhancement levels for all the ^{1}H hyperpolarized sites observed in case of 2- picoline, 3- picoline and 4-picoline as a function of temperature.***

A further hypothesis was explored whether deutration would increase signal intensity by reducing the number of protons that are enhanced. This can be thought of as proton dilution effect. Furthermore, it also allows the testing of efficiency for direct IrH transfer into *ortho, meta and para* protons rather than what might be related transfer in the molecules described above. For this purpose, two deuterium isotopomers (2-, 6-, d_2-pyridine and 3-, 4-, 5-, d_3-pyridine) were used. Perrin *et al.*[147] demonstrated that deutration increases the basicity of pyridine nitrogen due to the kinetic isotope effect. Kinetic isotope effect (KIE) refers to the change in the rate of a chemical reaction upon substitution of an atom in the reactants with one of its isotopes. In case of 2-, 6-d_2-pyridine and 3-, 4-, 5-, d_3-pyridine, their change in basicity is 0.095 and 0.052 when compared to pyridine with pKa of 5.17. The basicity of the substrate dictates the rate at which the dissociation from the metal takes place and also

increases the life time of the substrate spends in contact with the metal centre. These effects are likely to be small.

In case of 3-, 4-, 5-, d_3-pyridine, the *meta* and *para* positions were deutrated leaving one protonated site for interaction with the metal centre, while in case of 2-, 6-d_2-pyridine, the *ortho* positions were deuterated. A 16 fold increase in signal enhancement was observed by deutrating the *meta* and *para* position in 3-, 4-, 5-, d_3-pyridine relative to the parent pyridine. This confirms the proton dilution effect and suggests a route to bigger net signal enhancement on single sites. It also confirms that polarization transfer through and hydride-*ortho* proton coupling is possible.

The hyperpolarization data collected for 2-, 6-d_2-pyridine revealed that the polarization levels are reduced when compared to that achieved for 3-, 4-, 5-, d_3-pyridine, although still substantial. The ratio of efficiencies is 4:1 and hence we can conclude that a 4 fold reduction is efficiency results when a *meta* or *para* coupling is employed compared to the *ortho* coupling.

The horizon of hyperpolarization studies was further broadened by taking into account more precisely the effect of steric hindrance, basicity and how the change in the position of a substituent on the aromatic ring of pyridine affects the polarization transfer process using SABRE. For this purpose, 2- substituted, 3- substituted, 4-substituted pyridines were polarized (S_{VII}, S_{VIII}, S_{IX}, S_X, S_{XI}, S_{XII}, S_{XIII}, S_{XIV}, S_{XV}, S_{XVI}, S_{XVII}, and S_{XVIII} in Figure 2.21).

When comparing halides in the same group, size (steric) becomes more important. Molecules with smaller substituents are strongly attracted to solvent

molecules have a decreased potential energy and are therefore less reactive. Smaller ions such as fluoride have a large charge- to- surface ratio than larger ions (Iodide). Moreover, smaller ions are stabilized by their stronger attraction to polar solvent molecules, in particular they more effective at hydrogen bonding with protic solvents than the large ions.

The enhancement levels for 2-fluoropyridine as a function of shake time achieved the lowest level of signal enhancement. This is due to the fact that the inductive effect reduces the basicity of nitrogen in 2-fluoropyridine, which results in weaker binding with the metal centre. An inductive effect is the displacement of an electron pair in a covalent bond due to electronegativity difference of the two joined atoms and consequent polarization of the bond. The signal enhancement levels observed as a function of temperature and shake time are in agreement as shown in Figures 2.44 and 2.45.

3-fluoropyridine exhibits higher signal enhancement when compared to 2-fluoropyridine due to its higher binding potential. The average signal enhancement is now 133 fold for the hyperpolarized proton sites in this molecule. The temperature data obtained for 3-fluoropyridine supports the aforementioned trend that increase in temperature leads to higher signal enhancement levels as demonstrated in Figures 2.44 and 2.45. In case of 4-fluoropyridine, the data shows comparatively lower signal enhancement when compared to 3-fluoropyridine. The temperature data suggest this complex improves with increase in temperature as illustrated in Figures 2.44 and 2.45.

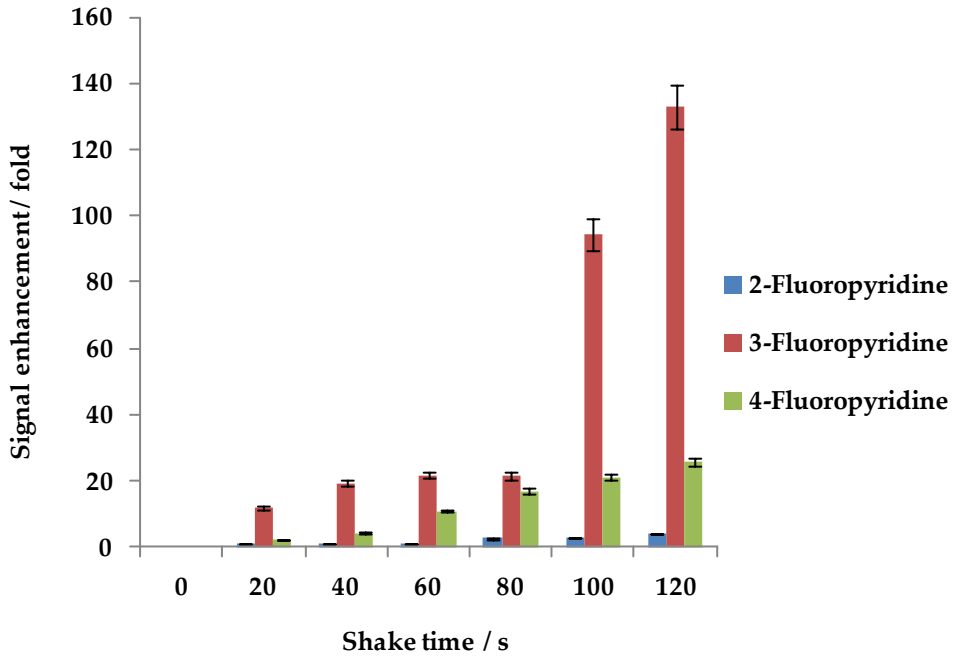

Figure 2.44: Sum of enhancement levels observed for all the hyperpolarized proton sites in case of 2- fluoropyridine, 3- fluoropyridine and 4-fluoropyridine as a function of shake time.

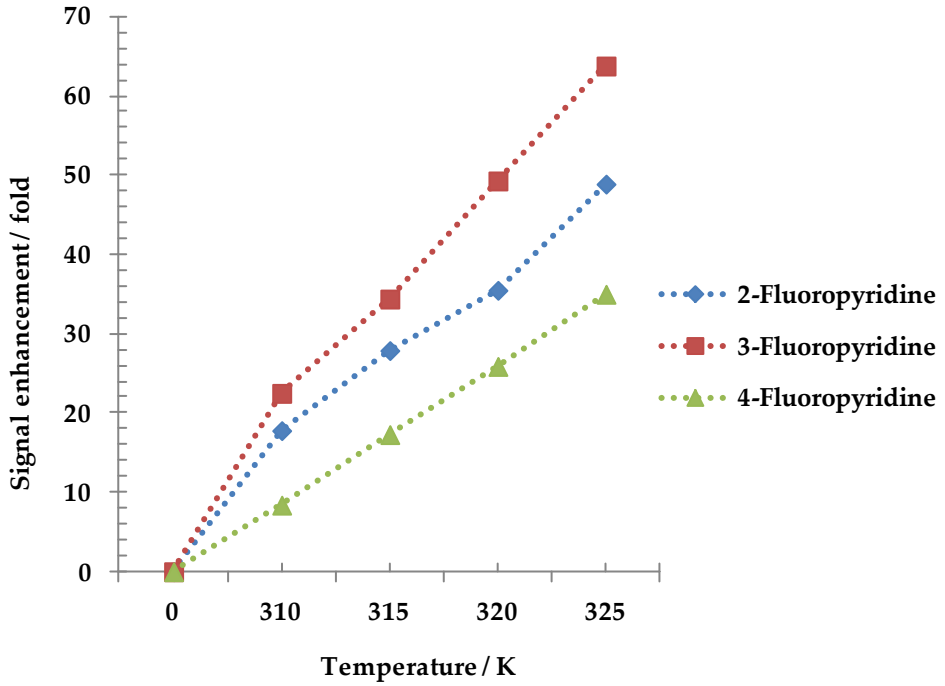

Figure 2.45: Sum of enhancement levels observed for all the hyperpolarized proton sites in case of 2- fluoropyridine, 3- fluoropyridine and 4-fluoropyridine as a function of temperature.

2-chloropyridine exhibits higher basicity when compared to 2-fluoropyridine. The higher basicity of 2-chloropyridine is due to a weaker inductive effect of chlorine when compared to fluorine. The comparatively higher basicity of 2-chloropyridine enhances polarization transfer process leading to better signal enhancement because steric hindrance is overcome by using the IMe ligand compared to IMes ligand (Figures 2.46 and 2.47). The covalent radii of F and Cl are 57 pm and 102 pm. The pKa's of 2-chloropyridine, 3- chloropyridine and 4-chloropyridine are 0.72, 2.84 and 3.88 respectively. This would suggest that 4-chloro pyridine will bind the strongest of the series, but less well than unsubstituted pyridine which has a pKa of 5.17.

The corresponding data are shown below in Figures 2.46 and 2.47. Clearly whilst pyridine is the best material, 3-chloropyridine is better than 4-chloropyridine. Furthermore while heating to 325 K improves the level of signal enhancement, the proportional increase for the chloride system is much smaller than for fluoride system. It would therefore appear that the coupling framework is optimised for transfer when a 3-substituent is present.

Moreover, the enhancement data shows that 3-fluoropyridine gives a 5 fold higher signal enhancement than 3-chloropyridine. Now the pKa is 2.97 which is very close to the 2.84 for 3-chloropyridine. Perhaps steric effects account for the better signal enhancement compared to 2-chloropyridine.

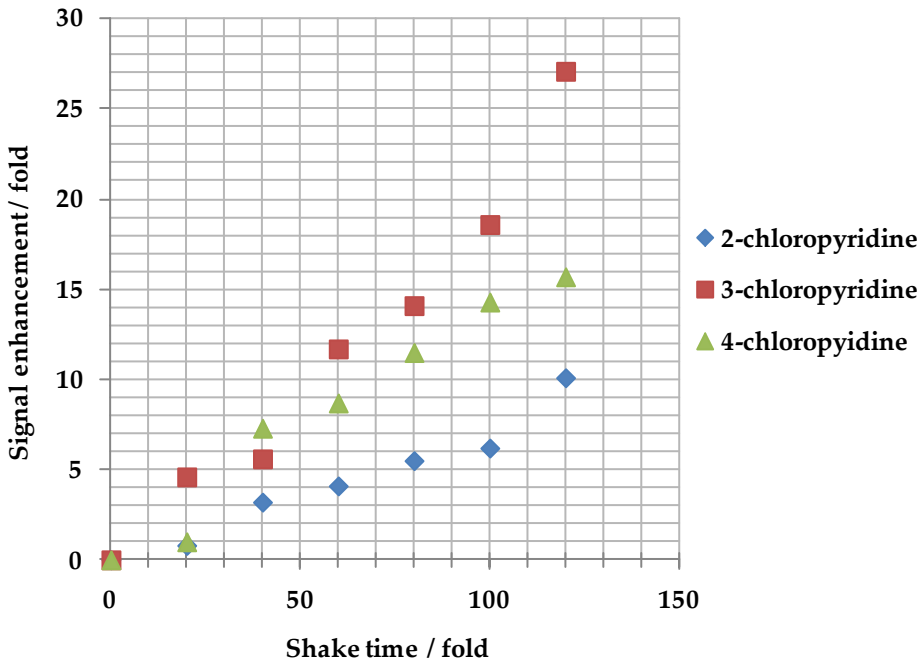

Figure 2.46: ***Sum of enhancement levels for all the hyperpolarized proton sites in case of 2- chloropyridine, 3- chloropyridine and 4-chloropyridine as a function of shake time.***

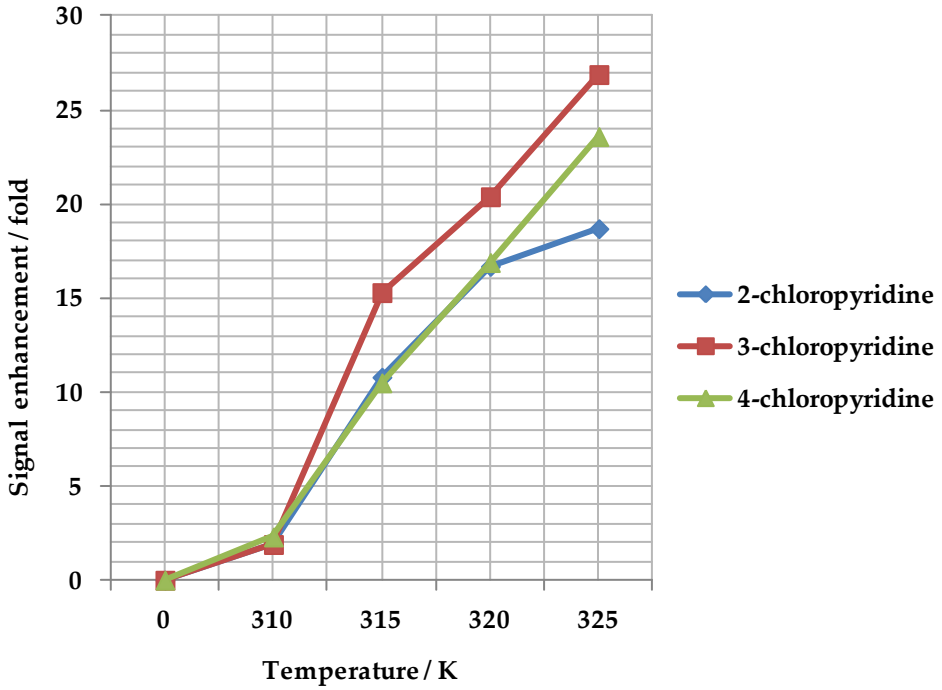

Figure 2.47: ***Sum of enhancement levels for all the hyperpolarized proton sites in case of 2- chloropyridine, 3- chloropyridine and 4-chloropyridine as a function of temperature.***

Literature pKa values for the corresponding bromides are readily available. They are 0.90, 2.84 and 3.82 respectively. Figures 2.48 and 2.49 show the corresponding data. The values of pKa for 3-chloro and 3-bromo are identical whilst the steric bulk is bigger for the bromide. 3-chloro is slightly better enhanced. In case of 4-bromopyridine, the chloride is slightly more basic but the levels of polarization are comparable.

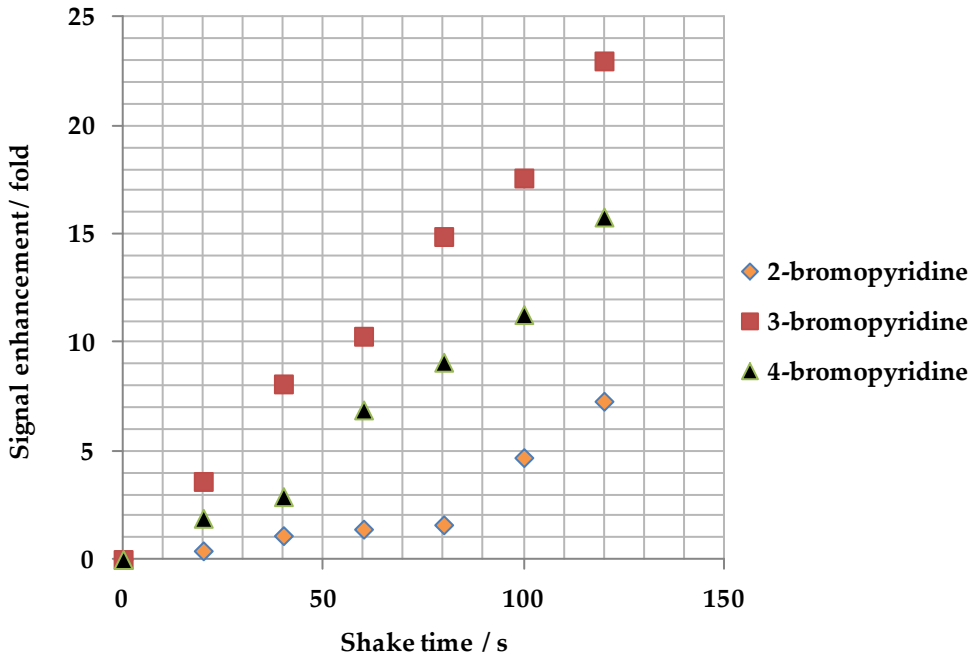

Figure 2.48: Sum of enhancement levels for all the ^{1}H hyperpolarized sites for 2-bromopyridine, 3-bromopyridine and 4-bromopyridine as a function of shake time.

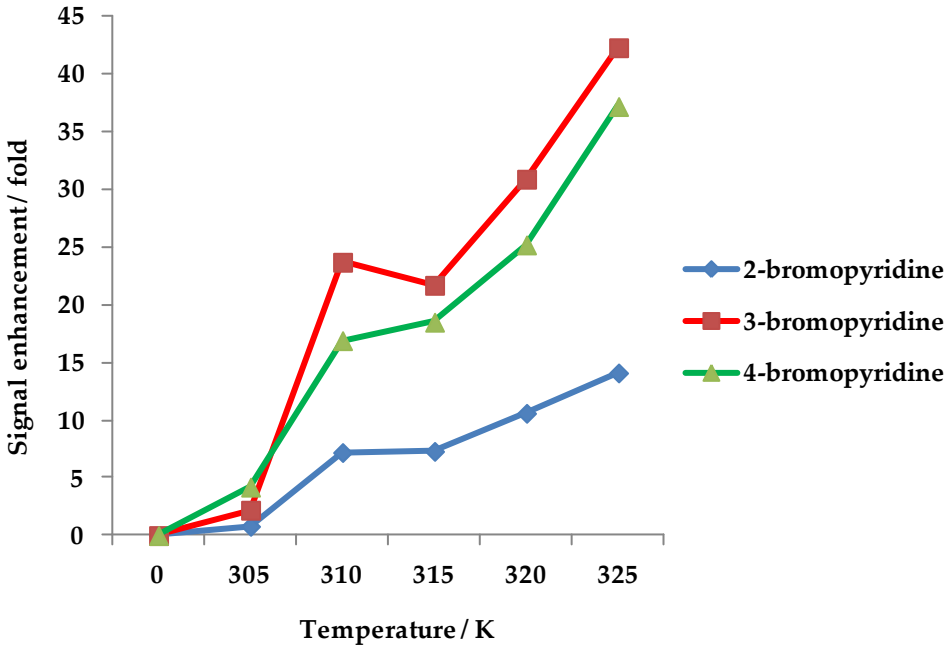

Figure 2.49: Sum of enhancement levels for all the ^{1}H hyperpolarized sites for 2-bromopyridine, 3-bromopyridine and 4-bromopyridine as a function of temperature.

In case of 2-iodopyridine, the signal enhancement is comparatively better than 2-bromopyridine even though the steric effect is bigger (Figures 2.50 and 2.51). The pKa value is now 1.82 rather than 0.90. For 3-iodopyridine the pKa is 3.25 and hence it is significantly more basic than the chloro or bromo substituents of pyridine. Now the signal enhancement is better. In case of 4-iodopyridine, the pKa of 4.02 and again slightly improved polarization level results.

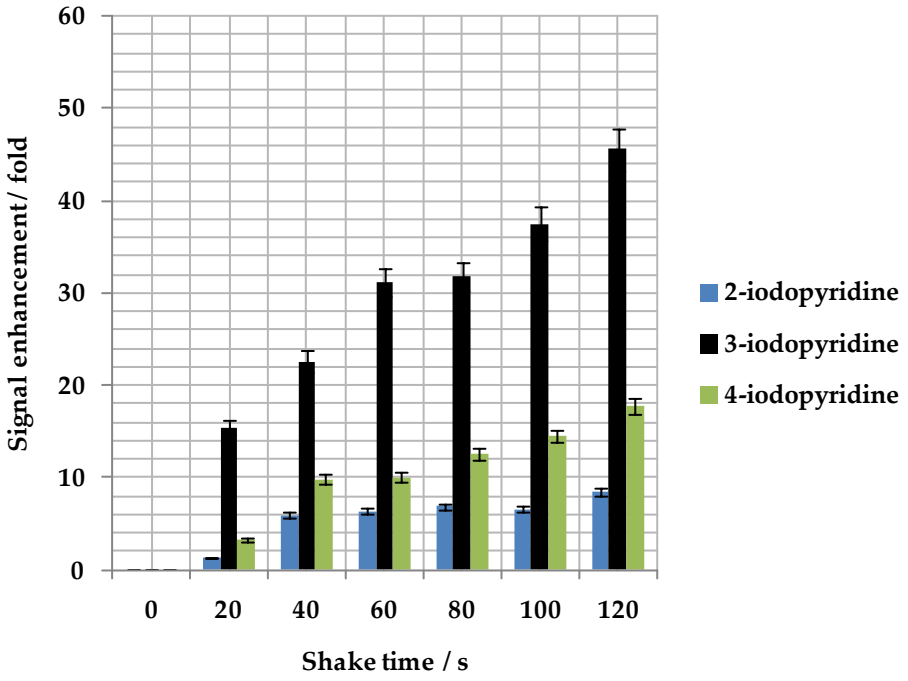

Figure 2.50: Sum of enhancement levels for all the hyperpolarized proton sites in case of 2- iodopyridine, 3- iodopyridine and 4-iodopyridine as a function of shake time.

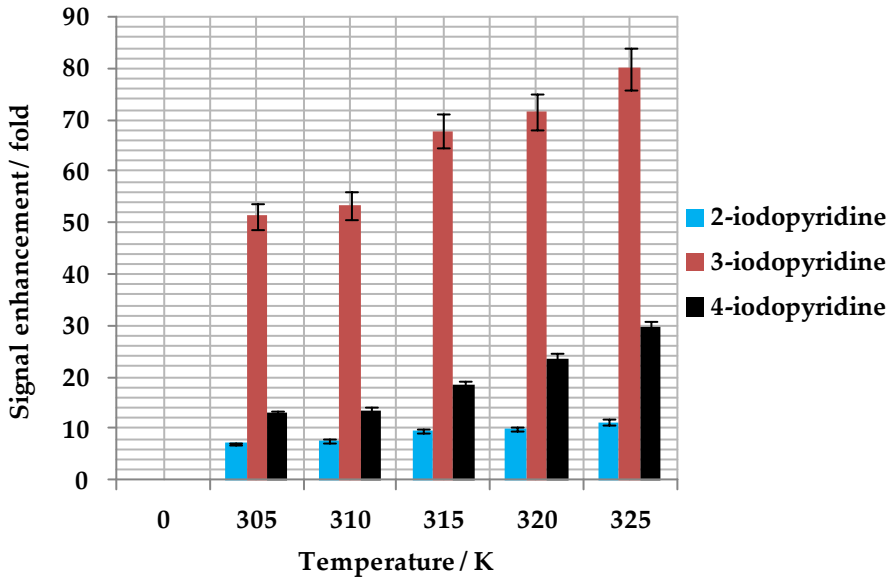

Figure 2.51: Sum of enhancement levels for all the hyperpolarized proton sites in case of 2- iodopyridine, 3- iodopyridine and 4-iodopyridine as a function of temperature.

It is therefore possible to conclude that in the case of IMe, steric effects associated with Me, F, Cl, Br and I substituents are minimal and sensitivity relates more closely to pKa and hence binding potential. It should also be noted that the coupling framework in the ligands plays a role and that the 2-substituent derivatives consistently yield lower polarization levels, even though they increase with increase in temperature.

CHAPTER THREE

Hyperpolarization studies of biologically relevant substrates using SABRE

3.1 Introduction

In this chapter, the performance of [Ir(COD)(IMe)Cl], ***1***, against biologically relevant substrates has been examined. These hyperpolarization studies ultimately provide an insight into the conditions necessary for an efficient and effective polarization transfer from a catalyst to biologically relevant substrates. The purpose of these studies was to optimize hyperpolarization phenomena for biologically relevant substrates.

SABRE has been successfully applied to hyperpolarize biologically relevant molecules.[101] A recent study reported the application of SABRE to detect nanomoles of pyridine in low-field NMR.[148] In a similar study by Duckett and co-workers a derivative of the Crabtree catalyst, [Ir(COD)(PCy_3)(MeCN)][BF_4], was used to hyperpolarize pyridine. The Crabtree catalyst, a transition metal catalyst, has been productively used in studies related to SABRE. These studies were then further extended to embark on MRI studies; the MR image (see Figure 3.1) obtained exhibits a 160 fold enhancement, a substantial increase which could ultimately assist in transforming the world of medical diagnostics. Figure 3.1 shows a cross section

image of hyperpolarized (left) and unpolarized (right) solutions containing glass tubes. The unpolarized solution is generated using 128 scans, while the more intense hyperpolarized solution required only one scan.[148]

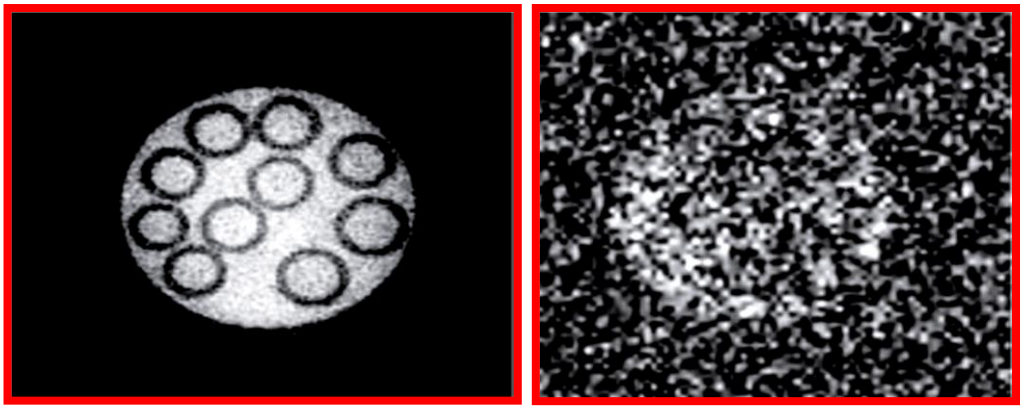

A ***B***

Figure 3.1: ***(A) Signals from polarized pyridine in d_4-methanol; (B) Signals from the same sample after the decay of polarization. (Reproduced with permission from reference 148).***

Of the various factors which could influence the SABRE technique, one is the type of the metal; iridium is widely used as a transition metal in catalysis. The carbene ligands used in SABRE also play a pivotal role in controlling the steric and electronic characteristics of a metal complex. It has been established that it is possible to quantify the electronic affects of ligands by calculating their bond lengths, NMR properties and examining their *trans* effects. Recently, a study has been undertaken which illustrates the ways to measure the electronic properties as well as Tolman's cone angle and the percentage buried volume.[149] The percentage buried volume is the percent of the total volume of a sphere occupied by a ligand as illustrated in Figure 3.2.

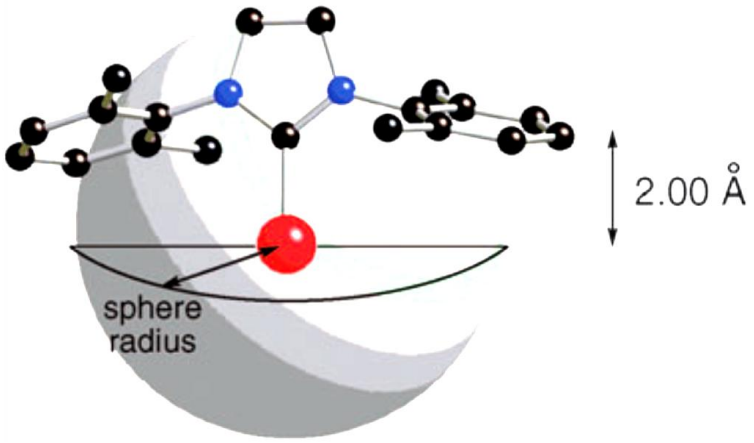

Figure 3.2: ***Percent buried volume % V_{bur}. (Reproduced with permission from reference 149).***

The percent of the total volume is calculated using crystallographic data. The sphere has defined radius and has the metal centre at the core [150, 151] and the volume of this sphere depicts the potential coordination sphere space around the metal occupied by a ligand / ligand fragment. Software called Samb*V*ca developed by Cavallo *et al*.[152] is used to measure the spatial occupation value of the ligands. The software is originally developed to measure the "percent buried volume" of *N*-heterocyclic complexes of ruthenium,[150] iridium,[153] palladium,[154] rhodium,[155] nickel,[156] gold[157] and silver.[158]

N-heterocyclic carbenes have been used as a substitute to phosphines, but the key finding is that NHCs prove to be an efficient polarization transfer catalysts because of their greater bulk and electron donating properties.[159] In a separate study, it has also been observed that ligands located *trans* to the bulky NHCs / phosphines dissociate first as compared to the ligand present *trans* to the hydrides because of their longer Ir-N bond distances. These observations

show that they are steric dependant thermodynamically controlled substitutions.[159]

A recent paper by Gutmann *et al*.[160] opened up the possibility of using Ir trichloride as a catalyst in hyperpolarization studies. In this paper they showed that the $IrCl_3.H_2O$ is highly water soluble and can be employed to enhance the signal intensity. To carry out the experiments, they dissolved 4-chloro-styrene (50 μL) / $IrCl_3.H_2O$ (7-9 mg) in methanol-d_4 and 4-chloro-styrene (50 μL) / $RhCl_3.H_2O$ (7-9 mg) in methanol-d_4. The samples were then exposed to *p*-H_2 and ^1H NMR spectra were acquired at room temperature. The observations made in the experiments showed PHIP enhancements both in $IrCl_3.H_2O$ and $RhCl_3.H_2O$ containing systems.

The aforementioned experiments[160] revealed that enhancement levels are strongly dependant on the temperature. At room temperature, the reaction rate is relatively slow which leads to a lower level of signal enhancement of 0.5 fold. In contrast, when similar experiments were carried out at the boiling temperature of the solvent, substantial levels of signal enhancement were observed which depends on the solvation of the catalyst and the substrate.

SABRE is a newly developed technique in the field of hyperpolarization and there is not ample literature and reviews are available to understand the factors affecting the polarization transfer process. In most of the recent studies on SABRE, pyridine was considered as the substrate of preference because it is a simple heterocyclic molecule and a model for biologically relevant substrates such as nicotinic acid, purine and pyrimidine.[148] A lot of work is being carried out on SABRE to provide us with a database of fundamental factors that govern

an efficient polarization transfer process. In *para*hydrogen induced polarization (PHIP), unsaturated molecules have been used due to their binding affinity with *p*-H_2 but the SABRE make use of substrates with unsaturated π-electron system, which are thought to assist in the polarization transfer process.[102-104]

The theoretical studies on SABRE acquaint us with the fact that the process of polarization transfer is dependent on the scalar coupling network within the substrate molecule and also on the difference of precession frequencies in the active iridium complex.[59] The polarization transfer process was found to be linearly dependent on the magnetic field and demonstrated a strong dependence of enhancement on the magnetic field in which the polarization transfer takes place. The SABRE studies carried out at variable temperatures revealed that the polarization transfer efficiency is also dependent upon the exchange rate of *p*-H_2 and a substrate molecule.[103]

3.2 Catalyst Activation

The polarization transfer catalyst [Ir(IMe)(COD)Cl], ***1***, was prepared according to a literature method.[146] 1.3 mg of ***1*** is allowed to react with *p*-H_2 in the presence of the substrates $\boldsymbol{S_1}$-$\boldsymbol{S_8}$ (ca. 3 mg) (see Figure 3.3) in 0.6 mL of deutrated methanol within a Young's NMR tube. The structures of biologically relevant substrates except isonicotinic acid which is an isomer of nicotinic acid, $\boldsymbol{S_1}$-$\boldsymbol{S_8}$ (nicotinic acid, isonicotinic acid, methyl nicotinate, isonicotinamide, pyrazine, isoniazid, purine and pyrimidine respectively) are shown in Figure 3.3. During this process, ***1*** is converted into a dihydride complex with chemical composition $[Ir(IMe)(S_n)_3(H)_2]^+$ as shown in Figure 3.4. This change readily manifests itself in the resulting hyperpolarized ^1H NMR spectra as the hydride

signal appears in the high field region around δ -20. Once the catalyst is activated in this way the SABRE phenomenon can be observed.

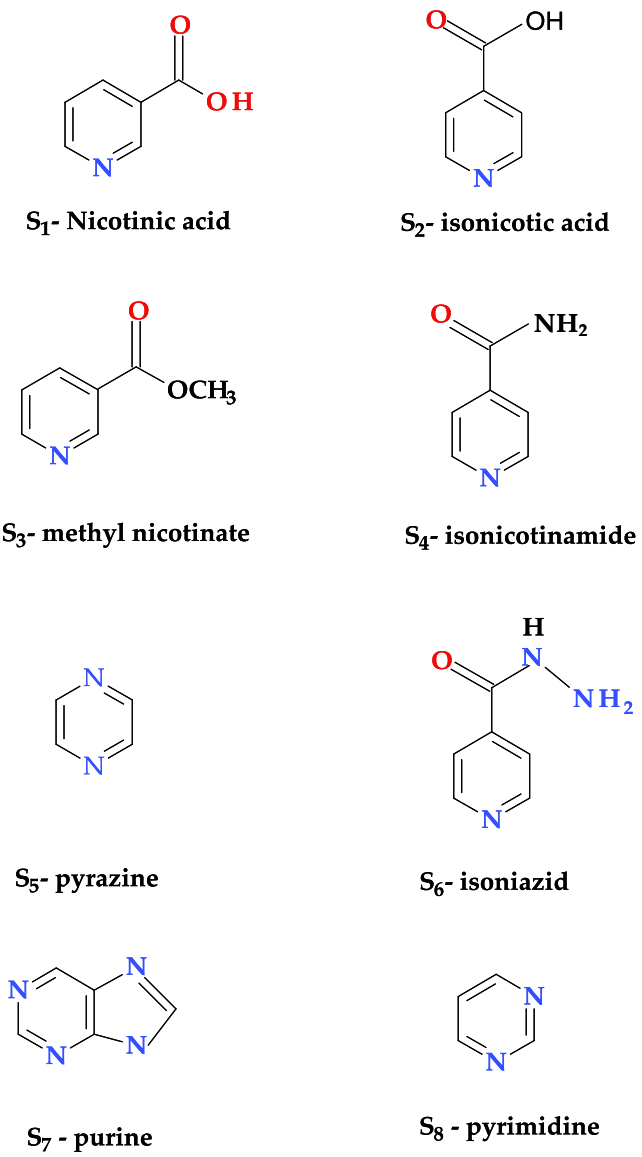

Figure 3.3: Chemical structures of the N-heterocyclic substrates (S_1-S_8) examined in this chapter.

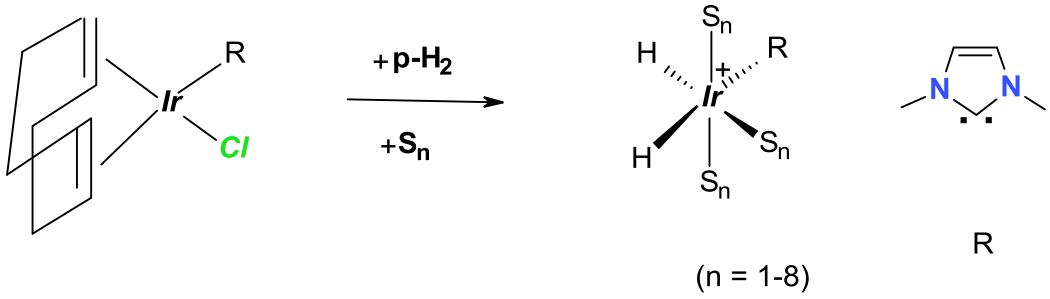

Figure 3.4: Formation of an active iridium complex from 1 by a reaction with substrate molecules (S_1-S_8) in the presence of p-H_2.

3.3 Hyperpolarization of substrates

In order to achieve the maximum hyperpolarized signal enhancement in the substrates **S_1-S_8**, the effect of three variables on the polarization transfer process was investigated. These are: (a) the shake time with *p*-H_2; (b) the effect of substrate concentration; (c) the effect of temperature. A flow diagram depicting the steps involved from sample preparation through to data acquisition in the NMR magnet is shown in Scheme 3.1.

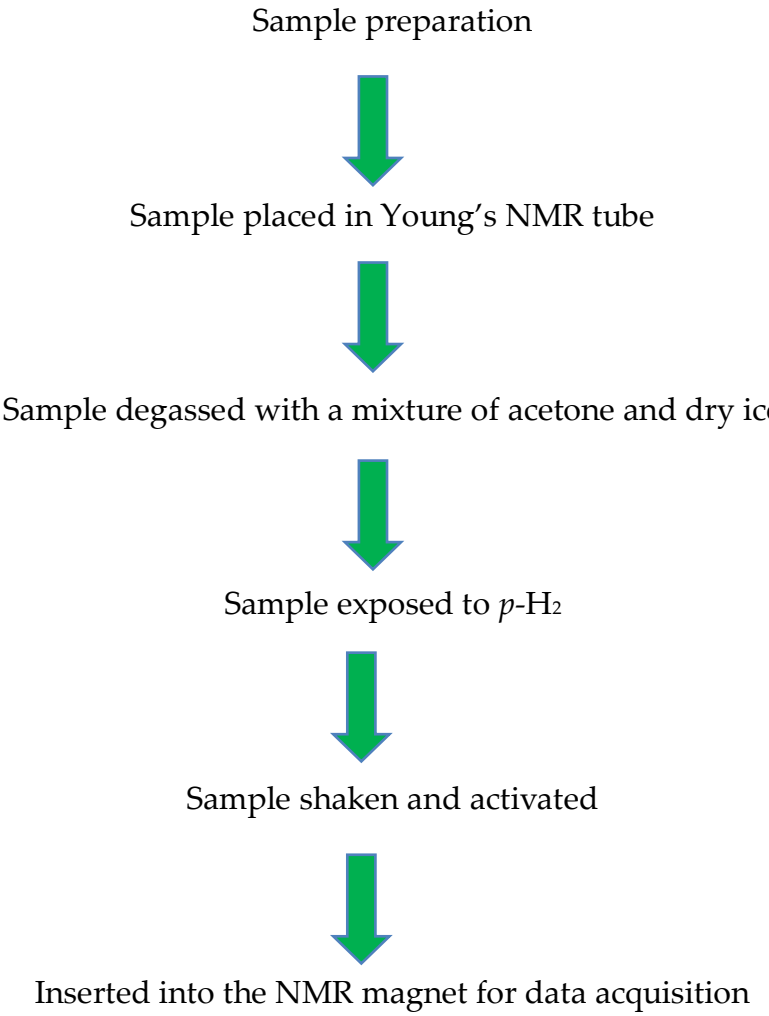

Scheme 3.1: ***Flow diagram depicting the steps involved in the acquisition of a hyperpolarized NMR spectrum.***

Polarization transfer from the *p*-H_2 to a substrate takes place by using ***1***. This polarization transfer is performed in an NMR tube fitted with a Young's valve in a known magnetic field, typically 65 G, by varying the contact time/ shake time between 20-120 s. This process facilitates the *p*-H_2 dissolving in the solution which promotes the formation of a dihydride complex. The sample is then transferred into the NMR magnet for data acquisition.

The following section describes the hyperpolarization studies of the substrates (S_1-S_8).

3.3.1 Nicotinic acid

Nicotinic acid (S_1 in Figure 3.3) is one of the most essential water soluble vitamins. Nicotinic acid has been used for the treatment of dyslipidemias (an abnormal amount of lipids (e.g. cholesterol and/or fat) in the blood) and is particularly effective in controlling HDL cholesterol.[161] Because of its biological relevance it was selected as a potential substrate to study using SABRE. Nicotinic acid possesses a substituent on the heterocyclic ring and is far more interesting to study than the pyridine. Tables B1-B4, Appendix B illustrate the ^{1}H and ^{13}C NMR data for the hyperpolarized sites, the effect of shake time, concentration, temperature on the enhancement and polarization levels.

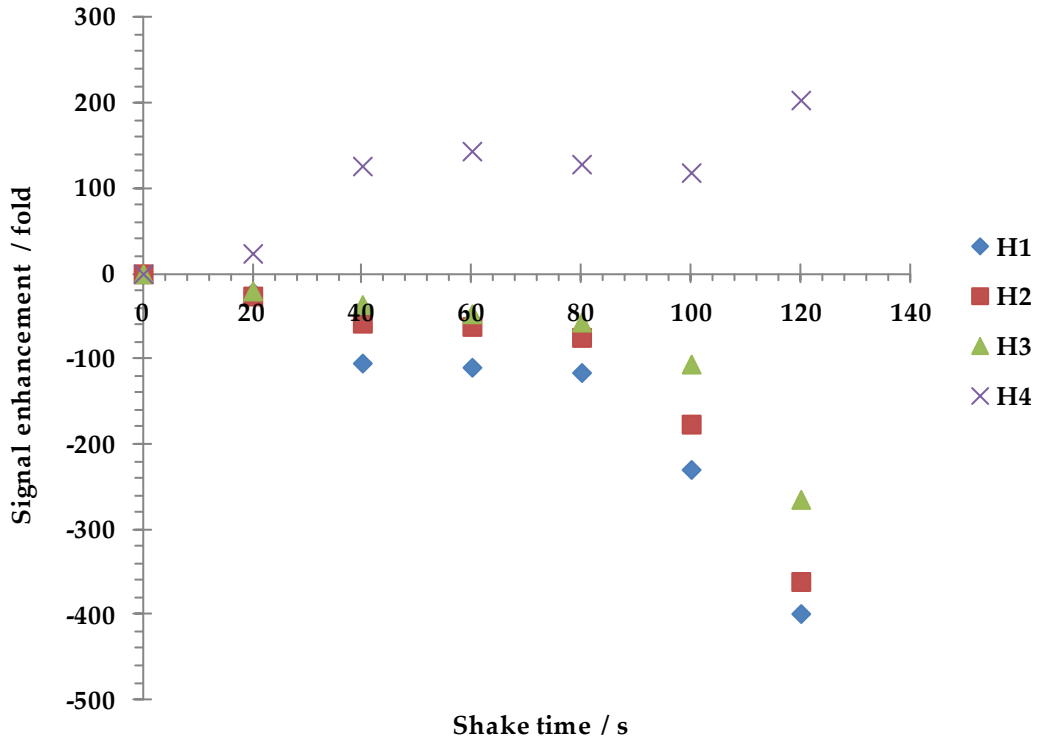

Figure 3.5: Effect of shake time on the extent of the ^{1}H NMR signal enhancement for the indicated proton sites of nicotinic acid (0.055 mmol) when the polarization transfer step is completed in a magnetic field of 65 G.

The hyperpolarization of nicotinic acid (0.055 mmol) in the shake time studies was achieved by activating the sample at 320 K and then bringing *p*-H_2 at a pressure of 3 atm into contact with nicotinic acid through shaking the sample in a magnetic field of 65 G. The sample was then screened by ^{1}H NMR spectroscopy. Figure 3.5 demonstrates that for a shake time of 20 s the signals of its H_1, H_2, H_3 and H_4 resonances were -21.5, -26.1, -20.1 and 23.9 times larger than normal. The enhancement levels for a 120 s shake were -398, -360, -264.6 and 203.8 fold respectively. As the signal to noise ratio S/N scales with the square of the number of scans, the comparable results for the highest enhancement level would require 158,404 scans if a thermally polarized sample

was employed. This measurement would take 132 hours, rather than the 3 s used in this experiment to complete. Figure 3.5 also shows that a shake time of 120 s proved to be optimal to achieve a hyperpolarized state.

Figure 3.5 also illustrates that proton H_1 is more enhanced than all the other proton sites present within the nicotinic acid molecule, thus it is thought to be due to its close proximity to the binding site. The H_2 proton also shows a promising enhancement level because of it's coupling to H_1. The enhancement levels were found to become weaker with increase in number of bonds away from the main route for polarization transfer.[103] Consequently, H_3 and H_4 experience lower levels of enhancement. The carboxylic acids protons do not show any polarization activity due to proton-deuterium exchange with the deutrated protic solvent. Typical thermal and hyperpolarized NMR spectra obtained in case of nicotinic acid are shown in Figure B5, Appendix B.

In the reported theoretical studies, it has been cited that a mixture of longitudinal-z magnetization and longitudinal two spin order of the type I_zS_z is created through the interaction with *p*-H_2.[30] To probe the type of magnetization, a gradient based method is used that employs OPSY (Only *para*hydrogen Spectroscopy), to investigate the presence of zero quantum, single quantum, double quantum and triple quantum terms. Application of a double quantum filter as dq-OPSY results in a removal of the thermally polarized resonances so that only hyperpolarized signals derived from $2I_zS_z$ magnetization are observed. The ^{1}H NMR dq-OPSY spectrum acquired (Figure B6, Appendix B) under the aforementioned conditions therefore consists of signals derived as a result of magnetization transfer from *p*-H_2. Polarization transfer is shown to proceed to all sites within the nicotinic acid molecule using SABRE.

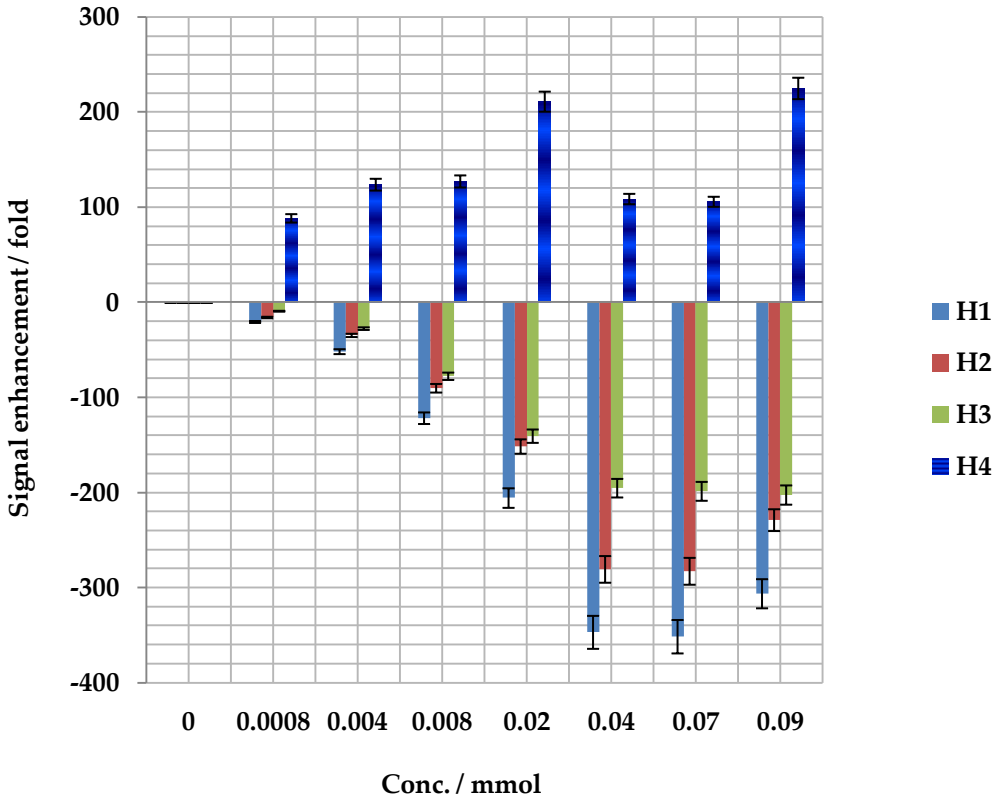

Figure 3.6: *Effect of concentration on the level of ^{1}H NMR signal enhancement for the indicated proton sites of nicotinic acid when the polarization transfer step is completed in a magnetic field of 65 G at 325 K.*

A series of samples were prepared that contained ***1*** and nicotinic acid in order to explore the effect of concentration. These samples were then filled with *p*-H_2 and warmed to 325 K before being shaken for approximately 100 s prior to sample insertion into the NMR magnet for ^{1}H NMR spectral acquisition. ^{1}H NMR spectra were then recorded to assess the degree of signal enhancement shown by the four nicotinic acid proton sites. The data obtained is illustrated graphically in Figure 3.6 and reveals that the degree of signal enhancement has

been maximized at the 0.07 mmol substrate loading level. The enhancement levels achieved for the H_1, H_2, H_3 and H_4 protons sites were -351.5, -282.7, -198.6 and 105.9 times stronger than those of an unpolarized sample.

When the same experiment was repeated for samples where the absolute concentration of ***1*** and nicotinic acid was decreased by a factor of three, the signal enhancement for all H_1, H_2, H_3 and H_4 protons reduced to -205.7, -151.5, -140.6 and 211.5 fold respectively. When the substrate concentration was further decreased to 0.0008 mmol, polarization transfer was still observed and the enhancement levels achieved for all four protons sites were -20.5, -15.8, -9.2 and 88.5 fold. These experiments confirm that even when the substrate is present in low concentration it can be effectively detected, and hence characterised, using SABRE.

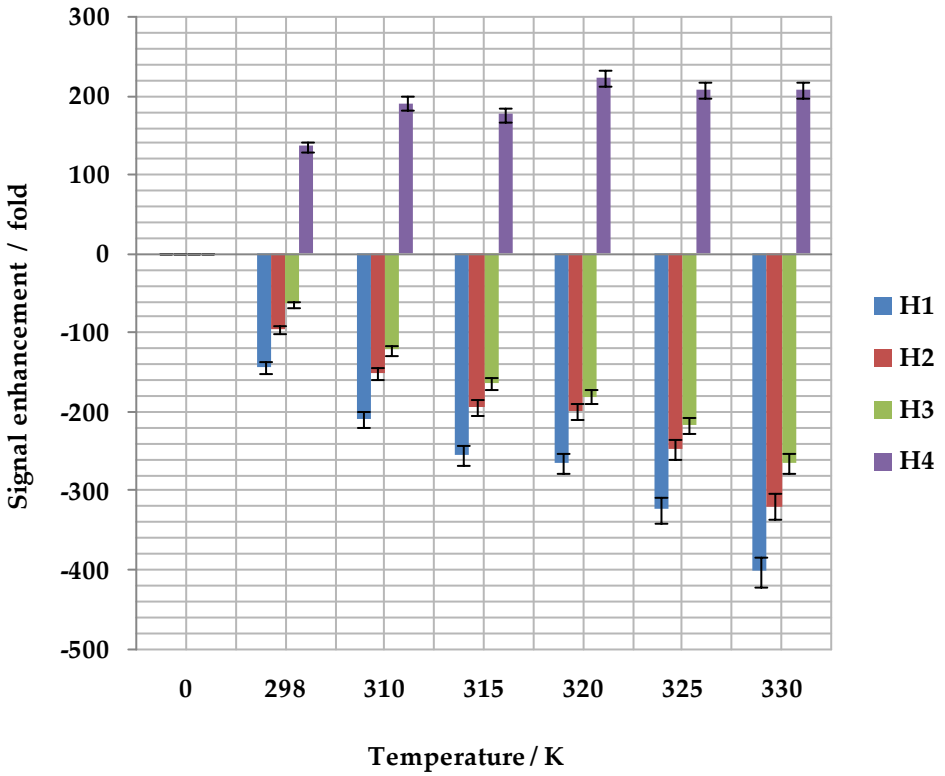

Figure 3.7: ***Effect of temperature on the degree of the ^{1}H NMR signal enhancement for the indicated proton sites of nicotinic acid when the polarization transfer step is completed in a magnetic field of 65 G.***

Figure 3.7 shows that efficient polarization transfer depends on the rate of exchange between *p*-H_2 and the substrate. It shows data from a range of SABRE studies at 65 G. The level of signal enhancement increases with temperature. The highest enhancement level is accomplished for the H_1 proton. Similar effects were observed for the other three proton sites.

The hydride loss exchange rate constant for the complex formed with nicotinic acid was determined to be 1.8 s^{-1} at 310 K. This is higher than that of pyridine which is 0.16 s^{-1} at 310 K in the analogous complex. This is consistent

with the higher levels of polarization achieved with nicotinic acid. As the p*Ka* of nicotinic acid is lower than pyridine (4.85 compared with 5.17),[162] a weaker Ir-N bond is expected which favours ligand exchange. Another fascinating feature of this study was the polarization transfer to all carbon sites in nicotinic acid.

^{13}C NMR data were collected to monitor the transfer of polarization to the ^{13}C nuclei within nicotinic acid. All carbon resonances were observed to be enhanced in the corresponding hyperpolarized ^{13}C NMR spectrum when the magnetization transfer step was completed at 65 G. The corresponding hyperpolarized ^{13}C NMR spectrum contains substantially enhanced resonances for C_1 (δ 166.10), C_2 (δ 152.32), C_3 (δ 149.97), C_4 (δ 137.76), C_5 (δ 126.01) and C_6 (δ 123.61) as shown in Figure B7, Appendix B. Interesting, C_6, which is a carboxylate carbon is also enhanced. Table B8, Appendix B, illustrates the enhancement levels obtained for the carbon sites in nicotinic acid.

The ^{13}C NMR data given in Table B8, Appendix B, was acquired in a single-scan and depicts all the resonances present within the molecule of nicotinic acid. The carbon at δ 153.32, which is close to the nitrogen centre, is very strongly polarized (102.8 fold) and this may enable the transfer of polarization to the aromatic ring system. The relative polarization obtained for the aromatic ring carbons close to the binding site are suitably more polarized than those carbons such as δ 137.76, δ 126.01, and δ 123.61, situated away from the binding site and achieved enhancement levels of 25.1, 20.4 and 18.4 fold respectively. The presence of protons on the C_4 and C_5 positions, combined with the low polarization factor observed for the carbon atom, may imply that the bulk of polarization shared between this pair is located on the proton atom. The

lowest enhancement (5.1 fold) was shown by C_1 (carboxylate carbon), thought to be due to the fact it is located outside the aromatic ring and the proton located on it is not polarized at all. The hyperpolarized ^{1}H and ^{13}C NMR spectra would emphasize this conjecture given that the proton (δ 9.13) as well as carbon on the 1-position (δ 152.32) of the aromatic ring system are strongly enhanced compared with the other resonances on the aromatic ring. Moreover, the carbon atoms which are highly polarized may well be a result of polarization being shared with the hydrogen nuclei located in their vicinity.

3.3.2 Isonicotinic acid

Isonicotinic acid (S_2 in Figure 3.3) is an isomer of nicotinic acid with a carboxyl group on the 4-position on the aromatic ring. The carboxyl group is present at the 3-position in nicotinic acid.[162] Isonicotinic acid has two equivalent protons, H_1 and H_2, giving rise to two resonances in the ^{1}H NMR spectrum. Tables B9-B12, Appendix B, show the proton and carbon NMR data for the hyperpolarized sites, the effect of shake time concentration on temperature on the enhancement and polarization levels.

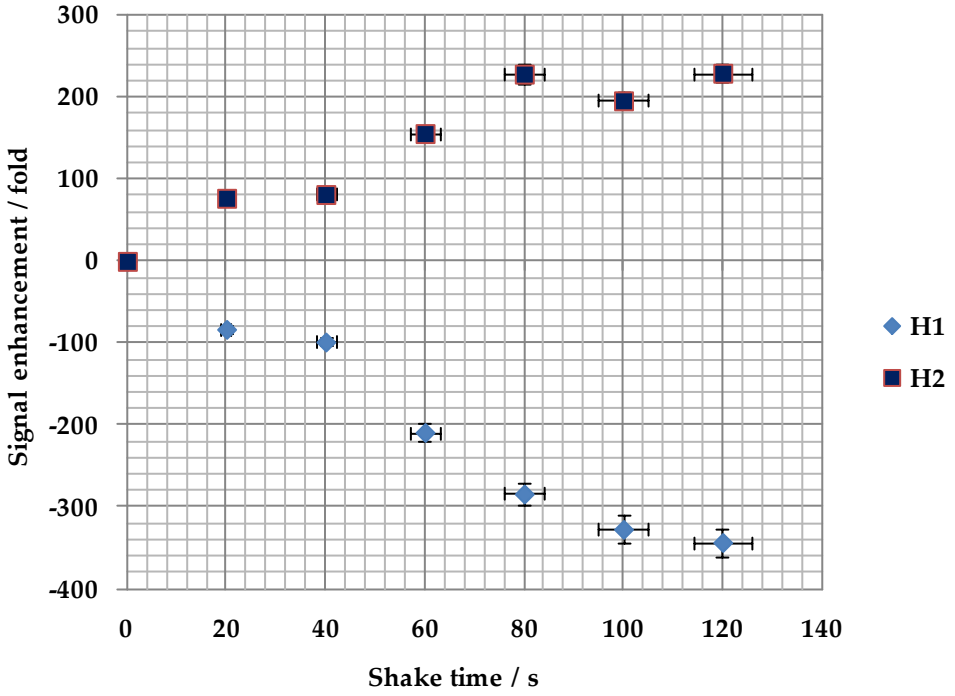

Figure 3.8: Effect of shake time on the extent of the ^1H NMR signal enhancement for the indicated proton sites of isonicotinic acid when the polarization transfer step is completed in a magnetic field of 65 G.

As shown in Figure 3.8, the shake time dependence of isonicotinic acid revealed that both protons H_1 and H_2 can be increased in intensity by increasing the shake time up to 120 s. The OH resonance of carboxylic group does not show any observable enhancement, presumably because of deutration. For the shake time studies carried out at 20 s, the enhancement levels for the heterocyclic ring protons H_1 and H_2 were -83.03 and 76.99 fold, while the enhancement levels observed at 120 s were -343.2 and 229.65 fold, respectively. The polarization transfer ability demonstrated by both the heterocyclic ring protons in isonicotinic acid is therefore comparable.

Typical thermal and hyperpolarized spectra obtained in the case of isonicotinic acid are shown in Figure B13, Appendix B, while Figure B14, Appendix B, represents the dq-OPSY spectrum which demonstrates *p*-H_2 transfer to all sites within the isonicotinic acid molecule under SABRE.

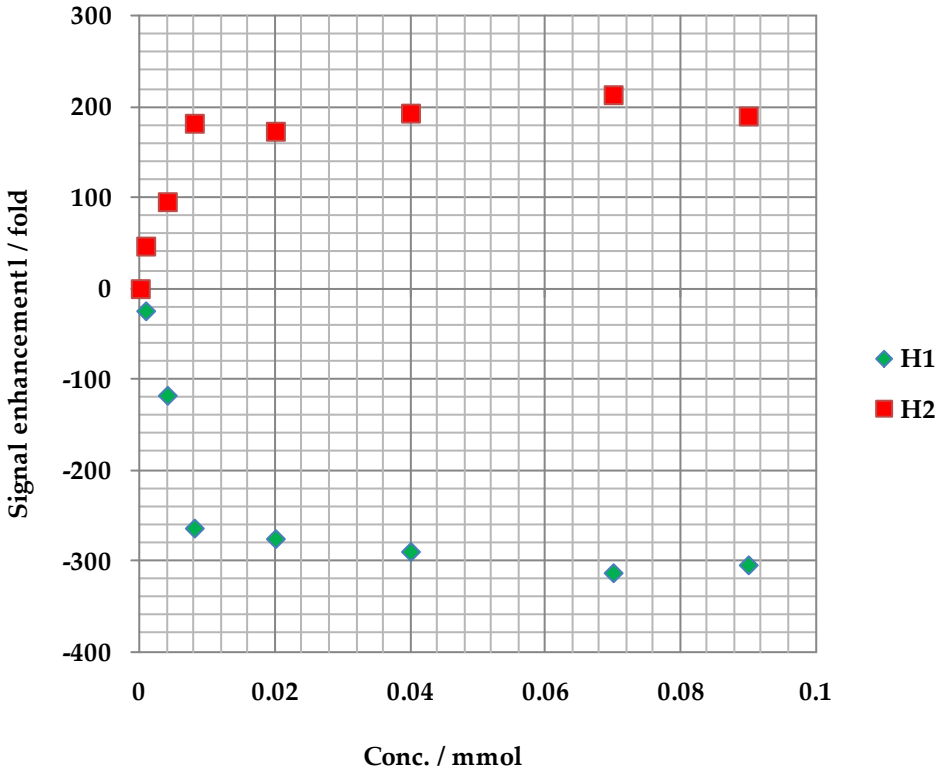

Figure 3.9: ***Effect of substrate concentration on the extent of the ^1H NMR signal enhancement for the indicated proton sites of isonicotinic acid when the polarization transfer step is completed in a magnetic field of 65 G.***

As demonstrated in Figure 3.9, the effect of concentration on isonicotinic acid polarization is similar to that observed for nicotinic acid. The enhancement levels observed for H_1 and H_2 protons with concentration of 0.0008 mmol were -

24.4 and 46.9 fold, while the maxima were observed at a concentration of 0.09 mmol and led to the signal enhancements of -304.3 and 190.2 fold respectively. The overall trend in enhancement levels was to increase in concentration over the range studied.

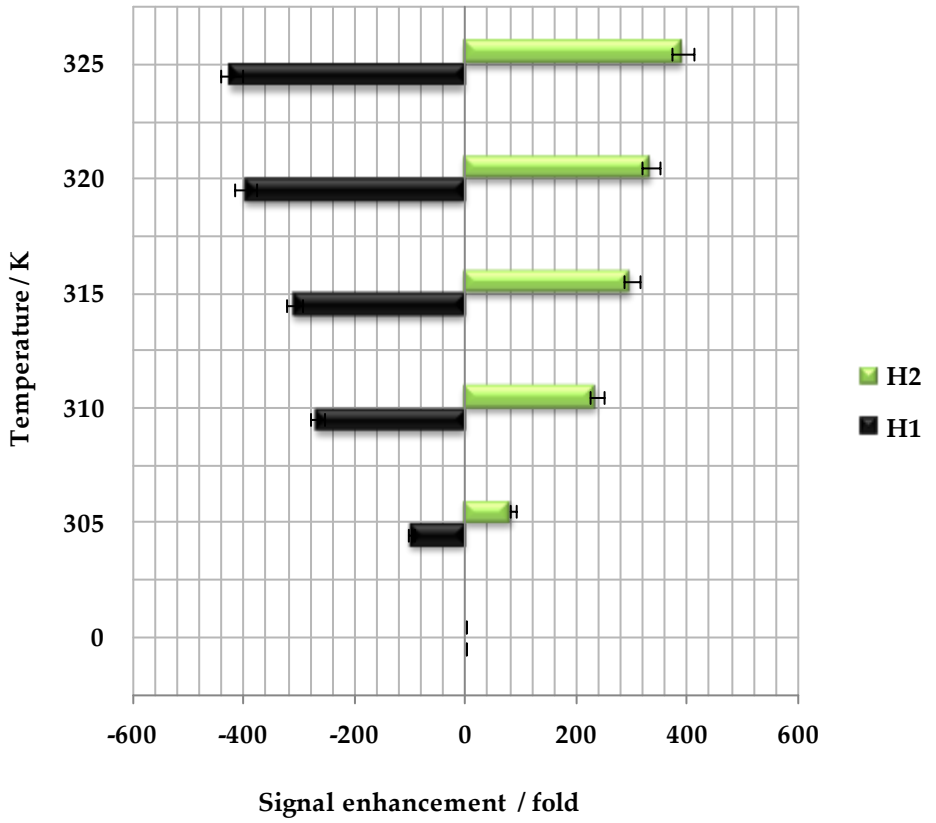

Figure 3.10: ***Effect of temperature on the extent of the ^{1}H NMR signal enhancement for the indicated proton sites of isonicotinic acid when the polarization transfer step is completed in a magnetic field of 65 G.***

The temperature studies were conducted in order to know how the exchange rates of *p*-H_2 and the substrates affect the polarization transfer efficiency to different functionalities within the same molecule as demonstrated

in Figure 3.10. Polarization of isonicotinic acid was achieved at various temperatures using the standard SABRE procedure in a magnetic field of 65 G. The maximum enhancement levels were obtained at 325 K (- 422.6 and 391.8 fold for H_1 and H_2 protons as graphically shown in Figure 3.10). The EXSY experiment revealed a rate constant of 2.1 s^{-1} for the hydride exchange in isonicotinic acid at 310 K as compared to 1.8 s^{-1} for nicotinic acid, although the reported pKa of isonicotinic acid is the same as that of nicotinic acid with a value of 4.85.

The observation of slightly more rapid H_2 exchange for isonicotinic acid would suggest a higher polarization level might be expected. This is observed experimentally since for samples concentrations of 0.09, 0.07, 0.04 and 0.02 mmol the relative enhancement levels are - 422.6, -396.2, -309.1 and -267.8 fold for isonicotinic acid and - 402.5, -323.6, -264.8 and -255.4 fold for nicotinic acid. The change in position of the carboxylic group to the *para* position in isonicotinic acid therefore results in more efficient polarization sharing.

^{13}C NMR data were also acquired to examine the transfer of polarization to the ^{13}C nuclei within isonicotinic acid. The corresponding hyperpolarized ^{13}C NMR spectrum revealed the polarization transfer to all carbon sites in isonicotinic acid. The corresponding hyperpolarized ^{13}C NMR spectrum exhibits enhanced resonances for C_1 (δ 166.07), C_2 (δ 149.58), C_3 (δ 138.10) and C_4 (δ 121.56) as shown in Figure B15, Appendix B. Table B16, Appendix B, illustrates the enhancement levels obtained for the carbon sites in isonicotinic acid.

^{13}C NMR data in Table B16, Appendix B, illustrate the enhancement levels observed for isonicotinic acid. C_2 and C_4 (δ 149.58 and δ 121.56) carbons are strongly polarized and the relative signal enhancement levels achieved for these carbons are (94.7 and 79.1 fold). The carbons C_1 (δ 166.07) and C_3 (δ 138.10) achieved enhancement levels of 10.4 and 15.4 fold respectively. Furthermore, C_1, the carboxylate carbon which is least enhanced and the proton on that carbon site is not enhanced. Moreover, akin to nicotinic acid, the carbon atom which is most polarized is located close to binding site.

4.3.3 Methyl nicotinate

Methyl nicotinate (S_3 in Figure 3.3) is an ester of methyl alcohol and nicotinic acid. It is used in the formation of face creams.[162, 163] Tables B17-B20, Appendix B, show the proton and carbon NMR, the effect of shake time, substrate concentration and temperature on its enhancement and polarization levels.

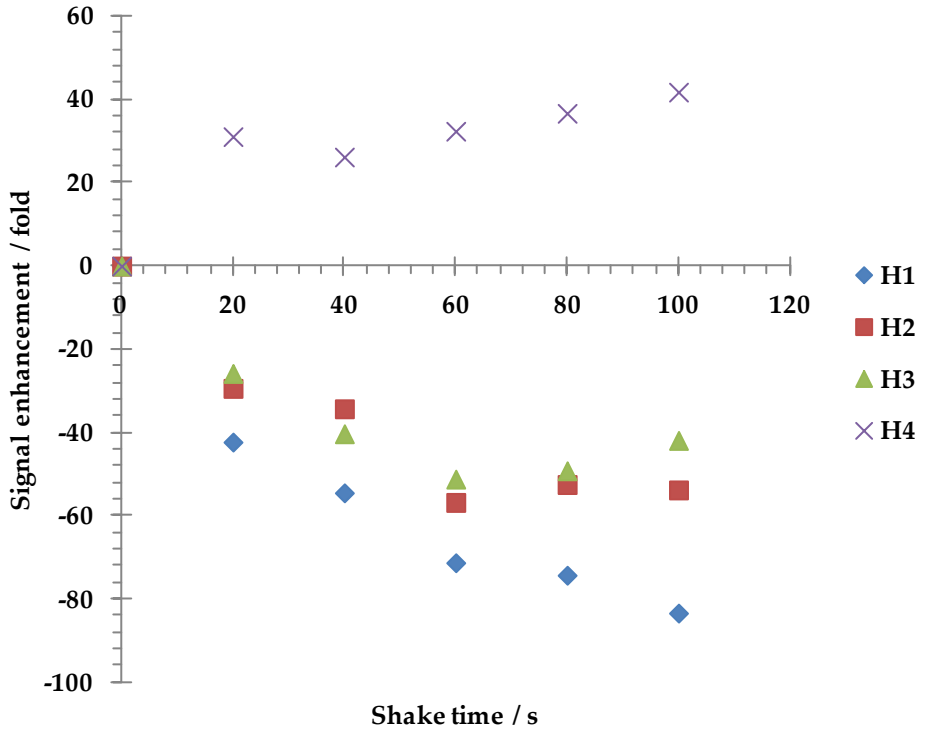

Figure 3.11: Effect of shake time on the extent of the ^1H NMR signal enhancement for the indicated proton sites of methyl nicotinate when the polarization transfer step is completed in a magnetic field of 65 G at 310 K.

In the shake time studies at 310 K, the signal enhancement levels seen for the methyl nicotinate were substantial (Figure 3.11), but significantly smaller than those observed for isonicotinic acid. After a shake time of 20 s the enhancement level reached - 42.3, -29.4, -25.1 and 31.1 fold for H_1, H_2, H_3 and H_4 protons, whilst with a shake time of 100 seconds these enhancement levels were increased to -83.4, -53.8, -41.9 and 41.8 fold respectively. This trend matches that observed for the previously described substrates in this chapter.

Typical thermal and hyperpolarized spectra obtained in the case of methyl nicotinate are shown in Figure B21, Appendix B, while Figure B22, Appendix B, depicts the dq-OPSY spectrum which demonstrates *p*-H_2 transfer to all sites within methyl nicotinate using SABRE.

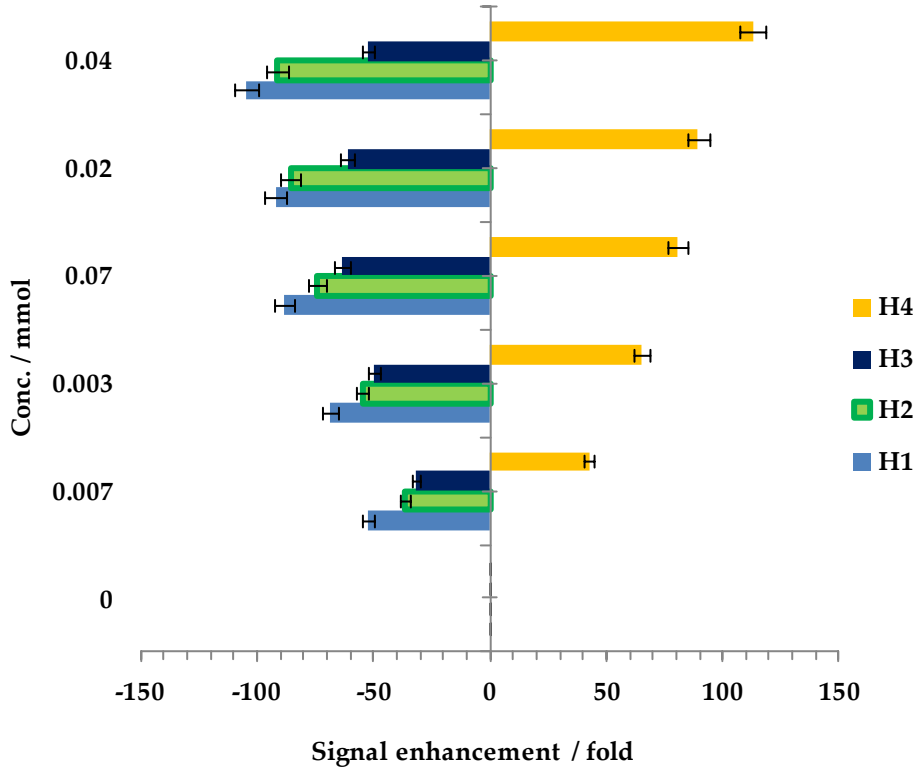

Figure 3.12: Effect of substrate loading on the extent of the ^1H NMR signal enhancement for the indicated proton sites of methyl nicotinate when the polarization transfer step is completed in a magnetic field of 65 G.

In concentration studies at 320 K, the H_1 proton showed an enhancement of -52.5 fold at a concentration of 0.007 mmol, while with the same substrate concentration H_2, H_3 and H_4 protons present on the aromatic ring showed -36.5 -31.9 and 42.7 fold signal enhancements respectively. The acetate protons showed no polarization transfer activity. The enhancement levels obtained in the case of methyl nicotinate were much smaller in magnitude compared to the concentration studies carried out with the aforementioned substrates. The maximum polarization transfer was observed at a substrate concentration of 0.04 mmol conducted in a magnetic field of 65 G with enhancement levels reaching up to -104.6, -91.5, -52.1 and 112.8 fold for H_1, H_2, H_3 and H_4 protons, as summarised in Figure 3.12.

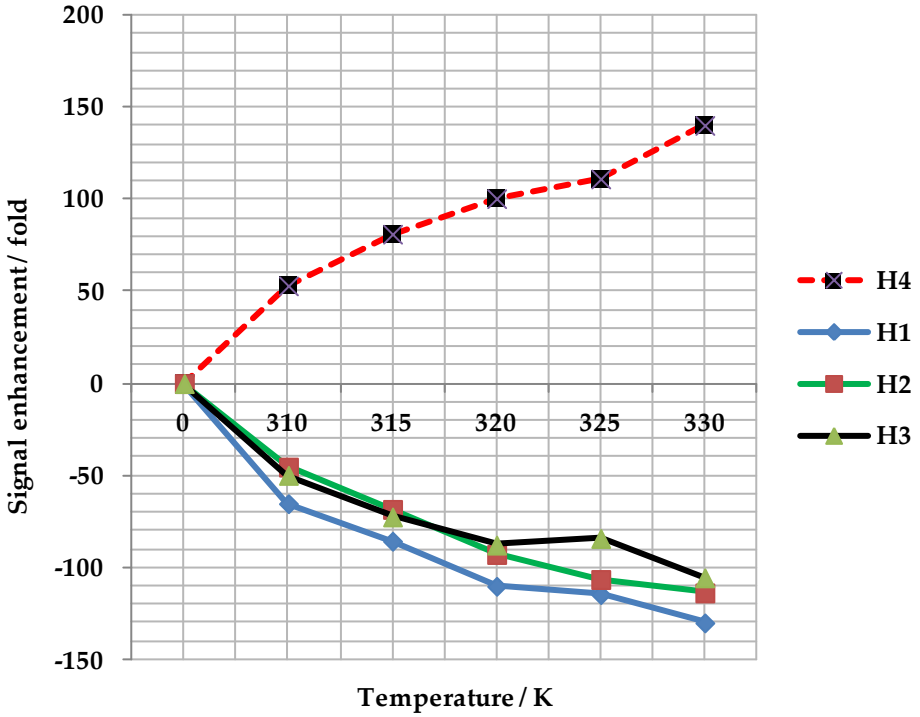

Figure 3.13: Effect of temperature on the extent of the ^1H NMR signal enhancement for the indicated proton sites of methyl nicotinate when the polarization transfer step is completed in a magnetic field of 65 G.

Figure 3.13 shows that the highest enhancement level is achieved for a temperature of 330 K and at the proton which is close to the binding site. The acetate group protons do not experience any detectable enhancement at any temperature; this might again be because of the very fast exchange with the deutrated solvent results in resonances that are undetectable at an NMR time scale. In case of methyl nicotinate, the rate constant for hydride exchange at 310 K was determined to be 0.90 s^{-1}. The reported pKa for methyl nicitonate[142] is 2.8 which suggests it will bind weakly through the lone pair of electrons associated with the nitrogen centre.

^{13}C NMR data acquired for methyl nicotinate demonstrates the polarization transfer to the ^{13}C nuclei. The corresponding hyperpolarized ^{13}C NMR spectrum exhibits enhanced resonances for C_1 (δ 165.03), C_2 (δ 153.58), C_3 (δ 148.08) and C_4 (δ 137.14), C_5 (δ 126.01), C_6 (δ 123.54) and C_7 (δ 55.2) as shown in Figure B23, Appendix B. Table B24, Appendix B, illustrates the enhancement levels obtained for the carbon sites in methyl nicotinate.

^{13}C NMR data given in Table B24, Appendix B, demonstrates that all the carbon resonances are observable in methyl nicotinate. C_2 and C_3 (δ 153.58 and δ 148.08) carbons are strongly polarized. The comparative signal enhancement levels achieved for the aromatic ring carbons (C_4, C_5, C_6) are greater than for C_1 (δ 165.03) and C_7 (δ 55.2) located outside the aromatic ring. The quaternary carbon atom shows little polarization transfer, which may well be a result of the polarization not being shared with any hydrogen nuclei, as happened for C_2 and C_3 . It would seem that the transfer of polarization from proton to carbon nuclei is promoted and therefore the polarization transfer to C_2 and C_3 carbons was significant.

3.3.4 Isonicotinamide

Isonicotinamide (S_4 in Figure 3.3) is an isomer of nicotinamide with great biological significance. In isonicotinamide, the amide group is present on the 4-position as compared to the nicotinamide in which it is present on 3-position. Isonicotinamide compounds are antagonists of orexin receptors (chemicals that are naturally produced by an area of the brain called the hypothalamus) which are useful in the treatment or prevention of neurological and psychiatric disorders.[165] Because of its biological significance; it is selected as a substrate to

study using SABRE. Tables B25-B28, Appendix B, demonstrate the proton and carbon NMR assignments, the effect of shake time concentration and the effect of temperature on the enhancement and polarization levels.

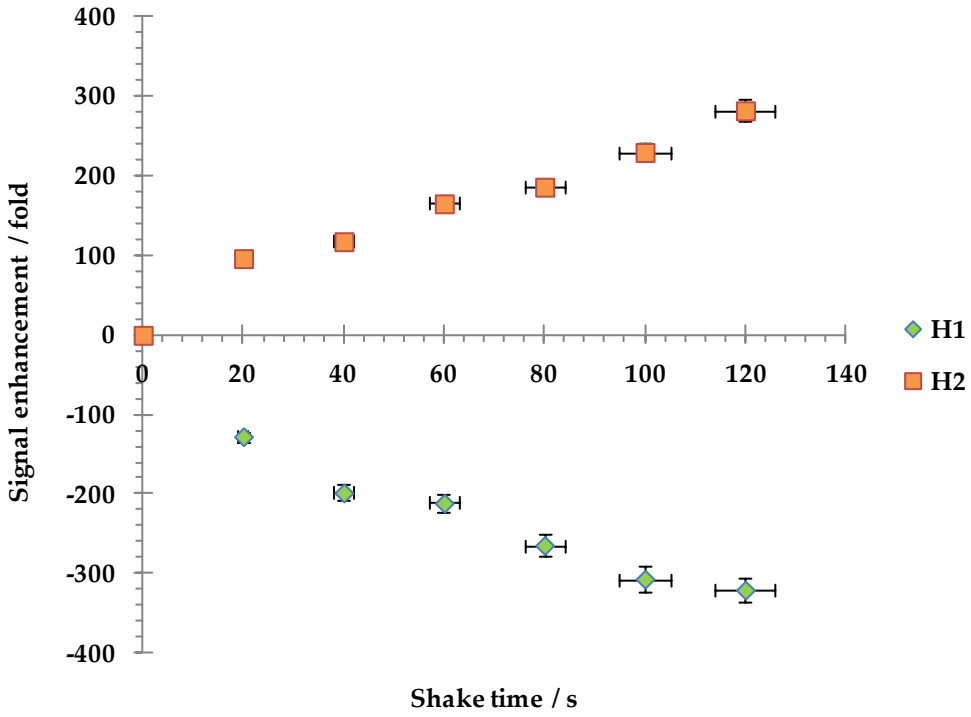

Figure 3.14: Effect of shake time on the extent of the ^1H NMR signal enhancement for the indicated proton sites of isonicotinamide when the polarization transfer step is completed in a magnetic field of 65 G.

In shake time studies at 320 K, the enhancement levels achieved for isonicotinamide (0.048 mmol) were still smaller than those of isonicotinic acid as can be seen in Figure 3.14. The enhancement levels reached are -127.6 and 96.5 fold for H_1 and H_2 protons after 20 s, while with a shake time of 120 s the enhancement levels were amplified to -320.7 and 282.5 fold respectively.

Typical thermal and hyperpolarized spectra obtained in case of isonicotinamide are shown in Figure B29, Appendix B, while Figure B30, Appendix B, illustrates the corresponding single-scan dq-OPSY spectrum which demonstrates that *p*-H_2 transfer proceeds to all sites in case of isonicotinamide.

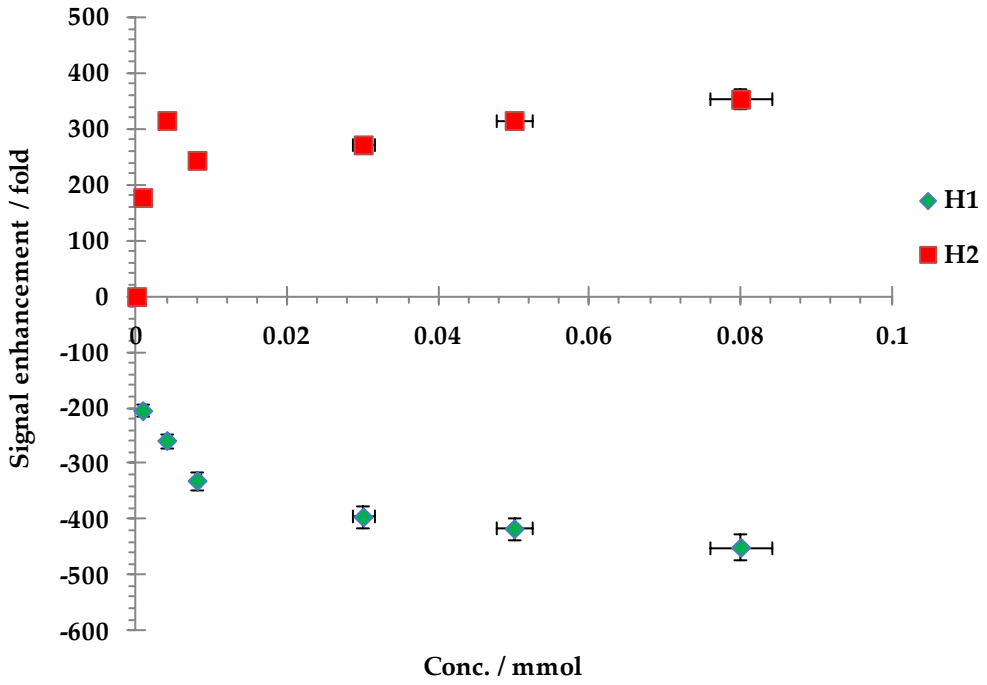

Figure 3.15: ***Effect of substrate loading on the extent of the ^{1}H NMR signal enhancement for the indicated proton sites of isonicotinamide when the polarization transfer step is completed in a magnetic field of 65 G at 325 K.***

The concentration studies of isonicotinamide demonstrated that the maximum signal enhancement observed was - 449 fold for the protons at the *ortho* position on the aromatic ring (Figure 3.15), while the protons present at the *meta* position on the aromatic ring showed an enhancement of 354 fold with a concentration of 0.08 mmol at 325 K. The enhancement levels obtained for

isonicotinamide were much higher in magnitude than those of isonicotinic acid under similar conditions.

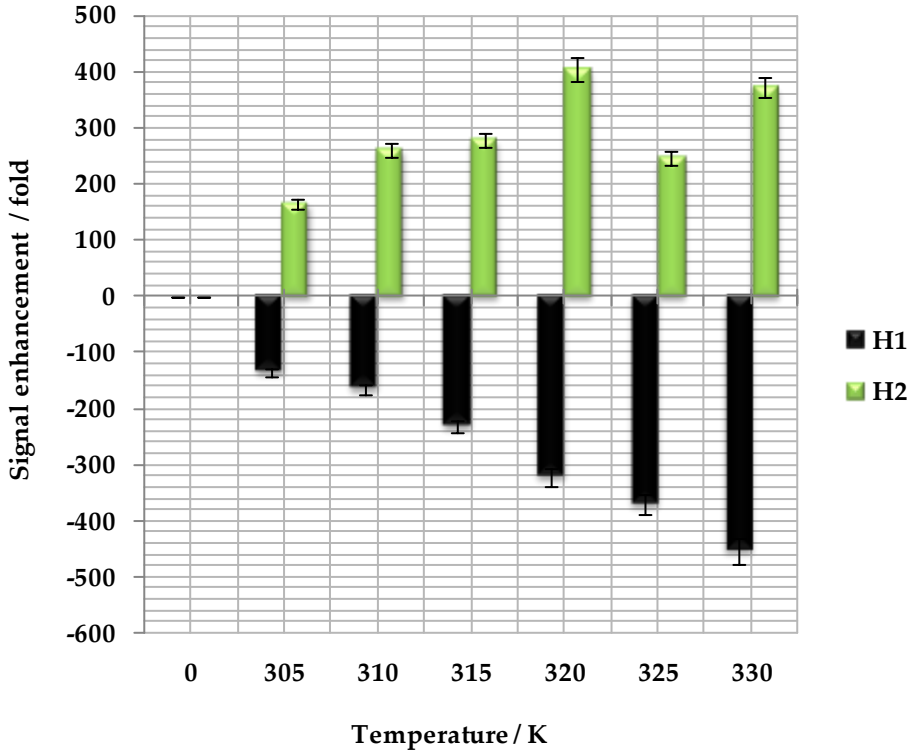

Figure 3.16: ***Effect of temperature on the extent of the ^{1}H NMR signal enhancement for the indicated proton sites of isonicotinamide when the polarization transfer step is completed in a magnetic field of 65 G at 330 K.***

As demonstrated in Figure 3.16 a maximum enhancement level for the *ortho* protons of -453 is achieved with a temperature of 330 K. The *meta* protons receive less polarization from the active iridium complex at this point and their signal enhancement is only 372.4 fold. The rate constant for hydride exchange in isonicotinamide was determined to be 3.6 s^{-1} at 310 K which is higher than the isonicotinic acid (2.1 s^{-1}). As isonicotinamide has pKa 3.3 when compared to the

isonicotinic acid pKa value of 4.8, faster exchange is possible for isonicotinamide.

Single scan ^{13}C NMR hyperpolarized spectrum acquired for isonicotinamide show polarization transfer to ^{13}C nuclei. The hyperpolarized ^{13}C NMR spectrum exhibited enhanced resonances for C_1 (δ 165.02), C_2 (δ 150.58), C_3 (δ 137.06) and C_4 (δ 122.01) as shown in Figure B31, Appendix B. Table B32, Appendix B, illustrates the ^{13}C data and enhancement levels obtained for the carbon sites in isonicotinamide.

^{13}C data given in Table B32, Appendix B, demonstrates that the carbon C_1 at δ 165.02 is the most polarized in comparison to the carbons C_2, C_3 and C_4 located at δ 158.58, δ 137.06, and δ 122.01 within the aromatic ring. Like isonicotinic acid, the polarization transfer to the C_1 carbon atom is more pronounced due its presence in close proximity to the binding site than its counterparts C_2, C_3 and C_4.

3.3.5 Pyrazine

Pyrazine (S_5 in Figure 3.3) is a symmetrical molecule that possesses a single proton resonance in ^1H NMR spectroscopy. Pyrazine belongs to the point group D_{2h}. Derivatives of pyrazine are of great biological importance, with phenazines being well known for their antitumor diuretic and antibiotic characteristics;[165] consequently it was chosen as a prospective substrate to study SABRE. The proton and carbon NMR data of pyrazine, the effect of shake time, substrate concentration and the effect of temperature on the enhancement and polarization level are given in Tables B33-B36, Appendix B.

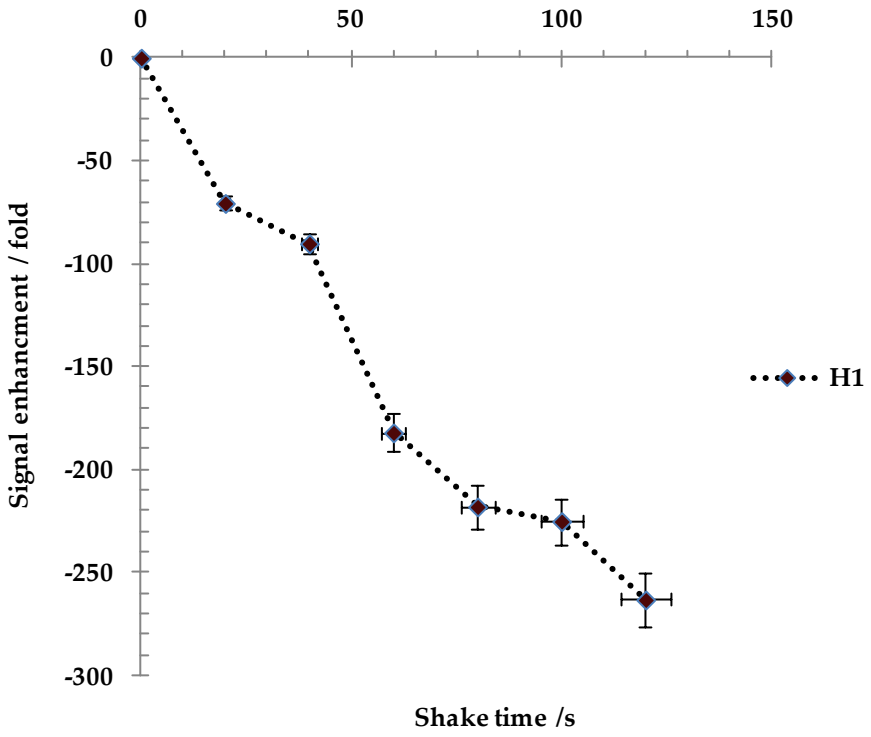

Figure 3.17: ***Effect of shake time on the extent of the ^{1}H NMR signal enhancement for the indicated proton sites of pyrazine when the polarization transfer step is completed in a magnetic field of 65 G.***

The hyperpolarization studies involving pyrazine were accomplished by activating the sample at 310 K by exposure to *p*-H_2 at 3 bar pressure and then shaking he sample in a magnetic field of 65 G. The sample was then monitored by ^{1}H NMR spectroscopy. For a shake time of 20 s, the magnitude of the H_1 resonance was -70.6 times larger than the spectrum acquired under the Boltzmann conditions. The enhancement levels for a 60 s shake time was -182.1; while those for 120 s shake time was -263.3 respectively. Figure 3.17 shows that the H_1 proton is substantially enhanced because of the magnetic and chemical equivalence and the lower number of spins receiving the polarization. Typical thermal and hyperpolarized spectra obtained in case of pyrazine are shown in

Figure B37, Appendix B, while Table B38, Appendix B, depicts the dq-OPSY spectrum which demonstrates the *p*-H_2 transfer to pyrazine is substantial.

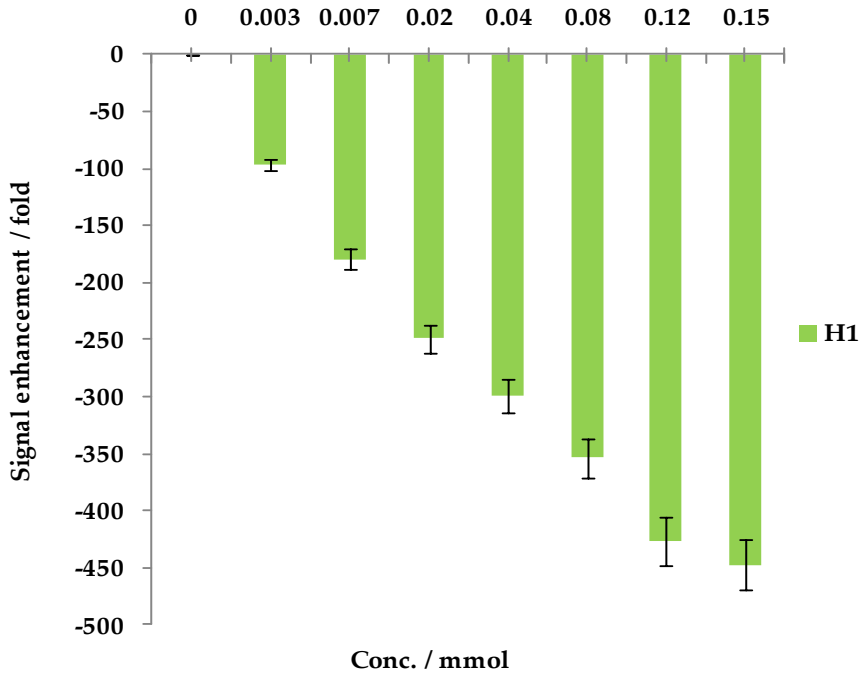

Figure 3.18: ***Effect of substrate loading on the extent of the ^{1}H NMR signal enhancement for the indicated proton sites of pyrazine when the polarization transfer step is completed in a magnetic field of 65 G.***

The concentration studies of pyrazine were performed at 320 K by using a series of samples that contained ***1*** (0.0031 mmol) and pyrazine with concentration varied from 0.15 mmol to 0.003 mmol. These samples were exposed to *p*-H_2 and warmed to 325 K before being shaken for approximately 20 s prior to sample insertion. ^{1}H NMR spectra were recorded to assess the degree of signal enhancement in the pyrazine. The data are illustrated graphically in Figure 3.18 and this reveals that the degree of enhancement is maximized at the

0.15 mmol substrate loading, where proton H_1 is - 447.5 times stronger than normal (polarization temperature 320 K). When the same experiment is repeated for samples where the absolute concentration of ***1*** is kept constant and the pyrazine is reduced to 0.003 mmol, the signal enhancement is reduced to - 96.9 fold. It is therefore clear that there is a substrate concentration dependence on the efficiency of the polarization transfer process.

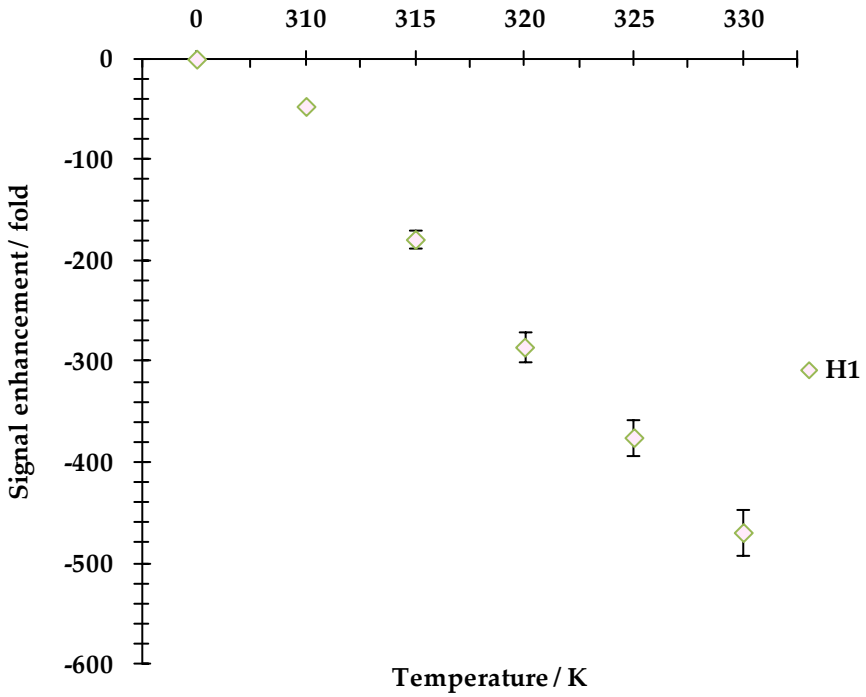

Figure 3.19: ***Effect of temperature on the extent of the ^1H NMR signal enhancement for the indicated proton sites of pyrazine when the polarization transfer step is completed in a magnetic field of 65 G.***

The temperature study data is shown graphically in Figure 3.19 and this illustrates that an increase in temperature has a profound effect on the proton

signal in terms of enhancement level. The higher levels of signal enhancement observed in the case of pyrazine are attributed to the formation of an active iridium complex instantly on addition of *p*H_2. At 310 K, the hydride exchange rate constant observed for the pyrazine is 4.2 s^{-1}. The reported pKa for pyrazine [141, 143] is 0.65 compared to 3.3 for isonicotinamide and 4.85 isonicotinic acid. The higher level of signal enhancement achieved for pyrazine suggested that the pKa favours a dissociative process necessary for the hyperpolarized state to be formed in bulk. A single-scan ^{13}C NMR spectrum collected in case of pyrazine is shown in Figure B39, Appendix B. Table B40, Appendix B depicts the ^{13} C data acquired for pyrazine. This hyperpolarized ^{13}C NMR spectrum consists of only a single resonance because it is a highly symmetrical molecule. The carbon C_1 at δ 144.95 is strongly polarized along with the proton located on the analogous position within the aromatic ring system.

3.3.6 Isoniazid

Isoniazid (S_6 in Figure 3.3) has great medical significance because it is used for the prevention and treatment of tuberculosis (TB).[166] Tuberculosis is a chronic disease of lungs and in humans it is caused by bacteria called Mycobacterium tuberculosis. Table B41 in Appendix B illustrates the proton and carbon NMR data for the hyperpolarized sites in Isoniazid. Tables B42-B44, Appendix B, mirror the effect of shake time, concentration and temperature on enhancement and polarization levels respectively.

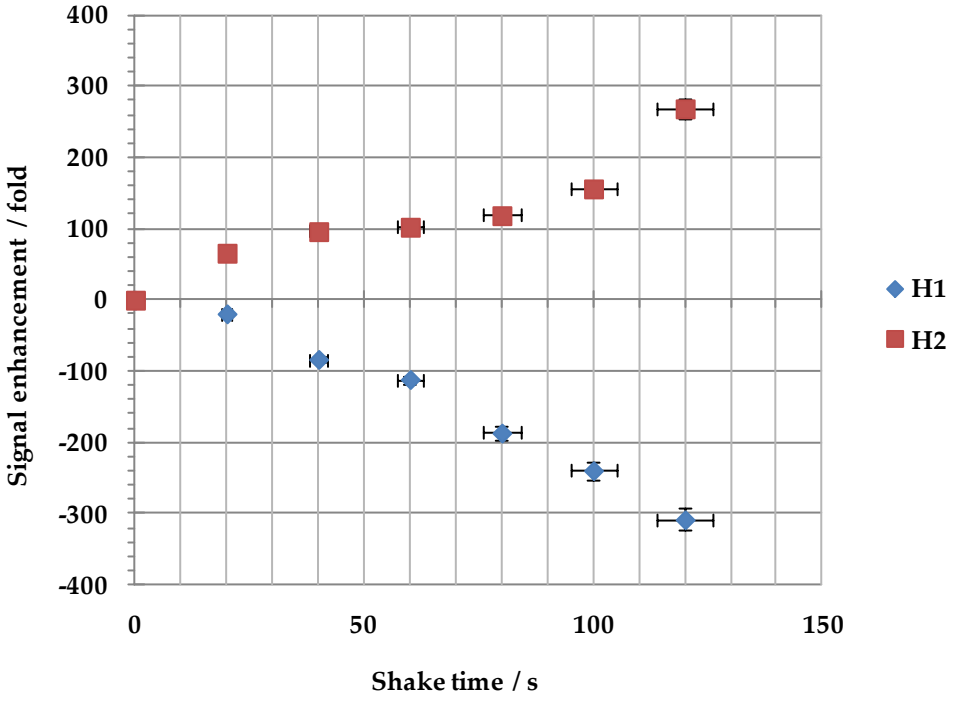

Figure 3.20: ***Effect of shake time on the extent of the ^{1}H NMR signal enhancement for the indicated proton sites of isoniazid when the polarization transfer step is completed in a magnetic field of 65 G.***

The hyperpolarization of isoniazid was achieved by activating the sample at 323 K and then bringing the *p*-H_2 into contact with isoniazid through shaking the sample in a magnetic field of 65 G. The sample is then monitored by ^{1}H NMR spectroscopy. For a shake time of 20 s, the enhancement levels for the proton sites H_1 and H_2 were -19.2 and 65.2 fold. The enhancement levels for a 60 s shake were -111.4 and 102.4 fold, while those for a 120 s shake were observed to be -308.3, and 268.6 fold respectively (see Figure 3.20).

As demonstrated in Figure 3.20, it is obvious shows that H_1 is the most enhanced proton sites within the isoniazid molecule. The H_2 proton also shows

promising enhancement levels. As the main route for polarization transfer is through scalar couplings the protons H_3 and H_4 experience lower level of enhancement. The amide protons do not show any polarization transferring activity because of proton-deuterium exchange upon addition of deutrated solvent.

Typical thermal and hyperpolarized spectra obtained for the case of isoniazid are shown in Figure B45, Appendix B, while Figure B46, Appendix B, depicts the dq-OPSY spectrum which demonstrates the *p*-H_2 transfer to all sites within isoniazid using SABRE.

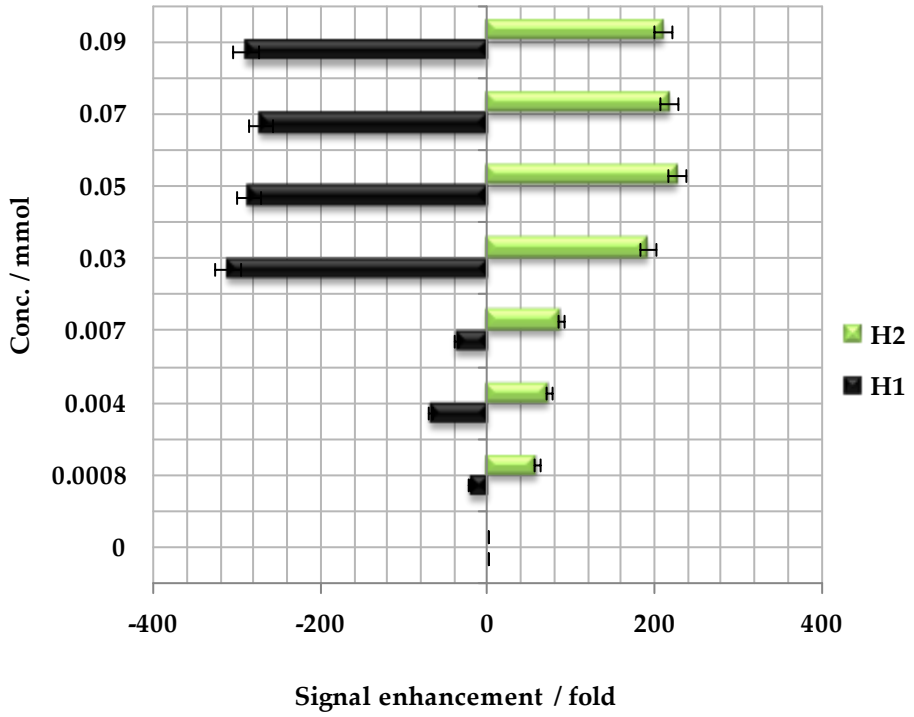

Figure 3.21: *Effect of concentration on the extent of the ^1H NMR signal enhancement for the indicated proton sites of isoniazid when the polarization transfer step is completed in a magnetic field of 65 G.*

A series of samples were prepared that contained the ***1*** (0.0031 mmol) and isoniazid containing 0.09, 0.07, 0.05, 0.03, 0.007, 0.004 and 0.0008 mmol in each sample. These samples were then filled with *p*-H_2 and warmed to 318 K before being shaken for approximately 20 s before sample insertion. ^{1}H NMR spectra were recorded to gauge the degree of signal enhancement shown by the two isoniazid proton sites. These data are illustrated graphically in Figure 3.21 and reveal that degree of enhancement is maximized at a substrate loading of 0.09 mmol where protons H_1 and H_2 are -290.7 and 209.9 times stronger than normal when polarization is undertaken at 318 K. When the same experiment is repeated for samples where the absolute concentration of ***1*** and isoniazid is reduced to 0.0008 mmol, the signal enhancement was observed to be reduced to -22.1 and 59.1 fold for H_1 and H_2 protons respectively.

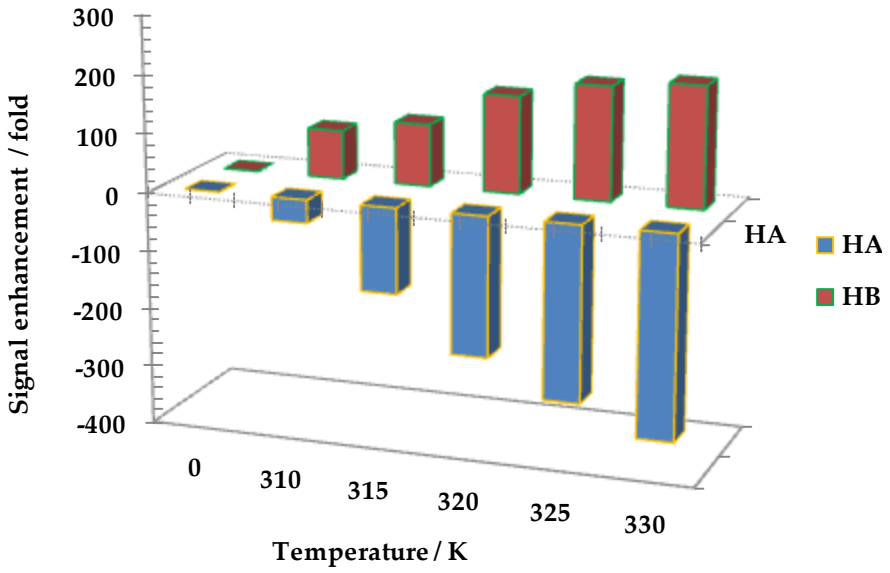

Figure 3.22: ***Effect of temperature on the extent of the ^{1}H NMR signal enhancement for the indicated proton sites of isoniazid when the polarization transfer step is completed in a magnetic field of 65 G.***

Figure 3.22 shows that the highest enhancement level is achieved at proton which is close to the binding site. An increase in temperature has a profound effect on the enhancement levels of this particular proton site and it exchanges efficiently with *p*-H_2 molecule. The rate constant for hydride exchange in isoniazid was determined to be 3.3 s^{-1} at 310 K. The isoniazid is more enhanced as compared to isonicotinamide which is indicative of formation of a more active iridium complex.

^{13}C NMR data acquired for isoniazid demonstrated the polarization transfer to all the ^{13}C site and the corresponding hyperpolarized ^{13}C NMR spectrum exhibits enhanced resonances for C_1 (δ 162.91), C_2 (δ 150.21), C_3 (δ 139.80) and C_4 (δ 121.14) shown in Figure B47, Appendix B. Table B48, Appendix B, illustrates the enhancement levels obtained for the carbon sites in isoniazid.

The hyperpolarized ^{13}C NMR spectrum as shown in Figure B47, Appendix B, was collected in a single scan in which all the resonances are observable. C_2 and C_4 (δ 139.80 and δ 121.14) carbons achieved polarized signal enhancement of 85.4 and 65.1 fold. The comparative enhancement levels achieved for the C_1, C_3 carbons located at δ 162.91 and δ 139.80 suitably least enhanced with enhancement levels of 14.9 and 21.4 fold. The information gained from the hyperpolarized ^1H NMR spectrum would certainly suggest that the proton on the *ortho* position is strongly enhanced compared with the other proton resonance at the *meta* position on the aromatic ring.

3.3.7 Purine

Purine (S_7 in Figure 3.3) is a heterocyclic compound, consisting of a pyrimidine ring fused to an imidazole ring. The derivatives of purine are guanine and adenine[164, 165]. The structures of purine, adenine and guanine are shown in Figure 3.23.

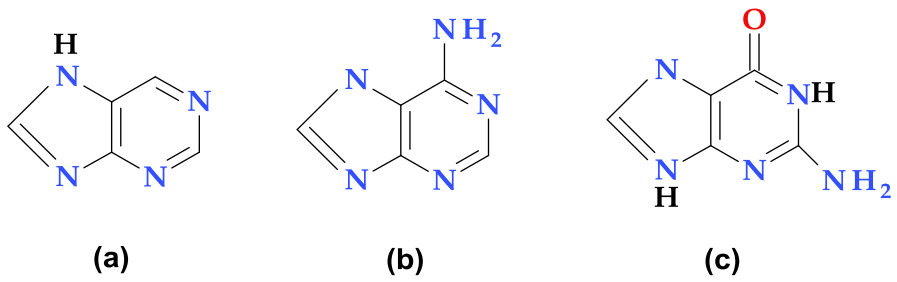

Figure 3.23: Structures of: (a) purine; (b) adenine; (c) guanine.

Table B49, Appendix B, shows the data for their proton and carbon NMR assignments. Tables B50-B52, Appendix B, show the data for the effect of shake time, substrate concentration and the effect of temperature on the enhancement and polarization levels.

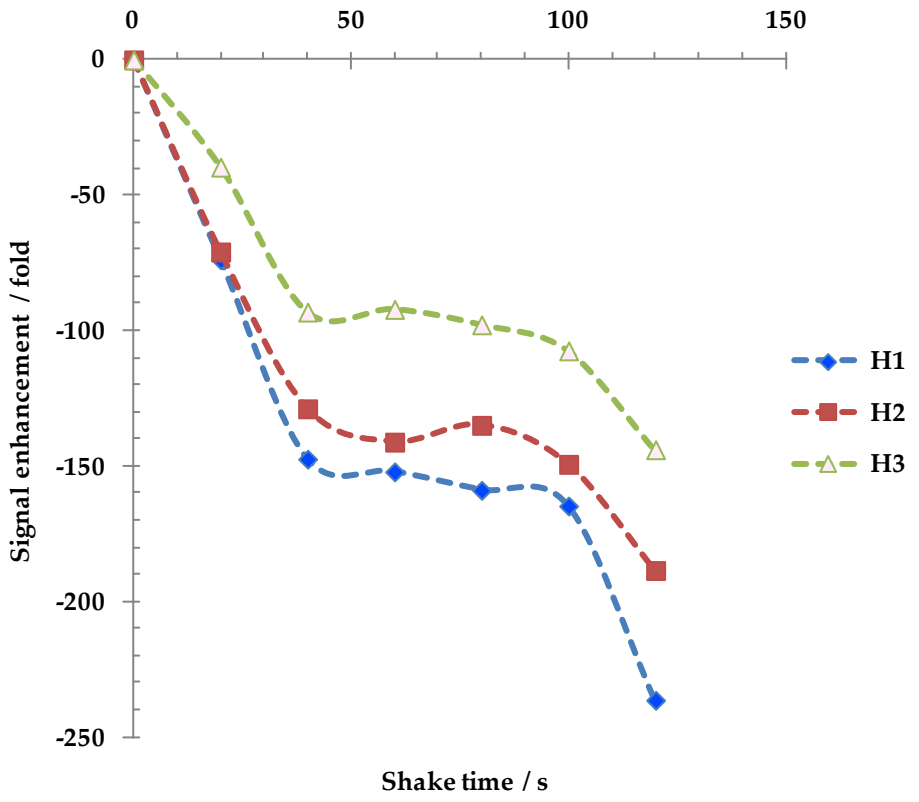

Figure 3.24: Effect of shake time on the extent of the ^{1}H NMR signal strength for the indicated proton sites of purine when the polarization transfer step is completed in a magnetic field of 65 G.

In the shake time experiments at 323 K, the hyperpolarization of purine was achieved by shaking an NMR tube to dissolve the *p*-H_2 from the headspace above the solution. The sample was then rapidly inserted into the NMR spectrometer while making sure to reproduce the same trajectory as precise as possible for each experiment. Acquisition of ^{1}H NMR spectrum using a 90° rf pulse was executed instantly after the sample settled in the spectrometer. This procedure was repeated by varying the shake times from 20-120 s. For a shake time of 20 s, the signals of the H_1, H_2 and H_3 resonances were -73.8, -70.9 and -39.6 times bigger than the resonances from the unpolarized sample. The enhancement levels for a 60 s shake were calculated to be -152.1, -141.1 and -

92.1 fold, while those for a 120 s shake were -236.4, -188.5 and -143.9 fold, respectively (Figure 3.24). The degree of signal enhancement was observed to increase with the length of time spent in contact with *p*-H_2.

From the graph in Figure 3.24, the enhancement levels achieved with variable contact times demonstrate that the signal enhancement level is of the order of several hundred. The largest enhancement demonstrated by a H_1 proton attaining an enhancement value of -235.4 fold was followed by the H_2 protons with an enhancement level of -188.5 for a shake time of 120 s. At 65 G, the enhanced signals all had negative intensities, while the amide protons showed no signal enhancement. Typical thermal and hyperpolarized ^{1}H NMR spectra obtained in the case of purine are shown in Figure B53, Appendix B.

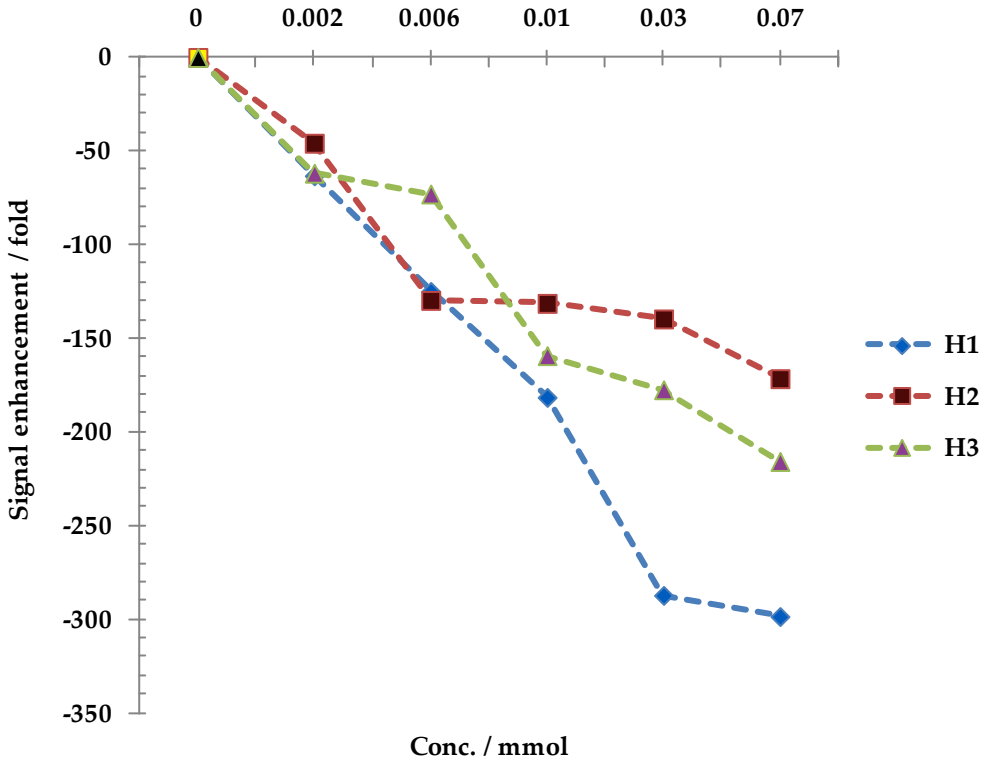

Figure 3.25: ***Effect of substrate concentration on the extent of the ^{1}H NMR signal enhancement for the indicated proton sites of purine when the polarization transfer step is completed in a magnetic field of 65 G.***

In concentration studies at 320 K, the polarization transfer to all the protons of pyrimidine and the imidazole rings was observed. The H_1, H_2 and H_3 protons sites within the purine molecule experienced substantial enhancement levels. The signal enhancement was comparatively lower at a concentration of 0.002 mmol with enhancement values of -63.2, -45.8 and -61.8 fold for the H_1, H_2 and H_3 protons. These data are illustrated graphically in Figure 3.25, which reveals that the degree of signal enhancement is maximized at a substrate loading of 0.07 mmol where protons H_1, H_2 and H_3 were -236.4, -188.5 and -143.9 times stronger than normal when polarization is undertaken at 320 K.

When the same experiment was repeated for samples where the absolute concentration of ***1*** was kept constant, and the purine level halved, the signal enhancement is reduced to -287.2, -139.6 and -177.4 fold respectively.

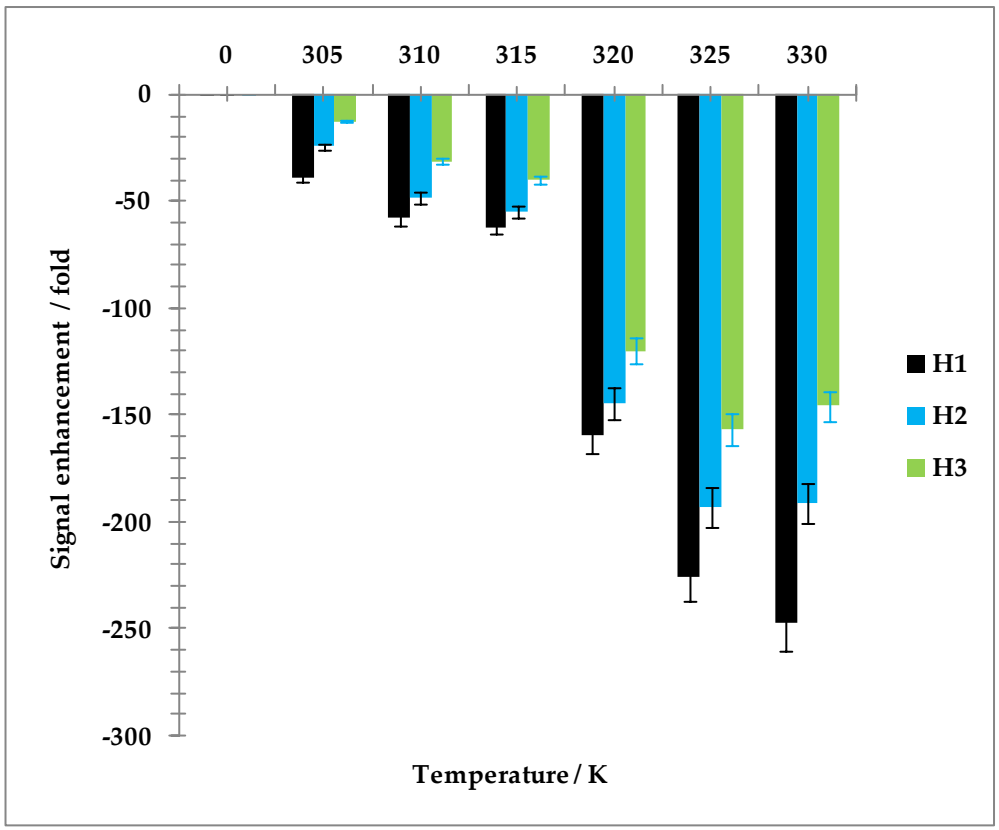

Figure 3.26: ***Effect of temperature on the extent of the ^{1}H NMR signal enhancement for the indicated proton sites of purine when the polarization transfer step is completed in a magnetic field of 65 G.***

The hyperpolarization studies at variable temperatures were able to deliver very impressive levels of signal enhancement reaching -247 fold for H_1 proton. The temperature for the largest enhancement was at 330 K for H_1 proton. Figure 3.26 shows that the purine protons are affected independently at

different temperatures with an interesting implication that exchange rate is one of the imperative factors to achieve non-Boltzmann conditions necessary for hyperpolarization. In these temperature studies, the temperature for the lowest enhancement was 305 K and the magnitude of signal enhancement for H_1, H_2 and H_3 protons at that particular temperature were -38.7, -24.3 and -12.6 fold respectively. At 330 K, the signal enhancement levels for H_1, H_2 and H_3 protons were increased significantly and calculated to be -247.6, -191.2 and -145.8 fold respectively. The hydride exchange rate constant in the case of purine was determined to be 1.5 s^{-1}, which is lower compared to pyrazine 4.2 s^{-1} at 315 K. The signals for NH protons of imidazole ring are not enhanced in the hyperpolarized NMR spectrum suggesting that the tautomeric exchange (see Figure 3.27) might broaden this resonance beyond detection.[162, 164]

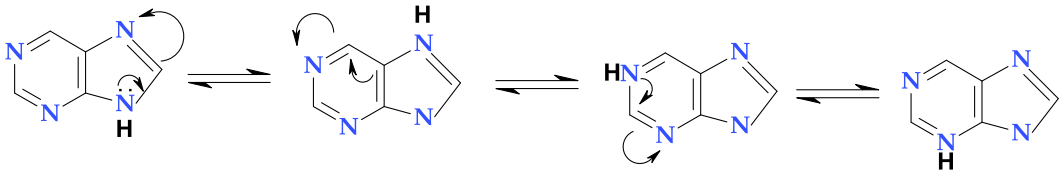

Figure 3.27: Tautomeric exchange in purine.

3.3.8 Pyrimidine

Pyrimidine (S_8 in Figure 3.3) is an aromatic heterocyclic organic compound of great biological relevance that structurally resembles pyridine. Pyrimidine belongs to group of biological molecules called diazines. It possesses a 6-membered heterocyclic ring with two nitrogen atoms that are located at the 1- and 3-positions within the aromatic ring.[167] Pyrimidine occurs naturally in the form of substituted and fused ring compounds such as vitamin B_1 (thiamine).[168, 169] Because of the biological significance of pyrimidine it too has been employed

as a potential substrate for SABRE. Table B54, Appendix B, shows data for the proton and carbon NMR assignments of pyrimidine. The data for the effect of shake time, effect of concentration and temperature on the enhancement and polarization levels are given in Tables B55-B57, Appendix B, respectively.

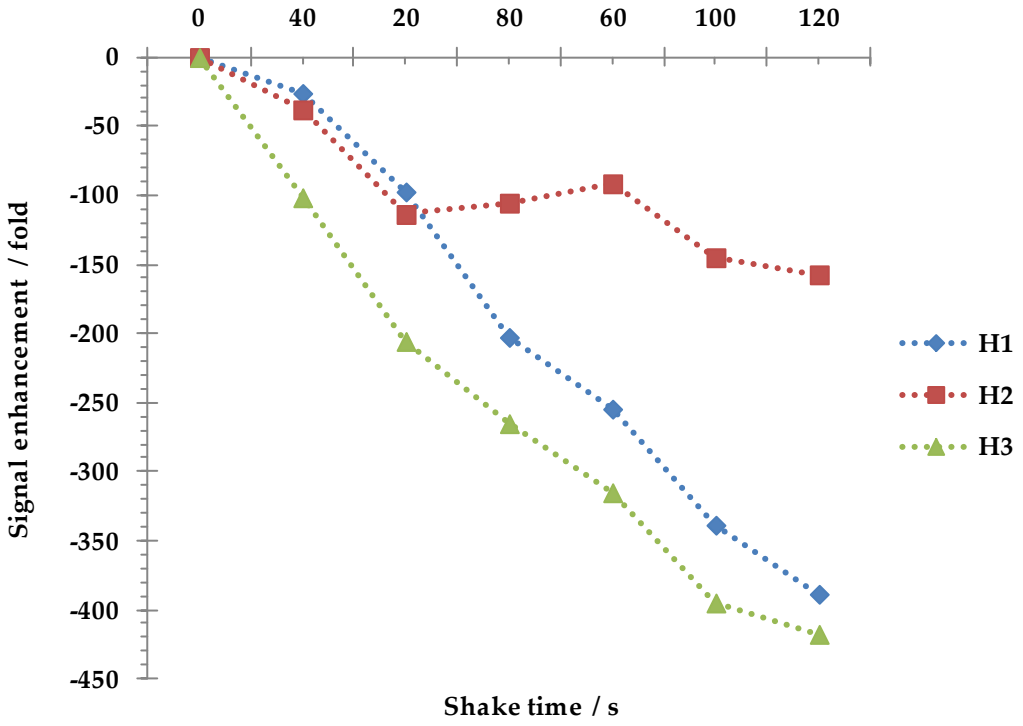

Figure 3.28: ***Effect of shake time on the extent of the ^1H NMR signal enhancement for the indicated proton sites of pyrimidine when the polarization transfer step is completed in a magnetic field of 65 G.***

The shake time studies at 320 K using pyrimidine as a substrate led to some fascinating observations as demonstrated in Figure 3.28. Proton H_3 is greatly enhanced, while the protons H_1 and H_2 exhibit a comparatively lower level of signal intensity. The reason for proton H_3 being greatly enhanced is because of its presence next to the binding site while all the other protons are a

few bonds away. From a chemical perspective, the π-electron density is lower in pyrimidine than pyridine which disfavours the electrophilic aromatic substitution and favours nucleophilic substitution. The basicity of pyrimidine is further lessened in comparison to pyridine with the pKa value for the protonated pyrimidine being 1.23 thus electrophilic addition takes place at 1-nitrogen.[170] In the case of H_3 proton, which is present at the *meta* position within the hetero-ring, a low level of signal enhancement is seen after a 20 s shake time while with shake time of 120 s its enhancement level increases to -417 fold. At this point H_1 and H_2 protons exhibit enhancement levels of -345.5 and -157.3 fold respectively. Typical thermal and hyperpolarized NMR spectra obtained in the case of pyrimidine are shown in Figure B58, Appendix B, while Figure B59, Appendix B, depicts the dq-OPSY spectrum.

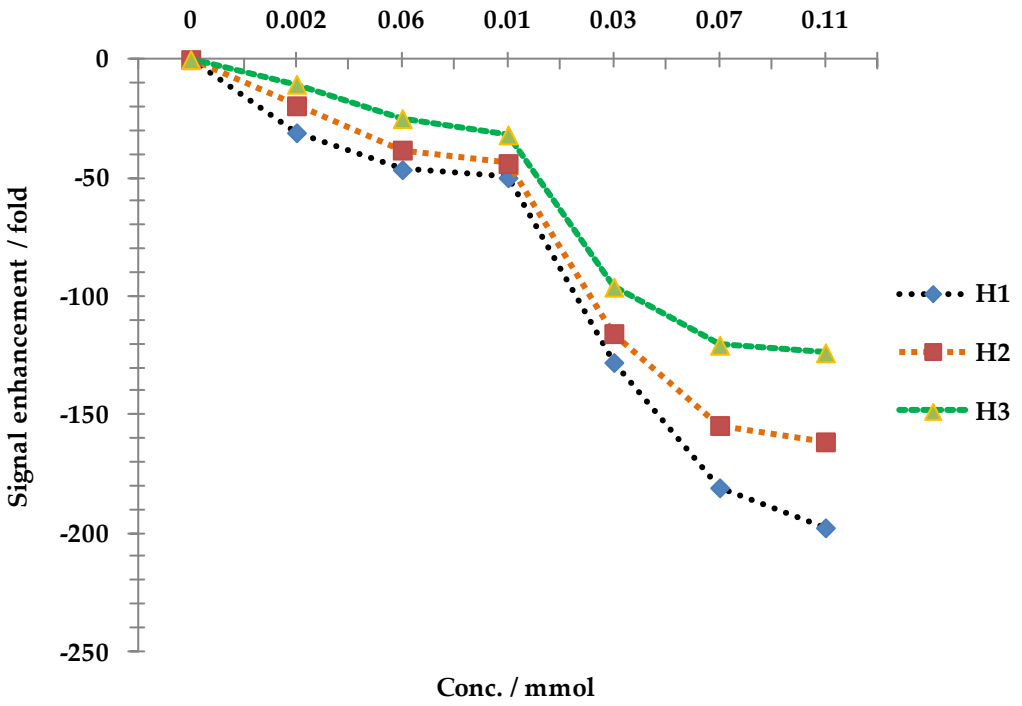

Figure 3.29: ***Effect of concentration on the extent of the ^{1}H NMR signal enhancement for the indicated proton sites of pyrimidine when the polarization transfer step is completed in a magnetic field of 65 G.***

In order to examine the effect of concentration on the polarization transfer process, a range of experiments have been conducted at 315 K. To carry out these experiments, the sample were individually exposed to *p*-H_2 and warmed to 315 K before being shaken prior to sample insertion into the NMR spectrometer. ^{1}H NMR spectra were acquired to gauge the degree of signal enhancement shown by the three proton sites present in pyrimidine molecule. These data are illustrated graphically in Figure 3.29 which divulges that the degree of enhancement is observed to be maximized at the 0.11 mmol substrate loading where the H_1, H_2 and H_3 protons are -197.7, -161.4 and -123.8 times

stronger than normal. When a similar experiment is repeated for samples where the absolute concentration of ***1*** and pyrimidine was lowered to 0.002 mmol, the signal enhancement proved to reduce to -30.9, -19.5 and -10.4 fold for H_1, H_2 and H_3 protons respectively. The proposed structure of an active iridium complex is shown in Figure 3.30.

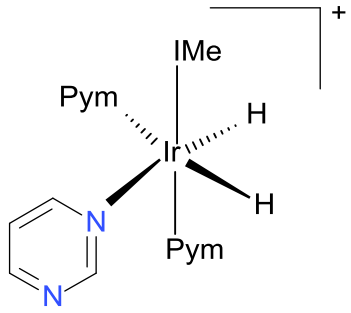

Figure 3.30: ***Structure of an active iridium polarization transfer catalyst when pyrimidine is used a substrate (Pym = pyrimidine. IMe = 1, 3 -dimethylimidazole-2-ylidene is a carbene ligand).***

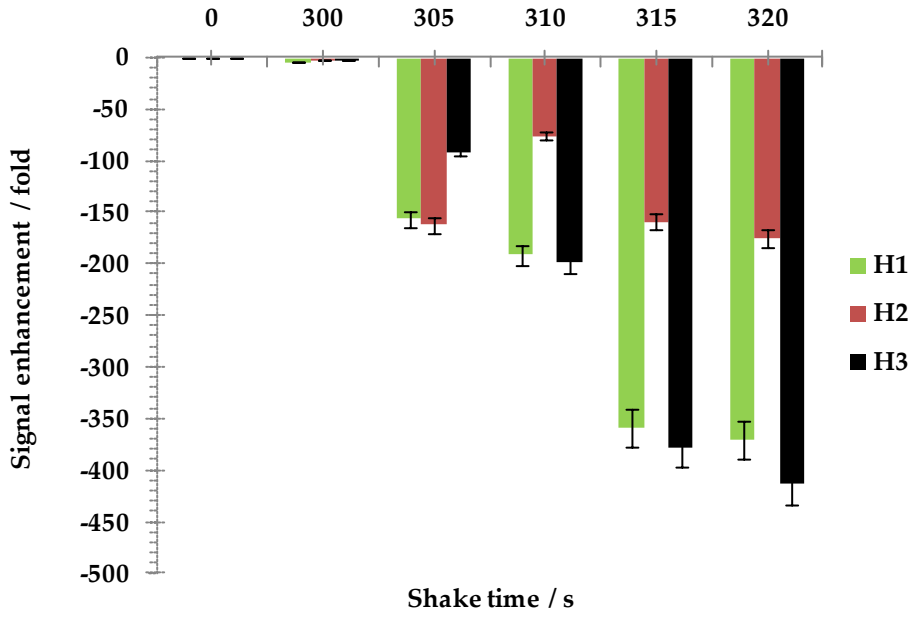

Figure 3.31: ***Effect of temperature on the extent of the ^{1}H NMR signal enhancement for the indicated proton sites of pyrimidine when the polarization transfer step is completed in a magnetic field of 65 G.***

In the corresponding variable temperature studies, the H_3 proton signal intensity surpasses that of H_1 and H_2 protons in terms of the level of hyperpolarization which reach -370.9 fold, -175.5 and -412.2 fold respectively as shown in Figure 3.31. The H_3 proton exhibited a stupendous enhancement of -412 fold, significantly better than that of purine in which the highly enhanced proton was H_1 with an enhancement value of -247.6 fold. All the protons present within the pyrimidine molecule share the optimum hyperpolarization at a temperature of 330 K. The higher temperatures favour the fast exchange necessary for an effective polarization transfer. The aforementioned observations suggested that the exchange rates of *p*-H_2 and the substrates molecules are imperative for an efficient polarization transfer process as was also demonstrated by the SABRE studies using purine at 65 G. The hydride

exchange rate constant in case of pyrimidine was determined to be 3.9 s^{-1}, which is higher compared to purine 1.5 s^{-1} at 310 K. The pKa of pyrimidine is much lower than purine (1.3 compared with 2.5). Conversely, the basicity difference between these two substrates would imply a much stronger binding affinity to the metal centre. In case of pyrimidine, the formation of stable and active iridium complex favours the polarization transfer mechanism and eventually the polarization build up is transferred from the metal centre to substrate resulting in the SABRE effect being observed in the free resonances of the substrate. Another interesting observation in the SABRE studies using pyrimidine was the signal enhancement for the hydroxyl and methyl resonance of methanol at δ 3.3 and δ 4.8 in the corresponding hyperpolarized NMR spectra as illustrated in Figure B60, Appendix B.

There can be two rationales for the polarization transfer to the hydroxyl and methyl resonances in the hyperpolarized NMR spectra using SABRE. One of the reasons could be that solvent acts as a substrate and binds directly to the active iridium polarization transfer catalyst, thus resulting in signal enhancement. Another approach would be for the solvent to undergo significant H/D exchange.

3.4 Conclusions

In this chapter, a series of biologically relevant substrates were polarized rather than the model substrates of chapter 2. The substrates nicotinic acid, isonicotinic acid, methyl nicotinate, isonicotinamide, pyrazine, isoniazid, purine and pyrimidine were chosen for this task.

Previously,[101-103] it has been demonstrated that in the hyperpolarization experiments the use of **2** at higher temperatures result in a decline in the efficiency of polarization transfer, which leads to lower levels of signal enhancement. However, when ***1*** **i**s employed as the polarization transfer catalyst, higher temperatures yield better polarization transfer. The sum of levels of signal enhancement seen for all the hyperpolarized sites in these substrates along with the pKa values of their nitrogen sites are shown in Figure 3.32.

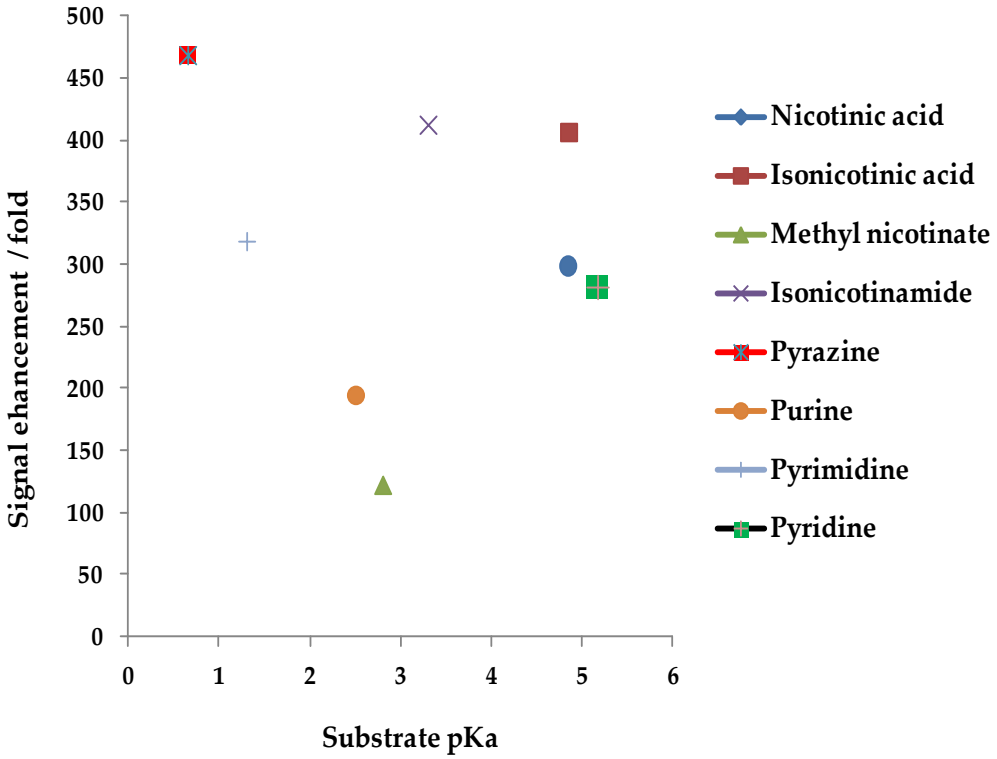

Figure 3.32: ***Sum of enhancement levels for all the ^{1}H hyperpolarized sites along with the pka values of their nitrogen centres of the substrates (S_1-S_8).***

The pKa of pyridine is 5.17, which makes a weak base. The presence of a COOH group at the *meta* position in the case of nicotinic acid has little effect on the basicity of nitrogen with a marginal decrease in pKa to 4.85. It appears that values close to 5.17 give rise to good levels of polarization. There is however a fall at below 2.2 where presumably the system is insufficiently basic.

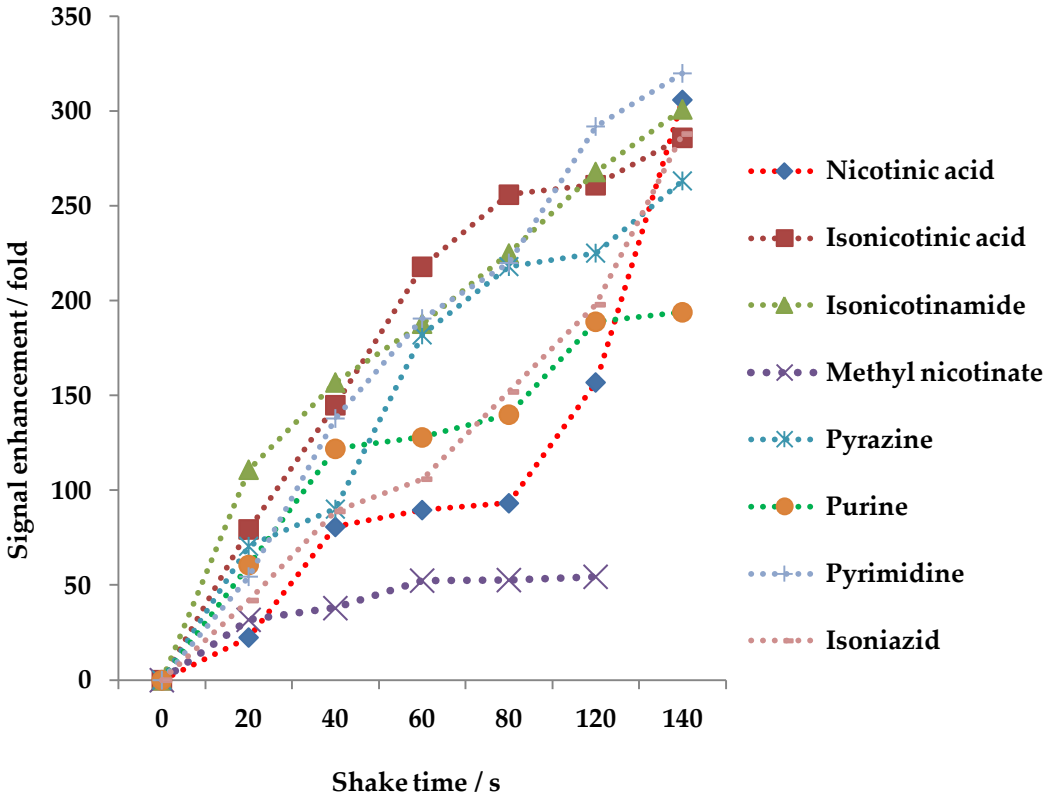

Figure 3.33: ***Sum of enhancement levels for all the ^1H hyperpolarized sites as a function of shake time for the substrates (S_1-S_8).***

Figure 3.33 shows that all the systems produce improved polarization levels with longer contact times. For methyl nicotinate the effect is however minimal and not surprisingly this system has an intermediate pKa close to 3.

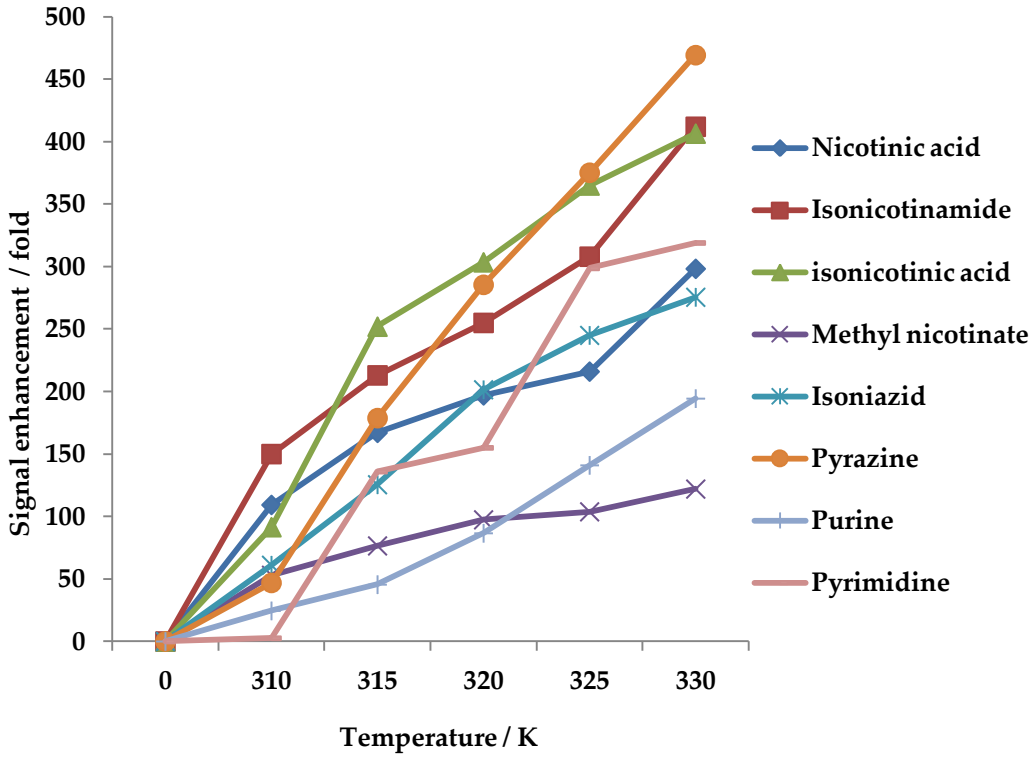

Figure 3.34: ***Sum of enhancement levels for all the ^1H hyperpolarized sites as a function of temperature for the substrates (S_1-S_8).***

Upon warming the exchange rates increase. In all cases more efficient transfer results (Fig 3.34). The polarization transfer to the substrate and molecular tumbling rate comparatively are faster at higher temperatures. In the extreme narrowing limit, the nuclear spin relaxation rates of proton and carbon are smaller at higher temperatures. The combination of faster exchange between substrate-catalyst and slower relaxation rate of nuclear spins leads to higher levels of signal enhancement. The gradient of the corresponding changes is highest for the least basic pyrazine systems. This suggests that pyrazine has the optimum lifetime and H_2 exchange rate at 330 K. For methyl nicotinate again weak polarization is evident and strong binding indicated (Figure 3.34).

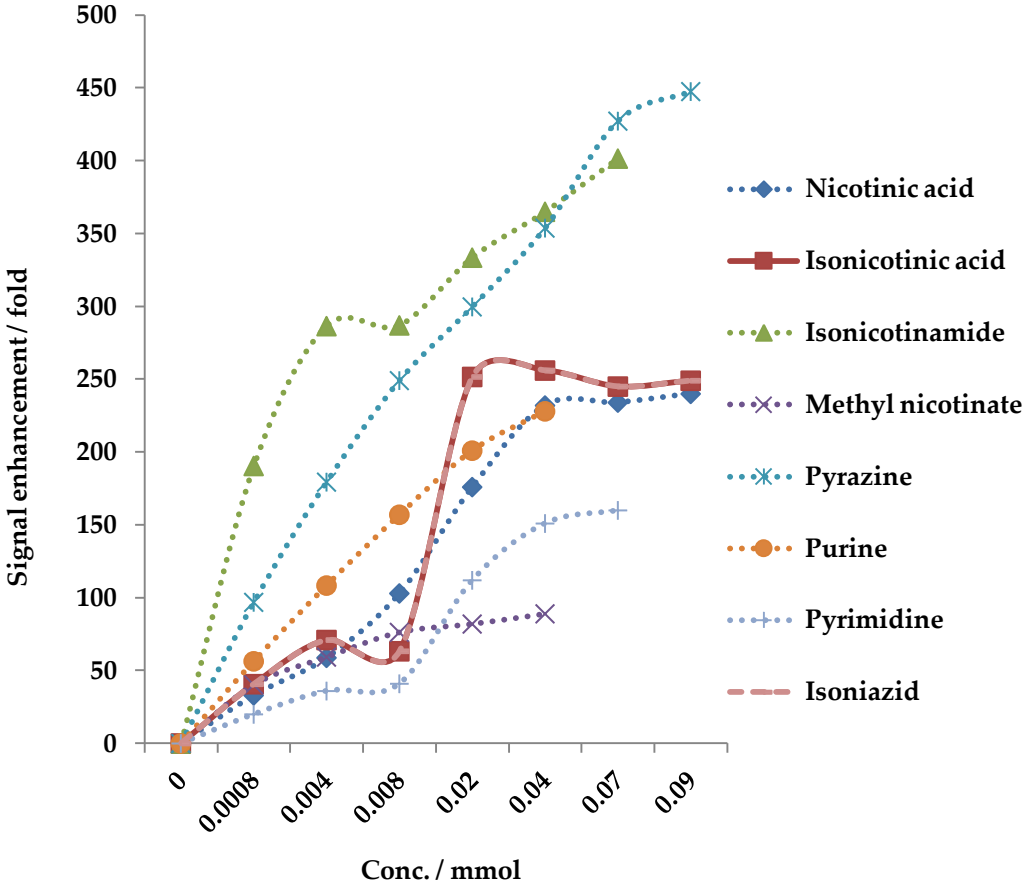

Figure 3.35: ***Sum of enhancement levels for all the ^{1}H hyperpolarized sites as a function of substrate concentration for the substrates (S_1-S_8).***

Isonicotinic acid out performs nicotinic acid and we can conclude that 4-substitution is viable if high levels of polarization are needed. For 4-substitution any steric effect is minimal. This trend is much clearer than Chapter 2 suggested. It should, however, be remembered that there are a lower number of spins receiving polarization from the *p*-H_2 in this system.

The signal enhancement studies on pyrazine complex with ***1*** show that it proved to be an even better substrate for hyperpolarization (Figure 3.35). This

happens despite pyrazine having a pKa of only 0.65. This could be reflected in its bi-dentate character.

During the aforementioned studies, it was also established that if the catalyst, [Ir(IMe)(COD)Cl], ***1***, is activated without a substrate present, the resulting compound becomes unstable as evidenced experimentally by the rapidly darkening solution. At low concentrations of substrate, this did prove to stabilise the catalyst and signal enhancement was still observable. It can be concluded that signal enhancement was observed for substrates studied in this chapter even when the substrate is present in solution at low concentration (Figure 3.35), so long as the catalyst can be kept stable. During the polarization reaction, the COD is hydrogenated and a substrate needs to be present to substitute the chloride. Then the substrate enters the coordination sphere of the metal, forming an active polarization transfer catalyst, $[Ir(IMe)(substrate)_3(H)_2]^+Cl^-$. Previous studies on SABRE have demonstrated it is possible to achieve an 8600 fold signal enhancement for pyridine[4], its potential to allow swift NMR analysis of very low concentration of analytes is an exhilarating future prospect for this emerging NMR technique.

In this chapter, the hyperpolarization studies carried out using SABRE proved that it is an effective technique for creating non-Boltzmann spin state populations in biologically relevant substrates by making use of *p*-H_2. Unlike *para*hydrogen induced polarization, no formal hydrogenation is required in SABRE. Spontaneous sharing of spin polarization takes place from the hydride ligands of the metal complex to the substrate within seconds. Consequently, the ligand exchange results in the free and bound substrate achieving a non-Boltzmann spin state population for its NMR active nuclei. This process of

polarization transfer has been demonstrated to ^{1}H and ^{13}C nuclei and this process of polarization transfer is found to be dependent on the shake time, temperature, pKa and concentration.

Polarization transfer to ^{13}C has also been achieved, which can be a milestone for routine ^{13}C analysis of drugs and metabolites. The acquisition of ^{13}C data is routinely difficult to achieve because of the inherent insensitivity of 6400 fold related to the direct observation ^{13}C resonance compared to that of ^{1}H. The resulting single-scan ^{13}C NMR spectrum of nicotinic acid was acquired after a 90° read pulse and polarization transfer at 65 G, in which all the resonances were discernible. In the case of ^{13}C measurement for nicotinic acid, the 102.8 fold signal gain for C_2 carbon requires a 10568 scan average to match the signal-to-noise ratios when normal magnetization is employed. If there is a 15 s delay between measurements, 45 h of spectrometer time would be needed to achieve this rather than the 3 s used for the polarized measurement. Thus, the experiments conducted using SABRE presented here have established the potential to polarize a range of substrates. It proves the applicability of this method in both the field of routine high-resolution NMR spectroscopy and diagnostic imaging.

CHAPTER FOUR

Parahydrogenation reactions of complex [IrCl(DMSO)$_3$], *4*

4.1 Introduction

This chapter encompasses investigations into the reactivity of the complex [IrCl(DMSO)$_3$], ***4***. A range of solvent studies were conducted in order to investigate how the use of different solvents affected the product distribution for the reaction of ***4*** with *p*-H$_2$. It is because a change in the solvating ability or dielectric constant of a solvent can thus influence the product distribution. Reactions of ***4*** have also been carried out with triphenylphosphine, pyridine and a range of L-amino acids, in the presence of *p*-H$_2$, and the reaction products and signal polarizations are characterized/ monitored by NMR spectroscopy.

Astoundingly in these reactions not only was the formation of dihydride amino acid complexes observed, but so was the direct observation of what is now referred to as the SABRE effect in the resonances of the free amino acids. The SABRE effect results when the temporary association of *p*-H$_2$ and a substrate is achieved through a suitable transition metal complex. Under these conditions, it leads to NMR polarization buildup that is detectable for the free amino acid substrate in solution.

4.2 [IrCl(DMSO)$_3$], *4*: Reactivity and relevance

Several studies have been reported in the literature that illustrate the reaction chemistry of a number of rhodium and iridium DMSO complexes.[170, 171] In addition, transition metal phosphine complexes of iridium and rhodium feature significantly in the chemistry of these metals because of their low valent character and readily soluble nature. They have also been used as homogenous catalysts that show high reactivity.[171] Since phosphine ligands are air sensitive, expensive and toxic, there has been a great interest in making new ligands with similar electron donating characteristics. Sulfoxides are potentially one class of such ligands, and their coordination chemistry has been investigated where their high water solubility is a distinctive feature.[173]

The oxidative addition of an OH group by a transition metal centre has also received great attention because of its relevance to a number of catalytic processes.[174] There is also an increasing interest in developing water-based catalysts because of their perceived environmentally friendly behavior.[4] Notwithstanding this, the oxidative addition of the OH bond of water is difficult to achieve and there are relatively few examples of it in the literature that involves a reaction with phosphine complexes.[175] ***4*** was first prepared by Milstein *et al*.[176] and shown to be water soluble. An addition of excess water to a yellow acetone slurry affords pale yellow crystal of syn-[DMSO)$_2$(H)Ir(μ-OH)$_2$(μ-Cl)Ir(H)(DMSO)$_2$][IrCl$_2$(DMSO)$_2$] and this reaction takes two hours to complete as shown in Figure 4.1.

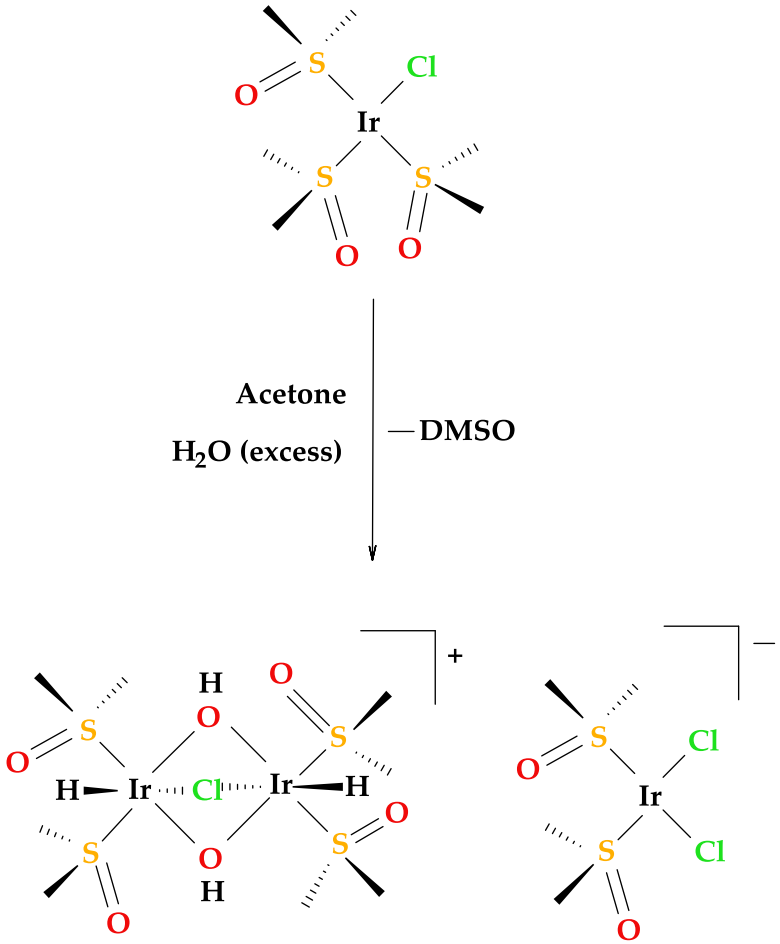

Figure 4.1: ***Formation of syn-[DMSO)$_2$(H)Ir(μ-OH)$_2$(μCl)Ir(H)(DMSO)$_2$][IrCl$_2$(DMSO)$_2$] from 4.***

The synthesis, characterization and the X-ray crystal structure of the complex, [IrCl(DMSO)$_3$], ***4,*** have been reported by Milstein *et al.*[176] The crystal structure of [IrCl(DMSO)$_3$], ***4,*** is shown in Figure 4.2.

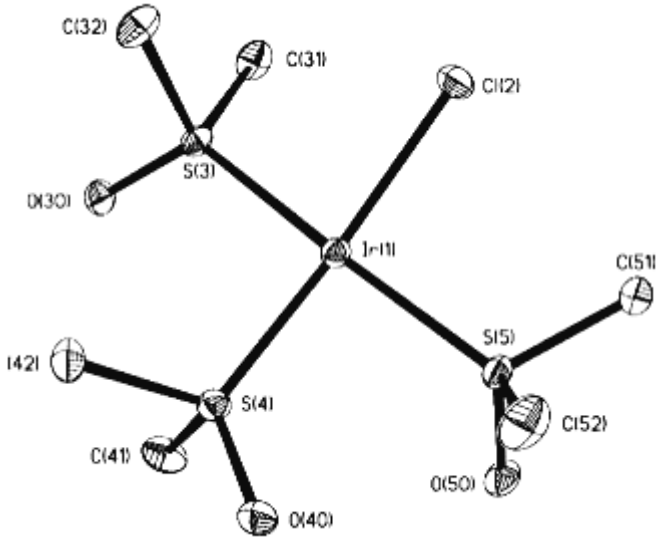

Figure 4.2: ***ORTEP plot of complex [IrCl(DMSO)$_3$], 4. Thermal ellipsoids are drawn at the 50 % probability level. Hydrogen atoms have been omitted for clarity.***[176]

Milstein *et al*. also demonstrated that, ***4,*** reacts with H_2 and two products are formed; their structures are shown in Figure 4.3. In this case, kinetically unstable, *fac*-[IrCl(H)$_2$(DMSO)$_3$], ***4a***, slowly converts to the more stable thermodynamic product *mer*-[IrCl(H)$_2$(DMSO)$_3$], ***4b***, in solution.[176]

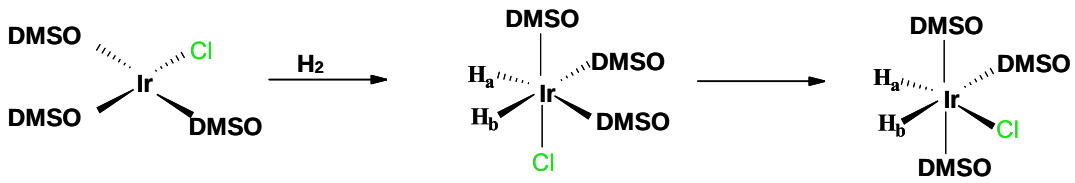

fac-[IrCl(H)$_2$(DMSO)$_3$] ***mer-[IrCl(H)$_2$(DMSO)$_3$]***

4 ***4a*** ***4b***

Figure 4.3: ***Kinetic and thermodynamic products of p-H$_2$ addition to 4.***

H_2 addition to ***4*** can take place over the S-Ir-S axis, leading to ***4a*** in which both newly formed hydride ligands are *trans* to an S-bound DMSO. A *fac* isomer has three identical ligands arranged on the same face of an octahedral complex. The formation of ***4b*** results from the addition of H_2 over the S-Ir-Cl axis. Now one hydride ligand is *trans* to chloride and the second hydride is *trans* to an S-bound DMSO ligand. Such a complex, in which the three identical ligands are co-planar, is referred to as a *m*eridional isomer.[176] This reaction sequence is illustrated in Figure 4.4.

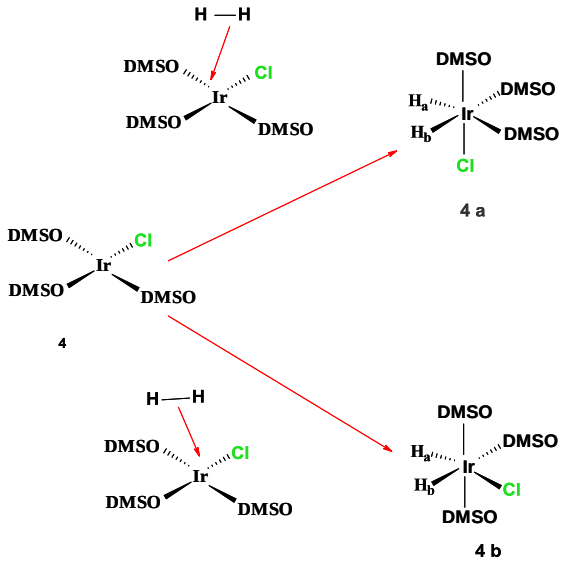

Figure 4.4: ***Oxidative addition of p-H_2 to 4 accounts for the formation of 4a and 4b.***

The oxidative addition of dihydrogen proceeds to increase the electron count of a metal centre by two units and 16 electron square planar d^8 complexes feature extensively as a system that readily add H_2. Analogous reactivity and stereochemistry has been observed in the oxidative addition of dihydrogen to related Ir(I) phosphine complexes such as *trans*-[IrCl(CO)(PPh_3)$_2$] (Vaska's

Complex),[177] [IrCl(CO)(dppe)],[178] and [IrCl(PMe_3)$_3$].[179] The oxidative addition reaction plays a pivotal role in homogenous catalysis and consequently understanding how is it controlled reflects an important aspect of an inorganic research.[177--179]

Theoretical studies pertaining to the reaction mechanism for oxidative addition of H_2 to the metal centre were proposed by Hoffmann *et al*.[180] in 1984. In this study, it has been anticipated that the oxidative addition of H_2 took place in three distinct steps.

a) In the first step, the H_2 molecule approaches the metal centre via η^2-coordination mode.

b) In the second step, a rapid alteration in orientation of the H-H bond takes place to attain stability.

c) In the final step, there is an increase in H-H bond length which leads to the formation of a dihydride species. The steps involved in the oxidative addition of H_2 to the metal centre are illustrated in Figure 4.5.

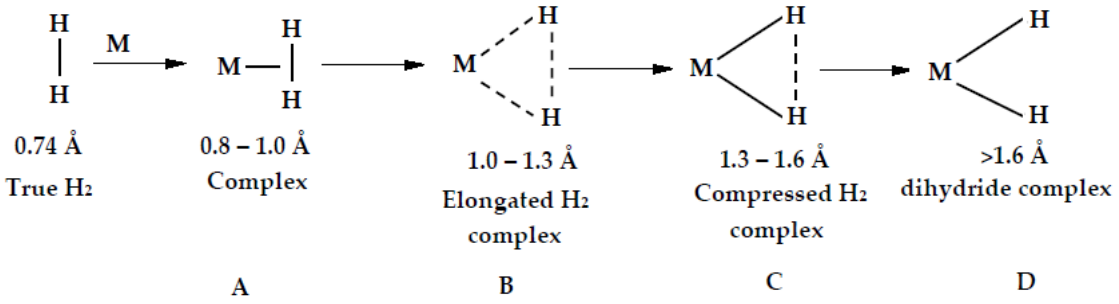

Figure 4.5: ***Schematic depicting the oxidative addition of H_2 to a transition metal complex along with their bond lengths, where: (A) η^1-coordination; (B) η^2-interaction; (C) increase in H-H bond length; (D) dihydride complex formation.***

For the d^8 complexes such as complexes, [IrCI(CO)$(PPh_3)_2$], and [IrCl(CO)(dppe)], there is a wide body of evidence to suggest that H_2 addition occurs in a concerted, pairwise manner, and places the hydrides in a mutually *cis* orientation. Eisenberg *et al*.[181] studied the oxidative addition of dihydrogen to the [IrX(CO)(dppe)] complex, where X is a halide. The mechanism of an oxidative addition of dihydrogen to [IrX(CO)(dppe)] (where X = Cl, Br, I, H or CN) complex involves the concerted *cis*-addition to a metal centre to form an octahedral complex with hydride ligands on the *cis* position. In case of aforementioned complexes, the addition of dihydrogen can occur via two possible routes, **a** and **b,** as shown in Figure 4.6. In route **a,** the H_2 ligand approaches the square planar complex with the molecular axis of H_2 parallel to the P-Ir-CO axis. The concerted addition along pathway **a,** takes place with concomitant bending of the *trans* P-Ir-CO arrangement, so that one hydride ligand of the product becomes *trans* to the CO ligand, with the other becoming *trans* to the phosphine ligand. On the other hand in Pathway **b,** the approach of

H_2 where it's molecular axis is parallel to P-Ir-X axis, and the addition proceeds with bending of the P-Ir-X arrangement.

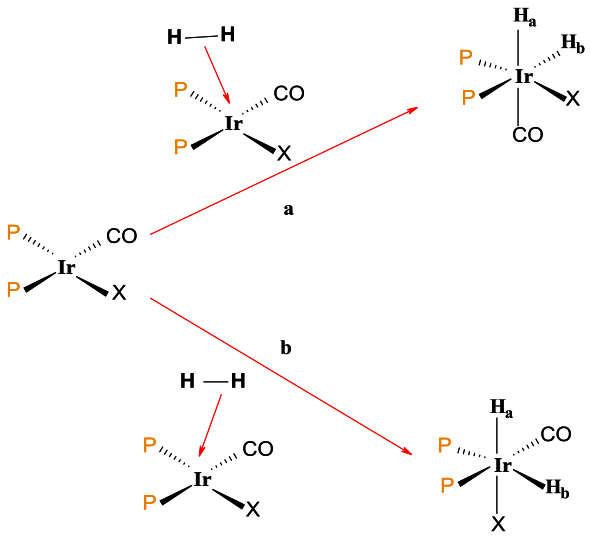

Figure 4.6: ***Stereochemistry involved in a reaction of complex, [IrX(CO)(dppe)], complex with p-H_2.***

The experimental results[181] have revealed that the reaction of complex, [IrCl(CO)(dppe)], with *p*-H_2 initially leads to the formation of product **A**. The stereo selectivity studies proved that the activation barrier for pathway **i** is lower than that of pathway **ii**. The product **B** was observed to form after a reaction time of an hour and it is depicted in Figure 4.7. The product **B** eventually favoured over the product **A** by a factor of more than ten, which shows that product formed in pathway **ii** is thermodynamically more stable than the product **A** formed during pathway **i**. Both these products exhibit PHIP in their hydride resonances.

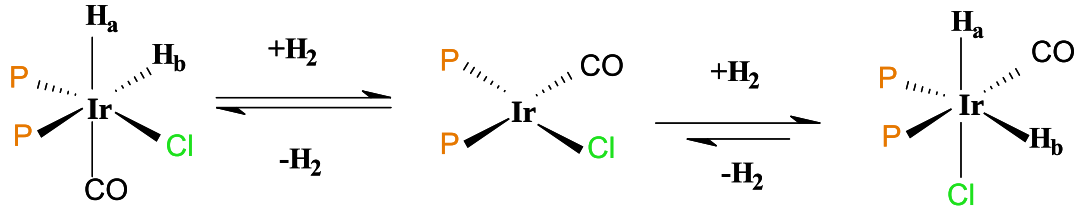

A *Route i* *Route ii* **B**

Kinetic product ***Thermodynamic product***

Figure 4.7: ***The oxidation addition products obtained in the reaction of complex, [IrCl(CO)(dppe),] with p-H2.***

Analogous stereo selectivity was also observed in a similar study by Longato and Bresadola,[182] for a complex carrying a carborane cluster ligand favouring an initial hydrogen addition over the P-Ir-CO axis. In this case, no ensuing isomerisation was observed, indicating that the initial kinetic product is also the most stable thermodynamic product. The steric congestion imposed by the carborane cluster ligand led to this suggestion since the formation of another isomer would require carborane cluster to be present on the *cis* position to both arms of the phosphine ligand.

A separate study by Eisenberg *et al.*[183] suggested that for electronic control, it is necessary to take into account the orbital interactions because as the H_2 molecule approaches the ligand bent back in order to occupy the *cis* position in the metal complex consequently it does not remain planar. When dihydrogen approaches the square planar metal complex, it gives rise to three key orbital interactions, which are as follows

1) σ-Bond formation

The donation takes place from the bonding σ orbital of H_2, σ(H_2), into an empty p_z or p_z-d_{z^2} orbital on the metal.

2) Back donation

The back donation occurs from the filled metal d_{xz} or d_{yz} orbital into an antibonding orbital of H_2, $\sigma^*(H_2)$. The main interactions involved between H_2 and a square planar d^8 metal centre are pictorially shown in Figure 4.8.

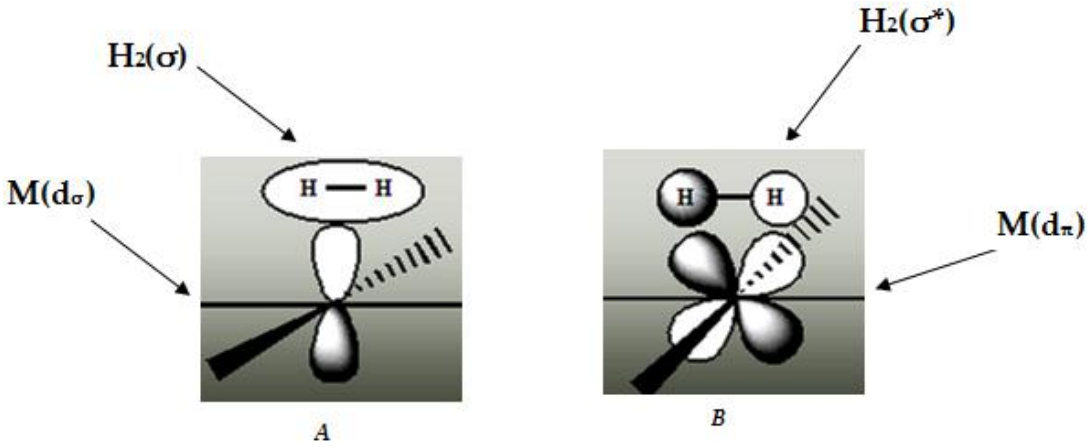

Figure 4.8: ***The key interactions involved between H_2 and a square planar d^8 metal centre: (A) σ-bond formation; (B) back donation.***

The donation of σ electron density from the H-H bond into the empty metal orbitals, H_2 (σ) ⟶ M(σ), is the most dominant interaction in metal-dihydrogen complexes. A second interaction is the back donation from filled d_π metal orbitals into empty σ* orbitals of H_2 (M(π) ⟶ H_2 (σ*), is also present. This interaction weakens the dihydrogen bond and is sensitive to electron density at the metal centre. With electron rich metal centres strong back

donation occurs and results in population of the σ*(H_2) orbital, which causes an increase in the length of the H-H bond. This encourages the formation of classical dihydride complexes. In the opposite sense, poor back donation from the electron deficient complexes will result in a weakly bound H_2 ligand, where the dihydrogen bond is as a result becomes stronger.

Hall and co-workers[184] studied *cis* PH_3 ligands in their computational model of the addition of a dihydrogen to [IrCl(CO)(dppe)]. This suggested that while addition over the P-Ir-Cl axis leads to the most stable thermodynamic isomer, addition over the P-Ir-CO axis proceeds via the most stable transition state. This behaviour arises because of interaction between the ligands in the plane of hydrogen addition and regions of charge density around the metal centre. As the square planar complex evolves to the six coordinate mode, the two ligands on the axis of an addition move past the regions of high charge density due to the metal lone pair electrons, which are a source of repulsion; electron with-drawing ligands are able to minimise this repulsion, and therefore stabilise the corresponding transition state. Strong σ and π-donor ligands destabilize the five-coordinate transition state by contributing to the repulsion between the electronic charge density of the ligands that concentrated around the metal centre. Electron with-drawing ligands thereby stabilize the five-coordinate transition state by delocalizing some of the electron charge density contributing to the repulsive interaction.

In the oxidative addition of dihydrogen to Vaska's type complexes,[185] *trans* –[IrX(CO)(PR_3)$_2$], the nature of the X ligand plays an imperative role in determining the direction of an addition. Weak electron donor ligands, such as chloride, favor addition in the X-Ir-CO plane, whereas for stronger electron

donor ligands, such as Ph^-, Me^-, and H^- addition is preferred in the P-Ir-P plane. For Ph^-, the most stable isomer of the final products refers to the species formed from an addition in the X-Ir-CO plane. This scrupulous isomer attains stability by orienting a weaker σ-donor or stronger π-donor ligand *trans* to a hydride ligand. The weak σ-donor character strengthens the strong Ir-H σ bond to which it is *trans*, while the strong π-donor character, which outcomes in an occupied antibonding interaction of π symmetry, is able to minimize the influence of the antibonding interaction by being *trans* to the strong *trans*-influence hydride ligand.[185]

4.3 Synthesis and characterization of [IrCl(DMSO)$_3$], *4*

4, was synthesized according to the literature procedure[176] which is fully described in the experimental section of the thesis. In short, $[IrCl(COE)]_2$ is reacted with excess DMSO in toluene at room temperature, resulting in the formation of a lemon yellow precipitate (Figure 4.9). The key NMR data for $[IrCl(DMSO)_3]$, ***4,*** is given in Table 4.1.

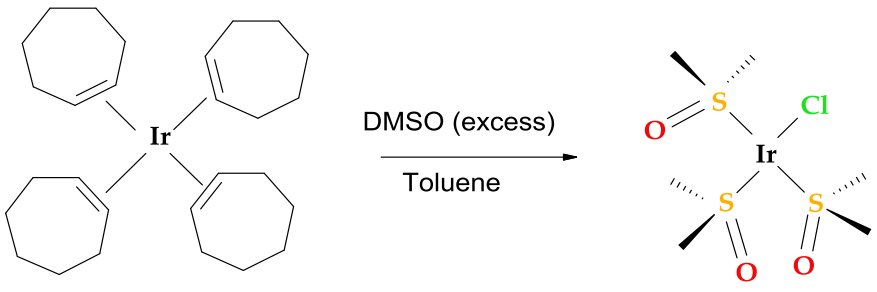

Figure 4.9: ***Reaction of formation [Ir(DMSO)$_3$] from [IrCl(COE)]$_2$.***

Table 4.1: NMR data for [IrCl(DMSO)$_3$], 4, at 298 K in DMSO-d$_6$.

Nucleus	*δ/ppm*	*Assignment*
^{1}H	2.80 - 3.50 (Shoulder)	CH_3 (DMSO)
^{13}C	41.75 (s)	CH_3 (DMSO)

4.4 Reactions of *4* with *p*-H$_2$ as a function of solvent

In 1862, Berthelot *et al*.[186, 187] reported the effect of solvent on the rate of a reaction, while the effect of solvent on chemical equilibrium came to light in 1896.[188] Solvent effects on the NMR spectra were first observed by Bothner-By and Glick[189] and independently by Reeves and Schneider[190] in 1957. Since then, the influence of solvent on chemical shifts and coupling constants has been thoroughly studied by a number of researchers.[191-196] A range of solvent studies was conducted in order to investigate how the uses of different solvents affect the product distribution for the reaction of ***4*** with *p*-H$_2$.

4.4.1 Reaction of *4* with *p*-H$_2$ in acetone-d$_6$

On placing an acetone-d$_6$ solution (0.6 mL) and ***4*** in a 5 mm NMR tube under 3 atm of *p*-H$_2$ at 298 K, no PHIP was evident in the high region of ^{1}H NMR spectrum for a dihydride product. This would suggest that reductive elimination of H$_2$ at this temperature does not take place, or that if it does it is below the limit of detection for *p*-H$_2$. In this case, the *p*-H$_2$ signals overlap with

the normal dihydride signals making detection of very small PHIP effects difficult.

When the same experiment was repeated after an interval of 15 minutes by adding fresh *p*-H_2 and shaken to allow the *p*-H_2 to react with the catalyst. The hyperpolarized ^1H NMR spectrum showed a pair of PHIP enhanced hydride signals were then immediately detected at δ -16.43 and δ -19.65 with J_{HH} = -6.34 Hz. The intensity of these signals was 1:0.04 at this point. In 2D COSY experiment, these signals proved to be coupled and hence originated from the same molecule. The 2D COSY spectrum is shown in Figure C1, Appendix C.

The observation of these two *p*-H_2 enhanced signals therefore indicates the formation of a new dihydride product with inequivalent hydrides. Isomer ***4b*** corresponds to such a species, where the hydride signals should have different chemical shifts because one hydride finds itself *trans* to chloride and the second hydride is *trans* to softer DMSO ligand.

The hydride resonances showed PHIP. Upon leaving the sample and recording the ^1H NMR spectrum with an interval of 15-20 minutes, the PHIP was still visible. This suggested that the addition reaction is slow. When the sample was shaken, the unreacted *p*-H_2 reacts with the sample solution and as a result the polarization comes back.

When the temperature was raised to 310 K, the intensity of PHIP derived signals started to increase and intensity of these signal found to be 1:0.8 at this point. Upon warming the sample to 315 K, no significant changes were observed in the intensity of the hydride signals. This might be due to the slow

reaction rate of ***4b*** at this temperature. The NMR data for [IrCl(H_2)(DMSO)$_3$], ***4b***, is given in Table 4.2.

Table 4.2: NMR data for mer-[IrCl(H_2)(DMSO)$_3$], 4b, at 298 K in acetone-d_6.

	^1H				^{13}C
Group	***δ_H / ppm***	***J / Hz***	***Integral***	***Assignment***	
CH_3 (DMSO^a)	2.38	-	2.95		50.9
CH_3 (DMSO^b)	2.49	-	3.05		43.1
H_a	-16.43	- 6.34	1.00	$^2J_{HH}$	-
H_b	-19.65	- 6.34	1.03	$^2J_{HH}$	-

To monitor the product distribution with temperature, the experiments were also carried out at variable temperatures but the dominant isomeric species in all observations were found to be the hydride ligands located at δ -16.43 and δ -19.65 and they exhibited the *m*eridional arrangement. The only *para*hydrogen spectroscopy (OPSY) also confirmed the resonances at δ -16.43 and δ -19.65 are derived from *p*-H_2. The OPSY spectrum is shown in Figure C2, Appendix C.

Enhancement of hydride resonances increased with temperature due to an increase in the exchange rate with *p*-H_2. At higher temperatures, *p*-H_2 enrichment is rapidly depleted. If NMR experiments need to be performed over a long period of time, a temperature where the enhancement is large enough, and where the rate of depletion of *p*-H_2 is not too fast, needs to be found. Once the signal enhancement has dropped due to depletion of *p*-H_2, the sample can be shaken to exchange *p*-H_2 in the gas phase for normal H_2 in solution. A slower,

but more effective way of regenerating good *p*-H_2 enhancement is to degas and refill the sample with *p*-H_2 from the high vacuum line.

To monitor the magnetization sharing process between the hydride ligands, the 1D EXSY experiments were conducted over a range of temperatures with variable mixing times. In 1D EXSY experiment, a shaped pulse selectively excites the specified resonance and measures the magnetization sharing between the two hydride ligands. In this experiment, the hydride resonance at δ -19.65 was excited, which found to share magnetization with the partner hydride resonance at δ -16.43. The rate constant data is given in Table C3, Appendix C and Eyring plot is given in Figure C4, Appendix C. The rate constants observed for an intra-molecular site exchange are given in Table 4.3.

The rate constants obtained for this intra-molecular hydride site exchange process were used to calculate the activation parameters $\Delta H^{\ddagger}$, $\Delta S^{\ddagger}$ and $\Delta G^{\ddagger}$. The activation parameters for this intra-molecular hydride site exchange are given in Table 4.4. The activation parameter data uses twice the rate constants in the analysis because when the transition state is reached there is an equal probability of the reaction returning to the starting point.

Table 4.3: ***Rate constants obtained for hydride site interchange of 4b in d_6-acetone.***

Temperature / K	*k / s^{-1} (hydride)*
305	0.18
310	0.19
315	1.5
320	1.6
325	3.1

Table 4.4: ***Activation parameters for hydride site interchange of 4b in d_6-acetone.***

4b		
Hydride exchange	$\Delta H^{\ddagger}$ / kJ mol^{-1}	126.8 ± 14
	$\Delta S^{\ddagger}$ / kJ mol^{-1}	154 ± 20
	$\Delta G^{\ddagger}_{300}$ / kJ mol^{-1}	82.2 ± 0.16

The activation parameters calculated for ***4b*** demonstrate that the large values of $\Delta H^{\ddagger}$ related to a process which involves significant bond breakage. This is also replicated in the large positive values of $\Delta S^{\ddagger}$ which are both consistent for a process involving a ligand loss.

4.4.2 Reaction of 4 with *p*-H_2 in toluene-d_8

A solution of ***4*** in 0.6 mL of toluene-d_8 in the presence of *p*-H_2 was monitored by ^{1}H NMR spectroscopy at 298 K. Initially, there was no indication of formation of any hydride products in the high field region of ^{1}H NMR spectrum which implies that reductive elimination of H_2 at this temperature does not take place. Upon warming the solution to 310 K and by adding fresh *p*-H_2 to the sample, weakly enhanced hydride resonances were appeared at δ -15.60 and δ -19.30 (J_{HH} = -6.50 Hz) as shown in Figure C5, Appendix C. The signal intensity of these resonances was 1:0.78. At 320 K, the resonance positions of these signals at δ -15.60 and δ -19.30 remained unchanged. When the temperature was increased to 323 K, a PHIP enhanced hydride signals were observed, and the signal intensity was calculated to be 1:1.15, but at that temperature no change in resonance positions of these signals was observed. The NMR data for complex, ***4b,*** is given in Table 4.5.

Table 4.5: NMR data for mer-[IrCl(H)$_2$(DMSO)$_3$], 4b, at 323 K in Toluene-d_8.

	^{1}H NMR				***^{13}C NMR***
Group	***δ_H / ppm***	***J / Hz***	***Integral***	***Assignment***	
CH_3 (DMSO^a)	2.38	-	3.10		51.9
CH_3 (DMSO^b)	2.49	-	3.01		42.3
H_a	-15.60	- 6.50	1.00	$^2J_{HH}$	-
H_b	-19.30	- 6.50	0.99	$^2J_{HH}$	-

The ^{1}H NMR data in Table 4.5 suggests that complex, ***4b,*** is of meridional arrangement of ligands in which the S-bound DMSO ligands were located at δ 2.38 and δ 2.49 respectively. The hydride ligand (stronger σ-donor) located at δ

-15.60 is *trans* to an S-bound DMSO ligand while the hydride signal at δ -19.30 is *trans* to chloride (weak σ-donor). The occurrence of polarization resulting in antiphase appearance to features that are separated by J_{HH} indicated that the hydride species was formed from the pairwise addition of H_2. The corresponding ^1H-^1H COSY NMR spectrum confirmed that these two hydride resonances are coupled to one another. This ^1H-^1H COSY spectrum is shown in Figure C6, Appendix C.

The addition of *p*-H_2 is further confirmed by an acquisition of ^1H OPSY spectrum, which also revealed PHIP derived hydride signals resonating at δ -15.60 and δ -19.30 in the high field region. The corresponding ^1H OPSY spectrum is shown in Figure C7, Appendix C. There is therefore a significant solvent effect on these resonance positions, which move dramatically on changing from acetone to toluene.

4.4.3 Reaction of *4* with *p*-H_2 in THF-d_8

To carry out this experiment, 1.2 mg of ***4*** and 0.6 mL of thf-d_8 is taken in an NMR tube fitted with a Young's tap. The ^1H thermal NMR spectrum was recorded using a 90° ^1H NMR pulse and in the next experiment *p*-H_2 was added to the sample at about 2.7 bar pressure. The hyperpolarized ^1H NMR spectrum was recorded by using a 45° ^1H NMR pulse at 298 K, which revealed enhanced hydride resonances at δ -18.89 and δ -19.50 respectively.

When the experiment was repeated at 310 K, new hydride signal was appeared at δ -16.33. Upon warming the solution to 320 K, the hydride resonances at δ -16.33 and δ -19.50 were strongly enhanced and the hydride signal which was initially observed at δ -18.89 disappeared over the course of

time which is indicative of their kinetic nature. When the temperature is increased to 323 K, there is a significant increase in the intensity of the hydride signal resonating at δ -16.33 and δ -19.50. These observations suggest that population of detected hydride species are solvent and temperature dependent. The ^{1}H NMR spectrum is shown in Figure C8, Appendix C. The NMR data for *fac*-[IrCl(H)$_2$(DMSO)$_3$], ***4a,*** and *mer*-[IrCl(H)$_2$(DMSO)$_3$], ***4b***, is given in the Tables 4.6 and 4.7.

Table 4.6: NMR data for fac-[IrCl(H)$_2$(DMSO)$_3$], 4a, at 323 K in THF-d$_8$.

	^{1}H NMR				^{13}C NMR
Group	***δ_H / ppm***	***J / Hz***	***Integral***	***Assignment***	
CH_3 (DMSO^a)	's' 3.22	-	3.15	-	52.1
CH_3 (DMSO^b)	's' 3.35	-	3.01		41.9
H_a	'd' -16.33	-6.72	1.00	$^{2}J_{HH}$	-
H_b	'd' -19.50	-6.72	1.05	$^{2}J_{HH}$	-

Table 4.7: NMR data for mer-[IrCl(H)$_2$DMSO)$_3$], 4b, at 323 K in THF-d$_8$.

	^{1}H NMR			
Group	***δ_H / ppm***	***J / Hz***	***Integral***	***Assignment***
CH_3 (DMSO)	's' 2.34	-	2.95	-
H	'd' -16.89	- 6.32	1.00	$^{2}J_{HH}$

The equivalent hydride resonance was instantly visible at δ -16.89, which corresponds to a product with the *facial* arrangement of ligands. The *mer* isomer with inequivalent hydride resonances located at δ -16.33 and δ -19.50 respectively and suggested being the thermodynamic products of the reaction. In a *m*eridional isomer, S-bound DMSO ligands were located at δ 3.22 and δ 3.35 respectively. It is quite intriguing, therefore, as to why ***4a*** is now formed so clearly.

The OPSY spectrum showed the *p*-H_2 derived signals for thermodynamically stable *mer* isomer, ***4b***. A ^{1}H-^{1}H COSY spectrum was then recorded which showed a correlation between these two hydride resonances (δ -16.33 and δ -19.50). The resultant spectrum is displayed in Figure C9, Appendix C.

4.4.4 Reaction of *4* with *p*-H_2 in benzene-d_6

A sample of ***4*** (ca. 1.2 mg) was taken and 0.6 mL of benzene-d_6 condensed into an NMR tube fitted with a Young's tap. The sample was exposed to *p*-H_2 at ***4*** atm pressure and then shaken to allow the reaction of *p*ara-enriched hydrogen with the sample solution. A ^{1}H NMR spectrum was recorded at 330 K. The ^{1}H hyperpolarized NMR spectrum showed one partially enhanced hydride resonance at δ -15.98 , which is suggested to be a kinetic product and then after an interval of 3 minutes antiphase doublets for the thermodynamically stable product appeared at δ -16.10 and δ - 20.95 (J_{HH} = -5.8 Hz) respectively. The NMR data for ***4b*** is given in Table 4.8.

Table 4.8: NMR data for mer-[IrCl(H)$_2$(DMSO)$_3$], 4b in benzene-d$_6$.

^{1}H NMR				
Group	*Chemical shift / δ_H*	*Coupling J/Hz*	*Integral*	*Assignment*
CH_3 (DMSO^a)	2.93	-	3.01	-
CH_3 (DMSO^b)	3.15	-	3.10	-
H_a	-16.10	-5.8	1.00	$^2J_{HH}$
H_b	-20.95	-5.8	1.03	$^2J_{HH}$

The newly formed complex, ***4b,*** also refers to such a dihydride complex in which one hydride ligand is located *trans* to an S-bound DMSO ligand and the second hydride ligand is present *trans* to the chloride. A ^{1}H-^{1}H COSY NMR experiment showed that these two hydrides resonances are coupled to one another and confirmed their origin in the same molecule. The ^{1}H-^{1}H COSY spectrum is displayed in Figure C10, Appendix C.

4.4.5 Reaction of *4* with *p*-H$_2$ in dmso-d$_6$

In order to carry out this experiment, a sample containing 1 mg (2.2 μM) of ***4*** was placed in an NMR tube fitted with a Young's tap, and 0.6 mL of DMSO-d$_6$ was transferred. The sample was then filled with *p*-H$_2$ at 2.9 atm pressure, and placed into the NMR spectrometer at 340 K for spectral analysis.

The ^{1}H NMR spectrum acquired under these conditions showed a strongly enhanced antiphase hydride signals at δ -16.67 with a partner signal at δ - 20.06. In addition, we see a further singlet at δ -14.92 of very weak intensity, and two

further enhanced hydride signals at δ -16.32 and δ -22.04. The ratio of peak intensities for the first two enhanced hydride species was 1:0.07. ^{1}H-^{1}H COSY spectrum spectroscopy confirmed that these two pair of hydride signals were coupled and hence originated in the same molecule (Figure C11, Appendix C). The minor pairs of hydride signals at δ -14.92, δ -16.32 and δ -22.04 disappeared over the course of an hour's reaction. The ^{1}H NMR spectrum depicting these hydrides is given in Figure C12, Appendix C.

This characteristic emission-absorption signal as shown in Figure 4.17 reveals the sign of the proton-proton couplings. In this case J_{HH} is negative because the hydride resonances are in emission-absorption mode. Positive couplings would give rise to absorption-emission signals. The 2D COSY showed ^{1}H-^{1}H coupling between hydrides at δ -20.03 and δ -16.67 is given in Figure C13, Appendix C.

An OPSY spectrum was acquired which made the observation of signals from *p*-H_2 derived protons possible. The OPSY spectrum further confirmed the *p*-H_2 transfer to the following resonances at δ -16.67 and δ -20.03. Typical ^{1}H OPSY NMR spectrum is shown in Figure C14, Appendix C.

These two *p*-H_2 enhanced signals at δ -16.67 and δ -20.03 therefore indicate the formation of a dihydride product with inequivalent hydrides. The dihydride complex, ***4b,*** refers to such a product in which one hydride ligand is located *trans* to (weak σ-donor) chloride and the second hydride is found *trans* to the soft DMSO ligand. The NMR data for complex [IrCl(H)$_2$(DMSO)$_3$]**, *4b,*** is given in Table 4.9.

Table: 4.9: NMR data for [IrCl(H)$_2$(DMSO)$_3$], 4b in dmso- d$_6$.

	^{1}H NMR				^{13}C NMR
Group	***δ_H / ppm***	***J / Hz***	***Integral***	***Assignment***	
CH_3 (DMSO^a)	's' 3.06	-	3.03	-	52.2
CH_3 (DMSO^b)	's' 3.23	-	2.97	-	42.5
H_a	'd' -16.67	- 6.39	0.97	$^2J_{HH}$	-
H_b	'd' -20.03	- 6.39	1.00	$^2J_{HH}$	-

In these hyperpolarized ^{1}H NMR spectra, strongly enhanced hydride resonances were observed at δ -16.67 and δ -20.03 throughout the measurements. These signals are only visible in dmso-d$_6$ through the *p*-H$_2$ effect. Upon waiting for 60 minutes, and shaking the sample in an NMR tube, the hydride signals reappear because PHIP is re-established. Only the product associated with a *m*erdional ligand arrangement is therefore detected.

The intensity of PHIP enhanced hydride signals increased significantly with temperature. At 335 K, the signal intensity of strongly enhanced resonances was 1:1.03, while at 340 K the signal intensity increased to 1:1.26. When the temperature rose to 345 K, signal intensity was 1:1.28. On warming the sample to 350 K and 355 K, the signal intensities were determined to be 1:1.31 and 1:1.35 respectively. The signal enhancement for these hydride products was observed at higher temperatures and the hydride peaks showed expected flattening as the rate of exchange with temperature increased. It is imperative to note that the line broadening was significant as the temperature increased which implies that the hydride peaks showed a solvent-dependent behavior with increasing temperature.

The detection of a weak set of signals in the original experiment at δ -16.32 and δ -22.04 suggests that loss of DMSO from ***4b*** is possible. In this case the formation of a species such as $[IrCl(H)_2(H_2O)(DMSO)_2]$ might be possible. This would suggest that the DMSO ligand is labile and in neat d_6-DMSO, the formation of $[IrCl(H)_2(DMSO)_3]$ is promoted. Given the propensity of this complex to react with H_2O to form this known dimer syn-$[DMSO)_2(H)Ir(\mu\text{-}OH)_2(\mu\text{-}Cl)Ir(H)(DMSO)_2][IrCl_2(DMSO)_2]$, such a reaction is possible.[170]

In order to monitor the dynamic behavior of complex, ***4***, in dmso-d_6, a series of ^1H EXSY spectra were acquired over a range of mixing times for a series of temperatures. The ^1H exchange spectroscopy (EXSY) experiment is used to obtain information about internuclear distances and exchange processes. In the EXSY experiment for ***4*** a shaped pulse selectively excited the hydride resonance at δ -16.67. An exchange process was detected, intra-molecular hydride exchange (magnetization transfer to the hydride resonance at δ -20.03).

The rate constants obtained for this intra-molecular hydride site exchange process were used to calculate the activation parameters $\Delta H^{\ddagger}$, $\Delta S^{\ddagger}$ and $\Delta G^{\ddagger}$. The rate data is given in Table C15, Appendix C and Eyring plot is given in Figure C16, Appendix C. The rate constants for this hydride site exchange process are given in Table 4.10, and the activation parameters for this intra-molecular hydride site exchange are given in Table 4.11.

Table 4.10: ***Rate constants obtained for hydride site interchange of 4b in dmso-d_6.***

4b		
Hydride exchange	$\Delta H^{\ddagger}$ / kJ mol^{-1}	59.9 ± 16
	$\Delta S^{\ddagger}$ / kJ mol^{-1}	60 ± 47
	$\Delta G^{\ddagger}_{300}$ / kJ mol^{-1}	77.9 ± 0.2

Table 4.11: ***Activation parameters for hydride site interchange of 4b in dmso-d_6.***

Temperature (K)	***k / s^{-1} (hydride)***
335	1.22
340	1.30
345	2.57
350	3.46
355	3.65

The activation parameters for hydride site interchange in dmso-d_6 determined to be $\Delta H^{\ddagger}$ = 59.9 ± 16 KJ/mol^{-1}, $\Delta S^{\ddagger}$ = 60 ± 47 KJ/mol^{-1} and $\Delta G^{\ddagger}_{300}$ = 77.9 ± 0.2 KJ/mol^{-1}. The values for enthalpy of activation ($\Delta H^{\ddagger}$) indicate that the associated process involves significant bond breakage. The entropy of activation ($\Delta S^{\ddagger}$) indicates the degree of randomness or disorder in a system. The values of $\Delta S^{\ddagger}$ show that disorder in the final state is more than in the initial

state. The large positive values for Gibb's free energy show that reaction is non-spontaneous.

4.5 Reaction of [IrCl(DMSO)$_3$], *4*, with PPh$_3$

The binding of PPh$_3$ to [IrCl(DMSO)$_3$], ***4***, in *p*-H$_2$ would be expected to be far more facile than H$_2$O. A sample of 1.2 mg of ***4*** and triphenylphosphine 0.5 mg was therefore prepared in 0.6 mL of d$_6$-acetone and exposed to 3 atm of *p*-H$_2$. When this reaction was monitored by ^{1}H NMR, two hydride containing products were immediately appeared.

These species provide two sets of hydride signals at δ -22.91, and δ -12.15 and δ -15.10, δ -20.85. The first hydride at δ -22.91 appears as a doublet of quartets where J_{HP} = 14.3 Hz, J_{HH} = 6 Hz. while the second signal at δ -12.15 appears as a doublet of triplets of doublets, where J_{HP} = 130.7 Hz, J_{HP} = 21 Hz and J_{HH} = 6 Hz. This species contain three phosphine ligands and two inequivalent hydrides. The three DMSO ligands are therefore replaced by PPh$_3$ in this product and they observed to be coupled in the corresponding 2D COSY spectrum as shown in Figure C17, Appendix *C*. An OPSY spectrum demonstrates the signals derived from *p*-H$_2$ addition is shown in Figure C18, Appendix C. The proposed structure for complex, ***4c,*** is shown in Figure 4.10 and the NMR data for complex, ***4c,*** is given in Table 4.12.

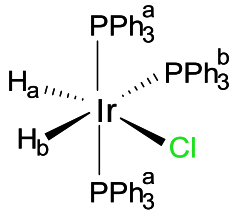

Figure 4.10: ***Structure of complex [IrCl(H)$_2$(PPh$_3$)$_3$], 4c.***

Table 4.12: ***Key NMR data for [IrCl(H)$_2$(PPh$_3$)$_3$], 4c.***

	^{1}H NMR			*^{31}P NMR*			*^{13}C*
Group	*δ_H / ppm*	*J/Hz*	*Integral*	*Group*	*δ_p / ppm*	*J/Hz*	*δ_c / ppm*
trans σ-H (PPh$_3$)	7.85	't' 8.14	6.01	-	-	-	140.1
cis σ-H (PPh$_3$)	7.74	'd' 4.50	12.01	-	-	-	138.5
trans m-H PPh$_3$)	7.30	't' 8.14	6.05	-	-	-	130.2
cis m-H (PPh$_3$)	7.18	'd' 4.50	12.07	-	-	-	128.1
trans p-H (PPh$_3$)	7.57	't' 7.98	3.05	-	-	-	136.1
cis p-H (PPh$_3$)	7.48	'm'	6.01	-	-	-	134.9
H$_a$	-22.91	'dq' 14.3, 6	1.02	PPh$_3^a$	8.49	'd' 14	-
H$_b$	-12.15	'dtd' 130.7 21, 6	1.00	PPh$_3^b$	-1.95	't' 14	-

The second product shows an evidence of containing two phosphine ligands with hydride resonances at δ -20.85 and δ -15.10. The PPh$_3$ ligand couples equally to the hydride ligands because the value of J_{HP} < 25 Hz and the

NMR data for that complex, ***4d***, is given in Table 4.13. The structure of complex, ***4d*** is shown in Figure 4.11. In $[IrCl(H)_2(PPh_3)_3]$, ***4c***, product the one hydride ligand is *trans* to chloride and the second hydride ligand is *trans* to phosphine ligand while in $[IrCl(H)_2(PPh_3)_2(DMSO)]$, ***4d***, One hydride ligand is *trans* to chloride ligand and second hydride is *trans* to DMSO.

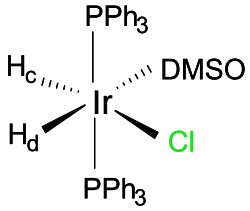

Figure 4.11: Structure of complex, $[IrCl(H)_2PPh_3)_2(DMSO)]$, 4d.

Table 4.13: Key NMR data of complex, $[IrCl(H)_2PPh_3)_2(DMSO)]$, 4d.

	^1H			^{31}P			^{13}C
Group	δ_H/ ***ppm***	***J/Hz***	***Integral***	***Group***	δ_P/ ***ppm***	***J/Hz***	
σ-H(PPh_3)	7.71	'd' 8.07	12.01	σ-H (PPh_3)	-	-	135.9
m-H(PPh_3)	7.63	't' 4.87	12.04	*m*-H (PPh_3)	-	-	128.5
p-H(PPh_3)	7.51	'm' 8.07	5.99	*p*-H (PPh_3)	-	-	133.7
CH_3 (DMSO)	2.95	's'	6.05	CH_3 (DMSO)	-	-	43.2
H_c	-20.85	'dt' 25, 6	1.03	PPh_3	14.4	's'	-
H_d	-15.10	'dt' 25, 6	1.00	-	-	-	-

It is clear from the structure that two DMSO ligands are replaced by phosphine ligands. When a 90° ^{1}H pulse is employed the ratio was between $[IrCl(H)_2(PPh_3)_3]$ and $[IrCl(H)_2(PPh_3)_2(DMSO)]$ was 1:1.03, however, with a 45° ^{1}H NMR pulse the ratio was used in conjunction with the PHIP effect, the ratio was 1:14.5. The equilibrium NMR data confirms that these products are present in very similar amounts. Complex, $[IrCl(H)_2(PPh_3)_3]$, is however less reactive to H_2 than $[IrCl(H)_2(PPh_3)_2(DMSO)]$ because it produces smaller PHIP enhancement signal. This might be expected due to an electron donating properties of phosphine stabilizing ***4c***.

To facilitate the further characterization of ***4c*** and ***4d*** an appropriate ^{1}H-^{31}P HMQC experiment was conducted at 298 K. This experiment revealed that the pair of hydride signals at δ -12.15 and δ -22.91 from ***4c*** coupled to the two ^{31}P centres at δ 8.49 and δ -1.95; this observation shows that these hydrides couple to two chemically in-equivalent ^{31}P nuclei. The second pair of hydride resonances at δ -15.10 and δ -20.85 from ***4d*** couple to a single ^{31}P centre; this observation, along with the doublet triplet splittings observed for each hydride resonance in the ^{1}H NMR spectrum, demonstrates that these hydrides couple to two chemically equivalent ^{31}P nuclei. The chemical shift of this ^{31}P nucleus is δ 14.47. The ^{1}H-^{31}P HMQC NMR spectrum is depicted in Figure C19, Appendix C.

In order to expand the available information for the ligand sphere of ***4d*** 1D EXSY experiments were performed on the same NMR sample. Irradiation of hydride resonance at δ -20.85 of ***4d*** yielded an nOe interaction to the other hydride resonance at δ -15.10, as well as to the protons of the bound triphenylphosphine ligand at δ 8.10, and an exchange peak to free H_2 at δ 4.55 respectively. The nOe interaction to the protons of the bound triphenylphosphine ligand also indicates that these hydride ligands are *cis* to a

PPh_3 ligand. The rate constant for the process of magnetization transfer corresponding to hydride site interchange in ***4d*** was determined to be 14.5 s^{-1}. The 1D EXSY spectrum acquired with selective irradiation of the hydride resonance at δ -20.85 of ***4d*** at 298 K is depicted in Figure C20, Appendix C.

4.5.1 Observation of SABRE within the PPh_3 system

An interesting aspect of the reaction of ***4*** with PPh_3 was the observation of signal enhancement for the free methyl protons of DMSO. The level of this signal enhancement proved to increase with the shake time as described in chapter 2. To explore the effect of shake time, the experiments were repeated by varying the reaction time from 20 to 90 s. Typical ^1H thermal and hyperpolarized NMR spectra depicting this effect is shown in Figure C21, Appendix C.

The enhancement level with a 20 s shake time was calculated to be 5.5 fold, while with 30 and 60 s, the signal enhancement level increased to 6.3 and 7.6 fold respectively. On increasing the shake time to 90 s, the enhancement level was determined to be 8.1 fold. At 120 s, the *p*-H_2 enrichment started to deplete and there was a decrease in the enhancement levels at this point. A graphical representation of variation in the enhancement levels with shake time is shown in Figure 4.12.

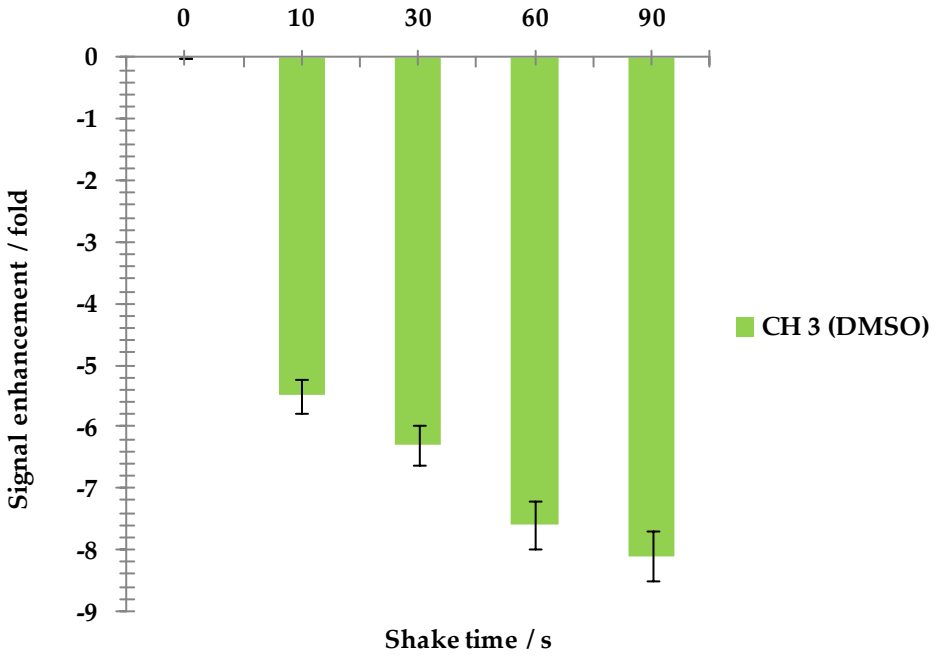

Figure 4.12: Variation in signal enhancement levels with shake time for the free DMSO signal when a sample of 4 in d_6-acetone containing PPh_3 is shaken with p-H_2.

The rate of hydride site interchange and H_2 loss in ***4d*** proved faster than in $[IrCl(H)_2(DMSO)_3]$. The effect of shake time on the intensity of hydride signals is graphically shown in Figure 4.13.

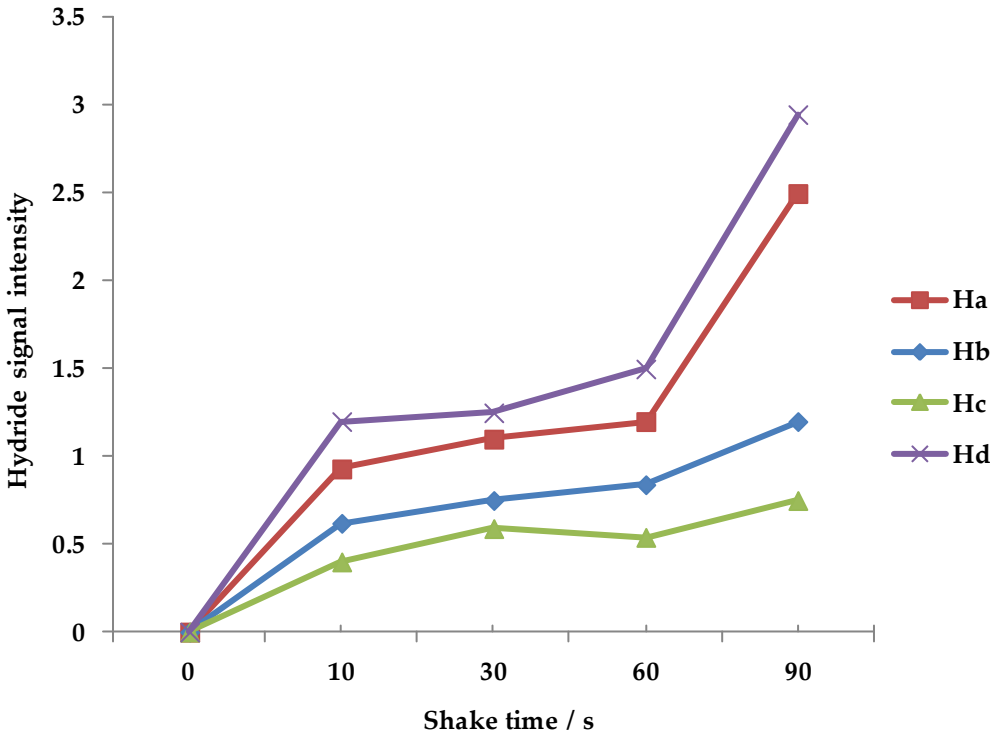

Figure 4.13: Variation in the intensities of hydride signals observed in case of complexes 4c and 4d with shake time.

Figure 4.13 shows that effect on the intensities of the hydride signals detected in both the complexes ***4c*** and ***4d*** as was also observed for the methyl resonance of free DMSO. The signal intensities of the hydride resonances demonstrated to be maximized at 90 s and started to decrease in a period between 90-120 s.

4.6 Reaction of [IrCl(DMSO)$_3$], *4*, with pyridine

This experiment was conducted to test the potential of the [IrCl(DMSO)$_3$] system, ***4***, as a biological sensor. Under an inert atmosphere, 1 mg (2.2 μM) of complex ***4*** and 5 μL (0.6 mmol) of pyridine were placed in an NMR tube that was fitted with a Young's tap and the NMR solvent *d*$_6$-DMSO taken into the tube. The sample was placed under 3 atm of *p*-H$_2$ and the ensuing reaction monitored by NMR spectroscopy at 310 K. The high-field region of the resultant ^{1}H NMR spectrum showed two hydride resonances at δ -19.10 and δ -21.90. These signals correspond to the dihydride pyridine containing species [IrCl(H)$_2$(py)(DMSO)$_2$], ***4e***. The structure of ***4e*** is displayed in Figure 4.14. The NMR data for ***4e*** is given in Table 4.14.

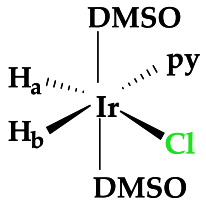

Figure 4.14: ***The structure of complex, 4e.***

Table 4.14: ***NMR data for [IrCl(H)$_2$(py)(DMSO)$_2$], 4e, at 310 K in d$_6$-dmso.***

	^{1}H NMR			^{13}C NMR
Group	***δ_H***	***J / Hz***	***Integral***	
σ-H (py)	8.47	'd' 4.08	2.01	146.5
m-H (py)	6.97	'm'	2.05	124.8
p-H (py)	7.64	't' 5.83	1.01	137.4
CH_3 (DMSO)		***'s'***	6.02	42.85
H_a	-19.10	'd' -7.8	1.00	
H_b	-21.90	'd' -7.8	1.02	

Typical thermal and hyperpolarized NMR spectra obtained in case of ***4e*** are shown in Figure C22, Appendix C.

Both of these new PHIP enhanced hydride signals appear δ -19.10 and δ-21.90 as antiphase doublets in the fully coupled ^{1}H NMR spectrum and enhancement of free pyridine was also observed. A ^{1}H-^{1}H COSY NMR experiment showed that these two hydride resonances coupled to one another and confirmed their origin in the same molecule. The ^{1}H-^{1}H COSY spectrum is displayed in Figure C23, Appendix C.

The *p*-H_2 addition was further confirmed by acquiring an OPSY spectrum which demonstrated the *p*-H_2 addition to the hydrides in the high field and pyridine resonances in the low field region of the ^{1}H OPSY-NMR spectrum is shown in Figure C24, Appendix C. It can be seen from these data that changing

from a hydride *trans* to DMSO, as in ***4b***, to hydride *trans* to pyridine, ***4e***, results in a movement of the hydride chemical shift from ca. δ -16 *to* δ -21**.**

4.7 Reactions of *4* with amino acids in the presence of *p*-H_2

The life sustainability process necessitates an interaction between organic (e.g., proteins, sugars and lipids) and inorganic (e.g., cations, often metals, and anions, such as phosphate) matter. At present, we discern that at least 13 metals that are imperative for plants and animals.[197, 198] The bulk metals include sodium, potassium, magnesium, and calcium and the trace metals include the d-block elements including vanadium, chromium, molbydenum, manganese, iron, cobalt, nickel, copper, and zinc.[198, 199] The bulk metals constitute 1-2% of the human body weight while the trace elements correspond to less than 0.01%. The concentrations of metals in the cells are strictly regulated at their respective optimum levels and the variation in metal concentration is often harmful and may even be detrimental to the living organism.[199]

Most of the trace metals are found as the natural component of proteins.[35] The metal ions possess distinctive features and tuned them by protein encapsulation to perform a wide variety of specific functions associated with the life processes.[197, 198] The specific functions in the cells are carried out by 30% of proteins, and about 40% of all enzymes consist of metals.[177] The thiolates of cysteines and aspartic acid act as ligands in proteins; for example binding of calcium with γ-carboxyglutamate side chains.[198, 200]

The role of metals in biological systems is of utmost significance. The first row transition elements are involved in various biochemical reactions. The heavier metallic elements are long known for their noxious effects on living organisms. The studies on platinum metal and its interaction with biologically relevant molecules open up a new vista of applications for platinum complexes possessing anticancer characteristics.[201] Additionally, ruthenium amino acid complexes have also been under study as potential antitumor compounds.[202] Research conducted on the interaction of transition metals with amino acid complexes also found their relevance in non-biological fields. The metal complexes such as osmium and ruthenium have found catalytic applications in hydrolysis.[203-205] Another interesting study was the formation of a DNA binding complex of amino acids with pentamethylcyclopentadienyl fragments.[206]

Metal hydrides play a pivotal role in transition metal catalysis.[207] Previously, various modes of amino acid binding to metals have been shown.[208] In this particular study of ***4*** and the amino acids, water has been used as a solvent. The complex, ***4,*** is water soluble and air stable in solution form and so that it has been selected as a potential polar soluble 'precursor receptor' complex that reacts with the amino acids in the presence of *p*-H_2 and the reaction products are characterized by NMR spectroscopy. The following section describes the *para*hydrogenation reactions of ***4*** with amino acids.

4.7.1 Reaction of *4* with alanine in the presence of *p*-H_2

Alanine is an amino acid with the chemical formula $CH_3CH(NH_2)COOH$. The structure of alanine is shown in Figure 4.15.

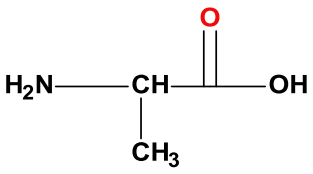

Figure 4.15: ***Structure of alanine.***

In this experiment, an NMR tube was charged with ***4*** (1 mg) and alanine 0.02 mg (224 nmol) in 0.6 mL of D_2O. A thermal ^1H NMR spectrum was acquired using a 90° ^1H NMR pulse. At about 3 bar pressure the *p*-H_2 was added to the sample and the hyperpolarized ^1H NMR spectrum was recorded using a 45° ^1H NMR pulse at 360 K. At 360 K, two set of hydride resonances were observed at δ -14.15, δ -23.70 and δ -16.05 and δ -25.10. Pairs of these resonances were found to be coupled in the corresponding 2D COSY spectrum. The COSY spectrum for complexes, ***4f***, and ***4g***, is shown in Figure C25, Appendix C and Figure C26, Appendix C demonstrates the dq-OPSY confirmed that the aforementioned complexes were formed as a result of *p*-H_2 addition.

The low field region of ^1H NMR spectrum exhibited resonances at δ 6.28, δ 4.71, δ 2.35, δ 2.64 and δ 1.40 along with two pairs of hydride resonances. First set of hydride resonance was observed at δ -23.70 with J_{HH} = -16 Hz and another hydride signal appeared at δ -14.15 with J_{HH} = -16 Hz. These hydride resonances correspond to a complex in which hydride ligand at δ -23.69 is *trans* to nitrogen of a bound amino acid ligand and the hydride resonance at δ -14.15 is *trans* to DSMO. The presence *of* ν(COO^-) band at 1677 cm^{-1} in the IR spectrum confirmed the chelation of $–NH_2$ and $– COO^–$ groups to iridium (I).

The second pair of hydride resonances appeared at δ -25.10 with J_{HH} = -15.58 Hz and δ -16.05 with J_{HH} = -15.58 Hz and. The hydride ligand at δ -25.10 observed to be *trans* to an O-bound amino acid site while the hydride signal at δ -16.05 is *trans* to an S-bound DMSO ligand and these hydride resonances were also found to be coupled in a corresponding 2D COSY NMR spectrum. The chelation of $–NH_2$ and $– COO^-$ groups to iridium (I) is confirmed by the presence *of* ν(COO^-) band at 1683 cm^{-1} in the IR spectrum.

The resonances for the bound DMSO ligands of these complexes are observed at δ 3.17, δ 3.25 and δ 2.38, δ 2.64 in the ^1H NMR spectrum. An integration of these resonances belonging to bound DMSO ligands satisfactorily yielded a 2:2 ratios and it can, therefore, be concluded that resonances at δ 2.38 and δ 2.64 belong to ***4f*** while the pair of resonances at δ 3.25 and δ 3.17 belong to ***4g***.

The high-field region of the ^1H NMR spectrum showed two pairs of hydride signals at δ -23.70, δ -14.15 and δ -25.10, δ -16.05 corresponding to ***4f*** and ***4g*** (initial ratio of ***4f*:*4g*** = 2:2) respectively. After about 10 minutes, the intensity of the resonances at δ -16.05 and δ-25.10 increased dramatically, while the intensity of the resonances at δ -14.15 and δ -23.70 started to decrease. This indicates that product ***4f*** is a kinetic product**,** while ***4g*** is a thermodynamic product. The structures of complexes ***4f*** and ***4g*** are shown in Figure 4.16, and the key NMR data for the complexes ***4f*** and ***4g*** is given in Tables 4.15 and 4.16.

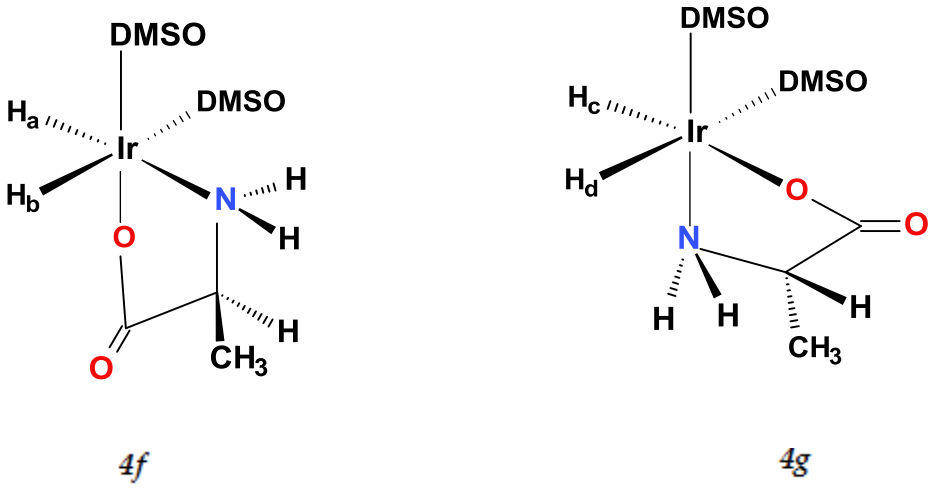

4f *4g*

Figure 4.16: Products obtained in an addition reaction of 4 with alanine in the presence of p-H_2.

Table 4.15: NMR data for $[Ir(H)_2(alanine)(DMSO)_2]^+Cl^-$, 4f.

	^{1}H NMR			*^{13}C NMR*	
Group	*δ_H / ppm*	*J / Hz*	*Integral*	*Group*	*δ_C / ppm*
CH_3 (Ala)	1.40	'm'	2.99	$\underline{C}H_3$	14.6
CH (Ala)	2.35	'm'	1.00	$\underline{C}O$	202.5
NH (Ala)	6.28	's'	1.02	$\underline{C}H$	51.3
NH (Ala)	4.71	's'	0.99	-	-
CH_3 (DMSO)[a]	2.38	's'	3.03	CH_3(DMSO)[a]	40.2
CH_3 (DMSO)[b]	2.64	's'	2.99	CH_3(DMSO)[b]	51.4
H_a	-23.70	'd' -16	1.01	-	-
H_b	-14.15	'd' -16	1.03	-	-

Table 4.16: ***NMR data for $[Ir(H)_2(alanine)(DMSO)_2]^+Cl^-$, 4g.***

	^1H NMR			***^{13}C NMR***	
Group	***δ_H / ppm***	***J / Hz***	***Integral***	***Group***	***δ_C / ppm***
CH_3 (Ala)	1.70	'm'	2.85	$\underline{C}H_3$	17.8
CH (Ala)	3.20	'm'	1.07	$\underline{C}O$	212.8
NH (Ala)	6.60	's'	1.05	$\underline{C}H$	53.9
NH (Ala)	4.20	's'	1.00	-	-
CH_3 (DMSO)[a]	3.17	's'	2.96	CH_3 (DMSO)[a]	41.7
CH_3 (DMSO)[b]	3.25	's'	1.01	CH_3 (DMSO)[b]	52.4
H_c	-25.10	'd'-15.56	1.02	-	-
H_d	-16.05	'd'-15.56	0.98	-	-

When the sample of ***4*** with an alanine was kept in water, the intensity ratio of hydride species observed to change with time. The integration areas of the hydride corresponding to ***4f*** and ***4g*** complexes with alanine as well as a monohydride complex formed as indicated in Table 4.17. The reaction of ***4*** with alanine however predominantly resulted in the formation of complex ***4g.***

Table 4.17: ***Distribution of complexes, 4f, 4g, and monohydride isomer formed with $[Ir(H_2)(alanine)(DMSO)_2]^+Cl^-$ as determined by the integration areas of the corresponding hydride resonances in the ^1H NMR spectra.***

Time / minutes	*4f* / %	*4g* / %	*Monohydride complex* / %
5	13	77	6
10	17.2	88	4
15	13	84	4
20	13.6	86	0.4
25	9.9	90	0.1

The monohydride species, observed as a signal at δ -26.90, was never significant and drops to 0.1 % after 25 minutes of reaction as demonstrated in Table 4.17. It was not identified. Product ***4g*** dominates at this point.

In order to explore the optimum signal enhancement, experiments were conducted with variable shake time to demonstrate that the enhancement levels found to increase and the shake time 120 s proved optimal and after that the enhancement levels started to drop and no further increase in enhancement levels has been observed. Another significant observation was the transfer of polarization to the CH and CH_3 protons of free alanine as shown in Figure C27, Appendix C.

In case of alanine, only the CH_3 and CH proton signals were enhanced. The enhancement was, however small. This observation suggests that it might be due to the insufficient stability of the iridium complex, as the effective and efficient way of polarization transfer also depends on the lifetime of the formed complex with alanine and changing the substrate or complex might help to increase the achievable enhancement levels. Another interesting observation was the enhanced methyl protons of DMSO.

The reaction of ***4*** with alanine resulted in signal enhancement for the free methyl protons of DMSO along with CH and CH_3 protons of free alanine. The level of signal enhancement found to increase with the shake time as demonstrated in chapter 2. To explore the effect of shake time, the experiments were carried out by varying the reaction time from 10 s to 120 s. At 10 s shake time, the signal enhancement levels for CH_3 protons of free DMSO, CH and CH_3 protons of free alanine were -1.9, -0.3 and -0.9 fold and the enhancement levels observed to increase with shake time reaching up to -7.2, -2.4 and -4.4 fold at 120 s for all the aforementioned proton sites. The graphical representation of signal enhancement observed in case of CH_3 protons of free DMSO, CH and CH_3 protons of free alanine is given in Figure 4.17.

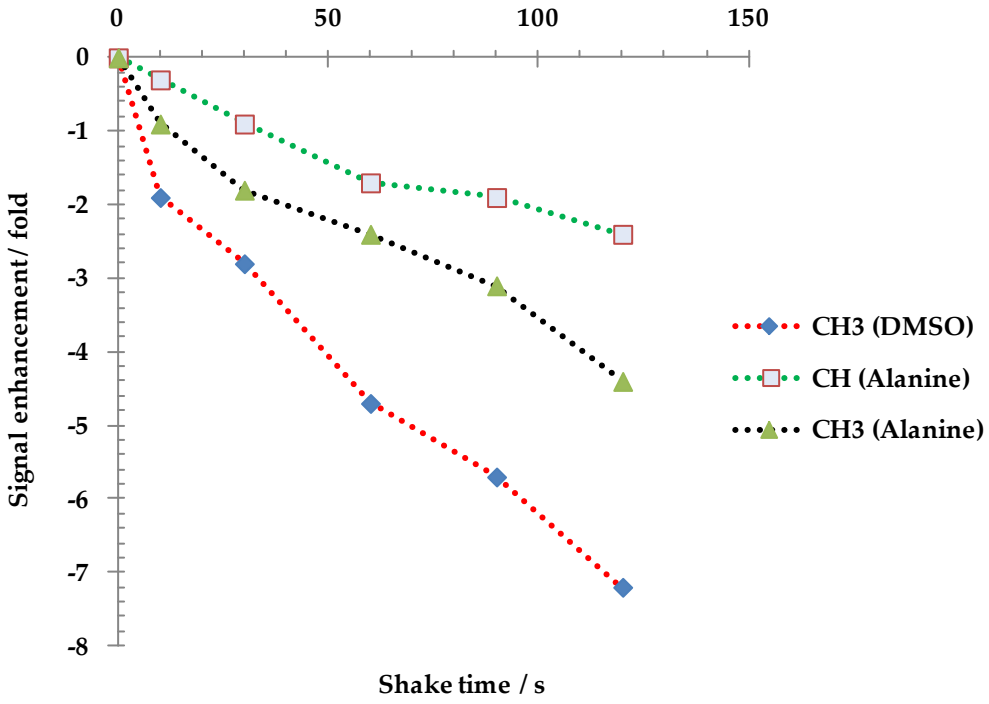

Figure 4.17: Variation in signal enhancement with shake time for the free DMSO signal and CH, CH_3 protons of free alanine when a sample of 4 in D_2O containing alanine is exposed to p-H_2.

To explore the magnetization sharing process, 1D EXSY experiments were conducted. The rate constant for the hydride exchange process was determined to be 0.17 s^{-1} at 320 K. This slow process is consistent with the low levels of SABRE. The reported pKa of alanine is 9.69.[209] The H_2 reductive elimination rate of the aforementioned complex is related to the identity of the nitrogen donor. The more basic the nitrogen, the lager the pKa value, and the stronger the Ir-N bond strength which corresponds to a slower H_2 elimination rate.

4.7.2 Reaction of *4* with leucine in the presence of *p*-H_2

The structure of leucine is shown in Figure 4.18.

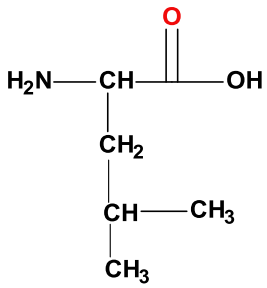

Figure 4.18: ***Structure of Leucine.***

A sample was prepared by the same method as used in case of alanine but in this experiment 0.03 mg (228 nmol) of leucine was used. Initially, there was no evidence of any hydride signal in the high field region of ^{1}H NMR spectrum. When the same experiment was repeated by adding fresh *p*-H_2, three hydride resonances were appeared at δ -14.45, δ -23.79 and δ -25.01 respectively. The acquisition of ^{1}H NMR spectrum after a waiting period of 15 minutes still contained these hydride signals. When the ^{1}H NMR spectrum was again acquired after 20 minutes, a new hydride signal appeared at δ -13.10. These resonances were found to be coupled in the corresponding ^{1}H-^{1}H COSY spectrum. The COSY spectrum acquired for complexes, ***4h***, and ***4i,*** is shown in Figure C28, Appendix C and C29, Appendix C demonstrates the dq-OPSY confirmed that the complexes, ***4h***, and ***4i***, were formed as a result of *p*-H_2 addition. The structures of the complexes, ***4h,*** and ***4i,*** are shown in Figure 4.19.

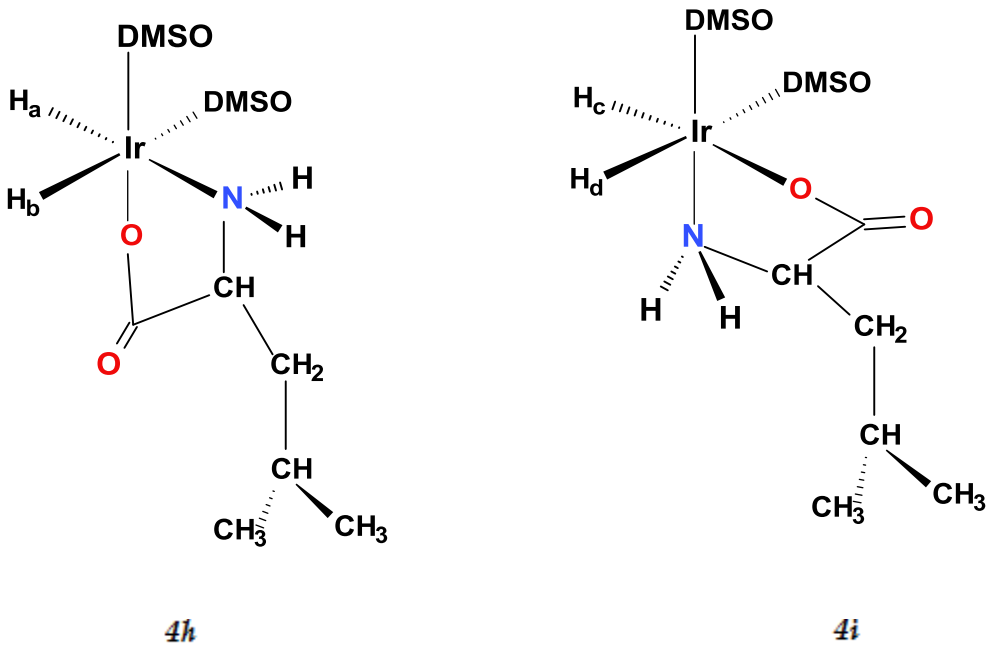

Figure 4.19: ***Products obtained in an addition reaction of 4 with leucine in the presence of p-H2.***

The hydride signal is a doublet located δ - 14.45 with J_{HH} = - 13 Hz while second hydride peak appeared at δ -23.79 with J_{HH} = -13 Hz. They are coupled in the corresponding 2D COSY spectrum. The hydride signal at δ -14.45 is *trans* to a DMSO ligand and the hydride resonance at δ -23.79 is *trans* to N-bound amino acid centre. The chelation of $–NH_2$ and $– COO^-$ groups to iridium (I) is confirmed by the presence *of* ν(COO^-) band at 1674 cm^{-1} in the IR spectrum. The NMR data for complex, ***4i*** is given in Table 4.18.

Table 4.18: ***NMR data for $[Ir(H)_2(Leu)(DMSO)_2]^+Cl^-$, 4h.***

	^1H NMR			***^{13}C NMR***	
Group	***δ_H / ppm***	***J / Hz***	***Integral***	***Group***	***δ_C / ppm***
CH_3(Leu)	0.87	't' 7.2	2.97	$\underline{C}_\alpha H$	50.5
CH_2(Leu)	1.73	'm'	1.95	$\underline{C}O$	198.6
CH_3(Leu)	1.17	'd' 8.4	3.03	$\underline{C}H_2$	40.9
$C_\alpha H$ (Leu)	2.15	'm'	1.00	$\underline{C}_\beta H$	25.4
$C_\beta H$(Leu)	3.05	'm'	0.97	$\underline{C}H_3$	12.8
NH (Leu)	6.89	'br s'	0.98	-	-
NH(Leu)	5.15	'br s'	1.03	-	-
CH_3 (DMSO)[a]	2.98	's'	3.07	CH_3 (DMSO)[a]	40.3
CH_3 (DMSO)[a]	2.67	's'	2.97	CH_3 (DMSO)[a]	50.4
H_a	-23.79	'd' - 13	1.25	-	-
H_b	-14.45	'd' - 13	1.12	-	-

In the second set of hydride resonances, the first hydride signal appeared at δ -13.10 with J_{HH} = -13.97 Hz, while the second hydride peak appeared at δ -25.01 with J_{HH} = -13.97 Hz. These hydride signals were coupled in the corresponding 2D COSY spectrum. The hydride ligand at δ -13.10 is *trans* to a soft DSMO ligand and the other hydride located at δ -25.01 is *trans* to O-bound amino acid site. The presence of IR ν(COO^-) band at 1680 cm^{-1} confirmed the chelation of $–NH_2$ and $– COO^–$ groups to iridium (I). The NMR data for ***4i*** isomer is given in Table 4.19.

Table 4.19: NMR data for $[IrH)_2(Leu)(DMSO)_2]^+Cl^-$, 4i.

	^1H NMR			^{13}C NMR	
Group	***δ_H / ppm***	***J / Hz***	***Integral***	***Group***	***δ_C / ppm***
CH_3(Leu)	0.92	't' 6.8	3.01	$C_\alpha H$	54.7
CH_2(Leu)	1.85	'm'	1.95	CO	201.7
CH_3 (Leu)	1.21	'd' 7.9	2.95	CH_2	42.8
$C_\alpha H$ (Leu)	2.35	'm'	1.00	$C_\beta H$	27.4
CH_β(Leu)	3.15	'm'	0.96	CH_3	16.9
NH(Leu)	6.01	'br s'	1.01	-	-
NH(Leu)	4.97	'br s'	0.97	-	-
CH_3 (DMSO)[a]	3.15	's'	2.75	CH_3 (DMSO)[a]	43.1
CH_3 (DMSO)[a]	3.29	's'	3.08	CH_3 (DMSO)[a]	52.7
H_c	-25.01	'd' - 13.97	1.39	-	-
H_d	-13.10	'd'-13.97	0.94	-	-

As the shake time is extended from 10 to 120 s, SABRE was also observed for the methyl protons of free DMSO and also for the CH_2 and CH protons as shown in Figure C30, Appendix C. The variation in levels of signal enhancement for the protons of free DMSO and for the CH_2 and CH_3 protons of free leucine is illustrated in Figures 4.20.

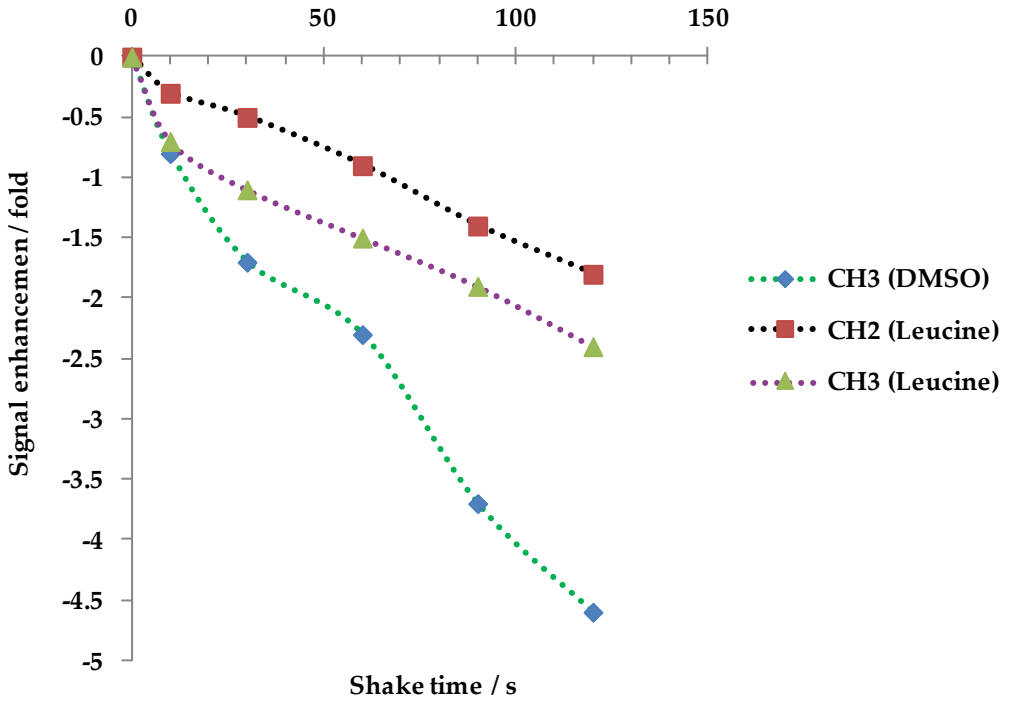

Figure 4.20: Signal enhancement observed with shake time for the free DMSO signal and CH_2, CH_3 protons of free leucine when a sample of 4 in D_2O containing leucine is shaken with p-H_2.

The enhancement levels found to increase with shake time. The levels of polarization transfer in case of leucine were comparatively weaker than those seen with alanine, which is due to the slower rate of H_2 reductive elimination.

4.7.3 Reaction of 4 with phenylalanine in the presence of *p*-H_2

Phenylalanine is an α-amino acid with the formula $O_2CCH(NH_2)CH_2C_6H_5$. The structure of phenylalanine is shown in Figure 4.21.

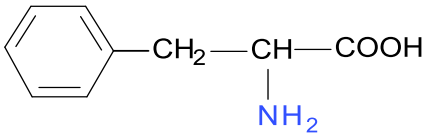

Figure 4.21: ***Structure of phenylalanine.***

A 0.6 mL D_2O solution of complex, ***4,*** and phenylalanine 0.05 mg (302 nmol) was placed in an NMR tube fitted with a Young's tap, and 3 atm of *p*-H_2 was introduced. NMR spectra were then collected on this sample using a 90° ^1H NMR pulse at 360 K, strong *p*-H_2 enhanced signals were immediately observed in the high-field region of the ^1H NMR spectrum at δ -14.20, δ -23.90 and δ -16.80, δ -25.02 respectively. These resonances were found to be coupled in the corresponding 2D COSY spectrum. The COSY spectrum obtained for complexes, ***4j*** and ***4k*** is shown in the C31, Appendix C and Figure C32, Appendix C demonstrates the dq-OPSY spectrum confirmed that the aforementioned products were formed as a result of *p*-H_2 addition.

One pair of hydride signals appeared at δ -14.20 with J_{HH} = -13.10 Hz and, while second pair of hydride resonances were observed at δ -23.90 with J_{HH} = -13.10 Hz. The resonance at δ -23.90 is *trans* to N-bound amino acid and

second hydride signal at δ -14.20 is located *trans* to the soft DMSO ligand. The isomeric products, ***4j, and 4k*** formed are shown in Figure 4.22. The key NMR data for complex ***4j*** is given in Table 4.20.

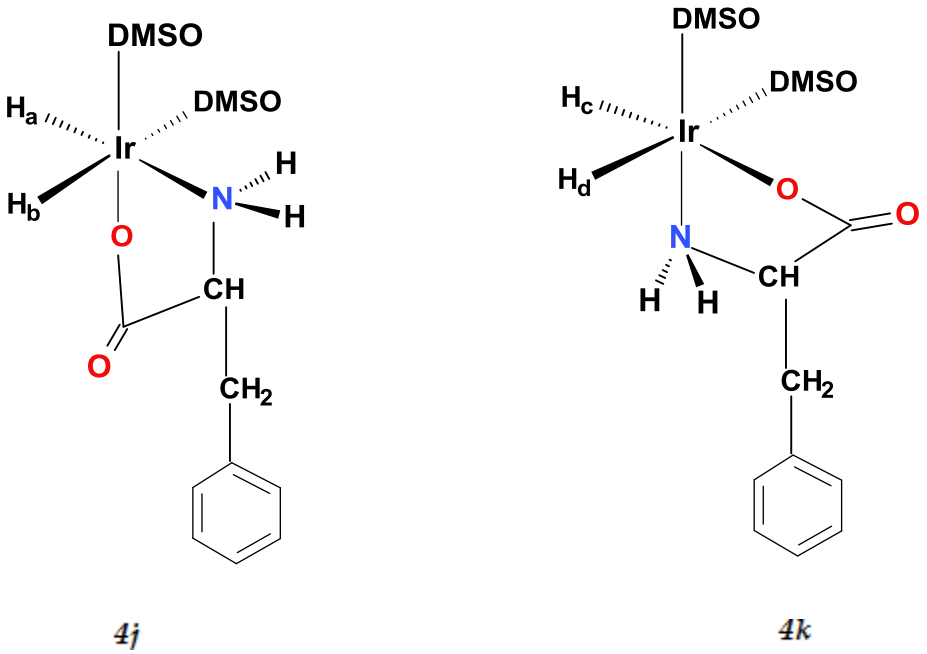

4j *4k*

Figure 4.22: Products obtained in an addition reaction of 4 with phenylalanine in the presence of p-H₂.

Table 4.20: NMR data for $[Ir(H)_2(phe)(DMSO)_3]^+Cl^-$, 4j.

	^{1}*H NMR*			^{13}*C NMR*	
Group	δ_H ***/ ppm***	***J / Hz***	***Integral***	***Group***	δ_C ***/ ppm***
$PhCH_a$	2.82	'dd'6, 13.6	1.12	<u>C</u>H	36.7
NH	2.92	'br s'	0.98	$\underline{C_\alpha}H$	56.1
$C_\alpha H$	3.19	'm'	1.00	<u>C</u>O	198.6
$PhCH_b$	3.62	'd' 13.6	1.11	Ar <u>C</u>	135.4
ArH	7.19	't'6.82	1.05	Ar <u>C</u>	130.3
ArH	7.28	't' 7.20	2.05	Ar <u>C</u>	128.8
ArH	7.54	'd' 4.30	2.03	Ar <u>C</u>	127.1
NH	7.72	'br s'	0.95	-	-
CH_3 (DMSO)[a]	2.28	's'	2.84	CH_3 (DMSO)[a]	41.7
CH_3 (DMSO)[b]	2.37	's'	3.01	CH_3 (DMSO)[b]	51.8
H_a	-23.90	-13.10'd'	1.01	-	-
H_b	-14.20	-13.10 'd'	1.05	-	-

The second pair of hydride resonances located at δ -16.80 with J_{HH} = -12.98 Hz and the other hydride signal observed at δ -25.02 with J_{HH} = -12.98 Hz. The hydride signal at δ -25.02 is *trans* to O-bound amino acid ligand while the resonance at δ -16.80 is *trans* to the S-bound DMSO ligand. The key NMR data for this dihydride complex, ***4k,*** is given in Table 4.21.

Table 4.21: NMR data for $[Ir(H)_2(phe)(DMSO)_3]^+Cl^-$, 4k.

^{1}H NMR				*^{13}C NMR*	
Group	*δ_H / ppm*	*J / Hz*	*Integral*	*Group*	*δ_C / ppm*
$PhCH_a$	3.05	'dd'5.98, 12.8	1.12	CH	38.4
$C_\alpha H$	3.45	'm'	1.06	$C_\alpha H$	58.8
$PhCH_b$	3.98	'd' 11.9	1.00	CO	202.5
ArH	7.63	't'6.98	1.05	Ar C	132.5
ArH	7.77	't' 7.80	2.10	Ar C	133.3
ArH	7.90	'd'5.05	2.05	Ar C	129.4
NH	7.85	'br s'	1.04	Ar C	126.3
NH	2.99	'br s'	1.01	-	-
CH_3 (DMSO)^a	3.44	's'	2.99	CH_3 (DMSO)^a	42.9
CH_3 (DMSO)^b	3.59	's'	3.05	CH_3 (DMSO)^b	52.7
H_a	-25.02	-12.98 'd'	1.19	-	-
H_b	-16.80	-12.98 'd'	1.05	-	-

In case of phenylalanine, the enhancement of methyl protons of free DMSO was observed. Its methine proton was not observed to polarize as in the case of alanine. This does not undergo amino acid ligand exchange.

4.7.4 Reaction of *4* with glycine in the presence of *p*-H_2

Glycine is an organic compound with the formula NH_2CH_2COOH. Glycine is a simple amino acid with one hydrogen atom on its side chain.[210] The structure of glycine is given in Figure 4.23.

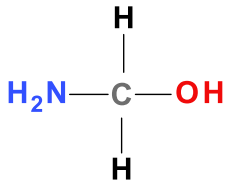

Figure 4.23: ***Structure of glycine.***

In order to complete this experiment, under an inert atmosphere, 1 mg of complex, ***4,*** with 0.02 mg (266 nmol) of glycine were placed in an NMR tube fitted with a Young's tap and dissolved in 0.6 mL of D_2O. The sample was placed under 3 atm of *p*-H_2 and placed in the NMR spectrometer at 360 K; two set of hydride resonances were immediately observed at δ -14.90, δ -24.12 and δ -16.10, δ -26.32. These resonances were found to be coupled in the corresponding 2D COSY spectrum. The COSY spectrum acquired in case of complexes, ***4l,*** and ***4m,*** is shown in the Figure C33, Appendix C and Figure C34, Appendix C demonstrates the dq-OPSY confirmed that both the complexes, ***4l,*** and ***4m,*** were formed as a result *p*-H_2 addition.

The first pair of hydride resonances in ***4l*** is seen at δ -14.05 with J_{HH} = -14.20 Hz and δ -24.10 with J_{HH} = -14.20 Hz. The resonance at δ -24.10 is assigned to an isomer in which the hydride is *trans* to an N-bound amino acid ligand. The second hydride signal at δ -14.05 is *trans* to an S-bound DMSO ligand as described earlier. The structures of complex complexes, ***4l,*** and ***4m,*** are shown in Figure 4.24 and NMR data for complex, ***4l*** is given in Table 4.22.

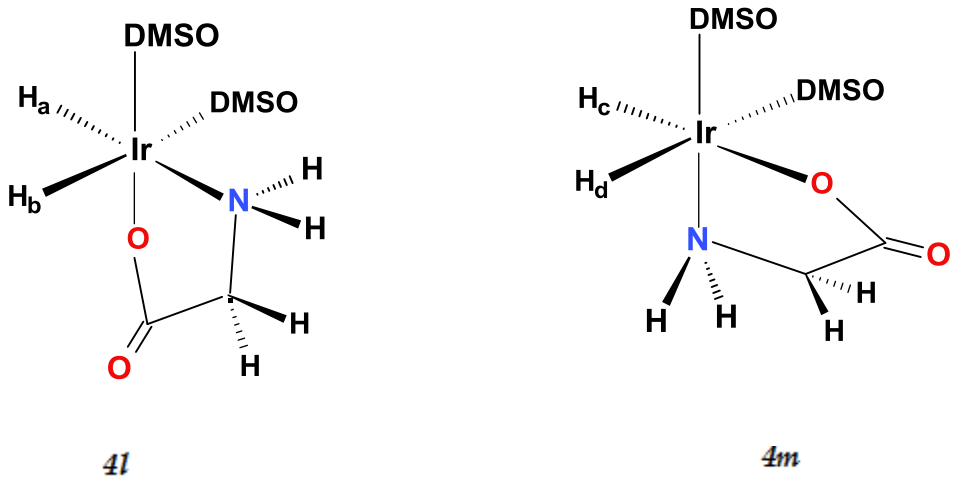

Figure 4.24: ***Products obtained in an addition reaction of 4 with glycine in the presence of p-H₂.***

Table 4.22: ***NMR data for $[Ir(H)_2(gly)(DMSO)_2]^+Cl^-$, 4l.***

	^{1}H NMR			***^{13}C NMR***	
Group	***δ_H / ppm***	***J / Hz***	***Integral***	***Group***	***δ_C / ppm***
CH_2 (Gly)	3.22	'd' 5.30	1.68	CO	197.5
NH (Gly)	5.06	's'	1.34	CH_2	42.6
NH(Gly)	6.05	's'	1.00	-	-
CH_3 (DMSO)[a]	3.53	's'	3.31	CH_3 (DMSO)[a]	42.7
CH_3 (DMSO)[b]	3.35	's'	3.01	CH_3 (DMSO)[b]	52.2
H_a	-24.10	'd' -14.20	1.12	-	-
H_b	-14.05	'd' -14.20	1.23	-	-

The second set of hydrides appeared at δ -26.32 with J_{HH} = -12.98 Hz and δ -16.01 with J_{HH} = -12.98 Hz. The hydride at δ -26.32 ligand is *trans* to O-bound glycine ligand and the hydride resonance at δ -16.01 is *trans* to DMSO-bound ligand. NMR data for ***4m*** is given in Table 4.23.

Table 4.23: NMR data for $[Ir(H)_2(gly)(DMSO)_2]^+Cl^-$, 4m.

	^{1}H NMR			*^{13}C NMR*	
Group	*δ_H / ppm*	*J / Hz*	*Integral*	*Group*	*δ_C / ppm*
CH_2 (Gly)	3.22	'd' 5.30	2.02	CO	199.4
NH (Gly)	5.43	'br s'	1.10	CH_2	44.9
NH (Gly)	4.39	's'	1.00	-	-
CH_3 (DMSO)[a]	3.21	's'	2.67	CH_3 (DMSO)[a]	41.7
CH_3 (DMSO)[b]	3.35	's'	2.94	CH_3 (DMSO)[b]	53.2
H_c	-26.32	'd' -12.98	0.94	-	-
H_c	-16.01	'd' -12.98	1.39	-	-

4.7.5 Reactions of *4* with Valine in the presence of *p-H_2*

Valine is an α-amino acid with the chemical formula $HO_2CCH(NH_2)CH(CH_3)_2$. Valine is considered to be an essential amino acid, as it must be supplied from an outside source.[210] The structure of valine is given in Figure 4.25.

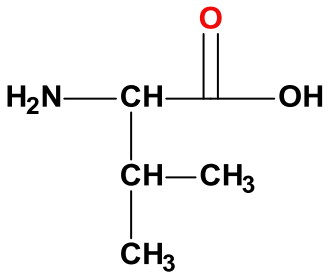

Figure 4.25: Structure of Valine.

A sample of ***4*** (ca. 1 mg) and valine 0.03 mg (256 nmol) was prepared in 0.6 mL of D_2O. A thermal ^1H NMR spectrum was recorded using a 90° ^1H NMR pulse at 360 K. The sample exposed to *p*-H_2 at 2.8 bar pressure and a hyperpolarized ^1H NMR spectrum was acquired using a 45° ^1H NMR pulse at 360 K. In case of valine, the hydride signals were observed immediately after an exposure to *p*-H_2. Two pair of hydrides resonances was observed. The first set of hydrides seen at δ -14.49 (J_{HH} = -15.57 Hz) and the second hydride resonance appeared at δ -23.16 (J_{HH} = -15.57 Hz). It is such a product in which the hydride at δ -23.16 is *trans* to an nitrogen bound valine ligand while the other hydride signal at δ -14.49 corresponds to such a species in which it is *trans* to an S-bound DMSO ligand. The ^1H-^1H coupling of these resonances in complexes, ***4n,*** and ***4o,*** was confirmed by 2D COSY as shown in Figure C35, Appendix C. The presence of ν(COO^-) band at 1678 cm^{-1} in the IR spectrum confirms the chelation of $–NH_2$ and $– COO^-$ groups to iridium(I). The products obtained in a reaction of ***4*** with valine are shown in Figure 4.26 and the key NMR data for complex, ***4n,*** is given in Table 4.24.

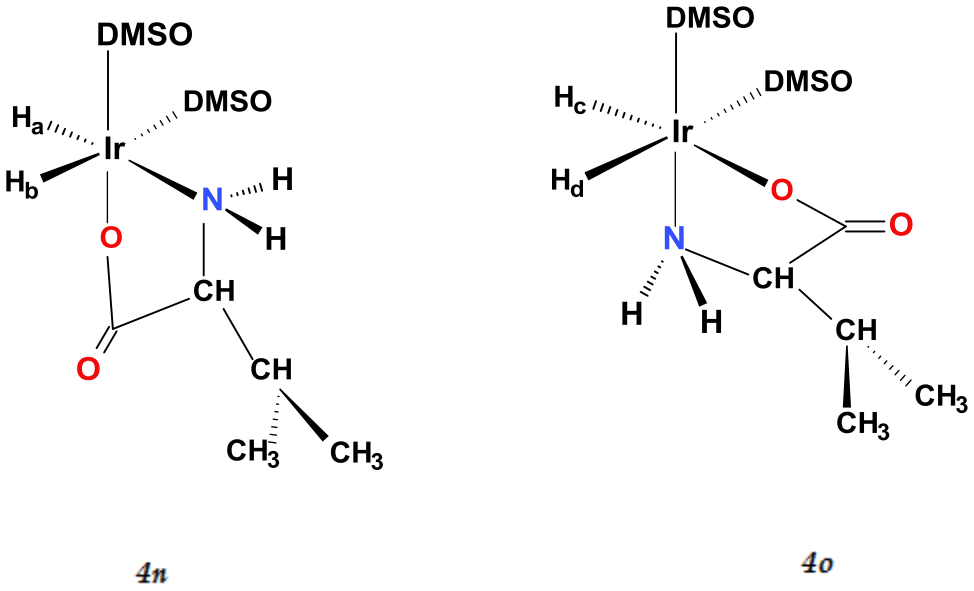

4n *4o*

Figure 4.26: Addition products obtained in a reaction of 4 with valine in the presence of p-H₂.

Table 4.24: NMR data for [Ir(H)₂(val)(DMSO)₂]⁺Cl⁻, 4n.

	¹H NMR			*¹³C NMR*	
Group	*δH / ppm*	*J / Hz*	*Integral*	*Group*	*δC / ppm*
$C(CH_3)_2$	0.81	'dd' 6, 12	5.98	$\underline{C}_\alpha H$	54.8
$C_\alpha H$	2.16	'm'	1.00	$\underline{C}O$	198.9
$C_\beta H$	2.38	'm'	1.05	$\underline{C}_\beta H$	30.6
NH (Val)	6.35	'br s'	1.11	$\underline{C}H_3$	18.9
NH (val)	4.38	'br s'	0.99	-	-
CH_3 (DMSO)[a]	2.86	's'	3.02	CH_3 (DMSO)[a]	40.8
CH_3 (DMSO)[b]	2.62	's'	3.01	CH_3 (DMSO)[b]	52.5
H_a	-23.16	'd' -15.57	1.02	-	-
H_b	-14.49	'd' -15.57	0.93	-	-

The second pair of hydride peaks were seen at δ -16.18 (J_{HH} = -14.10 Hz) and other hydride ligand appeared δ -24.55 (J_{HH} = -14.10 Hz). The hydride resonance at δ -24.55 is *trans* to an O-bound amino acid ligand and while other hydride resonance at δ -16.18 is *trans* to an S-bound DMSO ligand. These hydride resonances found to be coupled in corresponding 2D COSY experiment. The presence of ν(COO^-) band at 1685 cm^{-1} in the IR spectrum confirms the chelation of $–NH_2$ and $– COO^-$ groups to iridium(I). The key NMR data for this complex for ***4o*** is given in Table 4.25.

Table 4.25: NMR data for $[IrH)_2(val)((DMSO)_2]^+Cl^-$, 4o.

	^{1}***H NMR***			^{13}***C NMR***	
Group	***δ_H / ppm***	***J / Hz***	***Integral***	***Group***	***δ_C / ppm***
$C(CH_3)_2$	0.97	'dd' 6.20	6.01	$\underline{C}_\alpha H$	57.8
CH_α	2.26	'm'	1.03	$\underline{C}O$	202.6
CH_β	3.56	'm'	0.97	$\underline{C}_\beta H$	33.9
NH (Val)	3.98	'br, s'	1.08	$\underline{C}H_3$	21.7
NH (Val)	6.89	'br, s'	1.00		
CH_3 (DMSO)[a]	2.53	's'	3.07		
CH_3 (DMSO)[b]	2.62	's'	2.96		
H_c	-24.55	'd' -14.10	1.08		
H_d	-16.18	'd' -14.10	0.93		

An OPSY spectrum (Figure C36, Appendix C) was acquired, which further confirmed that these products are formed as result of interaction with *p*-H_2. The enhancement of methyl protons of DMSO ligand and methine protons of valine was observed in a reaction of ***4*** with valine in the low field region of ^{1}H NMR spectrum as shown in Figure 4.57.

The enhanced resonances shown in Figure C37, Appendix C are indicative of SABRE effect. The SABRE effect was more pronounced in case of the valine as compared to other dihydride amino acid complexes formed in a reaction with, ***4***. In this particular dihydride complex formed with valine, enhancement of methyl protons of dimethylsulfoxide along with CH_3 and CH protons of valine was a significant observation. The pKa of valine is 9.62.[209] The rate of hydride exchange observed for the alanine complex proved to be 0.17 s^{-1} while that of the valine complex was 0.10 s^{-1}. It is therefore clear that iridium alanine bond is less labile than the iridium valine bond. This reflects the fact alanine is the stronger base and hence a better donor which in turn leads to a slower H_2 elimination rate.

4.8 Conclusions

The reactions of ***4*** in selected solvents predominantly led to the formation of meridional dihydride complexes, in which one hydride ligand is *trans* to the poor sigma donor chloride and the other hydride is *trans* to soft DMSO ligand. In case of [Ir(MDSO)$_3$Cl], ***4***, a 16e square planer d^8 complex, the addition of H_2 results in formation 18e d^6 octahedral dihydride complex, [IrCl(H_2)(DMSO)$_2$], through a trigonal bipyramidal transition state (Figure 4.27) as was also observed in the case of H_2 addition to vaska's type complexes.[177-179]

Predominantly, the meridional isomer is detected in all the reactions of **4** with *p*-H_2. An interesting feature of this study was the observation of *facial* isomer in a reaction of ***4*** with d_8-THF.

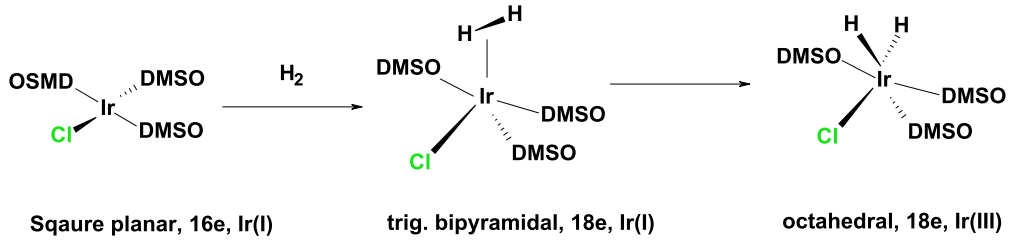

Figure 4.27: ***Oxidative addition of H_2 to [IrCl(DMSO)$_3$], 4, resulting in the formation of an octahedral complex through trigonal bipyramidal transition state.***

1D EXSY NMR spectroscopy revealed that the $IrCl(H)_2(DMSO)_2(L)$ systems undergo hydride site exchange and the formation of a 16-electron intermediate $[IrCl(H)_2(DMSO)_2]$ with in-equivalent hydride ligands is indicated. The activation parameters obtained for hydride site interchange in the reactions of ***4*** with *p*-H_2 in d_6-acetone and d_6-dmso have a large positive value of $\Delta S^{\ddagger}$ and are consistent with a dissociative process. For these systems, the activation free energy, $\Delta G^{\ddagger}_{300}$, proved better defined, and corresponded to 77.9 ± 0.2 kJ mol^{-1} in case of d_6-acetone, while for d_6-dmso the value is 82.2 ± 0.16 kJ mol^{-1}. This confirms that the barrier to the loss of the DMSO ligand in acetone is 4.3 ± 0.04 kJ mol^{-1} higher than that in d_6-dmos and confirms that there is a solvent dependence on this process.[211] Interestingly; it is the more strongly coordinating DSMO which has the higher barrier. Hence specific solvation of the intermediate cannot account for this effect. Instead non-specific salvation would

be indicated. The chemical shifts of hydride species observed in the reactions of ***4*** with *p*-H_2 in these solvent variation studies are summarized in Table 4.26.

Table 4.26: ***Hydride chemical shifts observed for the reactions of 4 in selected solvents.***

Solvent	***Hydride chemical shifts / ppm***	
DMSO-d_6	-16.67	-20.03
Acetone-d_6	-16.42	-19.73
THF-d_8	-16.33	-19.50
Toluene-d_8	-15.86	-18.96
Benzene-d_8	-16.35	-19.37

DMSO and acetone are polar solvents with dielectric constants of 20.7 and 46.7. The high dielectric constants of acetone and DMSO mean that they would be better at solvating species and more specifically charged species. Polar solvents would therefore lower the activation energy, resulting in a faster reaction, by lowering the $\Delta G^{\ddagger}$ for any process where stabilize of the transition state is achieved by neutralising charge build-up. This seems to happen for acetone here.

THF is a polar aprotic solvent with dielectric constant of 7.6. Benzene and toluene are classified as non-polar solvents having dielectric constants of 2.3 and 2.4. It can be seen from Table 4.26 that the hydride chemical shifts of ***4*** are highly solvent dependent.

Reaction of [IrCl(DMSO)$_3$], ***4***, with *p*-H$_2$ in the presence of triphenylphosphine at 310 K, yielded *p*-H$_2$ enhanced hydride resonances for two new complexes. These two new complexes were identified as the complex, [IrCl(H)$_2$(PPh$_3$)$_3$], ***4c***, and complex, [Ir(H)$_2$(DMSO)(PPh$_3$)$_2$Cl], ***4d***. The reaction of PPh$_3$ with ***4*** in the presence of *p*-H$_2$ proved to be facile compared to the reaction with pyridine. It is expected due to the electron donating properties of triphenylphosphine. The most noticeable feature of the ^{1}H NMR spectrum is however a large negative signal at δ 2.55 which matches that of free DMSO and indicates the occurrence of the SABRE effect. When this process was repeated with a 30 second sake, the free DMSO signal was increased dramatically in size to 8 times its original level.

The reaction of ***4*** with pyridine in the presence of *p*-H$_2$ and yielded well enhanced, long-lived, dihydride pyridine adduct, [IrCl(H)$_2$(py)(DMSO)$_2$], ***4e***. The complex, ***4e***, is a complex in which the higher field hydride signal results from a group which is *trans* to pyridine ligand and the lower field hydride ligand is *trans* to chloride. The hydride resonances were formed immediately upon exposure to *p*-H$_2$ along with enhancement of free pyridine ligands in the aromatic region of ^{1}H NMR spectrum. These observations confirm that the Ir-DMSO bond *trans* to hydride in **4** is prone to cleavage. Furthermore, it suggests that these systems can in fact be used to study the polarization of biological substrates in an analogous way to that described in Chapters 2 and 3.

Finally, it has been seen that ***4*** does indeed react with amino acids and a series of dihydrido amino acid complexes of the type [Ir(H)$_2$(amino acid)(DMSO)$_2$] are produced. In the case of reaction of 4 with amino acids (alanine, leucine, phenylalanine, glycine, and valine) two common types of

species detected which differ according to the relative orientations of the N/O centers of the amino acid as shown in Figure 4.28.

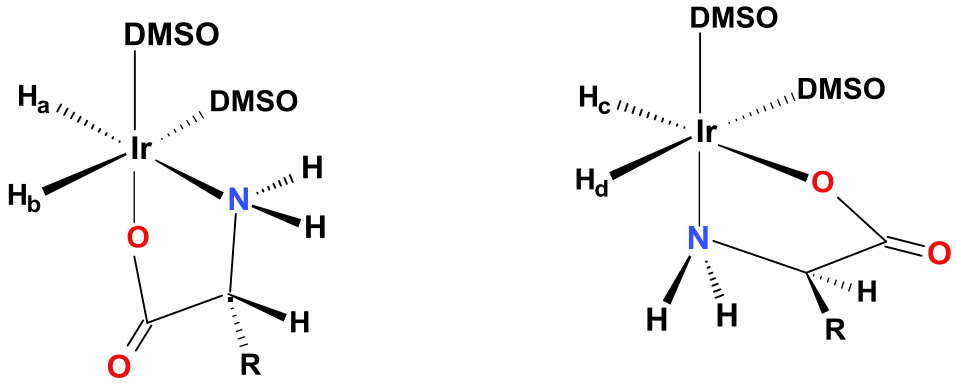

Figure 4.28: ***General structures of dihydrido amino acids complexes observed.***

It is possible to form these complexes by the addition of H_2 to $16e^-$ intermediate $Ir(DMSO)_2(O_2CCHRNH_2)$ where R is the amino acid substituent. This species forms if HCl and DMSO are lost from ***4***. The ratio of the H_2 addition adducts proved to be dependent on the identity of the amino acid as revealed in Table 4.27.

Table 4.27: ***Isomeric distribution of complexes of the type [Ir(H_2)(amino acid)$(DMSO)_2$]$^+Cl^-$ complexes formed in the presence of p-H_2 as determined by the integration areas of the corresponding hydride signals in the corresponding ^1H NMR spectra.***

Amino acid	*Isomeric ratio / %*	
	I	II
Alanine	9.9	90
Phenylalanine	13	87
Glycine	5	95
Leucine	8.8	91.2
Valine	10.9	89.1

Table 4.27 suggests that in case of all these amino acids, the thermodynamic product is II where the hydride ligand is *trans* to oxygen. In the thermodynamic product, the hydride ligand prefers to be *trans* to the more electronegative oxygen than the nitrogen centre as might be expected. The SABRE effect is also seen as these reactions progress, and excitingly the free amino acid and DSMO signals become polarized.

The polarization transfer to the methyl and methine protons in alanine was observed. When the substrate was changed to leucine, the methylene and methine protons were also polarized. In case of leucine, the polarization

transfer was weaker than that observed for alanine. In phenylalanine, its CH_2 and methine protons were not observed to polarize as observed in case aforementioned amino acids. This implies that steric hindrance provided by the bulky phenyl group might prevent efficient polarization transfer. The level of signal enhancement for the methyl and methylene protons in valine was significantly better compared to the other hyperpolarized amino acids.

It might be expected that optimization of this process offers a significant opportunity to hyperpolarize amino acids. Given the growing role of polypeptides as drugs and the need to optimize their synthesis this marks an important opportunity for SABRE.

CHAPTER FIVE

Experimental

5.1 General Experimental

Unless otherwise stated, chemical manipulations and samples for polarization studies were prepared under inert atmosphere conditions, using standard Schlenk (vacuum 10^{-2} mbar) or high vacuum (10^{-4} mbar) techniques, in order to exclude air and water. Dry N_2 for the Schlenk lines was purchased from BOC gases. Samples were stored under an atmosphere of N_2, using an Alvic Scientific Gas Shield glove box. The glove box was purged by N_2 gas provided by the evaporation of liquid N_2. NMR tubes were purchased from Apollo Scientific and were fitted with PTFE Young's taps.

5.1.1 Solvents and Reagents

The majority of the solvents were obtained as Analytical Grade from Fisher and dried by refluxing under N_2 over sodium wire (Aldrich) in the presence of benzophenone before storing under an inert atmosphere. Isopropanol (Fisher) was degassed by bubbling of Ar gas for 30 min. Water was distilled before use. Deutrated solvents for use in NMR were degassed and dried before use. Benzene-d_6 and toluene-d_8 were obtained from Aldrich and dried on potassium mirrors in ampoules fitted with a Young's tap. DMSO-d_6, and acetone-d_6 were obtained from Aldrich and dried over 3 Å molecular sieves in an ampoule and stored in the glove box.

5.2 NMR experiment

Typical NMR experiments consisted of the following steps. NMR samples were prepared in 5 mm NMR tubes fitted with PTFE Young's tap and degassed using freeze-pump-thaw cycles before addition of fresh *p*-H_2. Dry deuterated solvents were then either condensed into the sample tubes on a high vacuum line (d_8-toluene and d_6-benzene) or were transferred into the sample tubes under standard inert atmosphere conditions (d_6-acetone and d_6-DMSO) to a sample height of approximately 2.5 cm. When required, *p*-H_2 was added to the headspace of the sample tube to achieve approximately 3 atm of pressure, which was then shaken to dissolve the H_2 into solution. The sample was then ready for introduction into the NMR spectrometer, which was at a pre-selected temperature. The shake time was varied from 20-120 s to allow the sample to activate, so that hyperpolarization can be observed. All the hyperpolarization studies were conducted at a magnetic field of 65 G.

5.3 NMR Spectroscopy

The majority of NMR spectra were recorded on a Bruker 400 with ^{1}H at 400.13 MHz, ^{31}P at 161.90 MHz, ^{13}C at 100.00 MHz. The NMR spectra were also acquired on a Bruker 600 spectrometer with ^{1}H at 600.00 MHz, ^{13}C at 150.00 MHz. ^{1}H chemical shifts were calibrated from the residual ^{1}H signal present in the deuterated solvents, ^{31}P NMR shifts are reported relative to an external 85% solution of phosphoric acid, ^{13}C spectra were referenced using the chemical shifts for the deuterated solvent. Spectra were processed using the software programmes XWIN-NMR and TOPSPIN. The 1D ^{1}H, ^{31}P, ^{13}C, nOe and EXSY experiments as well as the 2D ^{1}H-^{1}H COSY experiment and ^{1}H-^{31}P, ^{1}H-^{13}C,

HMQC, and NOESY experiments were performed using pulse sequences described in the literature.[34-39]

5.4 Preparation of $[Ir(COD)Cl]_2$ (671.34 g mol^{-1})

$IrCl_3.3H_2O$ (2.2 g, 352.7 g mol^{-1}, 6.23 mmol) was suspended in water with 2-propanol (17:34 ml) in a round bottomed flask and degassed for 20 min. COD (6 ml, 5.292 g, 108 g mol^{-1}, 0.0489 mol) was added and the mixture was refluxed at 100° C for a minimum of 24 hours. After this time, the mixture was allowed to cool. The red precipitates were then filtered off and washed in a minimum amount of cold methanol. This was further dried on the high vacuum line. A red solid was collected (1.2 g, 671.4 g mol^{-1}, 1.78 mmol, 61.1 %).[212]

5.5 Preparation of $[IrCl(COE)]_2$ (896.13 g mol^{-1})

$[IrCl(COE)]_2$ was synthesised according to the standard literature procedure.[212] $IrCl_3.3H_2O$ (1.00 g, 2.83 mmol) and COE (3.0 ml) were refluxed in a mixture of isopropanol (11 ml) and water (5ml) under a steady stream of nitrogen. After 3 hours the dark red coloured solution changes to orange yellow and $[IrCl(COE)]_2$ precipitates out from the solution. The precipitates were collected quickly by filtration and washed with ice-cold methanol to remove the last traces of unreacted cyclooctene. Finally, the orange yellow powder was dried under vacuum. (Yield: 89%)

5.6 Preparation of [Ir(COD)(IMe)Cl] (432.1 g mol^{-1})

[Ir(COD)(IMe)Cl] complex was synthesized according to a method described by Crabtree *et al*.[146] The synthesis was carried out by using

$[Ir(COD)Cl]_2$ (60 mg, 89.2mmol) and *N*, *N*- dimethyl imidazolium carboxylate (30 mg, 212 μmol) in MeCN (5 mL). After 20 min of heating (oil bath, 75 °C) the colour of the solution changed from red to orange. The reaction mixture was cooled, and the solvent was removed in vacuum. The solid was dissolved in 2 mL of methylene chloride and was purified by column chromatography by elution with 1:1 hexane/ethyl acetate. The product was obtained by dissolving the solid in dichloromethane and recrystallizing by addition of ether to yield an orange microcrystalline solid. (Yield: 92%)

5.7 Preparation of $[IrCl(DMSO)_3]$ (462.19 g mol^{-1})

$[IrCl(DMSO)_3]$ was synthesised according to the method of Dorta *et al*.[176] Drop wise addition of DMSO (1 mL) to a bright orange suspension of $[IrCl(COE)]_2$ (0.38 g, 0.424 mmol) in toluene (6 mL) afforded a limpid yellow orange solution. Stirring at room temperature for *ca*. 3 hours, resulted in the formation of a lemon yellow precipitates, which were then filtered off, washed with diethyl ether, and dried under vacuum. (Yield: 81%)

5.8 Production of *p*-H_2

For the *p*-H_2 induced polarization (PHIP) experiments H_2 enriched in the *para* spin state was prepared by a method developed by Duckett *et al*,[22] produces 100% *p*-H_2. High purity H_2, taken from a cylinder is passed through a metal coil containing activated charcoal. The coil is maintained at 18 K by using a closed cycle helium refrigerator, via a copper block. The charcoal contains impurities, which catalyse the interconversion of the spin isomers of H_2; after a short time at 18 K the H_2 is enriched in the *para* isomer to 100%. The *para*-enriched H_2 is then drawn through a metal frit, which allows passage of gas but

keeps any charcoal particles inside the coil. The schematic representation of *p*-H_2 rig is displayed in Figure 5.2.

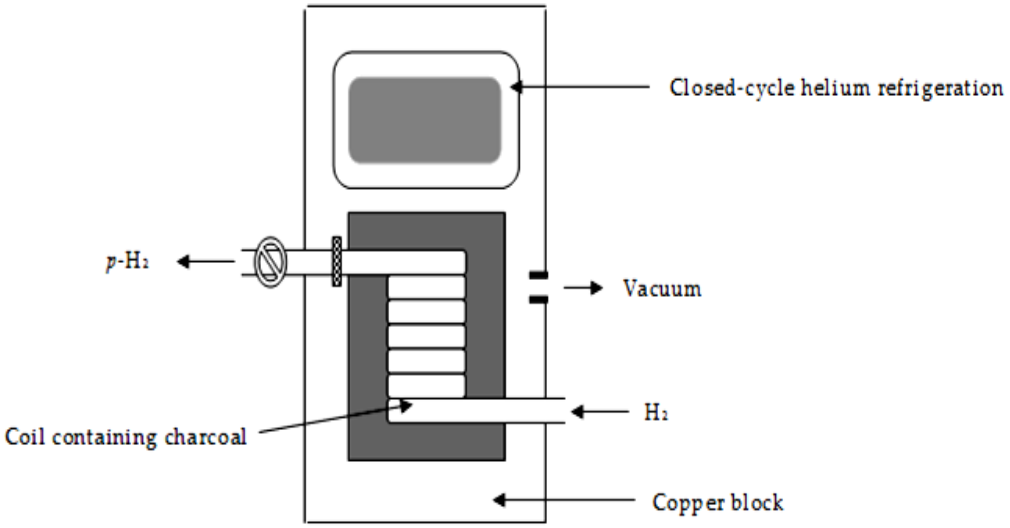

Figure 5.1: ***Schematic representation of p-H_2 rig.***

Sections 5.9 to 5.34 deal with the NMR results obtained for samples in Chapters 2 and 3. The substrates considered are pyridine, 2,- 6,- d_2-pyridine, 3-, 4-, 5-, d_3-pyridine, 2-picoline, 3-picoline, 4-picoline, 2-fluoropyridine, 3-fluoropyridine, 4-fluoropyridine, 2-chloropyridine, 3-chloropyridine, 4-chloropyridine, 2-bromopyridine, 3- bromopyridine, 4-bromopyridine, 2-iodopyridine, 3- iodopyridine, 4- iodopyridine, nicotinic acid, isonicotinic acid, methyl nicotinate, isonicotinamide, pyrazine, isoniazid, purine and pyrimidine. The NMR characterization data is included for most species in the following sections.

5.9 $[Ir(H)_2(IMe)(2,-6,-d_2\text{-py})_3]^+Cl^-$ (568.5 g mol^{-1})

A standard solution of $[Ir)(H)_2(IMe(d_2\text{-py})_3]Cl$ was prepared by using ***1*** (1.3 mg, 432.1 g mol^{-1}, 0.003 mmol) and 2-, 5-, d_2-pyridine (3 mg, 81.1 g mol^{-1}, 0.036 mmol) in methanol (0.6 mL). The solution was degassed in an NMR tube fitted with a Young's tap and then the solution exposed to *p*-H_2 (3 bar) to hydrogenate the sample. This resulted in $[Ir(IMe)(H)_2(d_2\text{-py})_3]Cl$ (1.5 mg, 568.5 g mol^{-1}, 0.0024 mmol) and free 2-, 5-, d_2-pyridine (2.5 mg, 81.1 g mol^{-1}, 0.021 mmol).

^{1}H NMR (MeOD, 400 MHz): 7.15 (d, *J* = 3.10 Hz, 4-*p*H *trans* to hydride), 7.02 (t, *J* = 5.45 Hz, 4-*p*H *cis* to hydride), 7.52 (m, 3-*m*H *trans* to hydride) 7.39 (t, *J* = 4.58, 1.54 Hz, 3-*m*H *cis* to hydride), 4.74 (methanol), 4.51 (s, free H_2), 4.72 (s, N-CH_2-CH_2-N), 6.98 (s, N-CH), 3.03 (methanol), 3.08 (s, CH_3^{IMe}), -22.66 (s, hydride).

^{13}C NMR (MeOD, 100 MHz): 122.3 (4-*p*H *trans* to hydride), 120.7, (4-*p*H *cis* to hydride), 140.8 (3-*m*H *trans* to hydride), 138.4 (3-*m*H *cis* to hydride), 51.2 (N-CH_2-CH_2-N), 117.3 (N-CH, carbene), 32.9 (N-CH_3, carbene).

5.10 $[Ir(H)_2(IMe)(3-,4-,5-,d_3\text{-py})_3]^+Cl^-$ (571.2g mol^{-1})

A standard solution of $[Ir)(H)_2(IMe(d_3\text{-py})_3]Cl$ was prepared by using [Ir(IMe)Cl(COD)] (1.3 mg, 432.1 g mol^{-1}, 0.003 mmol) was dissolved in methanol-d_4 (0.6 mL) and 3-, 4-, 5-, d_3-pyridine (3 mg, 82 g mol^{-1}, 0.036 mmol) was also added in an NMR tube fitted with a Young's tap. The solution was degassed and then exposed to *p*-H_2 at 3 bar to hydrogenate the sample. This resulted in $[Ir(IMe)(H)_2(d_3\text{-py})_3]Cl$ (1.5 mg, 571.2 g mol^{-1}, 0.0026 mmol) and free 3-, 4-, 5-, d_3-pyridine (2.5 mg, 82 g mol^{-1}, 0.030 mmol).

^{1}H NMR (MeOD, 400 MHz): 8.21 (m, σH *trans* to hydride), 7.98 (m, σH *cis* to hydride), 4.78 (methanol), 4.50 (s, free H_2), 4.72 (s, N-CH_2-CH_2-N), 7.01 (s, N-CH), 3.02 (methanol), 3.08 (s, CH_3^{IMe}), -22.68 (s, hydride).

^{13}C NMR (MeOD, 100 MHz): 122.3 (σH *trans* to hydride), 152.7, (σH *cis* to hydride), 51.2 (N-CH_2-CH_2-N), 117.3 (N-CH, carbene), 32.9-CH_3, carbene).

5.11 $[Ir(H)_2(IMe)(2\text{-pic})_3]^+Cl^-$ (604.6 g mol^{-1})

A solution of [Ir)$(H)_2$(IMe(2-pic)$_3$]Cl was prepared by using a complex, [Ir(IMe)Cl(COD)], ***1***, (1.3 mg, 432.1 g mol^{-1}, 0.003 mmol) and 2-picoline (3 mg, 93.13 g mol^{-1}, 0.032 mmol) were dissolved in methanol-d_4 (0.6 mL). The solution was degassed in an NMR tube fitted with a Young's tap and the solution was then exposed to *p*-H_2 (3 bar) to hydrogenate the sample. This resulted in [Ir(IMe)$(H)_2$(2-pic))$_3$]Cl (1.7 mg, 604.6 g mol^{-1}, 0.0028 mmol) and free 2-picoline (2.5 mg, 93.13 g mol^{-1}, 0.026 mmol).

^{1}H NMR (MeOD, 600 MHz): 8.42 (d, *J* = 5.49 4H, 3-*m*H *trans* to hydride), 8.30 (t, *J* = 6.97 Hz, 3-*m*H *cis* to hydride), 7.49 (t, *J* = 1.60, 7.95 Hz, 6-σH *trans* to hydride), 7.34 (d, *J* = 3.78 Hz, 6-σH *cis* to hydride), 7.02 (m, 4-*p*H *trans* to hydride), 6.95 (tt, *J* = 7.56, 1.64 Hz, 4-*p*H *cis* to hydride), 6.84 (t, 5.72, 5-*m*H *trans* to hydride), 6.74 (t, *J* = 6.72 Hz, 5-*m*H *cis* to hydride), 4.78 (methanol), 4.54 (s, free H_2), 4.72 (s, N-CH_2-CH_2-N), 7.01 (s, N-CH), 3.02 (methanol), 3.10 (s, CH_3^{IMe}), -24.8 (s, hydride).

^{13}C NMR (MeOD, 150 MHz): 160.2 (3-*m*H *trans* to hydride), 158.4, (3-*m*H *cis* to hydride), 153.0 (6-σH *trans* to hydride), 151.6 (6-σH *cis* to hydride), 144.4 (4-*p*H *trans* to hydride), 139.9 (4-*p*H *cis* to hydride), 124.2 (5-*m*H *trans* to

hydride), 122.8 (5-*m*H *cis* to hydride), 50.8 (N-CH_2-CH_2-N), 114.3 (N-CH, carbene), 33.1-CH_3, carbene).

5.12 $[Ir)(H)_2(IMe)(3\text{-pic})_3]^+Cl^-$ (604.6 g mol^{-1})

A standard solution of $[Ir)(H)_2(IMe(3\text{-pic})_3]Cl$ was prepared by using ***1*** (1.3 mg, 432.1 g mol^{-1}, 0.003 mmol) and 3-picoline (3 mg, 93.13 g mol^{-1}, 0.032 mmol) were dissolved in methanol-d_4 (0.6 mL). This was degassed in an NMR tube fitted with a Young's tap and then the solution was exposed to *p*-H_2 (3 bar) to hydrogenate the sample.

^{1}H NMR (MeOD, 600 MHz): 8.41 (m, Hz, 2-σH 3 *trans* to hydride), 8.37 (d, *J* = 3.22 Hz, 2H, 2-σH *cis* to hydride), 8.34 (m, 6-σH *trans* to hydride), 8.21 (d, *J* = 3.95 Hz, 2H, 6-σH *cis* to hydride), 7.37 (m, 4-*p*H *trans* to hydride), 7.28 (tt, *J* = 7.56, 1.64 Hz, 4-*p*H *cis* to hydride), 7.10 (dd, *J* = 4.18, 2.08, 5-*m*H *trans* to hydride), 6.95 (t, *J* = 6.72 Hz, 2H, 5-*m*H *cis* to hydride), 4.80 (methanol), 4.50 (s, free H_2), 4.75 (s, N-CH_2-CH_2-N), 6.98 (s, N-CH), 3.03 (methanol), 3.04 (s, CH_3^{IMe}), -22.8 (s, hydride).

^{13}C NMR (MeOD, 150 MHz): 154.0 (2-σH *trans* to hydride), 152.8 (2-σH *cis* to hydride), 149.0 (6-σH *trans* to hydride), 147.8 (6-σH *cis* to hydride), 136.4 (4-*p*H *trans* to hydride), 134.5 (4-*p*H *cis* to hydride), 125.2 (5-*m*H *trans* to hydride),124.4 (5-*m*H *cis* to hydride), 51.5 (N-CH_2-CH_2-N), 115.3 (N-CH, carbene), 31.9 (N-CH_3, carbene).

5.13 $[Ir(H)_2(IMe)(4\text{-pic})_3]^+Cl^-$ (604.6 g mol^{-1})

A standard solution of $[Ir)(H)_2(IMe(4\text{-pic})_3]Cl$ was prepared by using a complex, [Ir(IMe)Cl(COD)], (1.3 mg, 432.1 g mol^{-1}, 0.003 mmol) and 4-picoline (3 mg, 93.13 g mol^{-1}, 0.032 mmol) were dissolved in methanol-d_4 (0.6 mL). The sample was degassed in an NMR tube fitted with a Young's tap and then the solution was exposed to *p*-H_2 (3 bar) to hydrogenate the sample.

^{1}H NMR (MeOD, 600 MHz): 8.46 (t, *J* = 5.97 Hz, σH *trans* to hydride), 7.53 (d, *J* = 4.72 Hz, σH *cis* to hydride), 7.12 (t, *J* = 5.97 *m*H *trans* to hydride), 6.97 (d, *J* = 4.72 Hz, *m*H *cis* to hydride), 4.79 (methanol), 4.50 (s, free H_2), 4.70 (s, N-CH_2-CH_2-N), 7.01 (s, N-CH), 3.03 (methanol), 3.04 (s, CH_3^{IMe}), -22.8 (s, hydride).

^{13}C NMR (MeOD, 150 MHz): 154.0 (σH *trans* to hydride), 152.4 (*o*H *cis* to hydride), 126.2 (*m*H *trans* to hydride), 124.7 (*m*H *cis* to hydride), 51.8 (N-CH_2-CH_2-N), 115.7 (N-CH, carbene), 31.9 (N-CH_3, carbene).

5.14 $[Ir(H)_2(IMe)(2\text{-Fpy})_3]^+Cl^-$ (616.5 g mol^{-1})

A standard solution of $[Ir)(H)_2(IMe(2\text{-Fpy})_3]Cl$ was prepared by using [Ir(IMe)Cl(COD)] (1.3 mg, 432.1 g mol^{-1}, 0.003 mmol) and 2-flouropyridine (3 mg, 97.09 g mol^{-1}, 0.030 mmol) were dissolved in methanol-d_4 (0.6 mL). The solution was degassed in an NMR tube fitted with a Young's tap and the sample then exposed to *p*-H_2 and was kept in a mixture dry ice and acetone for about 20 minutes. This resulted in $[Ir(IMe)(H)_2(2\text{-Fpy})_3]Cl$ (1.7 mg, 616.5 g mol^{-1}, 0.0027 mmol) and free 2-flouropyridine (2.5 mg, 97.09 g mol^{-1}, 0.025 mmol).

^{1}H NMR (MeOD, 400 MHz): 8.24 (d, *J* = 2.49 4H, 3-*m*H *trans* to hydride), 8.17 (t, *J* = 6.97 Hz, 3-*m*H *trans* to hydride), 8.05 (d, *J* = 4.52 Hz, 6-σH *trans* to hydride), 7.94 (d, *J* = 3.78 Hz, 6-σH *cis* to hydride), 7.19 (m, 4-*p*H *trans* to hydride), 6.97 (tt, *J* = 5.20, 1.79 Hz, 4-*p*H *cis* to hydride), 6.79 (m, 5-*m*H *trans* to hydride), 6.66 (t, *J* = 6.72 Hz, 5-*m*H *cis* to hydride), 4.78 (methanol), 4.54 (s, free H_2), 4.72 (s, N-CH_2-CH_2-N), 7.01 (s, N-CH), 3.03 (methanol), 3.10 (s, CH_3^{IMe}), -26.1 (s, hydride).

^{13}C NMR (MeOD, 100 MHz): 161.3 (3-*m*H *trans* hydride), 158.9 (3-*m*H *cis* to hydride), 149.0 (6-σH *trans* to hydride), 147.6 (6-σH *cis* to hydride), 136.4 (4-*p*H, *trans* to hydride), 135.1 (4-*p*H *cis* to hydride), 125.2 (5-*m*H *trans* to hydride), 123.8 (5-*m*H *cis* to hydride), 49.9 (N-CH_2-CH_2-N), 116.3 (N-CH, carbene), 32.9-CH_3, carbene).

5.15 $[Ir(H)_2(IMe)(3\text{-}Fpy)_3]^+Cl^-$ (616.5 g mol^{-1})

A standard solution of [Ir)$(H)_2$(IMe(3-Fpy)$_3$]Cl was prepared by using ***1*** and free 3-flouropyridine (1.3 mg, 432.1 g mol^{-1}, 0.003 mmol) in methanol-d_4 (0.6 mL). The sample solution was degassed in an NMR tube fitted with a Young's tap and the solution was kept in a mixture dry ice and acetone for about 20 minutes and then exposed to *p*-H_2 (3 bar) to hydrogenate the sample. This resulted in [Ir(IMe)$(H)_2$(3-Fpy)$_3$]Cl (1.6 mg, 616.5 g mol^{-1}, 0.0025 mmol) and free 3-flouropyridine (2.6 mg, 97.09 g mol^{-1}, 0.026 mmol).

^{1}H NMR (MeOD, 600 MHz): 8.72 (d, *J* = 1.97 Hz, 2-σH *trans* to hydride), 8.69 (d, *J* = 3.22 Hz, 2-σH *cis* to hydride), 8.56 (t, *J* = 4.05 Hz, 6-σH *trans* to hydride), 8.49 (d, *J* = 3.40 Hz, 6-σH *cis* to hydride), 7.85 (m, 4-*p*H *trans* to hydride), 7.74 (t, *J* = 7.56, 1.64 Hz, 4-*p*H *cis* to hydride), 7.59 (q, *J* = 4.98 Hz, 5-*m*H

trans to hydride), 7.48 (t, *J* = 5.68 Hz, 5-*m*H *cis* to hydride), 4.77 (methanol), 4.48 (s, free H_2), 4.72 (s, N-CH_2-CH_2-N), 6.99 (s, N-CH), 3.05 (methanol), 3.17 (s, CH_3^{IMe}), -21.7 (s, hydride).

^{13}C NMR (MeOD, 100 MHz): 158.0 (2-σH *trans* to hydride), 156.8 (2-σH *cis* to hydride), 148.0 (6-σH *trans* to hydride), 147.1 (6-σH *cis* to hydride), 135.4 (4-*p*H *trans* to hydride), 133.0 (4-*p*H *cis* to hydride), 125.2 (5-*m*H *trans* to hydride),123.2 (5-*m*H *cis* to hydride), 50.9 (N-CH_2-CH_2-N), 114.5 (N-CH, carbene), 32.2 (N-CH_3, carbene).

5.16 $[Ir(H)_2(IMe)(4\text{-fpy})_3]^+Cl^-$ (616.5 g mol^{-1})

A standard solution of [Ir)$(H)_2$(IMe(4-fpy)$_3$]Cl was prepared by using ***1*** (1.3 mg, 432.1 g mol^{-1}, 0.003 mmol) and 4-flouropyridine (3 mg, 97.09 g mol^{-1}, 0.030 mmol) in methanol-d_4 (0.6 mL) in an NMR tube fitted with a Young's tap . The solution was kept in a mixture dry ice and acetone for about 20 minutes after its exposure to *p*-H_2 (3 bar) to hydrogenate the sample. This resulted in [Ir(IMe)$(H)_2$(4-fpy)$_3$]Cl (1.8 mg, 616.5 g mol^{-1}, 0.0029 mmol) and free 4-flouropyridine (2.4 mg, 97.09 g mol^{-1}, 0.024 mmol).

^{1}H NMR (MeOD, 600 MHz): 8.46 (t, *J* = 7.94 Hz, σH *trans* to hydride), 7.53 (d, *J* = 8.54 Hz, σH *cis* to hydride), 7.12 (t, *J* = 7.94 *m*H *trans* to hydride), 6.97 (d, *J* = 8.54 Hz, *m*H *cis* to hydride), 4.80 (methanol), 4.49 (s, free H_2), 4.72 (s, N-CH_2-CH_2-N), 7.01 (s, N-CH), 3.02 (methanol), 3.15 (s, CH_3^{IMe}), -25.7 (s, hydride).

^{13}C NMR (MeOD, 100 MHz): 152.2 (σH *trans* to hydride), 149.4 (σH *cis* to hydride), 136.4 (*m*H *trans* to hydride), 131.9 (*m*H *cis* to hydride), 52.2 (N-CH_2-CH_2-N), 117.3 (N-CH, carbene), 32.1 (N-CH_3, carbene).

5.17 $[Ir(H)_2(IMe)(2\text{-}Clpy)_3]^+Cl^-$ (665.8 g mol^{-1})

A standard solution of $[Ir)(H)_2(IMe(2\text{-}Clpy)_3]Cl$ was prepared by using [Ir(IMe)Cl(COD)] (1.3 mg, 432.1 g mol^{-1}, 0.003 mmol) (0.6 mL) and 2-chloropyridine (3 mg, 113.54 g mol^{-1}, 0.026 mmol) were dissolved in methanol-d_4 0.6 mL). This was degassed in an NMR tube fitted with a Young's tap and the *p*-H_2 was added to the sample and then it was kept in a mixture dry ice and acetone for about 20 minutes. This resulted in $[Ir(IMe)(H)_2(2\text{-}Clpy)_3]Cl$ (1.6 mg, 665.8 g mol^{-1}, 0.0024 mmol) and free 2-chloropyridine (2.4 mg, 113.54 g mol^{-1}, 0.021 mmol).

^{1}H NMR (MeOD, 600 MHz): 8.27 (d, *J* = 2.10 Hz, 3-*m*H *trans* to hydride), 8.15 (t, *J* = 7.15 Hz, 3-*m*H *trans* to hydride), 7.59 (t, *J* = 7.98 Hz, 6-σH *trans* to hydride), 7.49 (d, *J* = 3.78 Hz, 6-σH *cis* to hydride), 7.35 (m, 4-*p*H *trans* to hydride), 7.30 (t, *J* = 7.56, 1.64 Hz, 4-*p*H *cis* to hydride), 7.17 (t, 6.29, 5-*m*H *trans* to hydride),7.05 (t, *J* = 6.72 Hz, 5-*m*H *cis* to hydride), 4.74 (methanol), 4.51 (s, free H_2), 4.72 (s, N-CH_2-CH_2-N), 6.98 (s, N-CH), 3.01 (methanol), 3.08 (s, CH_3^{IMe}), -22.7 (s, hydride).

^{13}C NMR (MeOD, 100 MHz): 156.7 (3-*m*H *trans* to hydride), 152.7, (3-*m*H *cis* to hydride), 151.2 (6-σH *trans* to hydride), 149.4 (6-σH *cis* to hydride), 140.8 (4-*p*H *trans* to hydride), 138.4 (4-*p*H *cis* to hydride), 126.7 (5-*m*H *trans* to hydride), 122.9 (5-*m*H *cis* to hydride), 51.2 (N-CH_2-CH_2-N), 117.3 (N-CH, carbene), 32.9-CH_3, carbene).

5.18 $[Ir(H)_2(IMe)(3\text{-}Clpy)_3]^+Cl^-$ (665.8 g mol^{-1})

A standard solution of $[Ir)(H)_2(IMe(3\text{-}Clpy)_3]Cl$ was prepared by using a complex, [Ir(IMe)Cl(COD)], ***1***, and (1.3 mg, 432.1 g mol^{-1}, 0.003 mmol) and 3-chloropyridine (3 mg, 113.54 g mol^{-1}, 0.026 mmol) and dissolved in methanol-d_4 (0.6 mL) in an NMR tube fitted with a Young's tap. The solution was kept in a mixture dry ice and acetone for about 20 minutes after its exposure to *p*-H_2 (3 bar) to hydrogenate and activate the sample. This resulted in $[Ir(IMe)(H)_2(3\text{-}Clpy)_3]Cl$ (1.5 mg, 665.8 g mol^{-1}, 0.0025 mmol) and free 3-chloropyridine (2.7 mg, 113.54 g mol^{-1}, 0.023 mmol).

^{1}H NMR (MeOD, 600 MHz): 8.61 (d, *J* = 1.97 Hz, 2-*σ*H *trans* to hydride), 8.58 (d, *J* = 3.22 Hz, 2-*σ*H *cis* to hydride), 8.46 (t, *J* = 4.05 Hz, 6-*σ*H *trans* to hydride), 8.36 (d, *J* = 3.40 Hz, 6-*σ*H *cis* to hydride), 7.66 (t, *J* = 7.68 Hz, 4-*p*H *trans* to hydride), 7.54 (t, *J* = 7.47, 1.58 Hz, 4-*p*H *cis* to hydride), 7.28 (q, *J* = 4.66 Hz, 5-*m*H *trans* to hydride), 7.13 (t, *J* = 5.68 Hz, 5-*m*H *cis* to hydride), 4.78 (methanol), 4.52 (s, free H_2), 4.70 (s, N-CH_2-CH_2-N), 7.01 (s, N-CH), 3.04 (methanol), 3.18 (s, CH_3^{IMe}), -25.8 (s, hydride).

^{13}C NMR (MeOD, 100 MHz): 153.5 (2-*σ*H *trans* to hydride), 149.2 (2-*σ*H *cis* to hydride), 147.3 (6-σH *trans* to hydride), 146.1 (6-σH *cis* to hydride), 138.7 (4-*p*H *trans* to hydride), 136.7 (4-*p*H *cis* to hydride), 128.4 (5-*m*H *trans* to hydride),126.9 (5-*m*H *cis* to hydride), 51.1 (N-CH_2-CH_2-N), 116.9 (N-CH, carbene), 31.9 (N-CH_3, carbene).

5.19 $[Ir(H)_2(IMe)(4\text{-}Clpy)_3]^+Cl^-$ (665.8 g mol^{-1})

A standard solution of $[Ir)(H)_2(IMe(4\text{-}Clpy)_3]Cl$ was prepared by dissolving ***1*** (1.3 mg, 432.1 g mol^{-1}, 0.003 mmol) and 4-chloropyridine (3 mg, 113.54 g mol^{-1}, 0.026 mmol) in methanol-d_4 (0.6 mL) in an NMR tube fitted with a Young's tap. The solution was kept in a mixture dry ice and acetone for about 20 minutes and then exposed to *p*-H_2 (3 bar) to hydrogenate the sample. This resulted in $[Ir(IMe)(H)_2(4\text{-}Clpy)_3]Cl$ (1.7 mg, 665.8 g mol^{-1}, 0.0025 mmol) and free 4-chloropyridine (2.5 mg, 113.54 g mol^{-1}, 0.022 mmol).

^{1}H NMR (MeOD, 600 MHz): 8.49 (t, *J* = 7.75 Hz, *σ*H *trans* to hydride), 8.37 (d, *J* = 7.56 Hz, *σ*H *cis* to hydride), 7.12 (t, *J* = 7.75 Hz, H *trans* to hydride), 6.97 (d, *J* = 7.56 Hz, *m*H *cis* to hydride), 4.79 (methanol), 4.50 (s, free H_2), 4.70 (s, N-CH_2-CH_2-N), 7.01 (s, N-CH), 3.03 (methanol), 3.04 (s, CH_3^{IMe}), -22.8 (s, hydride).

^{13}C NMR (MeOD, 100 MHz): 153.8 (*σ*H *trans* to hydride), 151.4 (*σ*H *cis* to hydride), 137.8 (*m*H *trans* to hydride), 134.9 (*m*H *cis* to hydride), 50.5 (N-CH_2-CH_2-N), 116.3 (N-CH, carbene), 32.4 (N-CH_3, carbene).

5.20 $[Ir(H)_2(IMe)(2\text{-}Brpy)_3]^+Cl^-$ (799.2 g mol^{-1})

A standard solution of $[Ir)(H)_2(IMe(2\text{-}Brpy)_3]Cl$ was prepared by using a complex, [Ir(IMe)Cl(COD)], ***1***, (1.3 mg, 432.1 g mol^{-1}, 0.003 mmol) and 2-bromopyridine (3 mg, 158 g mol^{-1}, 0.018 mmol) in methanol-d_4 (0.6 mL). The solution was then degassed in an NMR tube fitted with a Young's tap and the solution was kept in a mixture dry ice and acetone for about 20 minutes and then exposed to *p*-H_2 (3 bar) to hydrogenate and activate the sample. This resulted in $[Ir(IMe)(H)_2(2\text{-}Brpy)_3]Cl$ (1.6 mg, 799.2 g mol^{-1}, 0.0020 mmol) and free 2-bromopyridine (2.6 mg, 158 g mol^{-1}, 0.016 mmol).

^{1}H NMR (MeOD, 600 MHz): 8.14 (d, *J* = 4.95, 3-*m*H *trans* to hydride), 8.01 (t, *J* = 6.97 Hz, 3-*m*H *trans* to hydride), 7.56 (t, *J* = 1.60, 7.95 Hz, 6-σH *trans* to hydride), 7.49 (d, *J* = 3.78 Hz, 6-σH *cis* to hydride), 7.46 (t, *J* = 6.98 Hz, 4-*p*H *trans* to hydride), 7.37 (tt, *J* = 7.56, 1.64 Hz, 4-*p*H *cis* to hydride), 7.01 (t, 5.72, 5-*m*H *trans* to hydride), 6.89 (t, *J* = 5.72 Hz, 5-*m*H *cis* to hydride), 4.78 (methanol), 4.50 (s, free H_2), 4.70 (s, N-CH_2-CH_2-N), 7.01 (s, N-CH), 3.03 (methanol), 3.12 (s, CH_3^{IMe}), -26.1 (s, hydride).

^{13}C NMR (MeOD, 150 MHz): 152.2 (3-*m*H *trans* to hydride), 147.6 (3-*m*H *cis* to hydride), 145.8 (6-σH *trans* to hydride), 141.4 (6-σH *cis* to hydride), 137.9 (4-*p*H *trans* to hydride), 136.1 (4-*p*H *cis* to hydride), 128.3 (5-*m*H *trans* to hydride), 122.7 (5-*m*H *cis* to hydride), 50.8 (N-CH_2-CH_2-N), 114.3 (N-CH, carbene), 33.1-CH_3, carbene).

5.21 $[Ir(H)_2(IMe)(3\text{-}Brpy)_3]^+Cl^-$ (799.2 g mol^{-1})

A solution of [Ir)$(H)_2$(IMe(3-Brpy)$_3$]Cl was prepared by using ***1*** (1.3 mg, 432.1 g mol^{-1}, 0.003 mmol) and 3-bromopyridine (3 mg, 158 g mol^{-1}, 0.018 mmol) in methanol-d_4 (0.6 mL) in an NMR tube fitted with a Young's tap. The solution was kept in a mixture dry ice and acetone for about 20 minutes and then exposed to *p*-H_2 (3 bar) to hydrogenate the sample. This resulted in [Ir(IMe)$(H)_2$(3-Brpy)$_3$]Cl (1.6 mg, 799.2 g mol^{-1}, 0.0020 mmol) and free 3-bromopyridine (2.6 mg, 158 g mol^{-1}, 0.016 mmol).

^{1}H NMR (MeOD, 400 MHz): 8.56 (m, 2-σH *trans* to hydride), 8.46 (d, *J* = 4.25 Hz, 2-σH *cis* to hydride), 7.60 (m, 6-σH *trans* to hydride), 7.55 (d, *J* = 3.22 Hz, 2H, 6-σH *cis* to hydride), 7.76 (t, *J* = 6.97 Hz, 4-*p*H *trans* to hydride), 7.66 (t, *J* = 7.56 Hz, 4-*p*H *cis* to hydride), 7.12 (m, 5-*m*H *trans* to hydride), 6.97 (t, *J* = 6.72

Hz, 5-*m*H *cis* to hydride), 4.81 (methanol), 4.51 (s, free H_2), 4.71 (s, N-CH_2-CH_2-N), 7.05 (s, N-CH), 3.03 (methanol), 3.03 (s, CH_3^{IMe}), -24.7 (s, hydride).

^{13}C NMR (MeOD, 100 MHz): 152.7 (2-σH *trans* to hydride), 150.8 (2-σH *cis* to hydride), 140.2 (6-σH *trans* to hydride), 138.9 (6-σH *cis* to hydride), 133.4 (4-*p*H *trans* to hydride), 132.0 (4-*p*H *cis* to hydride), 126.2 (5-*m*H *trans* to hydride), 121.2 (5-*m*H *cis* to hydride), 52.8 (N-CH_2-CH_2-N), 116.8 (N-CH, carbene), 30.9 (N-CH_3, carbene).

5.22 $[Ir(H)_2(IMe)(4\text{-}Brpy)_3]^+Cl^-$ (799.2 g mol^{-1})

A standard solution of [Ir)$(H)_2$(IMe(4-Brpy)$_3$]Cl was prepared by using [Ir(IMe)Cl(COD)] (1.3 mg, 432.1 g mol^{-1}, 0.003 mmol) and 4-bromopyridine (3 mg, 158 g mol^{-1}, 0.018 mmol) in methanol-d_4 (0.6 mL). The solution was degassed in an NMR tube fitted with a Young's tap and the solution was kept in a mixture dry ice and acetone for about 20 minutes and then exposed to *p*-H_2 (3 bar) to hydrogenate the sample. This resulted in [Ir(IMe)$(H)_2$(4-Brpy)$_3$]Cl (1.5 mg, 799.2 g mol^{-1}, 0.0018 mmol) and free 4-bromopyridine (2.7 mg, 158 g mol^{-1}, 0.017 mmol).

^{1}H NMR (MeOD, 600 MHz): 8.61 (t, *J* = 4.31 Hz, σH *trans* to hydride), 8.52 (d, *J* = 3.22 Hz, σH *cis* to hydride), 7.42 (t, *J* = 4.31 Hz *m*H *trans* to hydride), 7.34 (d, *J* = 3.22 Hz, *m*H *cis* to hydride), 4.79 (methanol), 4.50 (s, free H_2), 4.70 (s, N-CH_2-CH_2-N), 7.01 (s, N-CH), 3.03 (methanol), 3.04 (s, CH_3^{IMe}), -22.8 (s, hydride).

^{13}C NMR (MeOD, 100 MHz): 152.8 (σH *trans* to hydride), 150.3 (σH *cis* to hydride), 139.8 (*m*H *trans* to hydride), 138.4 (*m*H *cis* to hydride), 50.5 (N-CH_2-CH_2-N), 116.3 (N-CH, carbene), 32.4 (N-CH_3, carbene).

5.23 $[Ir(H)_2(IMe)(2\text{-}Ipy)_3]^+Cl^-$ (940.2 g mol^{-1})

A solution of $[Ir)(H)_2(IMe(2\text{-}Ipy)_3]Cl$ was prepared by taking [Ir(IMe)Cl(COD)] (1.3 mg, 432.1 g mol^{-1}, 0.003 mmol) and 2-iodopyridine (3 mg, 205 g mol^{-1}, 0.011 mmol) in methanol-d_4 (0.6 mL). The solution was then degassed in an NMR tube fitted with a Young's tap and the solution was kept in a mixture dry ice and acetone for about 25 minutes and then exposed to *p*-H_2 (2.8 bar) to hydrogenate the sample. 2-iodopyridine took bit longer to activate and this resulted in $[Ir(IMe)(H)_2(2\text{-}Ipy)_3]Cl$ (1.6 mg, 940.2 g mol^{-1}, 0.0016 mmol) and free 2-iodopyridine (2.4 mg, 205 g mol^{-1}, 0.011 mmol).

^1H NMR (MeOD, 600 MHz): 8.01 (d, *J* = 4.10 Hz, 3-*m*H *trans* to hydride), 7.94 (t, *J* = 6.97 Hz, 3-*m*H *trans* to hydride), 7.49 (d, *J* = 7.80 Hz, 6-*σ*H *trans* to hydride), 7.38 (d, *J* = 3.78 Hz, 6-*σ*H *cis* to hydride), 7.24 (m, 4-*p*H *trans* to hydride), 7.21 (t, *J* = 7.56, 1.64 Hz, 4-*p*H *cis* to hydride), 7.13 (m, 5-*m*H *trans* to hydride), 6.93 (t, *J* = 6.72 Hz, 5-*m*H *cis* to hydride), 4.79 (methanol), 4.50 (s, free H_2), 4.70 (s, N-CH_2-CH_2-N), 7.03 (s, N-CH), 3.03 (methanol), 3.12 (s, CH_3^{IMe}), -23.7 (s, hydride).

^{13}C NMR (MeOD, 100 MHz): 153.2 (3-*m*H *trans* to hydride), 148.4, (3-*m*H *cis* to hydride), 145.0 (6-*σ*H *trans* to hydride), 143.6 (6-*σ*H *cis* to hydride), 128.4 (4-*p*H *trans* to hydride), 126.9 (4-*p*H *cis* to hydride), 124.2 (5-*m*H *trans* to hydride), 121.8 (5-*m*H *cis* to hydride), 49.8 (N-CH_2-CH_2-N), 114.3 (N-CH, carbene), 32.1 (N-CH_3, carbene).

5.24 $[Ir(H)_2(IMe)(3\text{-}Ipy)_3]^+Cl^-$ (940.2 g mol^{-1})

A standard solution of [Ir)$(H)_2$(IMe(3-Ipy)$_3$]Cl was prepared by dissolving ***1*** (1.3 mg, 432.1 g mol^{-1}, 0.003 mmol) and 3-iodopyridine (3 mg, 205 g mol^{-1}, 0.011 mmol) in methanol-d_4 (0.6 mL). This was degassed in an NMR tube fitted with a Young's tap and the solution was kept in a mixture dry ice and acetone for about 25 minutes and then exposed to *p*-H_2 (3 bar) to hydrogenate the sample. This resulted in [Ir(IMe)$(H)_2$(3-Ipy)$_3$]Cl (1.5 mg, 940.2 g mol^{-1}, 0.0015 mmol) and free 3-iodopyridine (2.5 mg, 205 g mol^{-1}, 0.012 mmol).

^{1}H NMR (MeOD, 600 MHz): 8.74 (s, 2-σH *trans* to hydride), 8.64 (d, *J* = 4.10 Hz, 2-σH *cis* to hydride), 8.46 (d, *J* = 2.98 Hz, 6-σH *trans* to hydride), 8.37 (d, *J* = 3.41 Hz, 2H, 6-σH *cis* to hydride), 7.94 (d, *J* = 3.98 Hz, 4-*p*H *trans* to hydride), 7.84 (t, *J* = 6.56, 1.64 Hz, 4-*p*H *cis* to hydride), 6.98 (m, 5-*m*H *trans* to hydride), 6.85 (t, *J* = 5.72 Hz, 5-*m*H *cis* to hydride), 4.80 (methanol), 4.52 (s, free H_2), 4.71 (s, N-CH_2-CH_2-N), 7.03 (s, N-CH), 3.03 (methanol), 3.03 (s, CH_3^{IMe}), -24.2 (s, hydride).

^{13}C NMR (MeOD, 100 MHz): 152.0 (2-σH 3-Ipy *trans* to hydride), 149.3 (2-σH *cis* to hydride), 147.0 (6-σH *trans* to hydride), 145.8 (6-σH *cis* to hydride), 136.4 (4-*p*H *trans* to hydride), 134.0 (4-*p*H *cis* to hydride), 127.7 (5-*m*H *trans* to hydride),125.3 (5-*m*H *cis* to hydride), 50.5 (N-CH_2-CH_2-N), 116.8 (N-CH, carbene), 31.8 (N-CH_3, carbene).

5.25 $[Ir)(H)_2(IMe(4\text{-}Ipy)_3]^+Cl^-$ (940.2 g mol^{-1})

A sample solution of $[Ir)(H)_2(IMe(4\text{-}Ipy)_3]Cl$ was prepared by using [Ir(IMe)Cl(COD)] (1.3 mg, 432.1 g mol^{-1}, 0.003 mmol) and 4-iodopyridine (3 mg, 205 g mol^{-1}, 0.011 mmol) in methanol-d_4 (0.6 mL). This was degassed in an NMR tube fitted with a Young's tap and the solution was kept in a mixture dry ice and acetone for about 25 minutes and then exposed to *p*-H_2 (2.9 bar) to hydrogenate the sample. This resulted in $[Ir(IMe)(H)_2(4\text{-}Ipy)_3]Cl$ (1.5 mg, 940.2 g mol^{-1}, 0.0015 mmol) and free 4-iodopyridine (2.5 mg, 205 g mol^{-1}, 0.012 mmol).

^{1}H NMR (MeOD, 600 MHz): 8.72 (t, *J* = 3.45 Hz, *σ*H *trans* to hydride), 8.64 (d, *J* = 3.20 Hz, *σ*H *cis* to hydride), 8.45 (t, *J* = 3.45 Hz, *m*H *trans* to hydride), 8.31 (d, *J* = 3.45 Hz, *m*H *cis* to hydride), 4.81 (methanol), 4.51 (s, free H_2), 4.72 (s, N-CH_2-CH_2-N), 7.06 (s, N-CH), 3.03 (methanol), 3.03 (s, CH_3^{IMe}), -26.3 (s, hydride).

^{13}C NMR (MeOD, 100 MHz): 154.0 (*σ*H *trans* to hydride), 150.8 (*σ*H *cis* to hydride), 138.2 (*m*H *trans* to hydride), 134.5 (*m*H *cis* to hydride), 50.3 (N-CH_2-CH_2-N), 113.4 (N-CH, carbene), 32.9 (N-CH_3, carbene).

5.26 $[Ir)(H)_2(IMe(Nic)_3]^+Cl^-$ (694.8 g mol^{-1})

A standard solution of $[Ir)(H)_2(IMe(Nic)_3]Cl$ was prepared by using [Ir(IMe)Cl(COD)] (1.3 mg, 432.1 g mol^{-1}, 0.003 mmol) and) and nicotinic acid (3 mg, 123.2 g mol^{-1}, 0.025 mmol) in methanol-d_4 (0.6 mL). The sample was degassed in an NMR tube fitted with a Young's tap and the solution was exposed to *p*-H_2 (2.8 bar) to hydrogenate the sample. This resulted in $[Ir(IMe)(H)_2(Nic)_3]Cl$ (1.7 mg, 694.8 g mol^{-1}, 0.0024 mmol) and free nicotinic acid (2.5 mg, 123.1 g mol^{-1}, 0.020 mmol).

^{1}H NMR (MeOD, 600 MHz): 8.70 (d, *J* = 3.01 Hz, 2σH *trans* to hydride), 8.60 (m, 2-*σ*H *cis* to hydride), 8.47 (t, *J* = 3.97, 4-*p*H *trans* to hydride), 7.98 (tt, *J* = 6.98, 1.47 Hz, 4-*p*H *cis* to hydride), 8.39 (d, *J* = 5.78, 5-*m*H *trans* to hydride), 6.97 (m, 5-*m*H *cis* to hydride), 7.50 (m, Hz, 6-*σ*H *trans* to hydride), 7.53 (m, 6-*σ*H *cis* to hydride), 4.81 (methanol), 4.52 (s, free H_2), 4.75 (s, N-CH_2-CH_2-N), 7.11 (s, N-CH), 3.03 (methanol), 3.10 (s, CH_3^{IMe}), -22.5 (s, 2H, hydride).

^{13}C NMR (MeOD, 150 MHz): 147.3 (2-*σ cis* to hydride), 151.5 (2-*σ*H *trans* to hydride), 151.3 (6-*σ*H *cis* to hydride), 155.2 (6-*σ*H *trans* to hydride), 132.5 (4-*p*H *cis* to hydride), 140.8 (4-*p*H *trans* to hydride), 129.5 (4-*p*H *cis* to hydride), 119.1 (5-*m*H *cis* to hydride), 122.3 (5-*m*H *trans* to hydride), 50.4 (N-CH_2-CH_2-N), 116.5 (N-CH, carbene), 32.6 (N-CH_3, carbene).

5.27 [Ir)(H)$_2$(IMe(Inic)$_3$]$^+$Cl$^-$ (694.8 g mol^{-1})

A standard solution of [Ir)(H)$_2$(IMe(Inic)$_3$]Cl was prepared by dissolving [Ir(IMe)Cl(COD)] (1.3 mg, 432.1 g mol^{-1}, 0.003 mmol) and isonicotinic acid (2.8 mg, 123.2 g mol^{-1}, 0.022 mmol) in methanol-d$_4$ (0.6 mL). This was degassed in an NMT tube fitted with a Young's tap and the solution was exposed to *p*-H_2 (3 bar) to hydrogenate the sample. This resulted in [Ir(IMe)(H)$_2$(Inico)$_3$]Cl (1.6 mg, 694.8 g mol^{-1}, 0.0022 mmol) and free isonicotinic acid (2.4 mg, 123.1 g mol^{-1}, 0.019 mmol).

^{1}H NMR (MeOD, 400 MHz): 8.66 (t, *J* = 6.95 Hz, *σ***H** *trans* to hydride), 8.43 (d, *J* = 3.22 Hz, *σ***H** *cis* to hydride), 7.75 (t, *J* = 6.34, *m***H** *trans* to hydride), 6.97 (t, *J* = 7.70 Hz, *m***H** *cis* to hydride), 4.78 (methanol), 4.57 (s, free $\mathbf{H}_2$), 4.72 (s, N-C$\mathbf{H}_2$-C$\mathbf{H}_2$-N), 6.99 (s, N-CH), 3.03 (methanol), 3.05 (s, C$\mathbf{H}_3^{IMe}$), -23.5 (s, hydride).

^{13}C NMR (MeOD, 100 MHz): 143.2 (*σ***H** *cis* to hydride), 145.0 (*σ***H** *trans* to hydride), 125.5 (*m***H** *cis* to hydride), 127.2 (*m***H** *trans* to hydride), 51.4 (N-**C**H$_2$-**C**H$_2$-N), 114.3 (N-**C**H, carbene), 31.9 (N-**C**H$_3$, carbene).

5.28 [Ir)(H)$_2$(IMe(MN)$_3$]$^+$Cl$^-$ (736.8 g mol^{-1})

A standard solution of [Ir)(H)$_2$(IMe(MN)$_3$]Cl was prepared by dissolving [Ir(IMe)Cl(COD)] (1.3 mg, 432.1 g mol^{-1}, 0.003 mmol) and methyl nicotinate (3 mg, 137.2 g mol^{-1}, 0.021 mmol in methanol-d$_4$ (0.6 mL). This was degassed in an NMR tube fitted with a Young's tap and the solution was exposed to *p*-H$_2$ (3 bar) to hydrogenate the sample. This resulted in [Ir(IMe)(H)$_2$(MN)$_3$]Cl (1.6 mg, 736.8 g mol^{-1}, 0.0021 mmol) and free methyl nicotinate (2.6 mg, 137.2 g mol^{-1}, 0.018 mmol).

^{1}H NMR (MeOD, 600 MHz): 8.72 (d, *J* = 2.94, Hz, 2-*σ***H** *trans* to hydride), 8.60 (m, 2-*σ***H** *cis* to hydride), 8.41 (d, *J* = 3.75, 4-*p***H** *trans* to hydride), 7.98 (tt, *J* = 7.56, 1.64 Hz, 4-*p***H** *cis* to hydride), 8.01 (d, *J* = 1.98, 5-*m***H** *trans* to hydride), 7.87 (m, 5-*m***H** *cis* to hydride), 7.24 (dd, *J* = 4.93 Hz, 6-*σ***H** *trans* to hydride), 7.15 (m, 6-*o***H** *cis* to hydride), 4.80 (methanol), 4.51 (s, free **H**$_2$), 4.73 (s, N-C**H**$_2$-C**H**$_2$-N), 7.01 (s, N-CH), 3.03 (methanol), 3.14 (s, C**H**$_3^{IMe}$), -25.5 (s, 2H, hydride).

^{13}C NMR (MeOD, 100 MHz): 148.1 (2-*σ***H** *cis* to hydride), 150.7 (2-*σ***H** *trans* to hydride), 152.3 (6-*σ***H** *cis* to hydride), 154.4 (6-*σ***H** *trans* to hydride), 135.5 (4-*p***H** *cis* to hydride), 137.8 (4-*p***H** *trans* to hydride), 128.5 (4-*p***H** *cis* to hydride), 118.4 (5-*m***H** *cis* to hydride), 122.9 (5-*m***H** *trans* to hydride), 49.9 (N-**C**H$_2$-**C**H$_2$-N), 116.1 (N-**C**H, carbene), 33.2 (N-**C**H$_3$, carbene).

5.29 $[Ir)(H)_2(IMe(IN)_3]^+Cl^-$ (736.8 g mol^{-1})

A standard solution of $[Ir)(H)_2(IMe(IN)_3]Cl$ was prepared by dissolving [Ir(IMe)Cl(COD)] (1.3 mg, 432.1 g mol^{-1}, 0.003 mmol) and isoniazid (2.9 mg, 137.2 g mol^{-1}, 0.021 mmol) in methanol-d_4 (0.6 mL) and. This was degassed in an NMR tube fitted with a Young's tap and the solution was exposed to *p*-H_2 (3 bar) to hydrogenate the sample. This resulted in $[Ir(IMe)(H)_2(INH)_3]Cl$ (1.5 mg, 736.8 g mol^{-1}, 0.0022 mmol) and free isoniazid (2.5 mg, 137.2 g mol^{-1}, 0.018 mmol).

^{1}H NMR (MeOD, 600 MHz): 8.36 (t, *J* = 7.15, Hz, σ**H** *trans* to hydride), 8.13 (d, *J* = 4.25 Hz, σ**H** *cis* to hydride), 7.35 (t, *J* = 5.20, *m***H** *trans* to hydride), 7.21 (t, *J* = 6.45, Hz, *m***H** *cis* to hydride), 4.74 (methanol), 4.58 (s, free $\mathbf{H}_2$), 4.70 (s, N-C$\mathbf{H}_2$-C$\mathbf{H}_2$-N), 6.94 (s, N-CH), 3.02 (methanol), 3.10 (s, C$\mathbf{H}_3^{IMe}$), -24.5 (s, hydride).

^{13}C NMR (MeOD, 100 MHz): 142.2 (σ**H** *cis* to hydride), 144.6 (σ**H** *trans* to hydride), 124.4 (*m***H** *cis* to hydride), 126.2 (*m***H** *trans* to hydride), 51.8 (N-**C**H_2-**C**H_2-N), 115.3 (N-**C**H, carbene), 32.4-**C**H_3, carbene).

5.30 $[Ir)(H)_2(IMe(Pyz)_3]^+Cl^-$ (565.5 g mol^{-1})

A standard solution of $[Ir)(H)_2(IMe(pyz)_3]Cl$ was prepared by dissolving [Ir(IMe)Cl(COD)] (1.3 mg, 432.1 g mol^{-1}, 0.003 mmol) and pyrazine (3.1 mg, 80.1 g mol^{-1}, 0.038 mmol) in methanol-d_4 (0.6 mL). This was degassed in an NMR tube fitted with a Young's tap and the solution was exposed to *p*-H_2 (3 bar) to hydrogenate the sample. This resulted in $[Ir(IMe)(H)_2(pyz)_3]Cl$ (2.9 mg, 565.5 g mol^{-1}, 0.0024 mmol) and free pyrazine (2.6 mg, 80.1 g mol^{-1}, 0.032 mmol).

^{1}H NMR (MeOD, 400 MHz): 8.52 (t, *J* = 4.35 Hz, pyz *trans* to hydride), 8.38 (d, *J* = 3.05 Hz, pyz *cis* to hydride), 4.79 (methanol), 4.50 (s, free **H**$_2$), 4.70 (s, N-C**H**$_2$-C**H**$_2$-N), 7.01 (s, N-CH), 3.03 (methanol), 3.04 (s, C**H**$_3^{IMe}$), -23.8 (s, hydride).

^{13}C NMR (MeOD, 100 MHz): 139.8 (pyz *cis* to hydride), 143.6 (σ**H** pyz *trans* to hydride), 52.1 (N-**C**H$_2$-**C**H$_2$-N), 116.3 (N-**C**H, carbene), 32.4 (N-**C**H$_3$, carbene).

5.31 [Ir)(H)$_2$(IMe(Ina)$_3$]$^+$Cl$^-$ (691.8 g mol^{-1})

A standard solution of [Ir)(H)$_2$(IMe(Ina)$_3$]Cl was prepared by dissolving [Ir(IMe)Cl(COD)] (1.3 mg, 432.1 g mol^{-1}, 0.003 mmol) and isonicotinamide (3 mg, 122.2 g mol^{-1}, 0.025 mmol) in methanol-d$_4$ (0.6 mL). This was degassed in an NMR tube fitted with a Young's tap and the solution was exposed to *p*-H$_2$ (3 bar) to hydrogenate the sample. This resulted in [Ir(IMe)(H)$_2$(Ina)$_3$]Cl (1.7 mg, 691.8 g mol^{-1}, 0.0024 mmol) and free isonicotinamide (2.5 mg, 122.2 g mol^{-1}, 0.020 mmol).

^{1}H NMR (MeOD, 600 MHz): 8.56 (t, *J* = 6.54 Hz, σ**H** *trans* to hydride), 8.33 (d, *J* = 4.01 Hz, σ**H** *cis* to hydride), 7.65 (t, *J* = 5.95, *m***H** *trans* to hydride), 7.39 (t, *J* = 6.01 Hz, *m***H** *cis* to hydride), 4.72 (methanol), 4.53 (s, free **H**$_2$), 4.69 (s, N-C**H**$_2$-C**H**$_2$-N), 6.97 (s, N-CH), 3.03 (methanol), 3.02 (s, C**H**$_3^{IMe}$), -21.4 (s, hydride).

^{13}C NMR (MeOD, 100 MHz): 145.2 (*σ***H** *cis* to hydride), 147.4 (*σ***H** *trans* to hydride), 126.5 (*m***H** *cis* to hydride), 128.2 (*m***H** *trans* to hydride), 51.8 (N-**C**H$_2$-**C**H$_2$-N), 115.3 (N-**C**H, carbene), 31.4 (N-**C**H$_3$, carbene).

5.32 [Ir)(H)$_2$(IMe(pu)$_3$]$^+$Cl$^-$ (685.8 g mol^{-1})

A standard solution of [Ir)(H)$_2$(IMe(pu)$_3$]Cl was prepared by dissolving [Ir(IMe)Cl(COD)] (1.3 mg, 432.1 g mol^{-1}, 0.003 mmol) and purine (3.2 mg, 120.2 g mol^{-1}, 0.026 mmol) in methanol-d$_4$ (0.6 mL) and This was degassed in an NMR tube fitted with a Young's tap and the solution was exposed to *p*-H$_2$ (3 bar) to hydrogenate the sample. This resulted in [Ir(IMe)(H)$_2$(pu)$_3$]Cl (1.7 mg, 685.8 g mol^{-1}, 0.0024 mmol) and free purine (2.7 mg, 120.2 g mol^{-1}, 0.022 mmol).

^{1}H NMR (MeOD, 400 MHz): 9.01 (s, 4-*p***H** *trans* to hydride), 8.98 (s, 4-*p***H** *cis* to hydride), 8.78 (d, *J* = 2.395 Hz, 2-*σ***H** *trans* to hydride), 8.63 (s, 2-*σ***H** *cis* to hydride, 8.39 (s, 8-*m***H** *trans* to hydride), 8.29 (t, *J* = 5.70 Hz, 2H, 8-*m***H** *cis* to hydride), 3.03 (methanol), 4.51 (s, free **H**$_2$), 4.68 (s, N-C**H**$_2$-C**H**$_2$-N), 6.95 (s, N-CH), 4.76 (methanol), 2.90 (s, C**H**$_3^{IMe}$), -22.8 (s, hydride).

^{13}C NMR (MeOD, 100 MHz): 140.2 (4-*p***H** *trans* to hydride), 142.1 (4-*p***H** *cis* to hydride), 148.4 (2-*σ***H** *trans* to hydride), 150.1 (2-*σ***H** *cis* to hydride, 145.7 (8-*m***H** *trans* to hydride), 147.1 (8-*m***H** *cis* to hydride), 52.8 (N-**C**H$_2$-**C**H$_2$-N), 117.3 (N-**C**H, carbene), 32.9 (N-**C**H$_3$, carbene).

5.33 [Ir)(H)$_2$(IMe(pym)$_3$]$^+$Cl$^-$ (565.5 g mol^{-1})

A standard solution of [Ir)(H)$_2$(IMe(pym)$_3$]Cl was prepared by dissolving [Ir(IMe)Cl(COD)] (1.3 mg, 432.1 g mol^{-1}, 0.003 mmol) and pyrimidine (3.0 mg, 80.1 g mol^{-1}, 0.037 mmol) in methanol-d$_4$ (0.6 mL). The solution was degassed in an NMR tube fitted with a Young's tap and the solution was exposed to *p*-H$_2$ (3 bar) to hydrogenate the sample. This resulted in [Ir(IMe)(H)$_2$(pym)$_3$]Cl (1.8 mg, 565.5 g mol^{-1}, 0.0031 mmol) and free purine (2.5 mg, 80.1 g mol^{-1}, 0.031mmol).

^{1}H NMR (MeOD, 600 MHz): 8.81 (s , 2-σH *trans* to hydride), 8.60 (s, 2-σH *cis* to hydride), 8.49 (d, J = 2.95, 4- σH *trans* to hydride), 8.35 (t, J = 7.56 Hz, 4- σH *cis* to hydride), 7.19 (t, J = 1.55, 6.01 Hz, 6-pH *trans* to hydride), 6.98 (m, 6-pH *cis* to hydride), 4.78 (methanol), 4.5 (s, free H_2), 4.7 (s, N-CH_2-CH_2-N), 6.99 (s, N-CH), 3.03 (methanol), 2.99 (s, CH_3^{IMe}), -25.2 (s, 2H, hydride).

^{13}C NMR (MeOD, 100 MHz): 155.3 (2-σH *cis* to hydride), 157.5 (2-σH *trans* to hydride), 150.3 (6-σH *cis* to hydride), 152.4 (6-σH *trans* to hydride), 132.5 (4-pH *cis* to hydride), 119.8 (4-pH *trans* to hydride), 121.2 (4-pH *cis* to hydride), 51.1 (N-CH_2-CH_2-N), 114.9 (N-CH, carbene), 32.1 (N-CH_3, carbene).

This Appendix presents the data (Tables and Figures) from chapter 2.

Table A1: ***NMR data for [Ir(COD)(IMe)Cl], 1, recorded in d4-methanol at 298 K.***

	^{1}H NMR			^{13}C NMR	
Group	***δ_H / ppm***	***J / Hz***	***Integral***	***Group***	***δ_C / ppm***
N-CH	7.01	's'	1.00	N-CH	122.80
CH-COD	4.35	't' 2.80	2.02	CH-COD	83.64
N-CH_3	3.61	's'	3.38	N-CH_3	37.25
COD-CH	2.85	't'2.75	2.10	COD-CH	53.28
COD-CH_2	2.27	'm'	4.02	COD-CH_2	31.02
COD-CH_2	1.88	'm'	2.97	COD-CH_2	31.75

Table A2: ***^{1}H and ^{13}C NMR data for pyridine.***

	^{1}H NMR			^{13}C NMR	
Proton	***δ_H / ppm***	***J / Hz***	***Integral***	***Carbon***	***δ_C / ppm***
H_1	8.61	'd' 4.52	2.05	C_1	145.35
H_2	7.66	't' 7.61	1.00	C_2	137.22
H_3	7.27	'm'	2.02	C_3	124.56

Table A3: ***NMR data for [Ir(IMe)(py)$_3$(H$_2$)]$^+$, 3, acquired in d4-methanol at 298 K.***

	^{1}H NMR		***^{13}C NMR***	
Group	***δ_H / ppm***	***J / Hz***	***Group***	***δ_C / ppm***
trans-py, *ortho*	8.71	't' 7.42	*trans*-py, *ortho*	145.12
cis-py, *ortho*	8.45	'd' 4.42	*cis*-py, *ortho*	144.91
trans-py, *para*	7.99	't' 7.42	*trans*-py, *para*	137.47
cis-py, *para*	7.74	'm'	*cis*-py, *para*	136.51
trans-py, *meta*	7.70	't' 7.42	*trans*-py, *meta*	126.81
cis-py, *meta*	7.48	'd' 4.42	*cis*-py, *meta*	125.60
N-CH	7.11	's'	N-CH	116.54
N-CH$_2$	4.82	'm'	N-CH$_2$	71.39
N-CH$_3$	3.17	's'	N-CH$_3$	33.98
Ir-H	22.31	's'	-	-

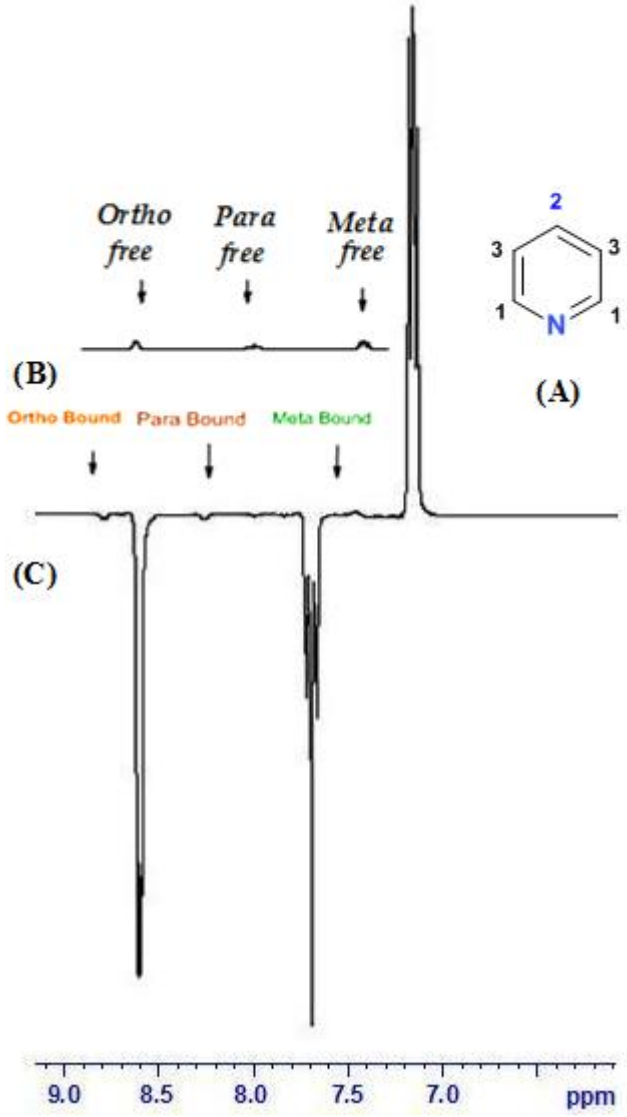

Figure A4: ***(A) Molecular structure of pyridine and labels indicating the enhanced ^{1}H sites in the hyperpolarized spectrum. (B) Single-scan ^{1}H NMR spectrum of the aromatic region of a sample of 1 showing resonances for free pyridine that were obtained prior to polarization; (C) corresponding ^{1}H hyperpolarized NMR spectrum acquired immediately after polarization in a magnetic field of 65 G exhibiting the newly enhanced proton signals for free pyridine***

Table A5: Observed rate constants for hydride exchange.

Set temperature (K)	Corrected temperature / K	1/T	lnk/T	k(H) /s^{-1}
303	304.1	0.0033	-7.296	0.11
303	304.1	0.0033	-7.295	0.11
308	309.5	0.00324	-6.808	0.17
308	309.5	0.00324	-6.807	0.17
313	314.1	0.00319	-6.400	0.26
313	314.1	0.00319	-6.398	0.26
318	319.1	0.00314	-5.934	0.42
318	319.1	0.00314	-5.931	0.42
323	323.9	0.003096	-4.962	1.13
323	323.9	0.003096	-4.959	1.14

In an Eyring plot, the value of $\Delta H^{\ddagger}$ can be obtained from the gradient of the line of best fit, whilst the value of $\Delta S^{\ddagger}$ is obtained from the intercept of the line with the y-axis by using the following equation:

$\ln(k/T) = \ln(k_B/h) - \Delta H/RT + \Delta S/R$,

Where $R = 8.314\ JK^{-1}mol^{-1}$ and $\ln(k_B/h) = 23.76$

Gibbs free energy of activation, ΔG, is calculated by extrapolating the graph to obtain a value for the rate constant, k, at the temperature of interest. This value is then substituted into the following equation:

$\Delta G = -RT\ln(k_h/k_b)$

An Eyring plot for intramolecular hydride exchange process is shown in Figure A6. The activation parameters of this exchange processes are given in Table A7.

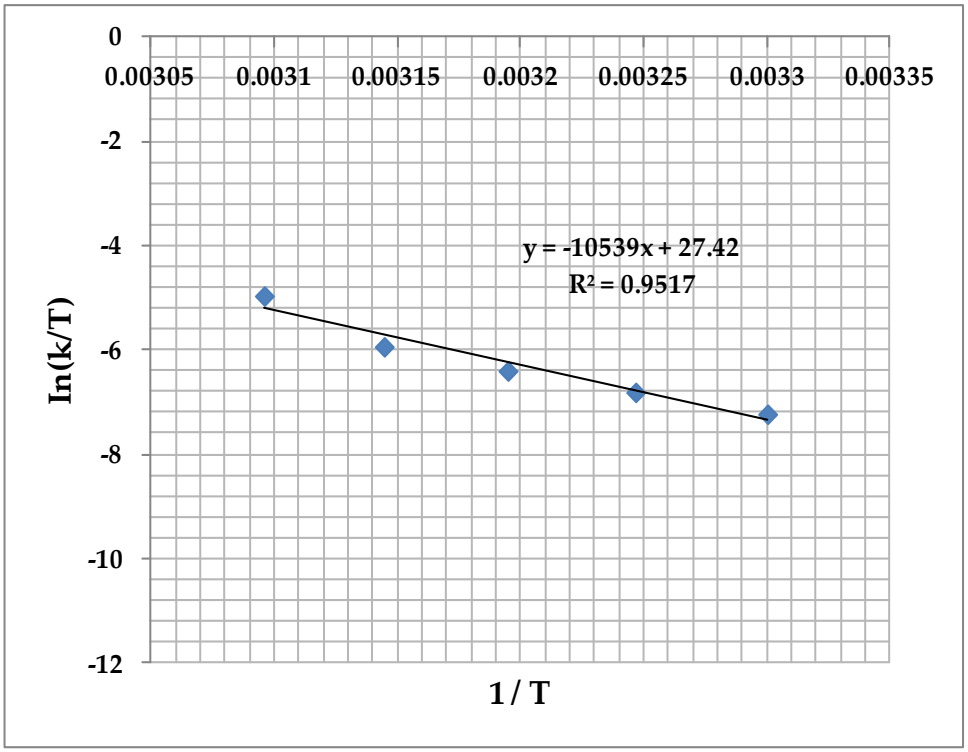

Figure A6: Eyring plots for Hydride exchange (using the data shown in Table A5.

Table A7: Activation parameters as determined for the hydride exchange process observed for complex 3 in d_4-methanol.

Hydride exchange	$\Delta H^{\ddagger}$ / kJ mol^{-1}	83.2 ± 7
	$\Delta S^{\ddagger}$ / kJ mol^{-1}	41.5 ± 10.2
	$\Delta G^{\ddagger}$ / kJ mol^{-1}	78.9 ± 0.2

Table A8: Observed rate constants for pyridine exchange.

Set temperature (K)	Corrected temperature / K	1/T	lnk/T	k(py) /s^{-1}
303	304.5	0.0033	-6.1600	0.32
303	304.1	0.0033	-6.1599	0.32
308	309.5	0.003247	-5.5149	0.62
308	309.5	0.003247	-5.5135	0.62
313	314.1	0.003195	-4.7883	1.31
313	314.1	0.003195	-4.7875	1.31
318	319.1	0.003145	-4.3222	2.11
318	319.1	0.003145	-4.3210	2.11
323	323.9	0.003096	-4.0729	2.75
323	323.9	0.003096	-4.0705	2.75

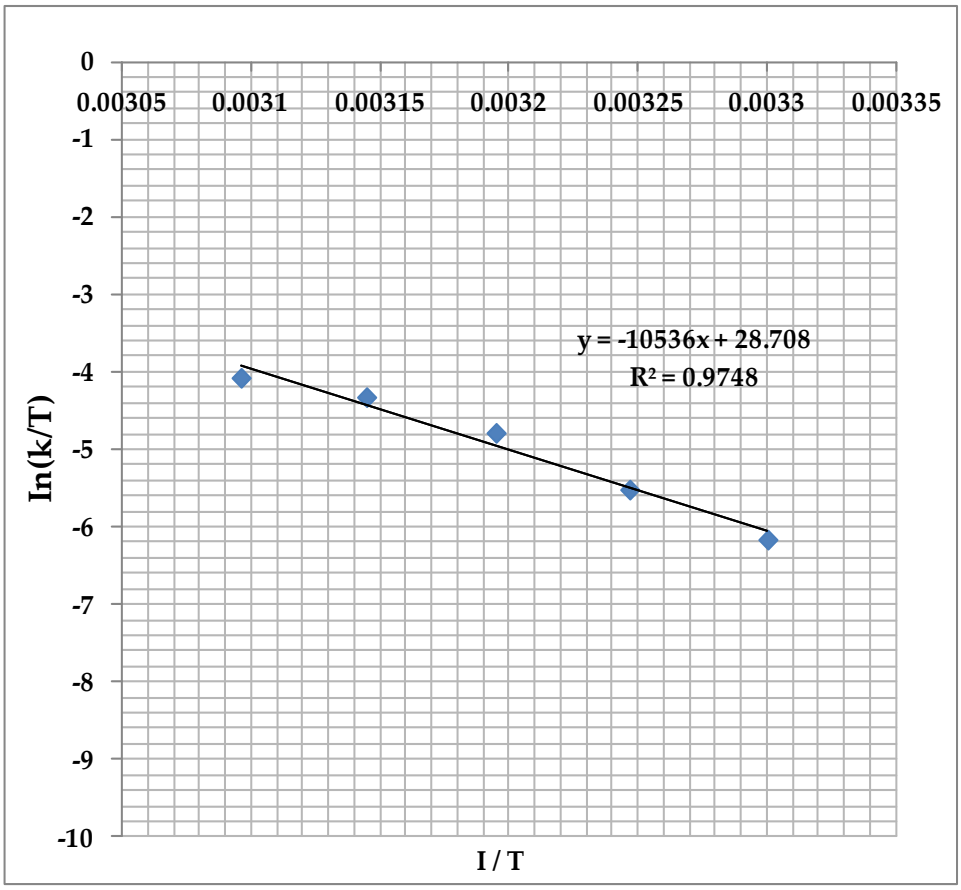

Figure A9: *Eyring plots for pyridine exchange (using the data shown in Table A8.*

Table A10: *Activation parameters as determined for the pyridine exchange process observed for complex 3 in d_4-methanol.*

Pyridine exchange	$\Delta H^{\ddagger}$ / kJ mol^{-1}	91.4 ±29
	$\Delta S^{\ddagger}$ / kJ mol^{-1}	40.7 ±12.3
	$\Delta G^{\ddagger}$/ kJ mol^{-1}	75.7 ± 0.3

Table A11: ***Enhancement and polarization levels observed as a function of shake time at 65 G for the protons of free pyridine.***

Shake time / s	*Signal enhancement / fold at 65 G*					
	Ortho	*Pol (Ortho)*	*Meta*	*Pol (Meta)*	*Para*	*Pol (Para)*
20	-7.9	-0.025	-2.5	-0.08	31.9	0.103
40	-9.8	-0.032	-10.2	-0.033	11.2	0.036
60	-25.1	-0.081	-19.4	-0.063	36.8	0.119
80	-55.7	-0.180	-79.5	-0.256	77.5	0.250
100	-47.9	-0.154	-96.6	-0.311	76.6	0.247
120	-63.9	0.206	-122.6	-0.395	86.2	0.278

Table A12: ***Enhancement and polarization levels as a function of substrate loading observed at a magnetic field of 65 G.***

Concentration		*Enhancement levels / fold at 65 G*					
Catalyst/ mmol	*Pyridine/ mmol*	*ortho*	*Pol (ortho)*	*meta*	*Pol (meta)*	*para*	*Pol (para)*
0.0031	0.051	-50.7	-0.163	-65.2	-0.210	69.1	0.223
0.0031	0.025	-32.8	-0.106	-49.4	-0.149	39.7	0.128
0.0031	7.6×10^{-3}	-23.6	-0.076	-40.7	-0.131	34.8	0.112
0.0031	6.4×10^{-3}	-22.7	-0.073	-41.5	-0.134	28.5	0.092
0.0031	3.7×10^{-3}	-10.9	-0.035	-19.2	-0.062	12.6	0.041
0.0031	1.3×10^{-3}	-8.6	-0.018	-11.9	-0.038	7.54	0.024

Table A13: ***Solvent studies data indicating the trend of an effect of solvent on the polarization transfer process using pyridine as a substrate in a magnetic field of 65 G at 310 K.***

			Enhancement levels / fold at 65 G					
Solvent	***1/ mg***	***Vol / cm^3***	***Ortho***	***Pol*** *(ortho)*	***Meta***	***Pol*** *(meta)*	***Para***	***Pol*** *(para)*
DMSO	1.3	0.6	-2.6	-0.008	-4.5	-0.015	1.8	0.006
Acetone	1.3	0.6	-2.5	-0.008	-3.4	-0.011	2.5	0.008
$CDCl_3$	1.3	0.6	-3.5	-0.011	-7.7	-0.025	4.1	0.013
D_2O	1.3	0.6	-0.5	-0.002	-0.2	-0.001	0.1	0.000
Methanol	1.3	0.6	-22.6	-0.073	-41.4	-0.133	28	0.090

Table A14: ***^{1}H and ^{13}C NMR data for the hyperpolarized sites in 2-, 6-, d_2-pyridine***

	^{1}H NMR			***^{13}C NMR***	
Group / label	***δ_H / ppm***	***J / Hz***	***Integral***	***Group / label***	***δ_C / ppm***
H_1	7.27	‘t’ 7.85	1.00	C_1	124.54
H_2	7.66	‘t’ 7.85	2.08	C_2	137.22
Hydride	-22.66	‘s’	1.05	**-**	-

Table A15: ***^{1}H and ^{13}C NMR data for the hyperpolarized sites in 3-, 4-, 5-, d_3-pyridine.***

^{1}H NMR				^{13}C NMR	
Group / label	***δ_H / ppm***	***J / Hz***	***Integral***	***Group / label***	***δ_C / ppm***
H_1	8.38	's'	2.00	C_1	124.56
Hydride	-22.68	-	-	-	-

Table A16: ***Enhancement levels observed as a function of shake time at 65G for 2-, 6-, d_2-pyridine protons.***

Shake time / s	***Signal enhancement / fold at 65 G***			
	H_1	***Pol (H_1)***	***H_2***	***Pol (H_2)***
20	-5.2	-0.017	13.1	0.042
40	-73.5	-0.237	23.4	0.075
60	-103.2	-0.333	38.8	0.125
80	-111.1	-0.358	50.5	0.163
100	-130.8	-0.422	60.1	0.194
120	-185.8	-0.599	92.3	0.297
140	-160.2	-0.516	75.5	0.243

Table A17: Enhancement and polarization levels achieved at the indicated sites in 2-, 6-, d_2-pyridine as a function of temperature at 65 G.

Temp / K	*Signal enhancement / fold at 65 G*			
	H_1	*Pol (H_1)*	*H_2*	*Pol (H_2)*
305	-78.6	-0.253	29.7	0.096
310	-155.1	-0.500	55.3	0.178
315	-167.1	-0.539	62.4	0.201
320	-185.5	-0.598	78.3	0.252
325	-218.5	-0.704	86.3	0.278

Table A18: Enhancement levels achieved at the indicated sites in 3-, 4-, 5, d_3-pyridine as a function of shake time in a magnetic field of 65 G at 330 K.

Shake time / s	*Signal enhancement / fold at 65 G*	
	H_1	*Pol (H_1)*
20	-105.3	-0.339
40	-245.5	-0.791
60	-480.3	-1.548
80	-665.7	-2.790
100	-899.7	-2.577
120	-936.6	-3.018

Table A19: Enhancement levels achieved at the indicated sites in 3-, 4-, 5, d_3-pyridine as a function of temperature at 65 G.

Temp / K	*Signal enhancement / fold at 65 G*	
	H_1	*Pol (H_1)*
305	-232.5	-0.749
310	-454.8	-1.466
315	-619.7	-1.997
320	-845.9	-2.726
325	-1022.3	-3.295

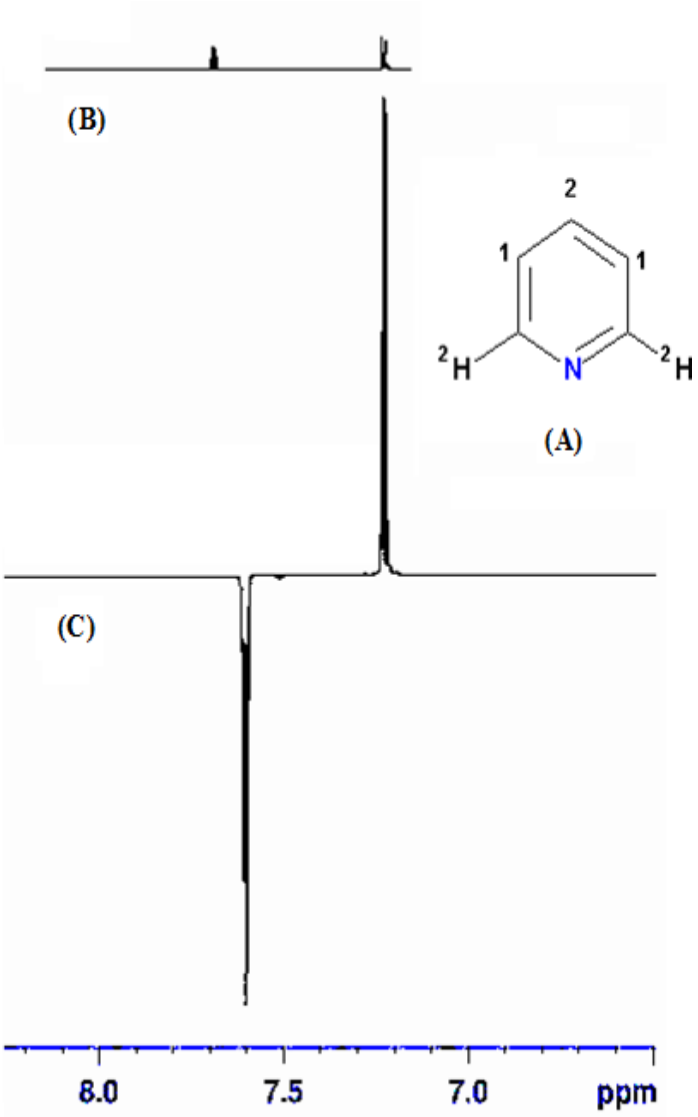

Figure A20: *(A) Molecular structure of 2-, 6-, d_2-pyridine and labels indicating the enhanced ^{1}H sites in the hyperpolarized spectrum. (B) Single-scan ^{1}H NMR spectrum of the aromatic region of a sample of 1 showing resonances for free 2-, 6-, d_2-pyridine that were obtained prior to polarization; (C) corresponding hyperpolarized ^{1}H NMR spectrum acquired immediately after polarization in a magnetic field of 65 G exhibiting the newly enhanced proton signals for free 2-, 6-, d_2-pyridine.*

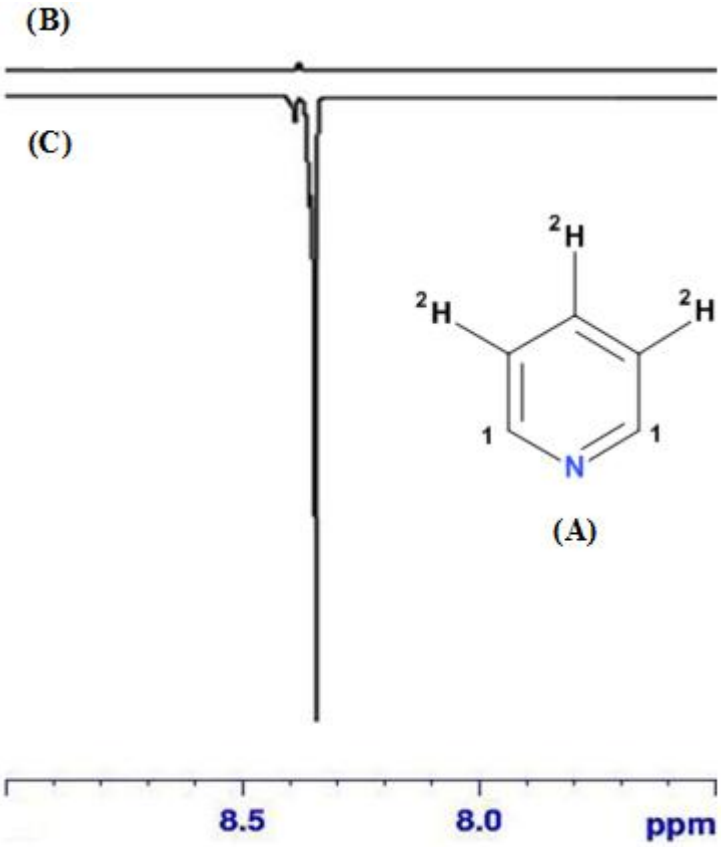

Figure A21: *(A) Molecular structure of 3-, 4-, 5-, d_3-pyridine. and labels indicating the enhanced ^{1}H sites in the hyperpolarized spectrum. (B) Single-scan ^{1}H NMR spectrum of the aromatic region of a sample of 1 showing resonances for free 3-, 4-, 5-, d_3-pyridine that were obtained prior to polarization; (C) corresponding hyperpolarized ^{1}H NMR spectrum acquired immediately after polarization in a magnetic field of 65 G exhibiting the enhanced proton signals for free 3-, 4-, 5-, d_3-pyridine.*

Table A22: Enhancement levels achieved for 3-, 4-, 5-, d_3-pyridine as a function of magnetic field using the flow probe.

Substrate	*Magnetic field / G*	*Signal enhancement / fold*	*polarization*
		Ortho	
3-, 4-, 5-, d_3-pyridine	-80	-18	-0.058
	-75	-17	-0.055
	-70	-25	-0.081
	-65	-35	-0.084
	-60	-27	-0.093
	-55	-24	-0.077
	-50	-22	-0.071

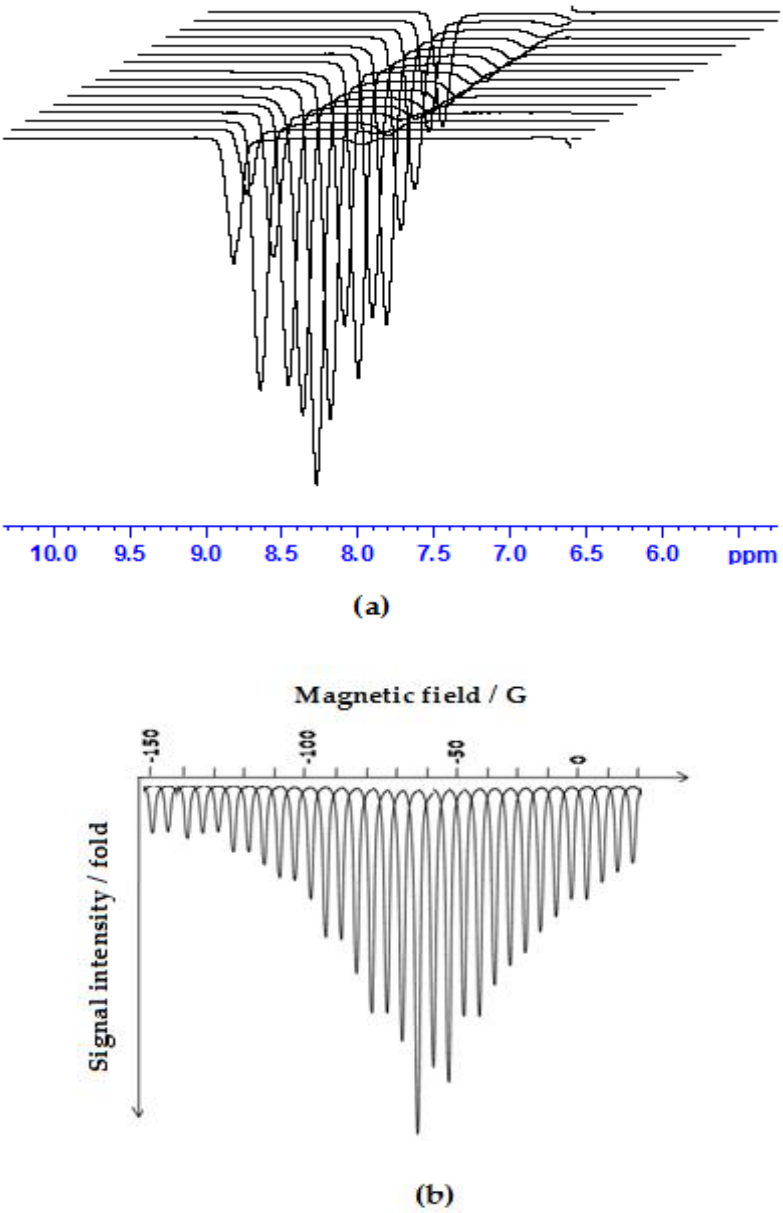

Figure A23: *(a) A series of hyperpolarized ^{1}H NMR traces showing the effect of changing the magnetic field during polarization transfer to 3-, 4-, 5-, d_3-pyridine for the IMe catalyst; (b) Magnetic field plot for ortho resonances (over the range of 0 – 150 G) in increments observed for a sample containing hyperpolarized 3-, 4-, 5-, d_3-pyridine.*

Table A24: ***^{1}H and ^{13}C NMR data for 2-picoline***

^{1}H NMR				^{13}C NMR	
Group / label	***δ_H / ppm***	***J / Hz***	***Integral***	***Group / label***	***δ_C / ppm***
H_1	8.60	'd' 5.64	1.00	C_1	158.20
H_2	7.57	't' 1.80, 8.66	1.02	C_2	149.20
H_3	7.19	'm'	1.03	C_3	136.40
H_4	7.01	't' 7.78	1.01	C_4	123.37
H_5 (CH_3)	2.55	's'	3.32	C_5	24.30

Table A25: ***^{1}H and ^{13}C NMR data for 3-picoline.***

^{1}H NMR				^{13}C NMR	
Group / label	***δ_H / ppm***	***J / Hz***	***Integral***	***Group / label***	***δ_C / ppm***
H_1	8.18	'm'	1.00	C_1	150.50
H_2	8.12	'm'	0.99	C_2	145.93
H_3	7.46	'm'	1.10	C_3	136.75
H_4	7.19	'dd' 4.88, 2.08	1.05	C_4	133.39
H_5 (CH_3)	2.32	's'	3.11	C_5	18.36

Table A26: ***^{1}H and ^{13}C NMR data for 4-picoline.***

^{1}H NMR				^{13}C NMR	
Group/ label	***δ_H / ppm***	***J / Hz***	***Integral***	***Group/ label***	***δ_C / ppm***
H_1	8.44	'd' 3.40	2.00	C_1	149.58
H_2	7.08	'd' 3.40	1.98	C_2	146.91
H_3 (CH_3)	2.17	's'	3.17	C_3	24.76

Table A27: ***^{1}H signal enhancement and polarization levels observed as a function of shake time in a magnetic field of 65 G for 2-picoline at 315 K.***

Shake time / s	*Signal enhancement / fold at 65 G*							
	H_1	*Pol (H1)*	H_2	*Pol (H2)*	H_3	*Pol (H3)*	H_4	*Pol (H4)*
20	-2.5	-0.008	-3.1	-0.010	4.8	0.015	5.2	0.017
40	-3.4	-0.011	-3.8	-0.012	5.4	0.017	5.9	0.019
60	-5.6	-0.017	-6.8	-0.022	7.4	0.024	8.2	0.026
80	-7.7	-0.025	-7.4	-0.024	8.2	0.026	9.5	0.031
100	-9.9	-0.032	-8.9	-0.029	9.1	0.029	10.7	0.034
120	-13.5	-0.044	-9.4	-0.030	10.2	0.033	12.2	0.039
140	-7.1	-0.023	-9.3	-0.030	9.7	0.031	10.4	0.034

Table A28: ***^{1}H signal enhancement and polarization levels observed as a function of temperature at 65 G for 2-picoline.***

Temp / K	*Signal enhancement / fold at 65 G*							
	H_1	*Pol (H1)*	H_2	*Pol (H2)*	H_3	*Pol (H3)*	H_4	*Pol (H4)*
305	-2.4	-0.008	-3.2	-0.010	2.1	0.007	3.5	0.011
310	-6.6	-0.021	-4.6	-0.015	10.2	0.033	8.1	0.026
315	-7.3	-0.024	-12.3	-0.040	7.7	0.025	10.2	0.033
320	-9.8	-0.032	-7.7	-0.025	10.9	0.035	11.2	0.036
325	-11.5	-0.037	-9.8	-0.032	7.4	0.024	12.3	0.040

Table A29: Enhancement and polarization levels observed as a function of shake time in a magnetic field of 65 G for 3-picoline at 310 K.

Shake time / s	Signal enhancement / fold at 65 G					
	H_1	Pol (H1)	H_2	Pol (H2)	H_3	Pol (H3)
20	-5.9	-0.019	1.9	0.006	4.2	0.014
40	-8.9	-0.029	1.4	0.005	4.8	0.015
60	-7.7	-0.025	2.3	0.007	5.2	0.017
80	-12.9	-0.042	2.1	0.007	1.7	0.005
100	-35.8	-0.115	4.3	0.014	12.6	0.041
120	-47.8	-0.154	7.3	0.024	11.3	0.036
140	-11.2	-0.036	7.5	0.024	10.5	0.034

Table A30: ^{1}H signal enhancement and polarization levels observed as a function of temperature at 65 G for 3-picoline.

Temp / K	Signal enhancement / fold at 65 G							
	H_1	Pol (H1)	H_2	Pol (H2)	H_3	Pol (H3)	H_4	Pol (H4)
305	-130.5	-0.419	-79.6	-0.257	-37.4	-0.121	12.5	0.040
310	-192.9	-0.622	-70.5	-0.227	-41.9	-0.135	17.2	0.055
315	-199.3	-0.642	-94.2	-0.304	-34.6	-0.112	13.4	0.043
320	-231.5	-0.746	-96.6	-0.311	-60.2	-0.194	21.1	0.068
325	-302.9	-0.976	-125.5	-0.404	-43.3	-0.140	24.5	0.079

Table A31: *^{1}H signal enhancement and polarization levels observed as a function of shake time in a magnetic field of 65 G for 4-picoline at 303 K.*

Shake time / s	Signal enhancement / fold at 65 G					
	H_1	Pol (H1)	H_2	Pol (H2)	H_3	Pol (H3)
20	-5.9	-0.019	1.9	0.006	4.2	0.014
40	-8.9	-0.029	1.4	0.005	4.8	0.015
60	-7.7	-0.025	2.3	0.007	5.2	0.017
80	-12.9	-0.042	2.1	0.007	1.7	0.005
100	-35.8	-0.115	4.3	0.014	12.6	0.041
120	-47.8	-0.154	7.3	0.024	11.3	0.036
140	-11.2	-0.036	7.5	0.024	10.5	0.034

Table A32: *^{1}H signal enhancement and polarization levels indicating the effect of temperature on the proton sites in 4-picoline.*

Temp / K	Signal enhancement / fold at 65 G					
	H_1	Pol (H1)	H_2	Pol (H2)	H_3	Pol (H3)
305	-24.1	-0.078	12.5	0.040	1.1	0.004
310	-37.2	-0.120	23.3	0.075	1.9	0.006
315	-42.7	-0.138	25.9	0.067	2.5	0.008
320	-59.3	-0.191	17.7	0.057	2.8	0.009
325	-74.2	-0.239	46.3	0.149	3.1	0.010

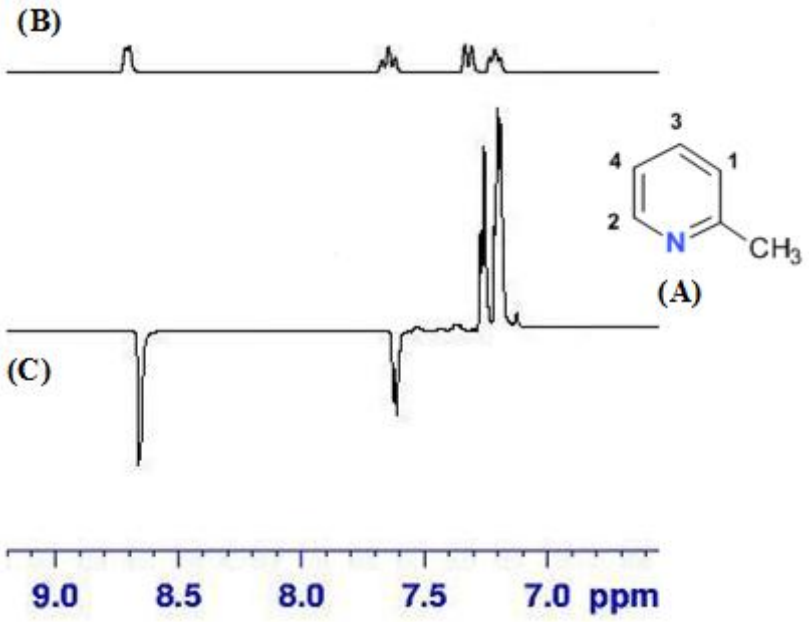

Figure A33: *(A) Molecular structure of 2-picoline and labels indicating the enhanced ^{1}H sites in the hyperpolarized spectrum. (B) Single-scan ^{1}H NMR spectrum of the aromatic region of a sample of 1 showing resonances for free 2-picoline that were obtained prior to polarization; (C) corresponding hyperpolarized ^{1}H NMR spectrum acquired immediately after polarization in a magnetic field of 65 G exhibiting the newly enhanced proton signals for free 2-picoline.*

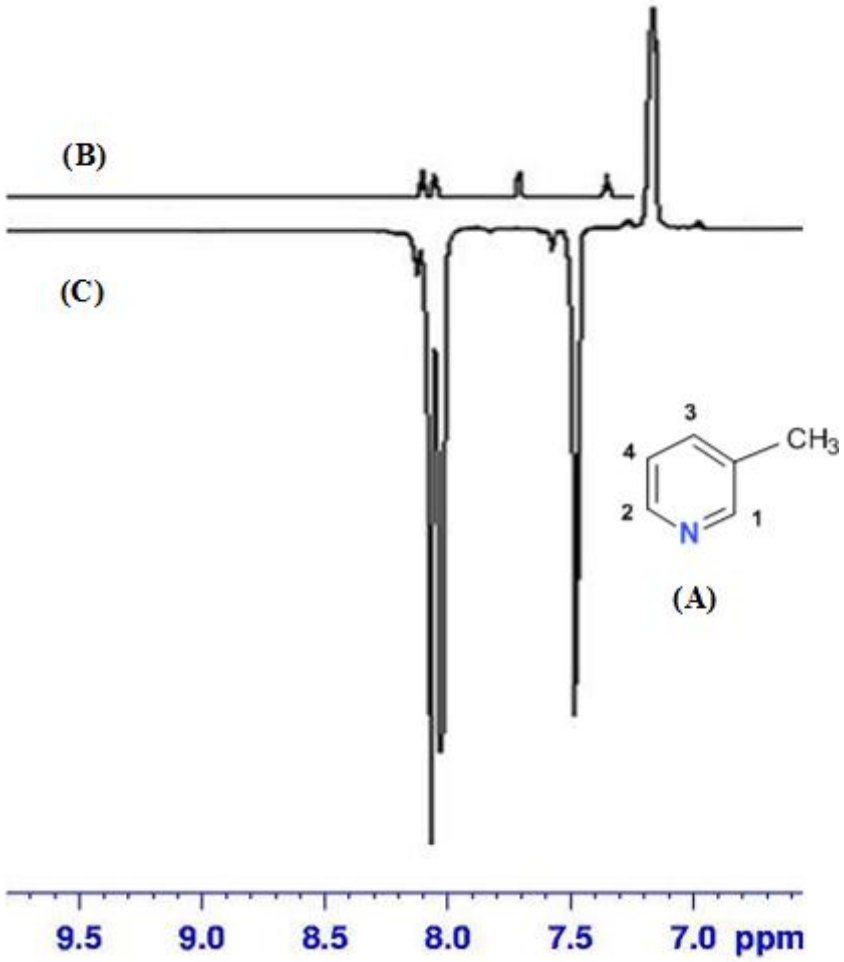

Figure A34: ***(A) Molecular structure of 3-picoline and labels indicating the enhanced ^{1}H sites in the hyperpolarized spectrum. (B) Single-scan ^{1}H NMR spectrum of the aromatic region of a sample of 1 showing resonances for free 3-picoline that were obtained prior to polarization; (C) corresponding hyperpolarized ^{1}H NMR spectrum acquired immediately after polarization in a 65 G exhibiting the newly enhanced proton signals for free 3-picoline.***

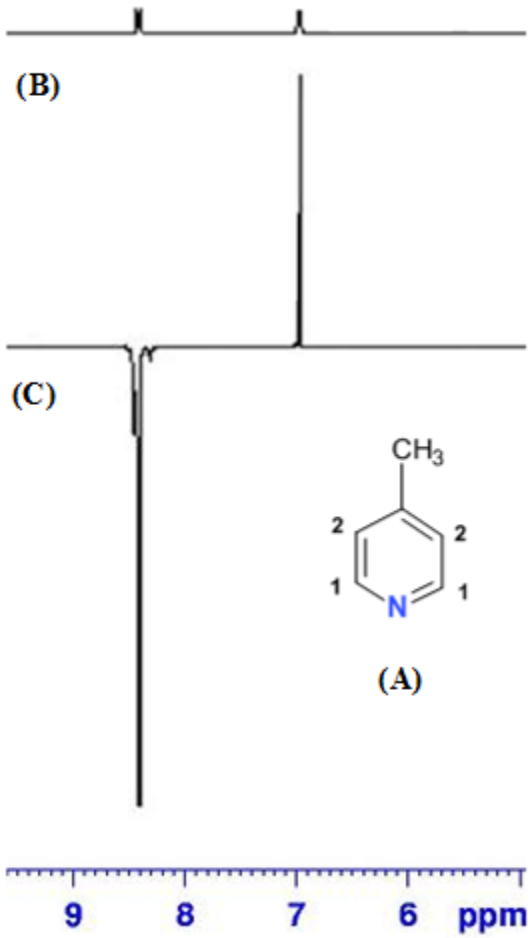

Figure A35: *(A) Single-scan ^{1}H NMR spectrum of the aromatic region of a sample of 1 showing resonances for free 4-picoline that were obtained prior to polarization; (B) corresponding hyperpolarized ^{1}H NMR spectrum acquired immediately after polarization in a magnetic field of 65 G exhibiting the newly enhanced proton signals for free 4-picoline. (C) The molecular structure of 4-picoline indicating the enhanced ^{1}H sites in the hyperpolarized spectrum.*

Table A36: ***^{1}H and ^{13}C NMR data for 2-fluoropyridine.***

^{1}H NMR				^{13}C NMR	
Group / label	***δ_H / ppm***	***J / Hz***	***Integral***	***Group/ label***	***δ_C / ppm***
H_1	8.31	'd' 1.89	1.00	C_1	149.58
H_2	8.11	'd' 4.19	1.06	C_2	146.91
H_3	7.30	'm'	0.82	C_3	124.76
H_4	6.90	'm'	1.09	C_4	128.68

Table A37: ***^{1}H and ^{13}C NMR data for 3-fluoropyridine.***

^{1}H NMR				^{13}C NMR	
Group / label	***δ_H / ppm***	***J / Hz***	***Integral***	***Group***	***δ_C / ppm***
H_1	8.80	'd'1.38	1.00	C_1	148.97
H_2	8.64	't' 3.90	1.01	C_2	145.78
H_3	7.92	'm'	1.04	C_3	123.14
H_4	7.68	'q' 5.04	1.02	C_4	127.91

Table A38: ***^{1}H and ^{13}C NMR data for 4-fluoropyridine***

^{1}H NMR				^{13}C NMR	
Group / label	***δ_H / ppm***	***J / Hz***	***Integral***	***Carbon***	***δ_C / ppm***
H_1	8.54	'd' 4.15	2.00	C_1	155.58
H_2	8.02	'd' 4.15	2.07	C_2	140.91

Table A39: ***^{1}H signal enhancement and polarization levels observed as a function of shake time at 65 G for 2-fluoropyridine.***

Shake time / s	*Signal enhancement / fold at 65 G*							
	H_1	*Pol (H1)*	H_2	*Pol (H2)*	H_3	*Pol (H3)*	H_4	*Pol (H4)*
20	-0.5	-0.002	-0.3	-0.001	-0.2	-0.001	2.1	0.007
40	-0.7	-0.002	-0.8	-0.003	-0.5	-0.005	1.1	0.004
60	-1.6	-0.005	-0.2	-0.001	-0.2	-0.001	1.7	0.005
80	-2.1	-0.007	-2.4	-0.008	-1.9	-0.006	2.8	0.009
100	-3.3	-0.011	-2.9	-0.009	-0.2	-0.001	3.8	0.012
120	-4.1	-0.014	-4.3	-0.016	-3.2	-0.010	4.0	0.013

Table A40: ***^{1}H signal enhancement and polarization levels observed as a function of temperature at 65 G for 2-fluoropyridine.***

Temp / K	*Signal enhancement / fold 65 G*							
	H_1	*Pol (H1)*	H_2	*Pol (H2)*	H_3	*Pol (H3)*	H_4	*Pol (H4)*
310	-19.2	-0.062	-23.2	-0.075	-21.3	-0.068	39.5	0.127
315	-21.9	-0.071	-25.9	-0.083	-11.6	-0.037	32.4	0.104
320	-39.5	-0.127	-28.7	-0.092	-16.2	-0.052	41.6	0.134
325	-31.1	-0.100	-43.6	-0.141	-37.8	-0.122	83.1	0.268

Table A41: *^{1}H signal enhancement and polarization levels observed as a function of shake time at 65 G fold for 3-fluoropyridine.*

Shake time / s	Signal enhancement / fold at 65 G							
	H_1	Pol (H1)	H_2	Pol (H2)	H_3	Pol (H3)	H_4	Pol (H4)
20	-10.3	-0.033	-11.2	-0.036	-6.4	-0.021	18.7	0.060
40	-13.9	-0.045	-18.4	-0.059	-11.4	-0.037	33.5	0.108
60	-20.6	-0.066	-19.7	-0.061	-12.2	-0.039	34.1	0.110
80	-20.8	-0.064	-21.9	-0.071	-15.2	-0.051	28.4	0.092
100	- 94.7	-0.130	-110.6	-0.057	-73.9	-0.105	97.3	0.191
120	- 136	-0.438	-154.2	-0.497	-103	-0.332	141	0.454

Table A42: *^{1}H signal enhancement and polarization levels observed as a function of temperature at 65 G for 3-fluoropyridine.*

Temp / K	Signal enhancement / fold at 65 G							
	H_1	Pol (H1)	H_2	Pol (H2)	H_3	Pol (H3)	H_4	Pol (H4)
310	-25.8	-0.083	-14.7	-0.047	-21.3	-0.069	28.8	0.093
315	-33.4	-0.108	-23.1	-0.074	-38.6	-0.124	42.5	0.137
320	-48.5	-0.156	-34.8	-0.112	-57.5	-0.185	56.3	0.181
325	-69.5	-0.224	-51.4	-0.165	-71.4	-0.229	62.7	0.201

Table A43: ***^{1}H signal enhancement and polarization levels observed as a function of shake time at 65 G for 4-fluoropyridine.***

Shake time / s	*Signal enhancement / fold at 65 G*			
	H_1	$Pol_{(H1)}$	H_2	$Pol_{(H2)}$
20	-1.3	-0.004	-3.2	-0.010
40	-3.9	-0.013	-4.4	-0.014
60	-6.6	-0.021	-8.7	-0.028
80	-9.8	-0.032	-13.9	-0.045
100	-12.7	-0.041	-16.6	-0.053
120	-16.4	-0.053	-18.2	-0.059

Table A44: ***^{1}H signal enhancement and polarization levels observed as a function of temperature at 65 G for 4-fluoropyridine.***

Temp / K	*Signal enhancement / fold at 65 G*			
	H_1	$Pol_{(H1)}$	H_2	$Pol_{(H2)}$
310	-6.8	-0.022	-10.6	-0.034
315	-15.7	-0.051	-18.9	-0.061
320	-25.4	-0.082	-26.4	-0.085
325	-30.6	-0.099	-39.4	-0.127

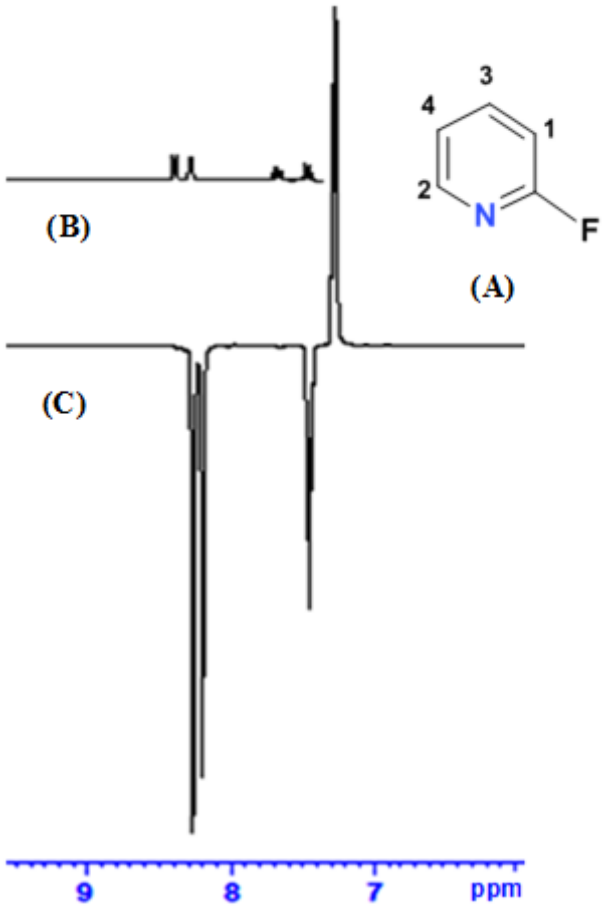

Figure A45: *(A) Molecular structure of 2-fluoropyridine and labels indicating the enhanced ^{1}H sites in the hyperpolarized spectrum. (B) Single-scan ^{1}H NMR spectrum of the aromatic region of a sample of 1 showing resonances for free 2-fluoropyridine that were obtained prior to polarization; (C) corresponding hyperpolarized ^{1}H NMR spectrum acquired immediately after polarization in a 65 G field exhibiting the newly enhanced proton signals for free 2-fluoropyridine.*

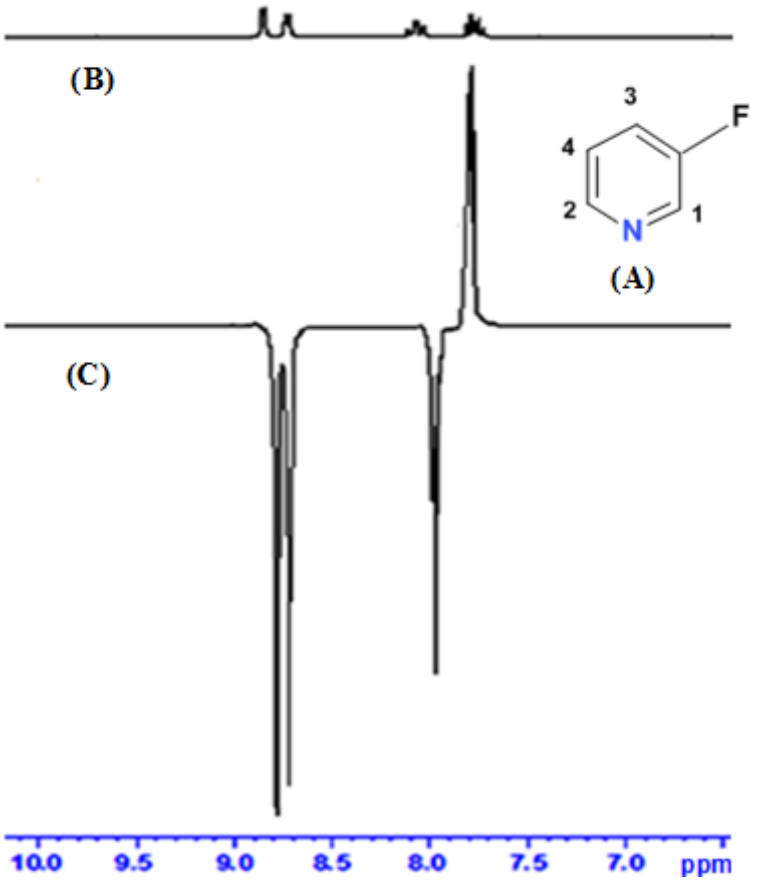

Figure A46: *(A) Molecular structure of 3-fluoropyridine and labels indicating the enhanced ^{1}H sites in the hyperpolarized spectrum. (B) Single-scan ^{1}H NMR spectrum of the aromatic region of a sample of 1 showing resonances for free 3-fluoropyridine that were obtained prior to polarization; (C) corresponding hyperpolarized ^{1}H NMR spectrum acquired immediately after polarization in a 65 G field exhibiting the newly enhanced proton signals for free 3-fluoropyridine.*

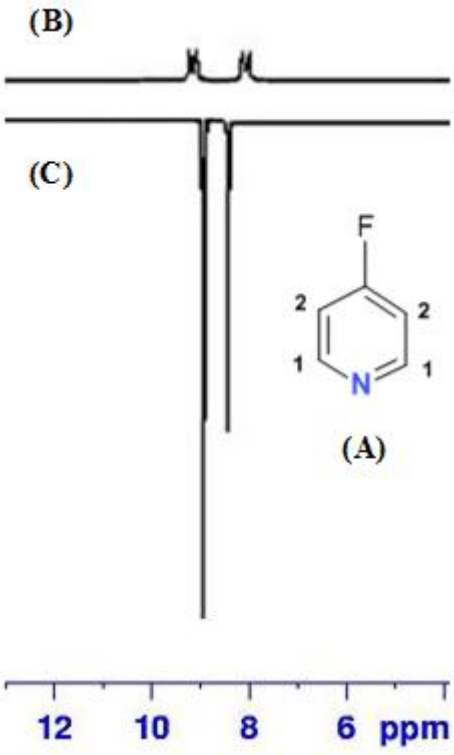

Figure A47: (A) Molecular structure of 4-fluoropyridine and labels indicating the enhanced ^{1}H sites in the hyperpolarized spectrum. (B) Single-scan ^{1}H NMR spectrum of the aromatic region of a sample of 1 showing resonances for free 4-fluoropyridine that were obtained prior to polarization; (C) corresponding hyperpolarized ^{1}H NMR spectrum acquired immediately after polarization in a magnetic field of 65 G exhibiting the newly enhanced proton signals for free 4-fluoropyridine.

Table A48: ***^{1}H and ^{13}C NMR data for 2-chloropyridine.***

	^{1}H NMR			^{13}C NMR	
Group	***δ_H / ppm***	***J / Hz***	***Integral***	***Group***	***δ_C / ppm***
H_1	8.34	'd'1.84	1.00	C_1	149.41
H_2	7.70	't' 8.32	1.02	C_2	146.54
H_3	7.40	'm'	1.01	C_3	124.41
H_4	7.25	't' 6.39	1.02	C_4	128.10

Table A49: ***^{1}H and ^{13}C NMR data for 3-chloropyridine.***

	^{1}H NMR			^{13}C NMR	
Group / label	***δ_H / ppm***	***J/Hz***	***Integral***	***Group / label***	***δ_C / ppm***
H_1	8.66	'd'2.17	1.00	C_1	148.58
H_2	8.56	'd' 4.01	0.98	C_2	147.55
H_3	7.76	't'7.79	0.97	C_3	123.76
H_4	7.39	'q' 4.66	1.02	C_4	127.87

Table A50: ***^{1}H and ^{13}C NMR data for 4-chloropyridine.***

	^{1}H NMR			^{13}C NMR	
Group / label	***δ_H / ppm***	***J / Hz***	***Integral***	***Group / label***	***δ_C / ppm***
H_1	8.61	'd' 5.1	2.00	C_1	157.41
H_2	7.98	'd' 5.1	2.02	C_2	141.10

Table A51: *^{1}H signal enhancement and polarization levels observed as a function of shake time at 65 G for 2-chloropyridine.*

Shake time / s	*Signal enhancement / fold at 65 G*							
	H_1	*Pol (H1)*	H_2	*Pol (H2)*	H_3	*Pol (H3)*	H_4	*Pol (H4)*
20	-0.7	-0.002	-0.4	-0.001	-0.7	-0.002	1.4	0.005
40	-3.7	-0.012	-3.2	-0.010	-2.6	-0.008	3.1	0.10
60	-4.1	-0.013	-4.0	-0.013	-3.2	-0.010	4.9	0.016
80	-5.6	-0.018	-5.7	-0.018	-4.8	-0.015	5.9	0.019
100	-6.9	-0.022	-6.6	-0.021	-5.8	-0.019	5.3	0.017
120	-7.8	-0.025	-8.8	-0.028	-7.9	-0.025	15	0.049

Table A52: *^{1}H signal enhancement and polarization levels observed as a function of temperature at 65 G for 2-chloropyridine.*

Temp / K	*Signal enhancement / fold 65 G*							
	H_1	*Pol (H1)*	H_2	*Pol (H2)*	H_3	*Pol (H3)*	H_4	*Pol (H4)*
310	-1.6	-0.005	-1.2	-0.004	-1.5	-0.005	3.4	0.011
315	-10.2	-0.033	-11.9	-0.038	-8.8	-0.028	12.1	0.039
320	-17.3	-0.056	-16.5	-0.053	-14.2	-0.046	18.5	0.060
325	-19.4	-0.063	-21.9	-0.071	-20.7	-0.067	12.8	0.041

Table A53: *^{1}H signal enhancement and polarization levels observed as a function of shake time at 65 G for 3-chloropyridine.*

Shake time / s	Signal enhancement / fold at 65 G							
	H_1	Pol (H1)	H_2	Pol (H2)	H_3	Pol (H3)	H_4	Pol (H4)
20	-5.9	-0.019	-1.9	-0.006	-4.2	-0.014	-6.1	-0.020
40	-8.9	-0.029	-1.4	-0.005	-4.8	-0.015	-7.2	-0.023
60	-7.7	-0.025	-12	-0.039	-15.2	-0.049	-11.3	-0.036
80	-12.9	-0.042	-19	-0.061	-10.7	-0.034	-13.5	-0.043
100	-32.4	-0.104	-8.3	-0.027	-12.6	-0.041	-31.5	-0.102
120	-47.8	-0.154	-9.3	-0.030	-15.3	-0.049	-38.4	-0.124

Table A54: *^{1}H signal enhancement and polarization levels observed as a function of temperature at 65 G for 3-chloropyridine.*

Temp / K	Signal enhancement / fold 65 G							
	H_1	Pol (H1)	H_2	Pol (H2)	H_3	Pol (H3)	H_4	Pol (H4)
310	-2.4	-0.008	-2.1	-0.007	-1.9	-0.006	-1.5	-0.005
315	-13.4	-0.043	-15.2	-0.049	-18.8	-0.061	-13.7	-0.044
320	-18.6	-0.060-	-21.5	-0.069	-19.3	-0.062	-22.1	-0.071
325	-26.4	-0.085	-27.3	-0.088	-31.7	-0.102	-21.9	-0.071

Table A55: ***^{1}H signal enhancement and polarization levels observed as a function of shake time at 65 G for 4-chloropyridine.***

Shake time / s	*Signal enhancement / fold at 65 G*			
	H_1	*Pol (H1)*	H_2	*Pol (H2)*
20	-0.8	-0.003	-1.2	-0.004
40	-7.8	-0.025	-6.8	-0.022
60	-8.9	-0.029	-8.5	-0.027
80	-13.5	-0.044	-9.4	-0.030
100	-16.7	-0.054	-11.9	-0.038
120	-19.2	-0.062	-12.2	-0.039

Table A56: ***^{1}H signal enhancement and polarization levels observed as a function of temperature at 65 G for 4-chloropyridine.***

Temp / K	*Signal enhancement / fold at 65 G*			
	H_1	*Pol (H1)*	H_2	*Pol (H2)*
310	-2.6	-0.008	-1.9	-0.006
315	-14.2	-0.046	-6.7	-0.022
320	-19.8	-0.064	-13.9	-0.045
325	-26.6	-0.086	-20.6	-0.066

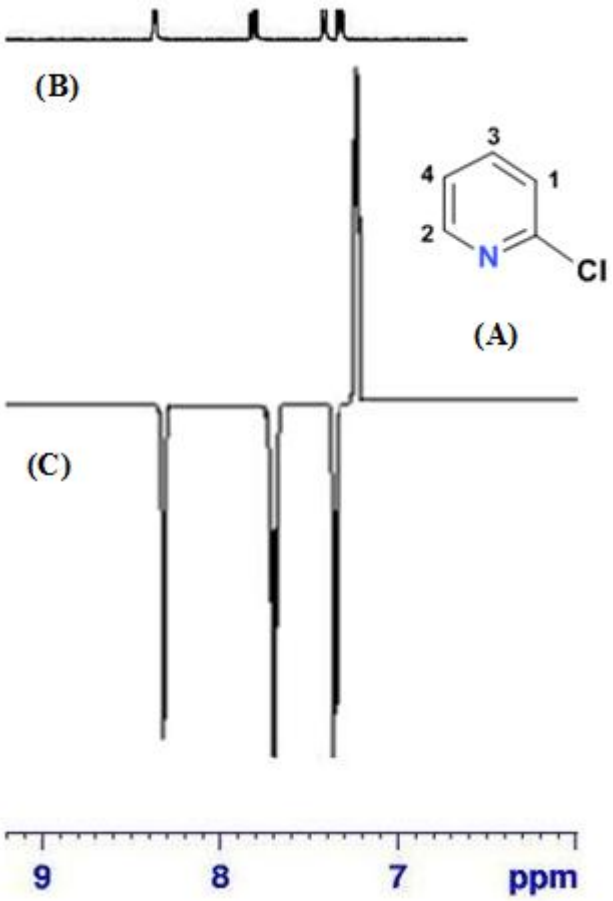

Figure A57: *(A) Molecular structure of 2-chloropyridine and the labels indicating the enhanced ^{1}H sites in the hyperpolarized spectrum. (B) Single-scan ^{1}H NMR spectrum of the aromatic region of a sample of 1 showing resonances for free 2-chloropyridine that were obtained prior to polarization; (C) corresponding hyperpolarized ^{1}H NMR spectrum acquired immediately after polarization in a magnetic field 65 G exhibiting the newly enhanced proton signals for free 2-chloropyridine.*

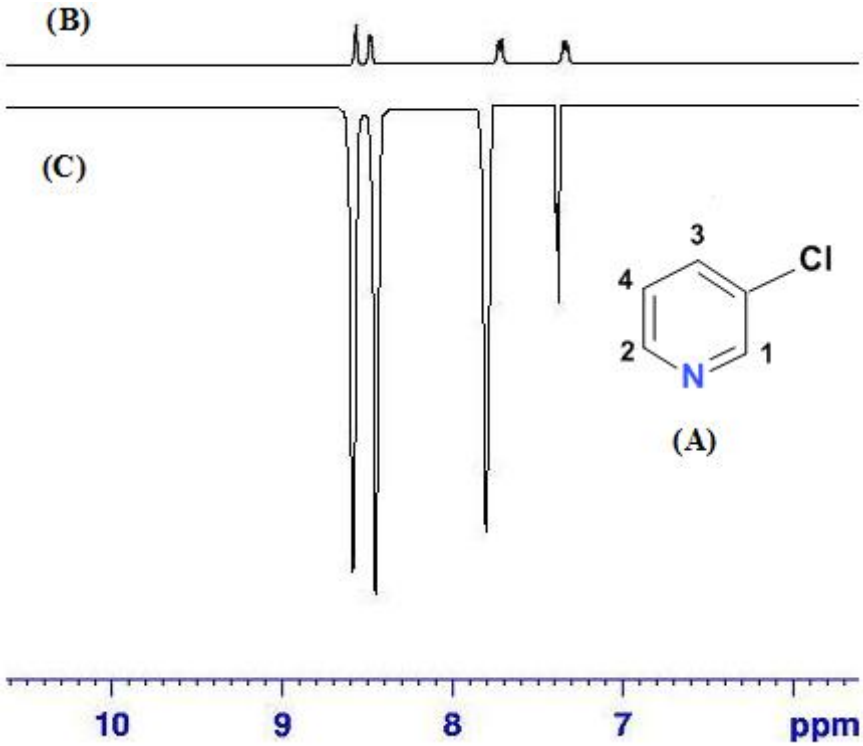

Figure A58: (A) Molecular structure of 3-chloropyridine and the labels indicating the enhanced ^{1}H sites in the hyperpolarized spectrum. (B) Single-scan ^{1}H NMR spectrum of the aromatic region of a sample of 1 showing resonances for free 3-chloropyridine that were obtained prior to polarization; (C) corresponding hyperpolarized ^{1}H NMR spectrum acquired immediately after polarization in a magnetic field of 65 G exhibiting the newly enhanced proton signals for free 3-chloropyridine.

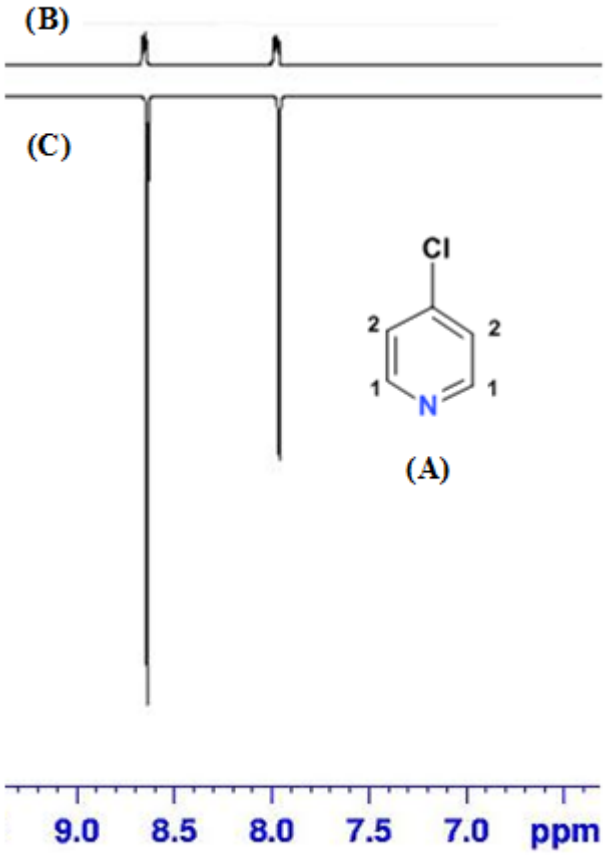

Figure A59: (A) Molecular structure of 4-chloropyridine and the labels indicating the enhanced ^{1}H sites in the hyperpolarized spectrum. (B) Single-scan ^{1}H NMR thermal spectrum; (C) corresponding hyperpolarized ^{1}H NMR spectrum acquired immediately after polarization in a magnetic field of 65 G exhibiting the newly enhanced proton signals for free 4-chloropyridine.

Table A60: ***^{1}H and ^{13}C NMR data for 2- bromopyridine.***

^{1}H NMR				^{13}C NMR	
Group / label	***δ_H / ppm***	***J / Hz***	***Integral***	***Group / label***	***δ_C /ppm***
H_1	8.23	'd' 4.39	1.00	C_1	148.30
H_2	7.62	't' 7.55	1.01	C_2	146.40
H_3	7.53	't' 8.33	1.05	C_3	124.76
H_4	7.38	't' 5.23	1.10	C_4	128.68

Table A61: ***^{1}H and ^{13}C NMR data for 3- bromopyridine***

^{1}H NMR				^{13}C NMR	
Group / label	***δ_H / ppm***	***J / Hz***	***Integral***	***Group / label***	***δ_C / ppm***
H_1	8.64	'm'	1.00	C_1	149.10
H_2	8.31	'm'	1.03	C_2	145.82
H_3	7.53	't' 7.99	1.02	C_3	122.96
H_4	7.41	'm'	1.01	C_4	127.05

Table* A62:** ***^{1}H and ^{13}C NMR data for 4-bromopyridine.

^{1}H NMR				^{13}C NMR	
Group / label	***δ_H / ppm***	***J / Hz***	***Integral***	***Group / label***	***δ_C / ppm***
H_1	8.71	'd' 4.82	2.00	C_1	151.37
H_2	7.56	'd' 4.82	2.07	C_2	143.15

Table A63: ***^{1}H signal enhancement and polarization levels observed as a function of shake time at 65 G for 2-bromopyridine.***

Shake time / s	*Signal enhancement / fold at 65 G*							
	H_1	*Pol (H1)*	H_2	*Pol (H2)*	H_3	*Pol (H3)*	H_4	*Pol (H4)*
20	-0.2	-0.001	-0.4	-0.001	-0.4	-0.001	0.3	0.001
40	-0.9	-0.003	-1.1	-0.009	-0.9	-0.003	1.2	0.004
60	-1.3	-0.004	-1.2	-0.004	-1.4	-0.005	1.4	0.005
80	-1.4	-0.005	-1.2	-0.004	-1.8	-0.006	1.9	0.006
100	-4.2	-0.014	-4.3	-0.014	-4.8	-0.006	5.2	0.017
120	-7.3	-0.024	-5.9	-0.019	-6.8	-0.022	8.9	0.029

Table A64: ***^{1}H signal enhancement and polarization levels observed as a function of temperature at 65 G for 2- bromopyridine.***

Temp / K	*Signal enhancement / fold at 65 G*							
	H_1	*Pol (H1)*	H_2	*Pol (H2)*	H_3	*Pol (H3)*	H_4	*Pol (H4)*
305	-0.4	-0.001	-0.3	0.001	-0.2	-0.001	2.1	0.007
310	-6.9	-0.022	-5.2	-0.017	-8.1	-0.026	8.5	0.027
315	-7.4	-0.024	-6.1	-0.020	-6.6	-0.021	8.9	0.029
320	-10.2	-0.033	-8.3	-0.027	-11.3	-0.036	12	0.040
325	-14.9	0.048	-11.7	-0.038	-12.9	-0.042	16	0.054

Table A65: ***^{1}H signal enhancement and polarization levels observed as a function of shake time at 65 G for 3-bromopyridine.***

Shake time / s	*Signal enhancement / fold 65 G*							
	H_1	*Pol (H1)*	H_2	*Pol (H2)*	H_3	*Pol (H3)*	H_4	*Pol (H4)*
20	-8.2	-0.026	-3.7	-0.012	-0.8	-0.003	0.7	0.002
40	-14.2	-0.046	-6.8	-0.022	-4.1	-0.013	7.3	0.024
60	-17.1	-0.055	-10.6	-0.033	-8.1	-0.026	5.4	0.017
80	-23.1	-0.074	-15.6	-0.050	-13.5	-0.044	7.4	0.024
100	-28.4	-0.092	-18.4	-0.059	-14.3	-0.046	9.2	0.030
120	-35.5	-0.114	-24.6	-0.079	-18.3	-0.059	13.4	0.043

Table A66: ***^{1}H signal enhancement and polarization levels observed as a function of temperature at 65 G for 3- bromopyridine.***

Temp / K	*Signal enhancement / fold at 65 G*							
	H_1	*Pol (H1)*	H_2	*Pol (H2)*	H_3	*Pol (H3)*	H_4	*Pol (H4)*
305	-1.3	-0.004	-0.3	-0.001	-0.8	-0.003	6.3	0.020
310	-20.9	-0.067	-15.8	-0.051	-24.2	-0.078	33.9	0.109
315	-22.1	-0.071	-18.2	-0.059	-19.8	-0.064	26.7	0.086
320	-30.6	-0.099	-24.8	-0.080	-30.6	-0.099	37.5	0.121
325	-44.5	-0.143	-35.1	-0.113	-38.7	-0.125	50.9	0.164

Table A67: *^{1}H signal enhancement and polarization levels observed as a function of shake time at 65 G for 4-bromopyridine.*

Shake time / s	*Signal enhancement / fold at 65 G*			
	H_1	$Pol_{(H1)}$	H_2	$Pol_{(H2)}$
20	-2.6	-0.008	-1.2	0.004
40	-2.5	-0.008	-3.2	-0.010
60	-8.4	-0.027	-5.4	-0.017
80	-10.8	-0.035	-7.4	-0.024
100	-13.2	-0.043	-9.3	-0.030
120	-18.2	-0.059	-13.2	-0.043

Table A68: *^{1}H signal enhancement and polarization levels observed as a function of temperature at 65 G for 4-bromopyridine.*

Temp / K	*Enhancements levels / fold at 65 G*			
	H_1	$Pol_{(H1)}$	H_2	$Pol_{(H2)}$
305	-1.2	-0.004	-5.9	-0.019
310	-18.8	-0.061	-14.9	-0.048
315	-20.2	-0.065	-16.9	-0.054
320	-28.2	-0.091	-22.9	-0.074
325	-41.6	-0.134	-32.8	-0.106

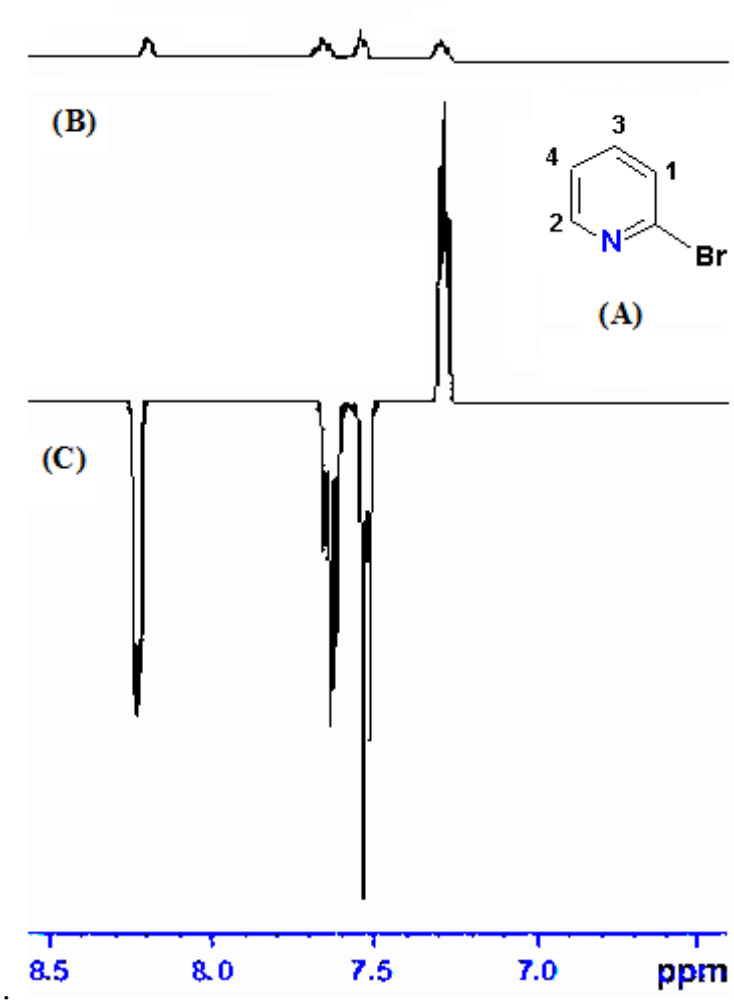

Figure A69: *(A) Molecular structure of 2-bromopyridine and the labels indicating the enhanced ^{1}H sites. (B) Single-scan ^{1}H NMR spectrum of the aromatic region of a sample of 1 showing resonances for free 2-bromopyridine that were obtained prior to polarization; (C) corresponding hyperpolarized ^{1}H NMR spectrum acquired immediately after polarization in a magnetic field of 65 G exhibiting the newly enhanced proton signals for free 2-bromopyridine.*

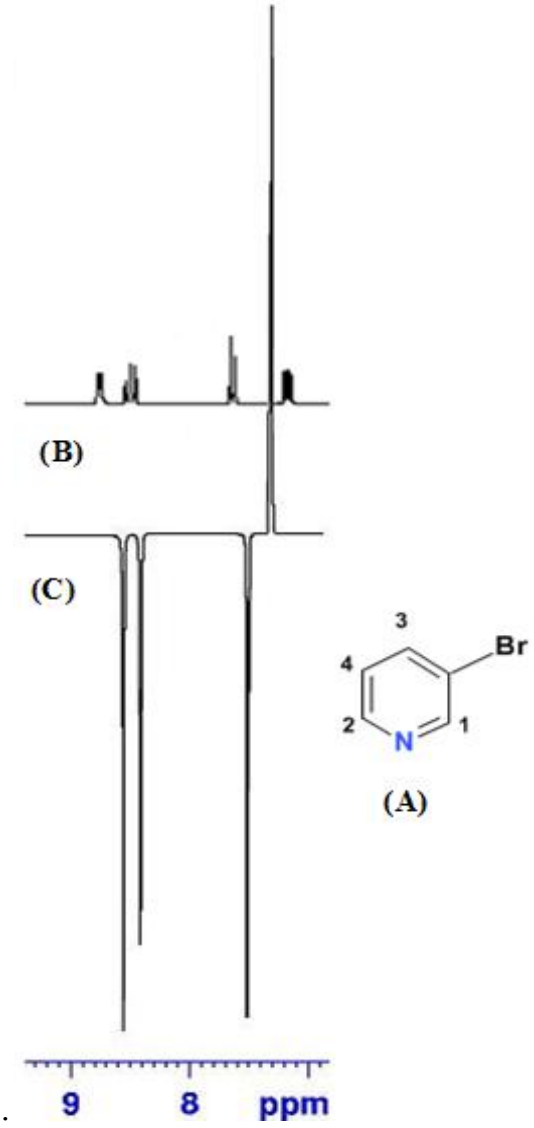

Figure A70: (A) Molecular structure of 3-bromopyridine with labels indicating the enhanced ^{1}H sites. (B) Single-scan ^{1}H NMR spectrum of the aromatic region of a sample of 1 showing resonances for free 3-bromopyridine that were obtained prior to polarization; (C) Corresponding hyperpolarized ^{1}H NMR spectrum acquired immediately after polarization in a magnetic field of 65 G exhibiting the enhanced proton signals for free 3-bromopyridine.

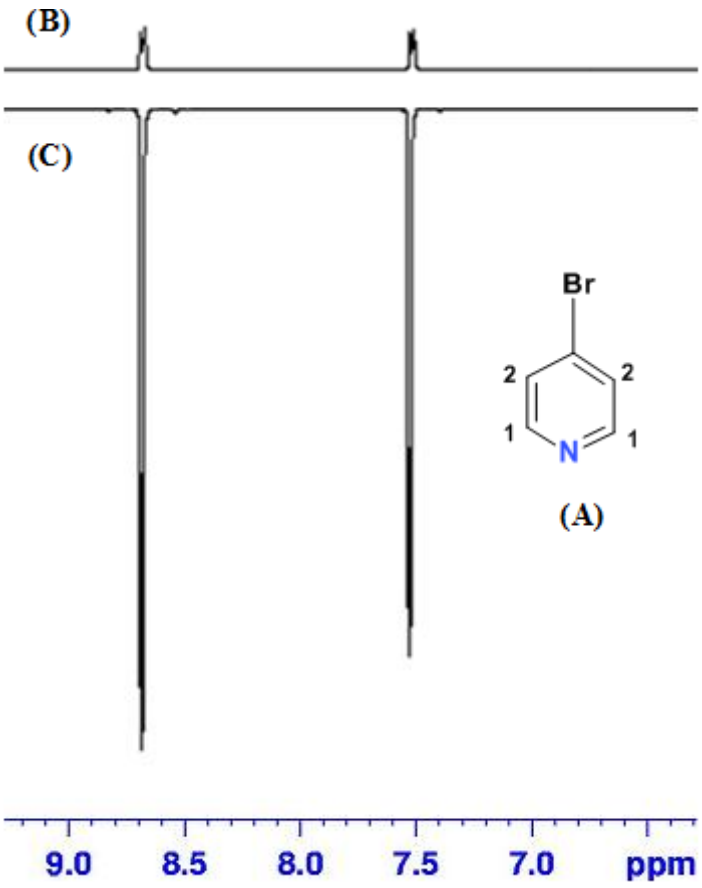

Figure A71: (A) Molecular structure of 4-bromopyridine with labels indicating the enhanced ^{1}H sites. (B) Single-scan ^{1}H NMR spectrum of the aromatic region of a sample of 1 showing resonances for free 4-bromopyridine that were obtained prior to polarization; (C) corresponding hyperpolarized ^{1}H NMR spectrum acquired immediately after polarization in a magnetic field of 65 G exhibiting the enhanced proton signals for free 4-bromopyridine.

Table A72: ***^{1}H and ^{13}C NMR data for 2-iodopyridine.***

^{1}H NMR				^{13}C NMR	
Group /label	***δ_H / ppm***	***J / Hz***	***Integral***	***Group / label***	***δ_C / ppm***
H_1	8.18	'd' 3.99	1.00	C_1	149.05
H_2	7.56	'd' 7.98	0.99	C_2	145.89
H_3	7.30	'm'	1.02	C_3	124.19
H_4	7.25	'm'	1.03	C_4	127.18

Table A73: ***^{1}H and ^{13}C NMR data for 3-iodopyridine.***

^{1}H NMR				^{13}C NMR	
Group / label	***δ_H / ppm***	***J / Hz***	***Integral***	***Group / label***	***δ_C / ppm***
H_1	8.80	's'	1.00	C_1	148.38
H_2	8.54	'd' 2.11	0.88	C_2	146.78
H_3	8.02	'd' 4.09	1.03	C_3	122.89
H_4	7.40	'm'	1.04	C_4	126.98

Table A74: ***^{1}H and ^{13}C NMR data for 4-iodopyridine.***

^{1}H NMR				^{13}C NMR	
Group / label	***δ_H / ppm***	***J / Hz***	***Integral***	***Carbon***	***δ_C / ppm***
H_1	8.80	'd' 6.2	2.00	C_1	150.05
H_2	8.54	'd' 6.2	2.02	C_2	146.45

Table A75: ***^{1}H signal enhancement and polarization levels observed as a function of shake time at 65 G for 2-iodopyridine.***

Shake time / s	*Signal enhancement / fold at 65 G*							
	H_1	*Pol (H1)*	H_2	*Pol (H2)*	H_3	*Pol (H3)*	H_4	*Pol (H4)*
20	-1.1	-0.004	-1.3	-0.003	-1.8	-0.006	-0.9	-0.003
40	-4.7	-0.015	-4.9	-0.016	-7.1	-0.023	-6.9	-0.022
60	-4.9	-0.016	-5.2	-0.017	-6.9	-0.022	-7.8	-0.025
80	-5.5	-0.018	-5.7	-0.018	-7.9	-0.025	-8.5	-0.027
100	-5.9	-0.019	-5.2	-0.017	-7.0	-0.023	-7.8	-0.025
120	-6.9	-0.022	-8.1	-0.026	-9.7	-0.030	-9.3	-0.030

Table A76: ***^{1}H signal enhancement and polarization levels observed as a function of temperature at 65 G for 2-iodopyridine.***

Temp / K	*Signal enhancement / fold at 65 G*							
	H_1	*Pol (H1)*	H_2	*Pol (H2)*	H_3	*Pol (H3)*	H_4	*Pol (H4)*
305	-6.7	-0.022	-5.4	-0.017	-6.5	-0.021	-9.8	-0.032
310	-8.5	-0.027	-3.9	-0.013	-5.9	-0.019	-11.2	-0.038
315	-11.4	-0.037	-4.6	-0.015	-8.6	-0.028	-13.3	-0.043
320	-11.8	-0.038	-5.1	-0.016	-9.1	-0.029	-13.8	-0.044
325	-13.5	-0.044	-5.6	-0.018	-10.7	-0.034	-14.5	-0.047

Table A77: ***^{1}H signal enhancement and polarization levels observed as a function of shake time at 65 G for 3- iodopyridine.***

Shake time /s	*Signal enhancement / fold at 65 G*							
	H_1	*Pol (H1)*	H_2	*Pol (H2)*	H_3	*Pol (H3)*	H_4	*Pol (H4)*
20	-15.2	-0.081	-8.6	-0.041	-12.4	-0.058	24.2	0.078
40	-25.4	-0.082	-12.9	-0.042	-17.8	-0.057	34.1	0.110
60	-34.1	-0.110	-14.4	-0.046	-25.1	-0.081	50.9	0.164
80	-35.2	-0.113	-15.8	-0.051	-27.6	-0.089	48.4	0.156
100	- 40.3	-0.130	-17.7	-0.057	-32.5	-0.105	59.3	0.191
120	- 46.3	-0.149	-24.2	-0.078	- 44.5	-0.143	66.8	0.215

Table A78: ***^{1}H signal enhancement and polarization levels observed as a function of temperature at 65 G for 3-iodopyridine.***

Temp / K	*Signal enhancement / fold at 65 G*							
	H_1	*Pol (H1)*	H_2	*Pol (H2)*	H_3	*Pol (H3)*	H_4	*Pol (H4)*
305	-48.2	-0.155	-38.9	-0.125	-47.6	-0.153	70.6	0.228
310	-61.2	-0.197	-29.2	-0.094	-42.5	-0.137	80.6	0.260
315	-81.8	-0.264	-33.5	-0.108	-61.7	-0.199	94.4	0.304
320	-84.5	-0.272	-37.3	-0.120	-65.8	-0.212	98.9	0.319
325	-96.8	-0.312	-40.9	-0.132	-77.6	-0.250	104.5	0.337

Table A79: ***^{1}H signal Enhancement and polarization levels observed as a function of shake time at 65 G for 4-iodopyridine.***

Shake time / s	*Signal enhancement / fold at 65 G*			
	H_1	$Pol_{(H1)}$	H_2	$Pol_{(H2)}$
20	-3.8	-0.012	-2.5	-0.008
40	-10.8	-0.035	-8.7	-0.028
60	-13.5	-0.044	-6.5	-0.021
80	-15.2	-0.049	-9.8	-0.032
100	-20.8	-0.067	-8.2	-0.026
120	-23.4	-0.075	-12.1	-0.039

Table A80: ***^{1}H signal enhancement and polarization levels observed as a function of temperature at 65 G for 4-iodopyridine.***

Temp / K	*Signal enhancement / fold at 65 G*			
	H_1	$Pol_{(H1)}$	H_2	$Pol_{(H2)}$
305	-14.2	-0.046	-11.5	-0.037
310	-18.1	-0.058	-8.5	-0.027
315	-27.1	-0.087	-9.8	-0.032
320	-32.9	-0.106	-13.9	-0.045
325	-37.5	-0.121	-21.6	-0.070

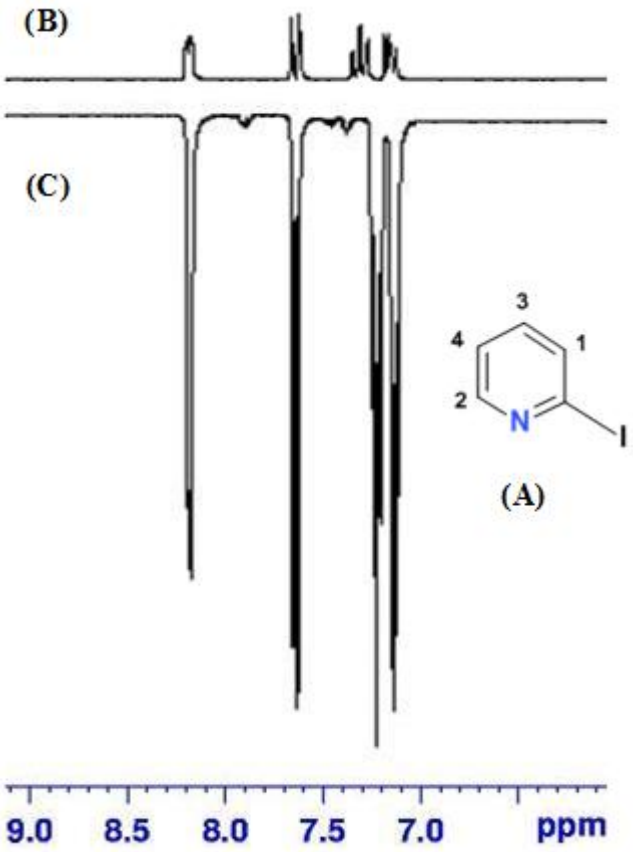

Figure A81: *(A) Molecular structure of 2-iodopyridine with labels indicating the enhanced ^{1}H sites. (B) Single-scan ^{1}H NMR spectrum of the aromatic region of a sample of 1 showing resonances for free 2-iodopyridine that were obtained prior to polarization; (C) corresponding hyperpolarized ^{1}H NMR spectrum acquired immediately after polarization in a magnetic field of 65 G exhibiting the newly enhanced proton signals for free 2-iodopyridine.*

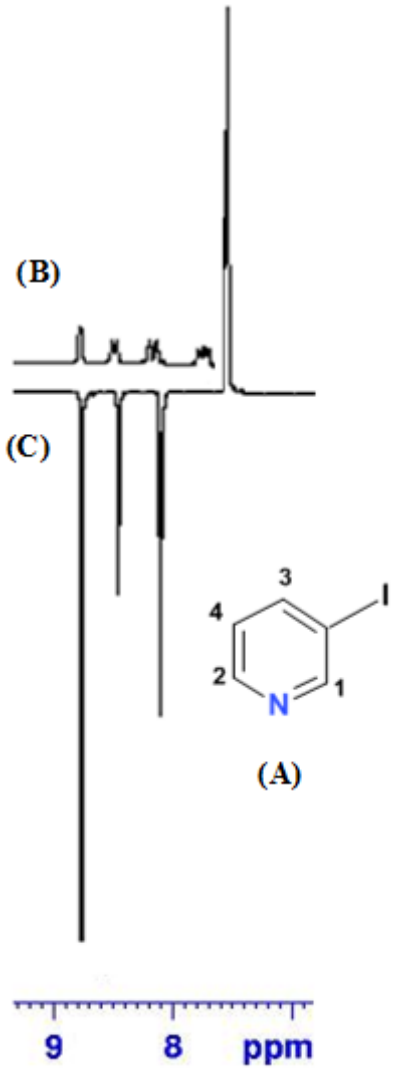

Figure A82: (A) Molecular structure of 3-iodopyridine with labels indicating the enhanced ^{1}H sites. (B) Single-scan ^{1}H NMR spectrum of the aromatic region of a sample of 1 showing resonances for free 3-iodopyridine that were obtained prior to polarization; (C) corresponding hyperpolarized ^{1}H NMR spectrum acquired immediately after polarization in a magnetic field of 65 G exhibiting the newly enhanced proton signals for free 3-iodopyridine.

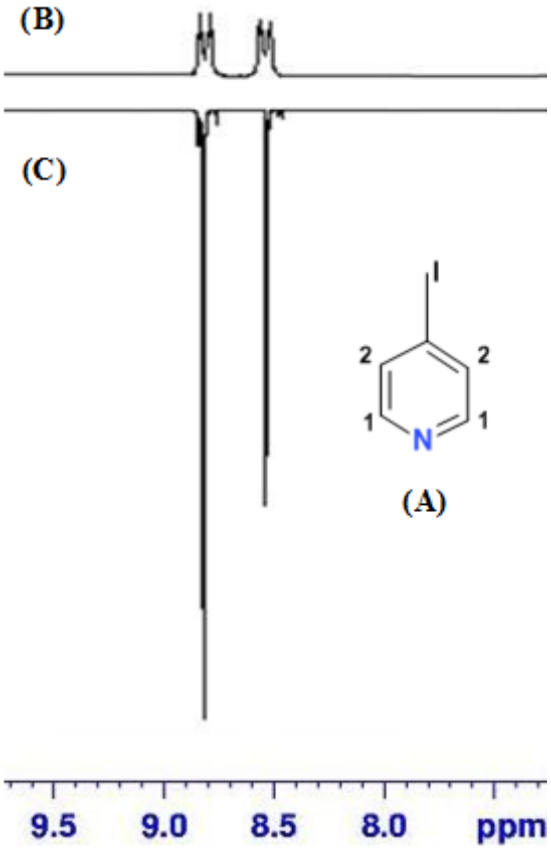

Figure A83: *(A) Molecular structure of 4-iodopyridine and the labels indicating the enhanced ^{1}H sites. (B) Single-scan ^{1}H NMR spectrum of the aromatic region of a sample of 1 showing resonances for free 4-iodopyridine that were obtained prior to polarization; (C) corresponding hyperpolarized ^{1}H NMR spectrum acquired immediately after polarization in a magnetic field of 65 G exhibiting the enhanced proton signals for free 4-iodopyridine.*

This Appendix presents the data (Tables and Figures) from chapter 3.

Table B1: ***^{1}H and ^{13}C NMR data for the hyperpolarized sites in nicotinic acid.***

	^{1}H NMR			***^{13}C NMR***	
Proton	***δ_H / ppm***	***J / Hz***	***Integral***	***Carbon***	***δ_C / ppm***
H_1	9.13	'd' 2.92	1.00	C_1	166.10
H_2	8.78	't' 4.97	1.09	C_2	152.32
H_3	8.43	'd' 6.29	1.02	C_3	149.97
H_4	7.56	'm'	1.04	C_4	137.76
-	-	-	-	C_5	126.01
-	-	-	-	C_6	123.61

Table B2: ***Enhancement and polarization levels observed as a function of shake time in a magnetic field of 65 G for nicotinic acid at 320 K.***

Shake time / s	***Signal enhancement / fold at 65 G***							
	H_1	***Pol (H_1)***	***H_2***	***Pol (H_2)***	***H_3***	***Pol (H_3)***	***H_4***	***Pol (H_4)***
20	-21.5	-0.07	-26.1	-0.09	-20.1	-0.07	23.9	0.08
40	-104.7	-0.34	-57.9	-0.19	-36.1	-0.12	126.4	0.41
60	-109.6	-0.36	-61.7	-0.11	-46.9	-0.16	143.9	0.47
80	-115.8	-0.38	-74.6	-0.25	-56.6	-0.19	128.6	0.42
100	-229.5	-0.75	-176.3	-0.57	-105.9	-0.35	118.7	0.39
120	-398.5	-1.29	-360.9	-1.17	-264.6	-0.86	203.8	0.66

Table B3: Enhancement and polarization levels observed as a function of substrate loading at 65 G for nicotinic acid at 325 K.

Conc. / mmol	*Signal enhancement / fold at 65 G*							
	H_1	*Pol (H_1)*	*H_2*	*Pol (H_2)*	*H_3*	*Pol (H_3)*	*H_4*	*Pol (H_4)*
0.0008	-20.5	-0.07	-15.8	-0.06	-9.2	-0.04	88.5	0.29
0.004	-51.7	-0.17	-34.6	-0.12	-27.5	-0.09	123.9	0.40
0.008	-121.7	- 0.40	-90.2	-0.30	-77.6	-0.26	127.3	0.42
0.02	-205.7	-0.67	-151.5	-0.49	-140.6	-0.46	211.2	0.69
0.04	-346.9	-1.12	-280.7	-0.91	-195.3	-0.63	108.8	0.36
0.07	-351.5	-1.14	-282.7	-0.92	-198.6	-0.65	105.9	0.35
0.09	-306.3	-0.99	-228.9	-0.74	-202.5	-0.66	225.1	0.73

Table B4: Enhancement and polarization levels observed for nicotinic acid as a function of temperature at 65 G.

Temp / K	*Signal enhancement / fold at 65 G*							
	H_1	*Pol (H_1)*	*H_2*	*Pol (H_2)*	*H_3*	*Pol (H_3)*	*H_4*	*Pol (H_4)*
305	-143.7	-0.47	-95.7	-0.31	-63.5	-0.21	136.2	0.44
310	-209.3	-0.68	-150.7	-0.49	-121.5	-0.40	191.6	0.62
315	-255.4	-0.83	-193.5	-0.63	-163.4	-0.53	177.1	0.58
320	-264.8	-0.86	-198.8	-0.65	-180.6	0.59	223.3	0.73
325	-323.6	-1.05	-247.5	-0.79	-216.7	-0.69	208.9	0.68
330	-402.5	-1.30	-319.4	-1.03	-265.1	-0.86	207.5	0.67

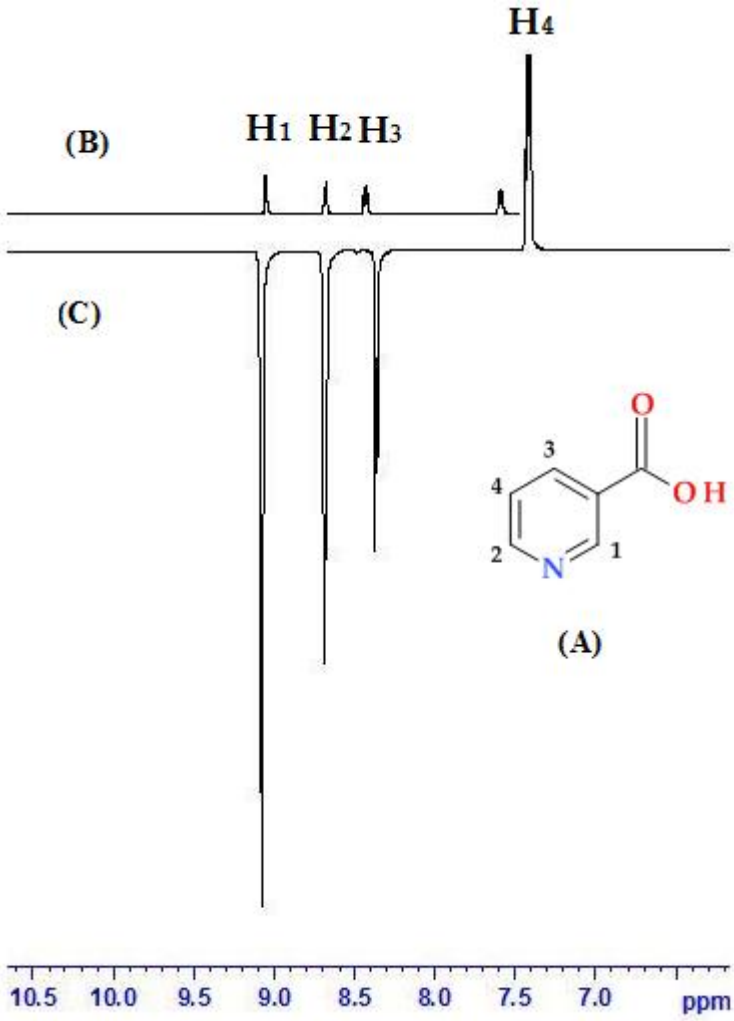

Figure B5: ***(A) Molecular structure of nicotinic acid with labels indicating the enhanced ^{1}H sites in the hyperpolarized spectrum; (B) Single-scan ^{1}H NMR spectrum showing resonances for free nicotinic acid that were obtained prior to polarization; (C) corresponding ^{1}H hyperpolarized NMR spectrum acquired in a magnetic field of 65 G exhibiting the enhanced proton signals for free nicotinic acid.***

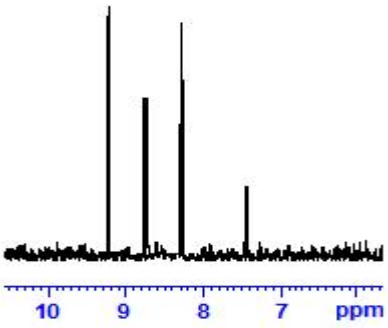

Figure B6: Depicts the dq-OPSY spectrum demonstrating the p-H_2 transfer to all hyperpolarized proton sites within the nicotinic acid using SABRE.

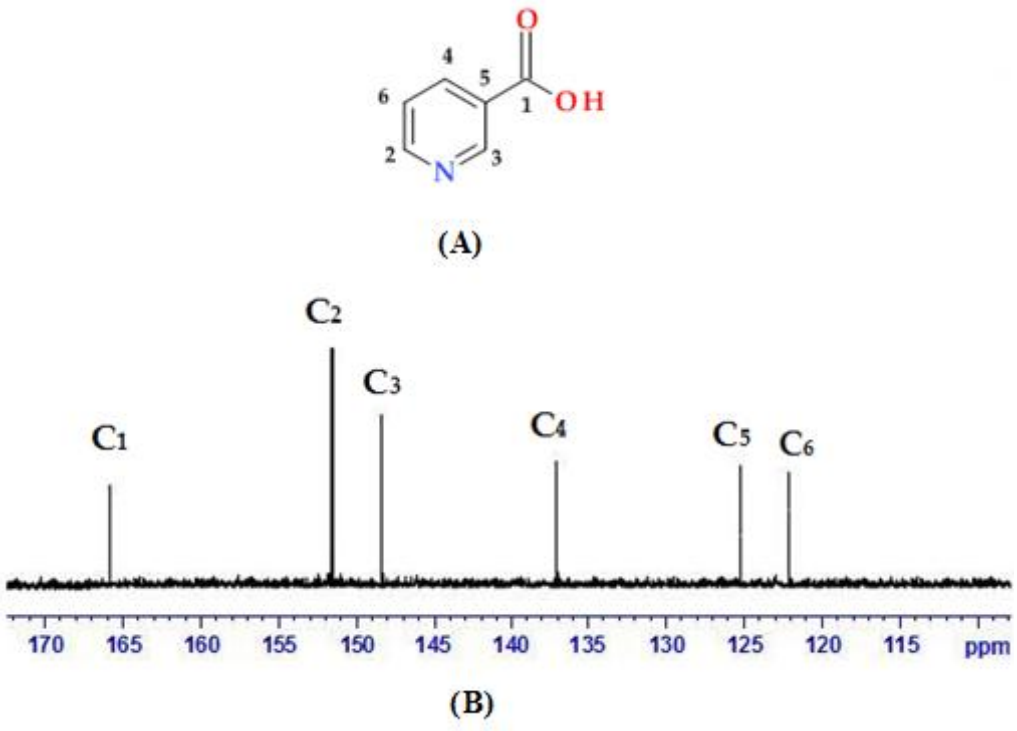

Figure B7: (A) Molecular structure of nicotinic acid with labels indicating the enhanced ^{13}C sites in the hyperpolarized spectrum; (B) Single-scan ^{13}C NMR spectrum of SABRE-hyperpolarized nicotinic acid after polarization transfer at 65 G with 1 in methanol-d_4 acquired using a 90° excitation pulse

Table B8: ***^{13}C NMR data and signal enhancement levels achieved for nicotinic acid relative to a non-hyperpolarized sample.***

Carbon / label	*δ / ppm*	*Signal enhancement / fold*
C_1	166.10	5.1
C_2	152.32	102.8
C_3	149.97	55.2
C_4	137.76	25.1
C_5	126.01	20.4
C_6	123.61	18.4

Table B9: ***^{1}H and ^{13}C NMR data for the hyperpolarized sites in isonicotinic acid.***

^{1}H NMR				*^{13}C NMR*	
Proton	*δ_H / ppm*	*J / Hz*	*Integral*	*Carbon*	*δ_C / ppm*
H_1	8.72	'd' 2.73	2.00	C_1	166.07
H_2	7.93	'd' 2.73	2.04	C_2	149.58
-	-	-	-	C_3	138.10
-	-	-	-	C_4	121.56

Table B10: ***Enhancement and polarization levels observed as a function of shake time in a magnetic field of 65 G for isonicotinic acid at 320 K.***

Shake time / s	*Signal enhancement / fold at 65 G*			
	H_1	*Pol* (H_1)	H_2	*Pol* (H_2)
20	-83.0	-0.268	76.9	0.248
40	-98.4	-0.317	81.5	0.263
60	-208.9	-0.673	155.9	0.503
80	-284.0	-0.915	228.5	0.737
100	-327.2	-1.055	196.0	0.632
120	-343.2	-1.106	229.6	0.740

Table B11: ***Enhancement and polarization levels observed as a function of substrate concentration in a magnetic field of 65 G for isonicotinic acid at 315 K.***

Conc. / mmol	*Signal enhancement / fold at 65 G*			
	H_1	*Pol* (H_1)	H_2	*Pol* (H_2)
0.0008	-24.4	-0.079	46.9	0.151
0.004	-117.5	-0.379	95.8	0.309
0.008	-263.8	-0.850	182.2	0.587
0.02	-275.4	-0.888	173.4	0.559
0.04	-289.6	-0.933	193.4	0.624
0.07	-313.0	-1.009	213.7	0.689
0.09	-304.3	-0.981	190.2	0.613

Table B12: Enhancement and polarization levels observed as a function of temperature at 65 G for isonicotinic acid.

Temp / K	*Signal enhancement / fold at 65 G*			
	H_1	*Pol* (H_1)	H_2	*Pol* (H_2)
305	-98.5	-0.318	85.6	0.276
310	-267.8	-0.863	237.2	0.765
315	-309.0	-0.996	298.7	0.963
320	-396.2	-1.277	334.8	1.079
325	-422.6	-1.362	391.8	1.263

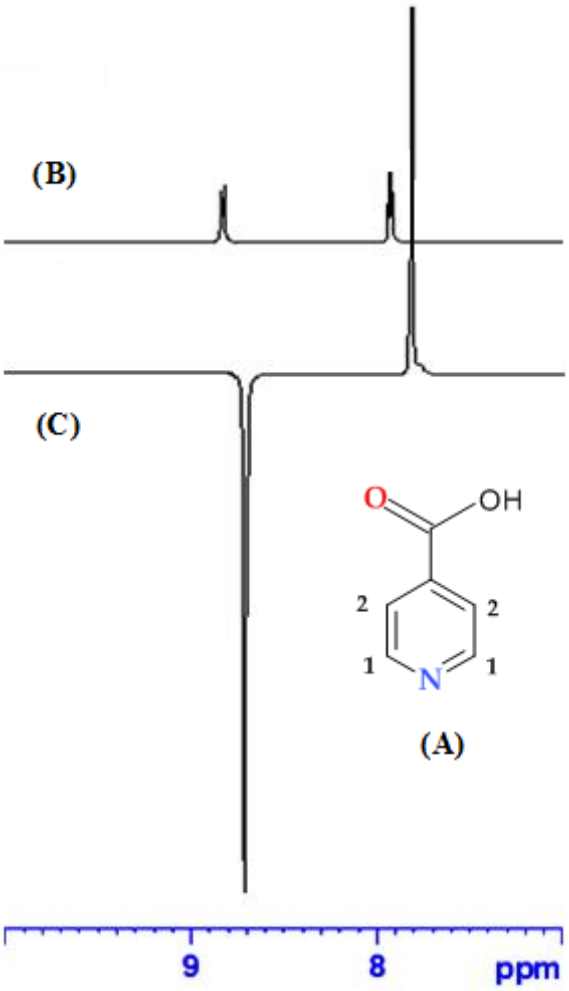

Figure B13: *(A) Molecular structure of isonicotinic acid with labels indicating the enhanced ^{1}H sites in the hyperpolarized spectrum; ^{1}H NMR spectra showing: (B) Single-scan thermally polarized trace of isonicotinic acid; (C) corresponding SABRE-hyperpolarized trace in methanol-d_4 achieved with the catalyst 1 in a 65 G polarization transfer field.*

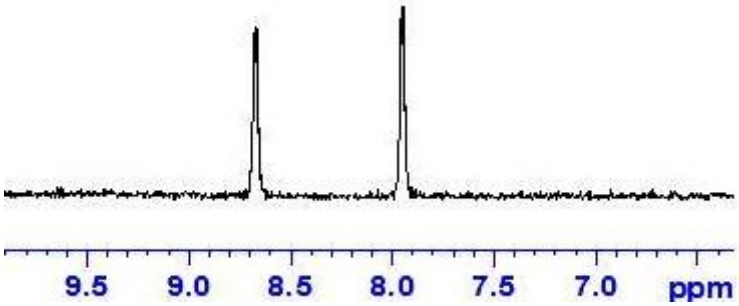

Figure B14: Depicts the dq-OPSY spectrum demonstrating the p-H_2 transfer to all sites within the isonicotinic acid using SABRE.

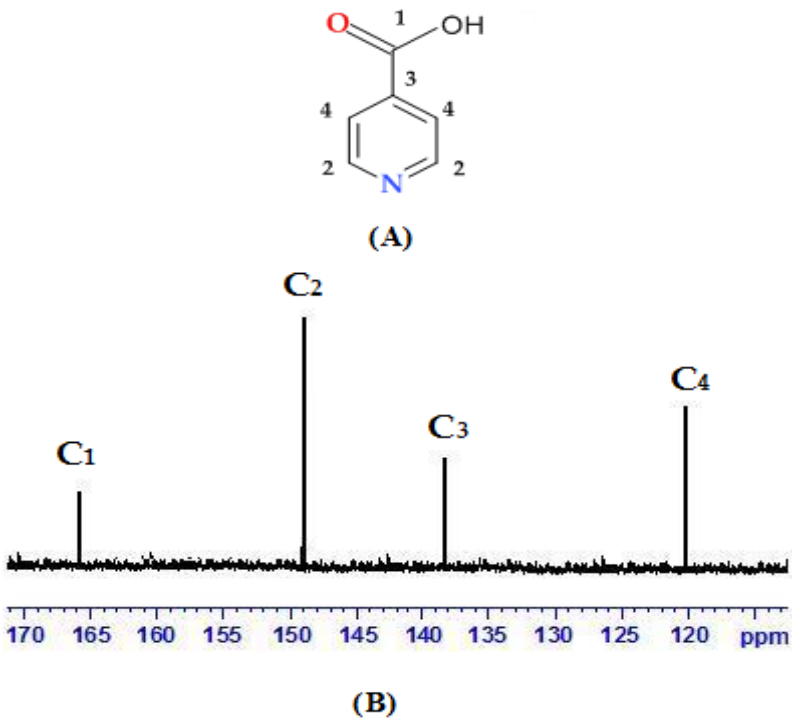

Figure B15: (A) Molecular structure of isonicotinic acid with labels indicating the enhanced ^{13}C sites in the hyperpolarized spectrum; (B) Single-scan ^{13}C NMR spectrum of SABRE-hyperpolarized isonicotinic acid after polarization transfer at 65 G with 1 in methanol-d_4 acquired using a 90° excitation pulse.

Table B16: ***^{13}C NMR data and enhancement levels obtained for isonicotinic acid.***

Carbon / label	*δ / ppm*	*Signal enhancement / fold*
C_1	166.07	10.4
C_2	149.58	94.7
C_3	138.10	15.4
C_4	121.56	79.1

Table B17: ***^{1}H and ^{13}C NMR data for the hyperpolarized sites in methyl nicotinate.***

^{1}H NMR				*^{13}C NMR*	
Proton	*δ_H / ppm*	*J / Hz*	*Integral*	*Carbon*	*δ_C / ppm*
H_1	8.89	'd' 1.41	1.00	C_1	165.03
H_2	8.53	'd' 3.15	1.01	C_2	153.58
H_3	8.17	'd' 1.80	1.03	C_3	148.08
H_4	7.34	'dd' 4.93	1.04	C_4	137.14
-	-	-	-	C_5	126.01
-	-	-	-	C_6	123.54
-	-	-	-	C_7	55.2

Table B18: ***Enhancement and polarization levels observed as a function of shake time in a magnetic field of 65 G for methyl nicotinate at 310 K.***

Shake time / s	*Signal enhancement / fold at 65 G*							
	H_1	*Pol* (H_1)	H_2	*Pol* (H_2)	H_3	*Pol* (H_3)	H_4	*Pol* (H_4)
20	-42.3	-0.136	-29.4	-0.095	-25.8	-0.08	31.1	0.100
40	-54.5	-0.176	-34.3	-0.111	-40.3	-0.13	26.2	0.084
60	-71.3	-0.230	-56.8	-0.183	-51.2	-0.16	32.4	0.104
80	-74.3	-0.239	-52.5	-0.169	-49.2	-0.15	36.7	0.118
100	-83.4	-0.269	-53.8	-0.173	-41.9	-0.13	41.8	0.135

Table B19: ***Enhancement and polarization levels observed as a function of substrate concentration in a magnetic field of 65 G for methyl nicotinate at 320 K.***

Conc. / mmol	*Signal enhancement / fold at 65 G*							
	H_1	*Pol* (H_1)	H_2	*Pol* (H_2)	H_3	*Pol* (H_3)	H_4	*Pol* (H_4)
0.007	-52.5	-0.169	-36.5	-0.11	-31.9	-0.10	42.7	0.138
0.003	-68.9	-0.222	-54.9	-0.17	-50.1	-0.16	65.2	0.210
0.07	-88.6	-0.286	-74.6	-0.24	-63.5	-0.20	80.7	0.260
0.02	-92.3	-0.297	-85.7	-0.27	-61.1	-0.19	89.4	0.288
0.04	-104.6	-0.337	-91.5	-0.29	-52.1	-0.16	112.8	0.364

Table B20: ***Enhancement and polarization levels observed as a function of temperature at 65 G for methyl nicotinate.***

Temp / K	*Signal enhancement / fold at 65 G*							
	H_1	*Pol* (H_1)	H_2	*Pol* (H_2)	H_3	*Pol* (H_3)	H_4	*Pol* (H_4)
310	-65.3	-0.21	-45.4	-0.14	-49.9	-0.16	53.1	0.171
315	-85.7	-0.27	-68.4	-0.22	-72.5	-0.23	81.2	0.262
320	-110	-0.35	-92.9	-0.29	-87.8	-0.28	100.5	0.323
325	-114	-0.37	-106.5	-0.34	-84.2	-0.27	111.2	0.358
330	-130	-0.41	-113.8	-0.36	-105.6	-0.34	140.3	0.452

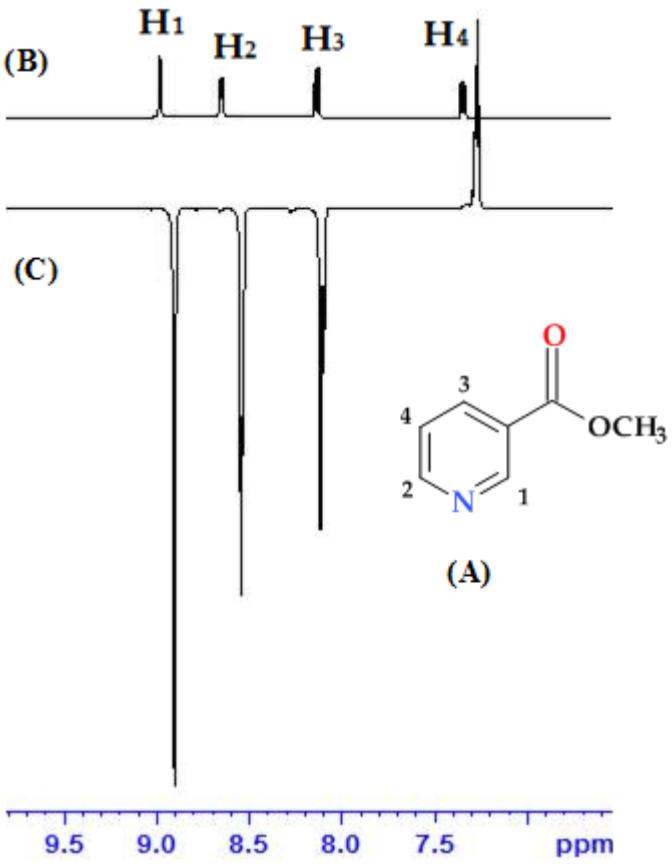

Figure B21: *(A) Molecular structure of methyl nicotinate with labels indicating the enhanced ^{1}H sites in the hyperpolarized spectrum; (B) Single-scan ^{1}H NMR spectrum showing resonances for free methyl nicotinate that were obtained prior to polarization; (C) corresponding hyperpolarized ^{1}H NMR spectrum acquired immediately after polarization in a magnetic field of 65 G exhibiting the newly enhanced proton signals for free methyl nicotinate*

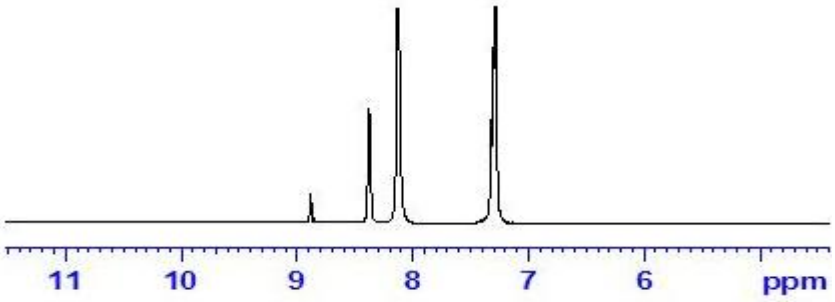

Figure B22: Depicts the dq-OPSY spectrum demonstrating the p-H_2 transfer to methyl nicotinate using SABRE.

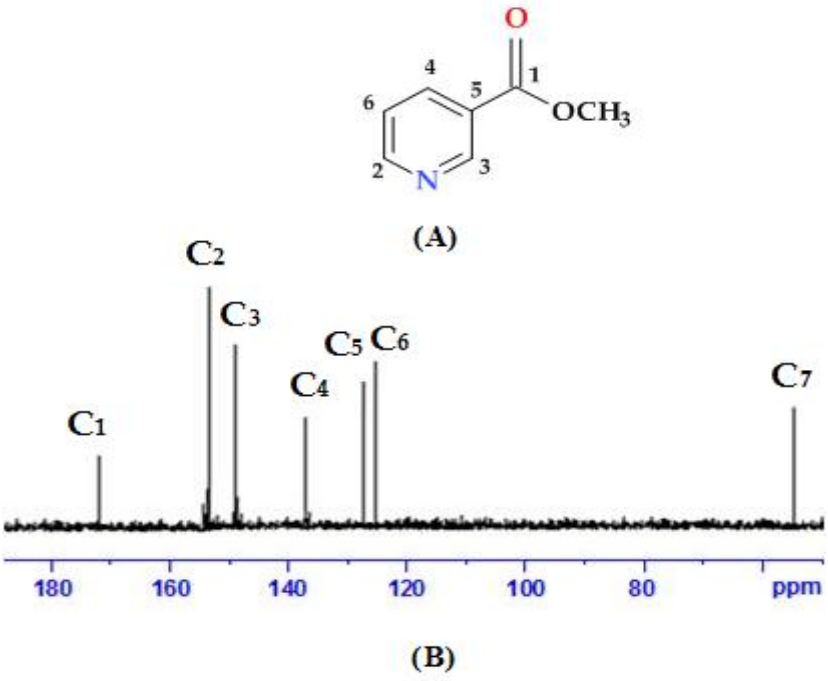

Figure B23: (A) Molecular structure of methyl nicotinate with labels indicating the enhanced ^{13}C sites in the hyperpolarized spectrum; (B) Single-scan ^{13}C NMR spectrum of SABRE-hyperpolarized methyl nicotinate after polarization transfer at 65 G with 1 in methanol-d_4 acquired using a 90° excitation pulse.

Table B24: ***^{13}C NMR data and enhancement levels observed for methyl nicotinate.***

Carbon / label	*δ / ppm*	*Signal enhancement / fold*
C_1	165.03	4.2
C_2	153.58	40.7
C_3	148.08	32.5
C_4	137.14	15.1
C_5	126.01	20.4
C_6	123.54	22.8
C_7	55.2	12.6

Table B25: ***^{1}H and ^{13}C NMR data for the hyperpolarized sites in isonicotinamide.***

	^{1}H NMR			*^{13}C NMR*	
Proton	*δ_H / ppm*	*J / Hz*	*Integral*	*Carbon*	*δ_C / ppm*
H_1	8.69	'd' 2.56	2.00	C_1	165.02
H_2	7.81	'd' 2.56	2.02	C_2	150.58
-	-	-	-	C_3	137.06
-	-	-	-	C_4	122.01

Table B26: ***Enhancement and polarization levels observed as a function of shake time in a magnetic field of 65 G for isonicotinamide at 320 K.***

Shake time / s	*Signal enhancement / fold at 65 G*			
	H_1	*Pol* (H_1)	H_2	*Pol* (H_2)
20	-127.6	-0.411	96.5	0.311
40	-198.4	-0.639	117.8	0.380
60	-211.3	-0.681	165.5	0.533
80	-264.5	-0.852	186.4	0.601
100	-306.9	-0.989	230.1	0.742
120	-320.7	-1.034	282.5	0.910

Table B27: ***Enhancement and polarization levels observed as a function of substrate concentration in a magnetic field of 65 G for isonicotinamide at 325 K.***

Conc. / mmol	*Signal enhancement / fold at 65 G*			
	H_1	*Pol* (H_1)	H_2	*Pol* (H_2)
0.0008	-204.6	-0.659	177.7	0.573
0.004	-258.2	-0.832	214.3	0.691
0.008	-330.1	-1.064	244.2	0.787
0.03	-395.1	-1.273	272.1	0.877
0.05	-416.3	-1.342	315.8	1.018
0.08	-449.8	-1.450	354.1	1.141

Table B28: Enhancement and polarization levels observed as a function of temperature at 65 G for isonicotinamide.

Temperature / K	*Signal enhancement / fold at 65 G*			
	H_1	*Pol (H_1)*	*H_2*	*Pol (H_2)*
305	-135.4	-0.436	165.5	0.533
310	-165.2	-0.532	261.2	0.842
315	-232.5	-0.749	278.3	0.897
320	-322.6	-1.040	404.9	1.305
325	-370.7	-1.195	246.1	0.793
330	-453.4	-1.461	372.4	1.200

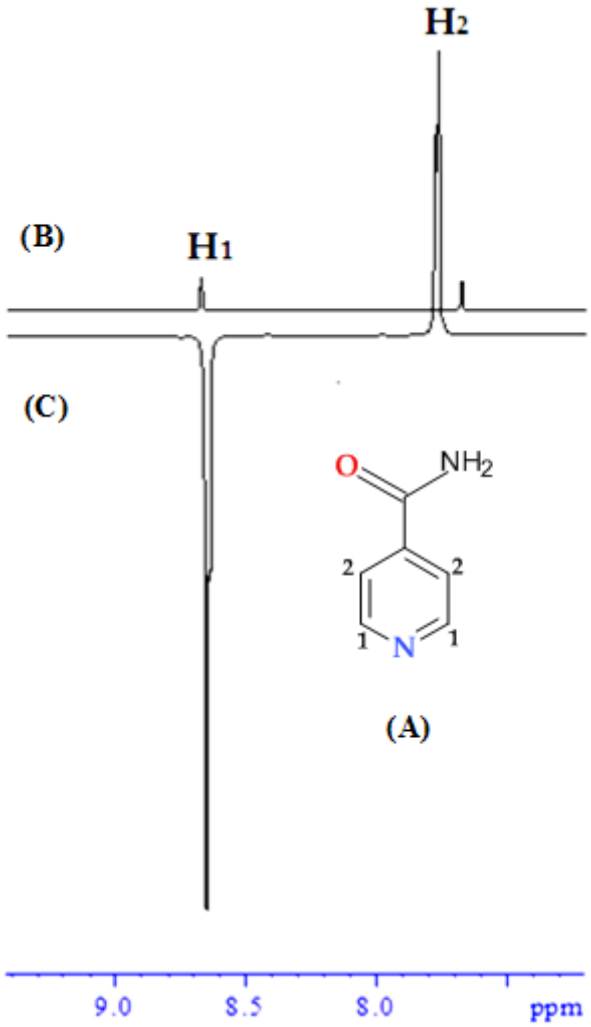

Figure B29: *(A) Molecular structure of isonicotinamide with labels indicating the enhanced ^{1}H sites in the hyperpolarized spectrum; (B) Single-scan ^{1}H NMR spectrum acquired under Boltzmann conditions presenting resonances for isonicotinamide that were obtained prior to hyperpolarization; (C) corresponding hyperpolarized ^{1}H NMR spectrum obtained immediately after polarization transfer in a magnetic field of 65G exhibiting the newly enhanced proton free signals for isonicotinamide.*

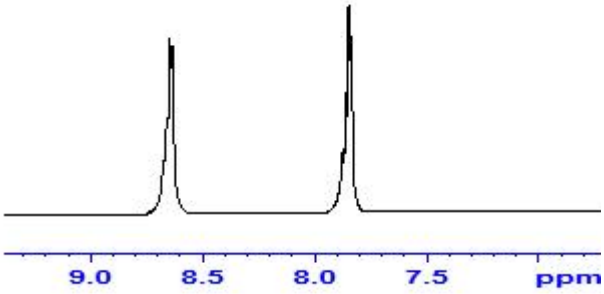

Figure B30: Depicts the dq-OPSY spectrum demonstrating the p-H_2 transfer to the proton sites in isonicotinamide using SABRE.

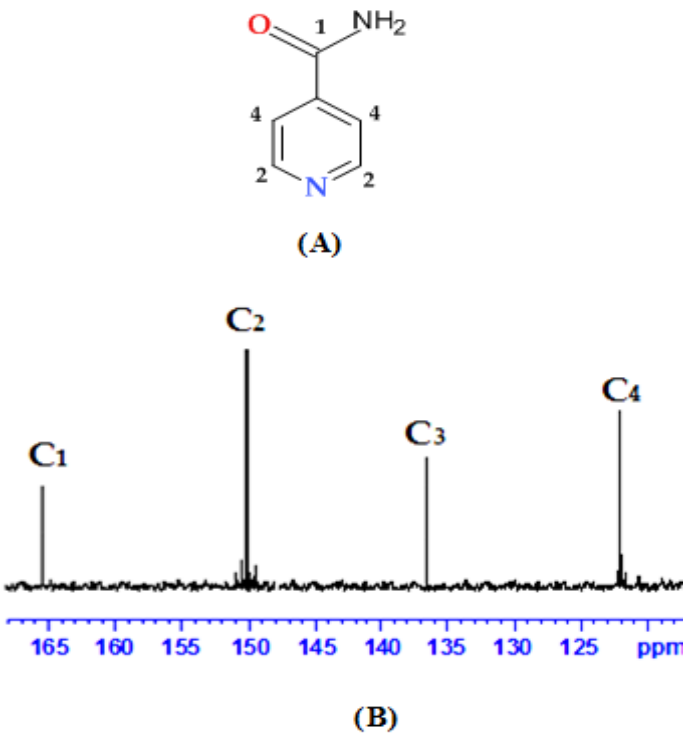

Figure B31: (A) Molecular structure of isonicotinamide with labels indicating the enhanced ^{13}C sites in the hyperpolarized spectrum; (B) Single-scan ^{13}C NMR spectrum of SABRE-hyperpolarized isonicotinamide after polarization transfer at 65 G with, 1, in methanol-d_4 acquired using a 90° excitation pulse.

Table B32: ***^{13}C NMR data and signal enhancement levels achieved in case of isonicotinamide.***

Carbon / label	*δ / ppm*	*Signal enhancement / fold*
C_1	165.02	5.8
C_2	150.58	59.4
C_3	137.06	12.8
C_4	122.01	41.5

Table B33: ***^{1}H and ^{13}C NMR data for the hyperpolarized sites in pyrazine.***

	^{1}H NMR			*^{13}C NMR*	
Group	*δ_H / ppm*	*J / Hz*	*Integral*	*Group*	*δ_C / ppm*
H_1	8.87	'd' 2.92	4.00	C_1	144.95

Table B34: ***Enhancement and polarization levels observed as a function of shake time in a magnetic field of 65 G for pyrazine at 310 K.***

Shake time / s	*Signal enhancement / fold at 65 G*	
	H_1	*Pol* (H_1)
20	-70.6	-0.228
40	-90.2	-0.291
60	-182.1	-0.587
80	-218.0	-0.703
100	-225.2	-0.726
120	-263.3	-0.849

Table B35: ***Enhancement and polarization levels observed as a function of substrate concentration in a magnetic field of 65 G for pyrazine at 320 K.***

Conc. / mmol	*Signal enhancement / fold at 65 G*	
	H_1	*Pol* (H_1)
0.003	-96.9	-0.312
0.007	-179.4	-0.578
0.02	-299.7	-0.803
0.04	-360.5	-0.966
0.08	-353.8	-1.141
0.12	-427.2	-1.377
0.15	-447.5	-1.442

Table B36: ***Enhancement and polarization levels observed as a function of temperature at 65 G for pyrazine.***

Temperature / K	*Signal enhancement / fold at 65 G*	
	H_1	*Pol* (H_1)
310	-46.9	-0.150
315	-178.8	-0.576
320	-285.5	-0.920
325	-375.2	-1.209
330	-469.3	-1.512

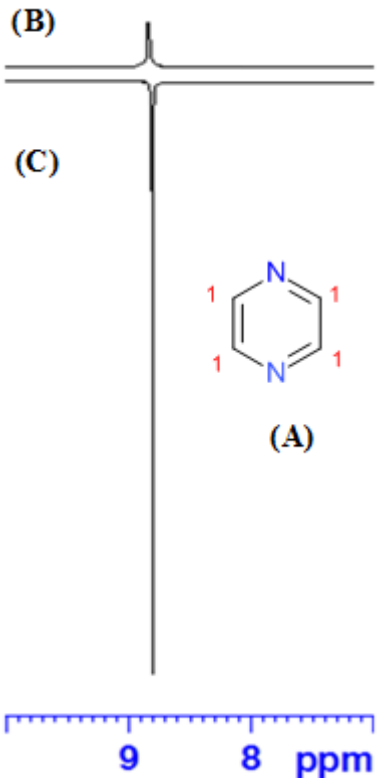

Figure B37: *(A) Molecular structure of pyrazine with labels indicating the enhanced ^{1}H sites in the hyperpolarized spectrum; Single-scan ^{1}H NMR spectrum of the aromatic region showing resonances for free pyrazine that were obtained prior to polarization; (B) corresponding hyperpolarized ^{1}H NMR spectrum acquired immediately after polarization in a magnetic field of 65 G exhibiting the newly enhanced proton signals for free pyrazine.*

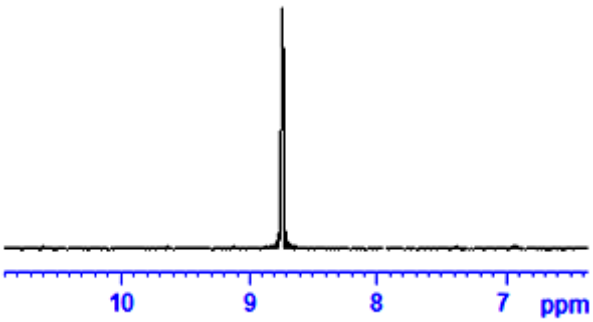

Figure B38: Depicts the dq-OPSY spectrum demonstrating the p-H_2 transfer to all sites within the pyrazine using SABRE.

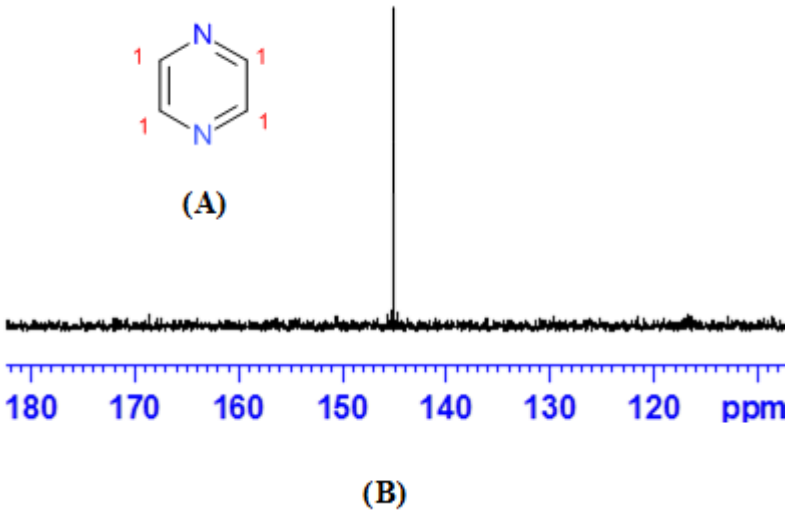

Figure B39: (A) Molecular structure of pyrazine with labels indicating the enhanced ^{13}C sites in the hyperpolarized spectrum; (B) Single-scan ^{13}C NMR spectrum of SABR-hyperpolarized pyrazine acid after polarization transfer at 65 G with 1 in methanol-d_4 acquired using a 90° excitation pulse.

Table B40: ***^{13}C NMR data and enhancement levels obtained for pyrazine relative to a non-hyperpolarized sample.***

Carbon / label	*δ / ppm*	*Signal enhancement / fold*
C_1	144.95	135.8

Table B41: ***^{1}H and ^{13}C NMR data for the hyperpolarized sites in isoniazid.***

^{1}H NMR				*^{13}C NMR*	
Proton	*δ_H / ppm*	*J / Hz*	*Integral*	*Carbon*	*δ_C / ppm*
H_1	8.47	'd' 3.18	2.00	C_1	162.91
H_2	7.54	'd' 3.18	1.98	C_2	150.21
-	-	-	-	C_3	139.80
-	-	-	-	C_4	121.14

Table B42: Enhancement and polarization levels observed as a function of shake time in a magnetic field of 65 G for isoniazid at 323 K.

Shake time / s	*Signal enhancement / fold at 65 G*			
	H_1	*Pol (H_1)*	*H_2*	*Pol (H_2)*
20	- 19.2	- 0.062	65.9	0.212
40	- 83.2	- 0.268	96.2	0.310
60	- 111.4	- 0.359	102.4	0.330
80	- 186.6	- 0.601	118.6	0.382
100	- 239.4	- 0.772	156.2	0.503
120	- 308.3	- 0.994	268.6	0.866

Table B43: Enhancement and polarization levels observed as a function of substrate concentration in a magnetic field of 65 G for isoniazid at 318 K.

Conc. / mmol	*Signal enhancement / fold at 65 G*			
	H_1	*Pol (H_1)*	*H_2*	*Pol (H_2)*
0.0008	- 22.1	- 0.071	59.4	0.091
0.004	- 69.2	- 0.223	72.8	0.235
0.007	- 38.8	- 0.125	87.8	0.283
0.03	- 312.2	- 1.006	191.9	0.618
0.05	- 286.5	- 0.923	226.3	0.729
0.07	- 273.1	- 0.880	217.4	0.701
0.09	- 290.7	- 0.937	209.9	0.676

Table B44: ***Enhancement and polarization levels observed as a function of temperature at 65 G for isoniazid.***

Temperature / K	***Signal enhancement / fold at 65 G***			
	H_1	***Pol (H_1)***	***H_2***	***Pol (H_2)***
310	- 39.6	- 0.128	83.2	0.268
315	- 146.2	- 0.471	105.7	0.341
320	- 238.5	- 0.769	165.2	0.532
325	- 298.9	- 0.963	193.4	0.623
330	- 346.3	- 1.116	205.7	0.663

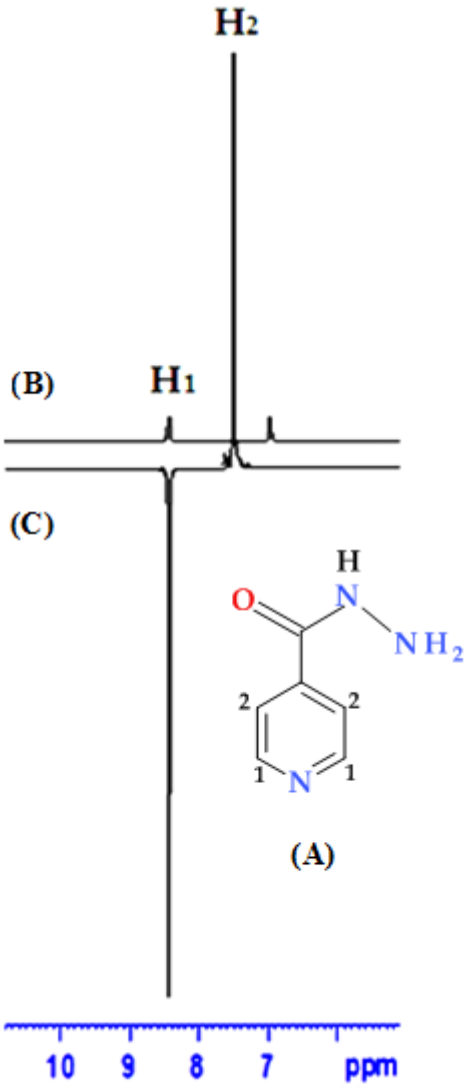

Figure B45: (A) Molecular structure of isoniazid with labels indicating the enhanced ^{1}H sites in the hyperpolarized spectrum; ^{1}H NMR spectra depicting: (B) Single-scan ^{1}H NMR spectrum of the aromatic region of a sample of 1 showing resonances for free isoniazid that were obtained prior to polarization; (C) corresponding ^{1}H NMR spectrum acquired immediately after polarization at 65 G magnetic field exhibiting the newly enhanced proton signals for free isoniazid.

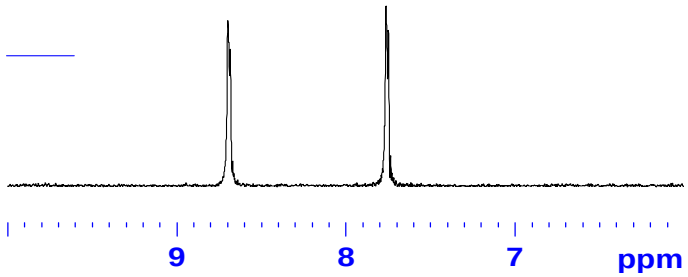

Figure B46: Depicts the dq-OPSY spectrum demonstrating the p-H_2 transfer to all sites within the isoniazid molecule using SABRE.

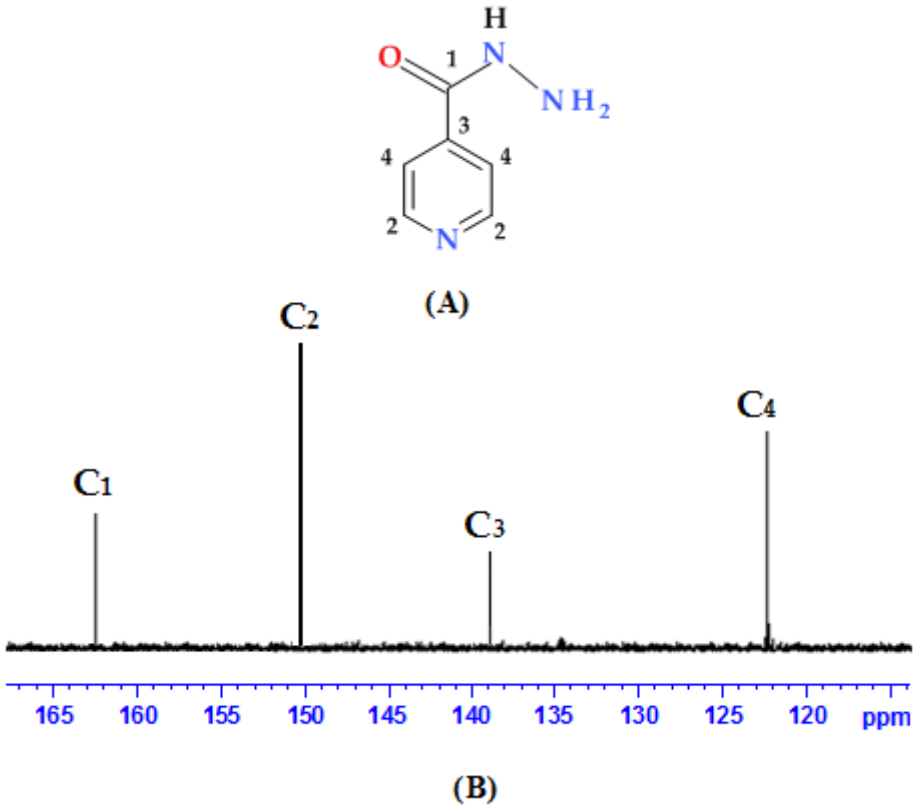

Figure B47: (A) Molecular structure of isoniazid with labels indicating the enhanced ^{13}C sites in the hyperpolarized spectrum; (B) Single-scan ^{13}C NMR spectrum of SABRE-hyperpolarized isoniazid after polarization transfer at 65 G with 1 in methanol-d_4 acquired using a 90° excitation pulse.

Table B48: ***^{13}C NMR data and enhancement levels obtained for isoniazid relative to a non-hyperpolarized sample.***

Carbon / label	*δ / ppm*	*Signal enhancement / fold*
C_1	162.91	14.9
C_2	150.21	85.4
C_3	139.80	21.4
C_4	121.14	65.1

Table B49: ***^{1}H and ^{13}C NMR data for purine.***

^{1}H NMR				*^{13}C NMR*	
proton	*δ_H / ppm*	*J / Hz*	*Integral*	*Carbon*	*δ_C / ppm*
H_1	9.12	's'	2.00	C_1	155.60
H_2	8.96	's'	1.09	C_2	152.45
H_3	8.58	's'	2.02	C_3	148.10
-	-	-	-	C_4	144.90
-	-	-	-	C_5	130.05

Table B50: ***Enhancement and polarization levels observed as a function of shake time at 65 G for purine at 323 K.***

Shake time / s	*Signal enhancement / fold at 65 G*					
	H_1	*Pol* (H_1)	H_2	*Pol* (H_2)	H_3	*Pol* (H_3)
20	-73.8	-0.238	-70.9	-0.228	-39.6	-0.128
40	-147.4	-0.475	-128.8	-0.415	-93.1	-0.300
60	-152.1	-0.490	-141.1	-0.455	-92.1	-0.297
80	-158.9	-0.512	-134.9	-0.435	-97.8	-0.315
100	-164.7	-0.531	-149.3	-0.481	-107.4	-0.346
120	-236.4	-0.762	-188.5	-0.607	-143.9	-0.464

Table B51: ***Enhancement and polarization levels observed as a function of substrate concentration in a magnetic field of 65 G for purine at 320 K.***

Conc. / mmol	*Signal enhancement / fold at 65 G*					
	H_1	*Pol* (H_1)	H_2	*Pol* (H_2)	H_3	*Pol* (H_3)
0.002	-63.2	-0.204	-45.8	-0.148	-61.8	-0.199
0.006	-124.9	-0.403	-129	-0.418	-72.9	-0.235
0.01	-181.5	-0.585	-131	-0.423	-159.2	-0.513
0.03	-287.2	-0.926	-139	-0.450	-177.4	-0.572
0.07	-298.5	-0.962	-171	-0.553	-215.7	-0.695

Table B52: Enhancement and polarization levels observed as a function of temperature at 65 G for purine.

Temp / K	*Signal enhancement / fold at 65 G*					
	H_1	*Pol (H_1)*	*H_2*	*Pol (H_2)*	*H_3*	*Pol (H_3)*
305	-38.7	-0.125	-24.3	-0.078	-12.6	-0.041
310	-58.1	-0.187	-48.3	-0.156	-31.1	-0.100
315	-62.3	-0.201	-54.5	-0.176	-39.7	-0.128
320	-159.8	-0.515	-144.5	-0.466	-120.1	-0.387
325	-225.9	-0.728	-193.2	-0.623	-156.7	-0.505
330	-247.6	-0.798	-191.2	-0.616	-145.8	-0.470

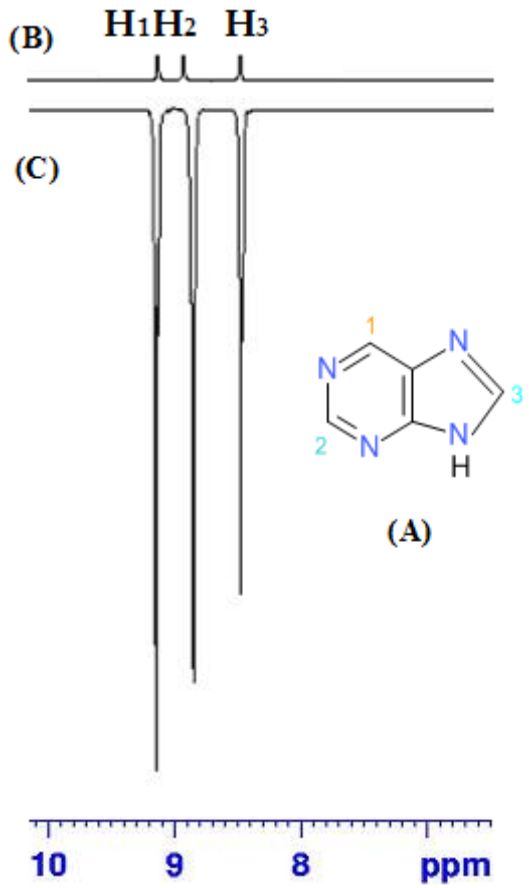

Figure B53: *(A) Molecular structure of isoniazid with labels indicating the enhanced ^{13}C sites in the hyperpolarized spectrum; (B) Single-scan ^{1}H NMR spectrum of the aromatic region illustrating the resonances for free purine that were obtained prior to polarization; (C) corresponding hyperpolarized ^{1}H NMR spectrum acquired immediately after exposure to p-H_2 in a magnetic field of 65 G exhibiting the newly enhanced proton signals for free purine.*

Table B54: ^{1}H and ^{13}C NMR data for pyrimidine

^{1}H NMR				^{13}C NMR	
Proton	***δ_H / ppm***	***J / Hz***	***Integral***	***Carbon***	***δ_C / ppm***
H_1	8.95	's'	1.00	C_1	158.12
H_2	8.59	'd' 2.38	1.05	C_2	155.58
H_3	7.31	't' 1.44, 5.8	1.02	C_3	122.96

Table B55: Enhancement and polarization levels observed as a function of shake time in a magnetic field of 65 G for pyrimidine at 320 K.

Shake time	***Signal enhancement / fold at 65 G***					
/ s	***H_1***	***Pol (H_1)***	***H_2***	***Pol (H_2)***	***H_3***	***Pol (H_3)***
20	55.9	-0.083	-37.	-0.366	-101	-0.856
40	-75.3	-0.243	-37.9	-0.122	-205.5	-0.327
60	-160.5	-0.517	-91.4	-0.295	-265.5	-0.853
80	-218.6	-0.705	-105.4	-0.340	-305.4	-0.662
100	-294.5	-0.949	-144.9	-0.467	-394.8	-1.272
120	-345.5	-1.113	-157.3	-0.507	-417.5	-1.346

Table B56: Enhancement and polarization levels observed as a function of substrate concentration in a magnetic field of 65 G for pyrimidine at 315 K.

Conc. / mmol	*Signal enhancement / fold at 65 G*					
	H_1	*Pol (H_1)*	*H_2*	*Pol (H_2)*	*H_3*	*Pol (H_3)*
0.002	-30.9	-0.100	-19.5	-0.063	-10.4	-0.034
0.06	-46.5	-0.150	-38.2	-0.123	-24.9	-0.080
0.01	-49.9	-0.161	-43.9	-0.141	-31.8	-0.120
0.03	-127.9	-0.412	-115	-0.373	-96.1	-0.310
0.07	-180.8	-0.583	-154	-0.498	-120	-0.389
0.11	-197.7	-0.637	-161	-0.520	-123	-0.399

Table B57: Enhancement and polarization levels observed as a function of temperature at 65 G for pyrimidine.

Temp / K	*Signal enhancement / fold at 65 G*					
	H_1	*Pol (H_1)*	*H_2*	*Pol (H_2)*	*H_3*	*Pol (H_3)*
310	-54.7	-0.015	-42.2	-0.007	- 63.8	-0.009
315	-156	-0.503	-162.4	-0.523	-91.1	-0.294
320	-191	-0.617	-76.5	-0.247	-198.9	-0.641
325	-359	-1.158	-159.1	-0.513	-378.5	-1.120
330	-370	-1.195	-175.5	-0.556	- 412.2	-1.328

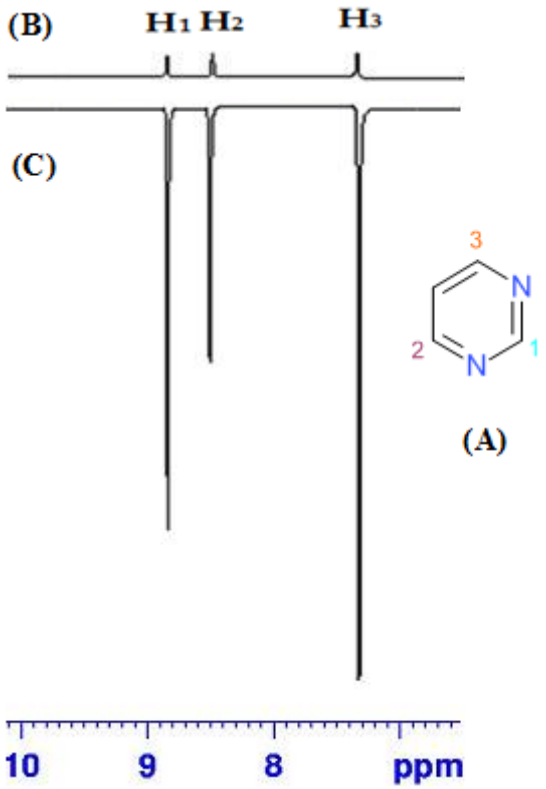

Figure B58: *^{1}H NMR spectra showing: (A) Single-scan thermally polarized ^{1}H NMR spectrum of pyrimidine; (B) corresponding hyperpolarized ^{1}H NMR spectrum acquired immediately after polarization in a magnetic field of 65 G exhibiting the newly enhanced proton signals for free pyrimidine.*

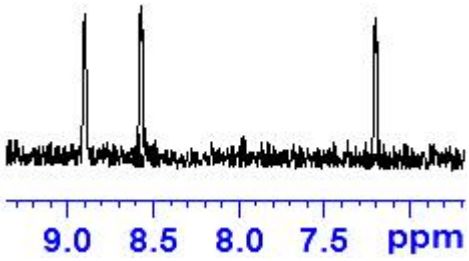

Figure B59: Depicts the dq-OPSY spectrum demonstrating the p-H_2 transfer to all sites within the pyrimidine using SABRE.

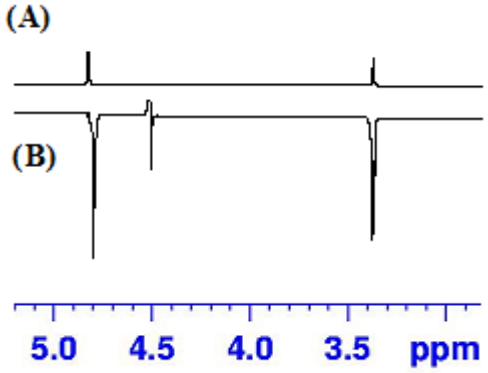

Figure B60: (A) Single-scan ^1H NMR spectrum of a sample of 1 showing hydroxyl and methyl resonances for methanol that were obtained prior to polarization; (B) ^1H NMR spectrum of SABRE-hyperpolarized hydroxyl and methyl resonances of methanol-d_4.

This Appendix presents the data (Tables and Figures) from chapter 4.

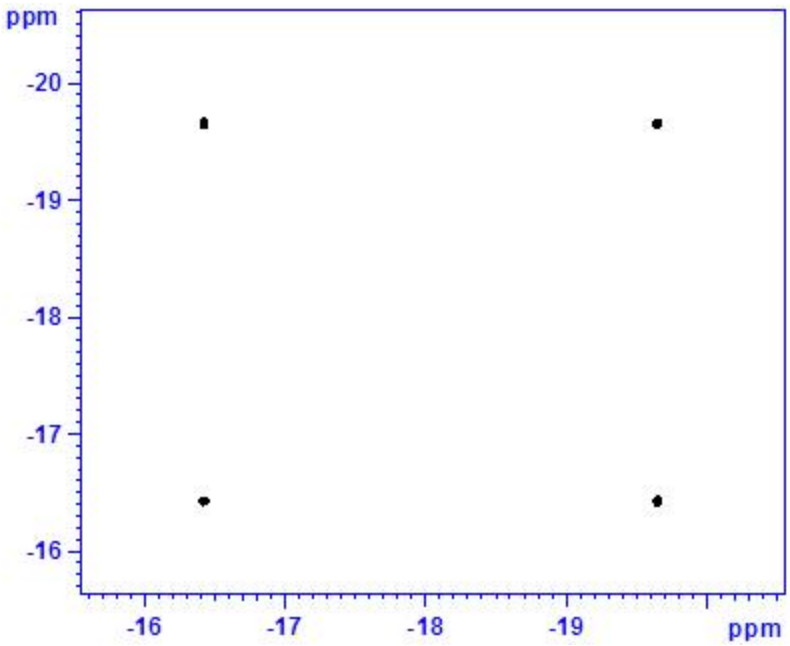

Figure C1: 2D COSY spectrum showing ^{1}H-^{1}H coupling between hydride signals resonating at δ -16.43 and δ -19.65 detected in a reaction of 4 with p-H_2 in acetone-d_6.

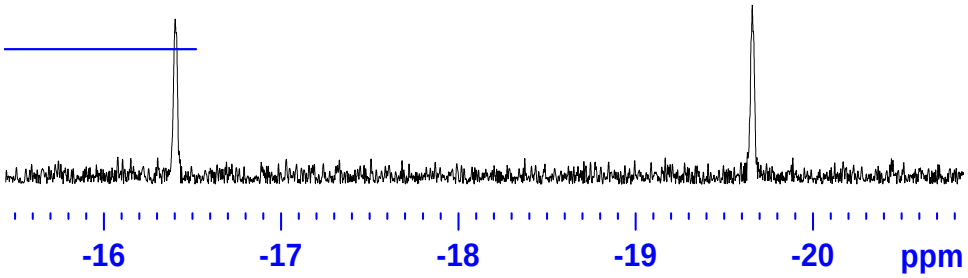

Figure C2: OPSY spectrum indicating the p-H_2 derived signals in a reaction of 4 with p-H_2 in aceton-d_6.

Table C3: Observed rate constants for hydride exchange.

Set temperature (K)	Corrected temperature / K	1/T	lnk/T	k(H) /s^{-1}
305	304.1	0.00327	-6.741	0.18
305	304.1	0.00325	-6.738	0.18
310	311.2	0.00322	-6.704	0.19
310	311.2	0.00321	-6.702	0.19
315	315.9	0.00317	-5.416	0.70
315	315.8	0.00316	-5.414	0.69
320	321.1	0.00312	-4.605	1.6
320	321.1	0.00310	-4.603	1.6
325	325.8	0.00307	-3.959	3.1
325	325.8	0.00305	-3.957	3.1

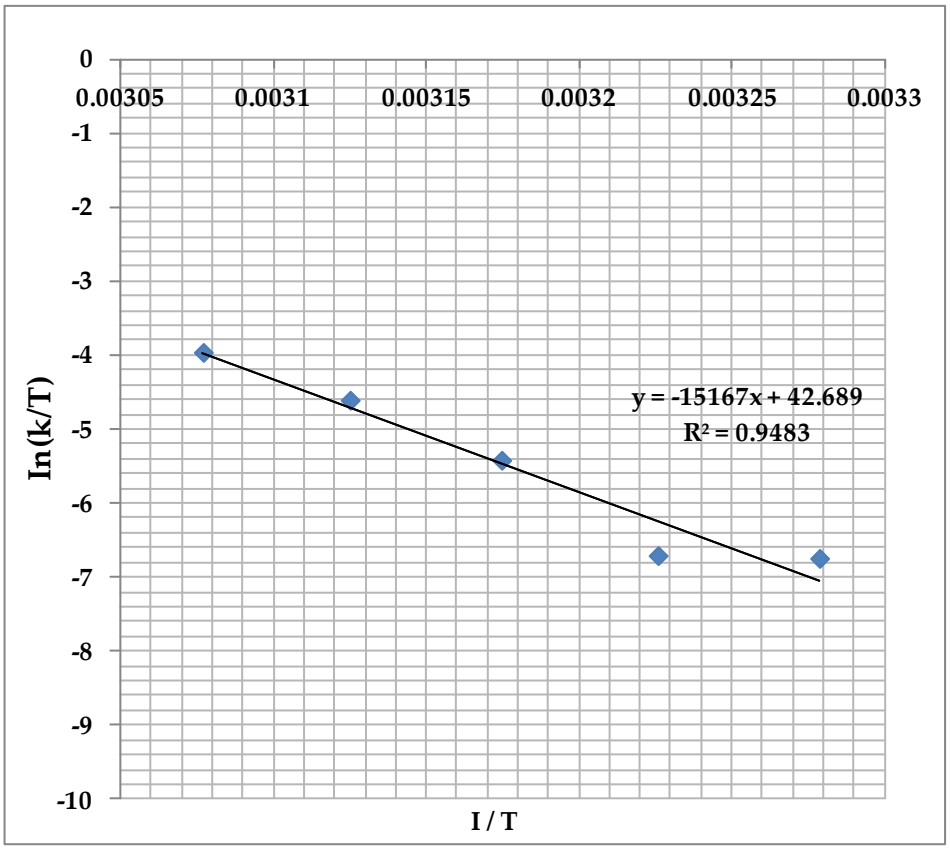

Figure C4: Eyring plots for Hydride exchange using the data shown in C3.

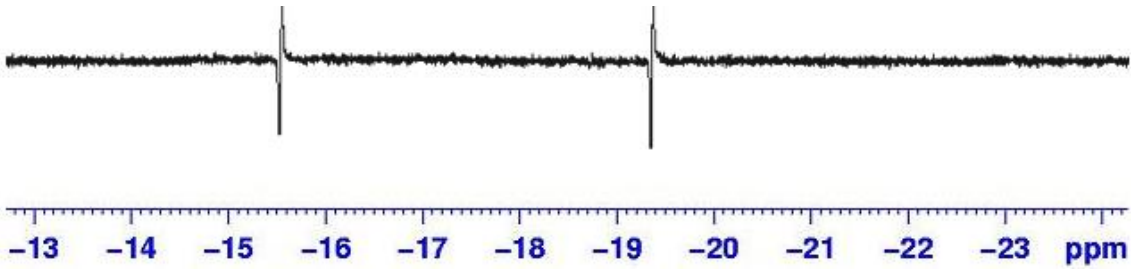

Figure C5: ^{1}H NMR spectrum showing enhanced antiphase peaks in a reaction of 4 in toluene-d$_8$.

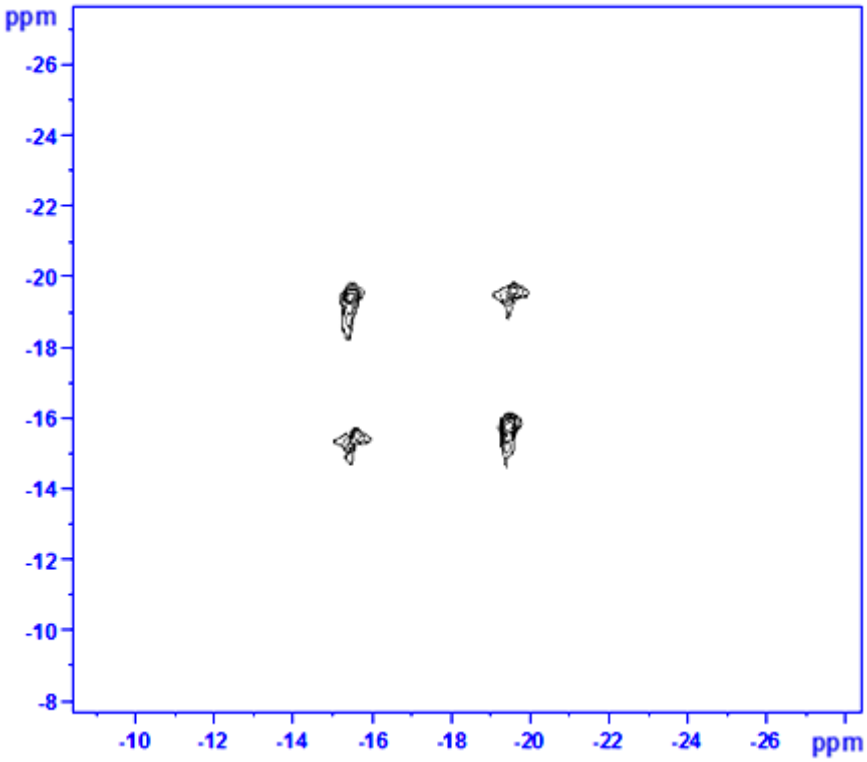

Figure C6: 2D COSY spectrum showing ^{1}H-^{1}H coupling between hydride signals resonating at δ -15.60 and δ -19.30 detected in the reaction of 4 with p-H_2 in toluene-d_8.

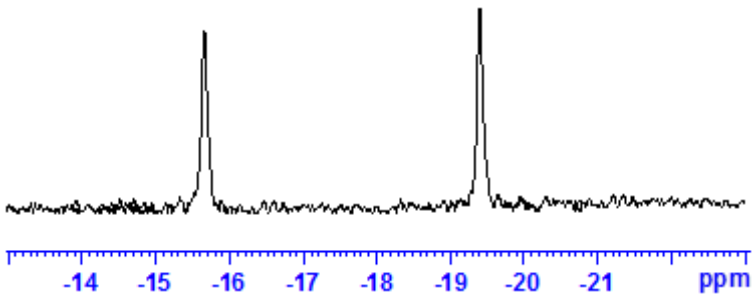

Figure C7: OPSY spectrum depicting the p-H_2 derived signals in a reaction of 4 with p-H_2 in toluene-d_8.

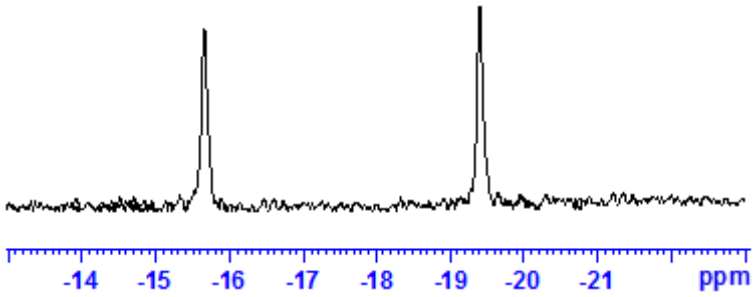

Figure C8: OPSY spectrum depicting the p-H_2 derived signals in a reaction of 4 with p-H_2 in toluene-d_8.

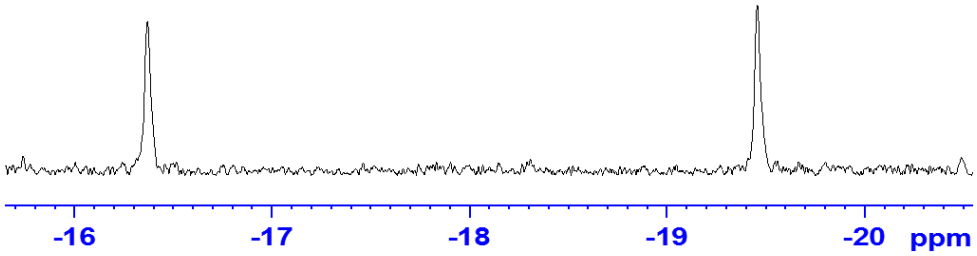

Figure C9: An OPSY spectrum showing the p-H_2 derived signals of mer isomer formed in a reaction of 4 with p-H_2 in THF-d_8.

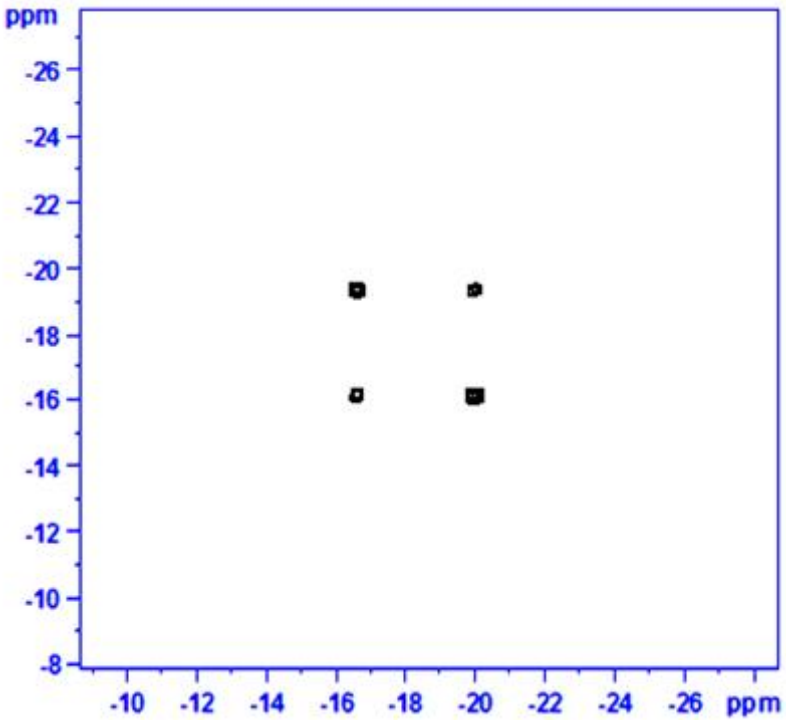

Figure C10: *^{1}H-^{1}H COSY spectrum of complex, 4b, recorded at 323 K.*

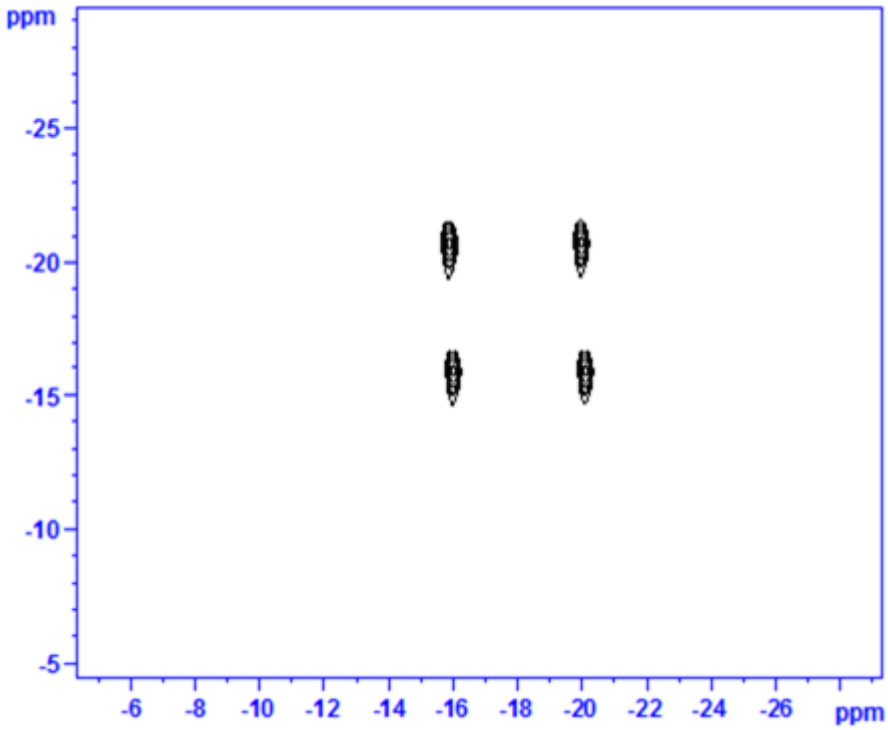

Figure C11: *^{1}H-^{1}H COSY spectrum of complex, 4b, recorded at 330 K.*

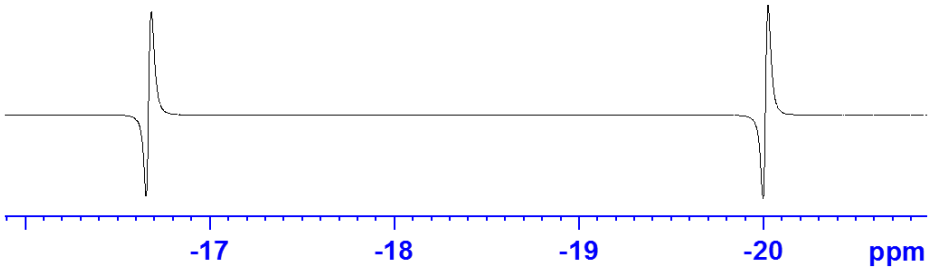

Figure C12: *^{1}H NMR spectrum showing the PHIP antiphase enhanced resonances obtained in a reaction of 4 with p-H_2 in dmso-d_6.*

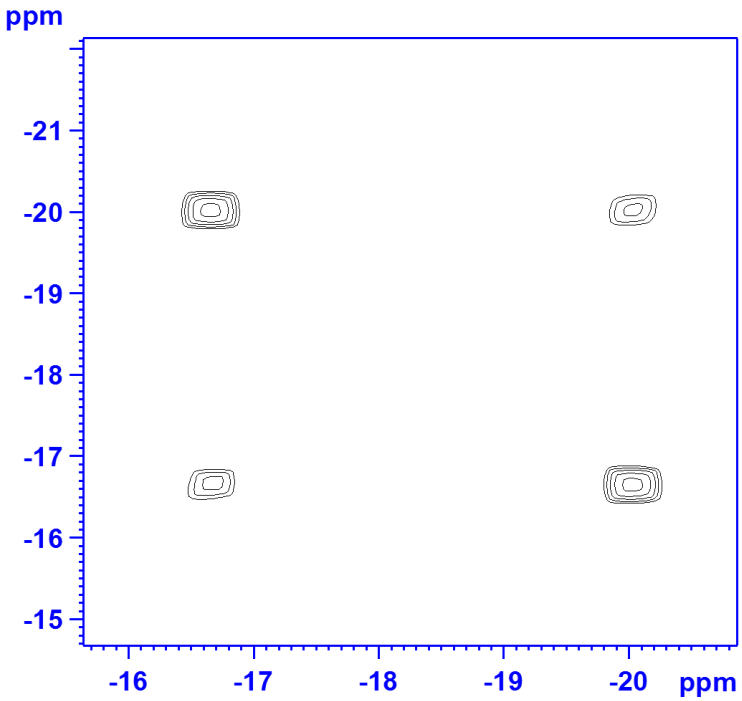

Figure C13: *2D COSY spectrum showing ^{1}H-^{1}H coupling between hydride signals resonating at δ -16.67 and δ -20.03 in a reaction of 4 with p-H_2 in dmso-d_6.*

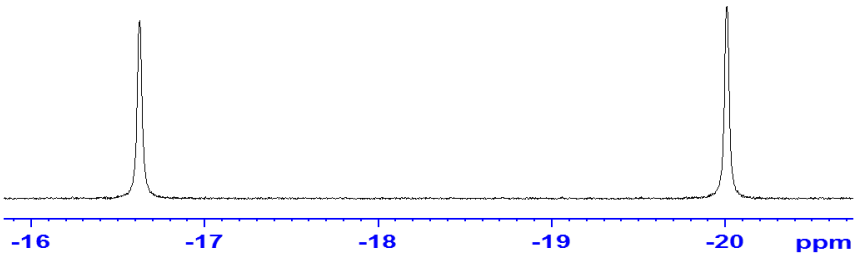

Figure C14: OPSY spectrum showing the p-H_2 derived signals of 4 in dmso- d_6.

Table C15: Observed rate constants for hydride exchange.

Set temperature (K)	Corrected temperature / K	1/T	lnk/T	k(H) /s^{-1}
335	336.1	0.00298	-4.922	1.22
335	336.1	0.00296	-4.920	1.22
340	341.2	0.00294	-4.873	1.30
340	341.2	0.00293	-4.872	1.30
345	345.9	0.00289	-4.206	2.57
345	345.8	0.00287	-4.203	2.57
350	350.2	0.00285	-3.923	3.46
350	350.2	0.00283	-3.921	3.46
355	356.2	0.00281	-3.884	3.65
355	356.2	0.00280	-3.881	3.65

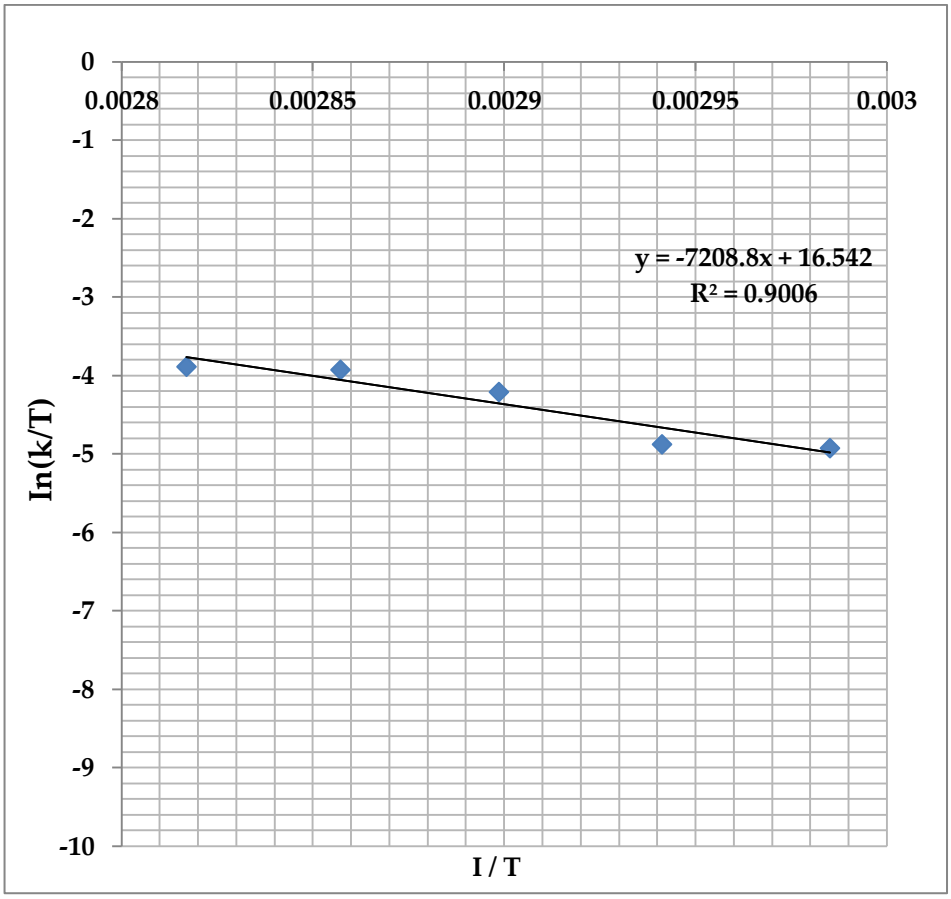

Figure C16: Eyring plots for Hydride exchange (using the data shown in Table C15.

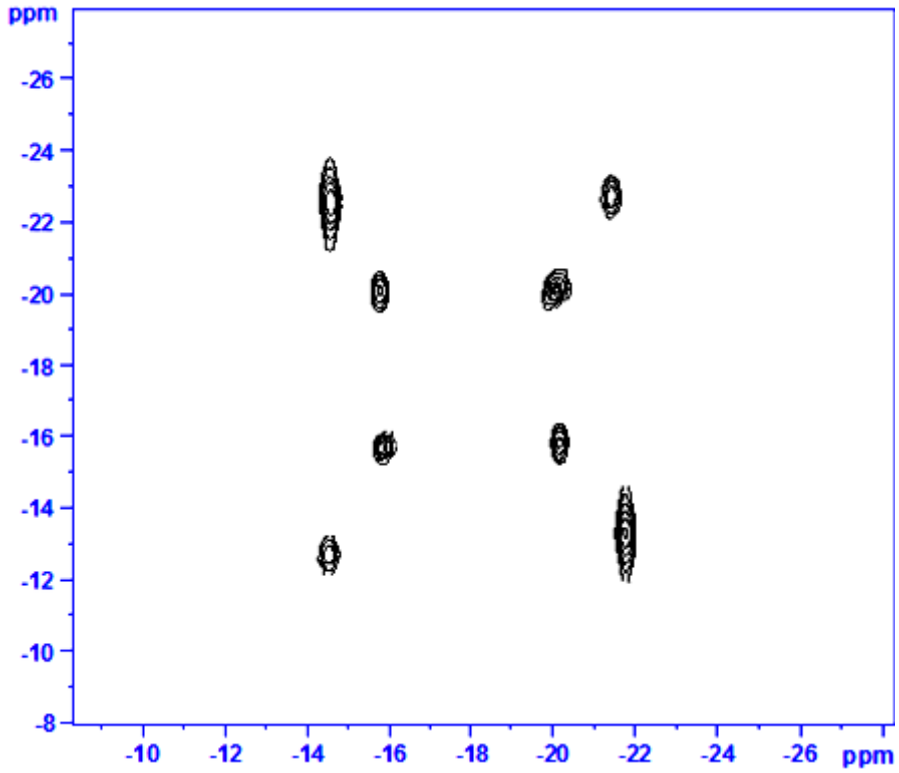

Figure C17: 2D COSY spectrum showing ^{1}H-^{1}H coupling between hydride signals resonating at δ -12.15, δ -22.91 and δ -15.10, δ -20.85 detected in the reaction of 4 with PPh_3 in the presence of p-H_2.

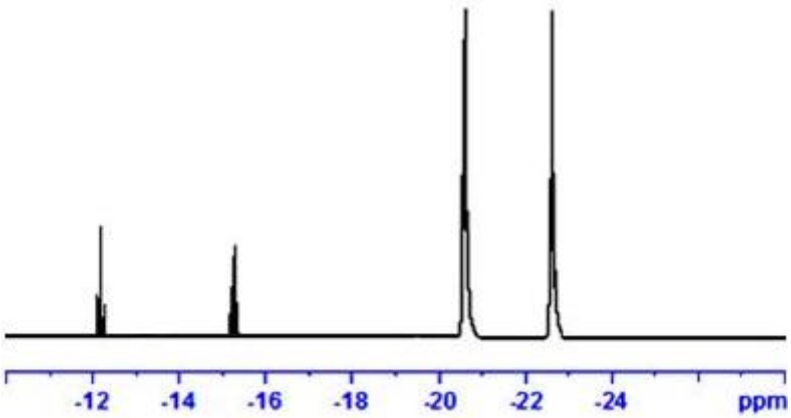

Figure C18: dq-OPSY spectrum showing the p-H_2 derived resonances for 4c and 4d.

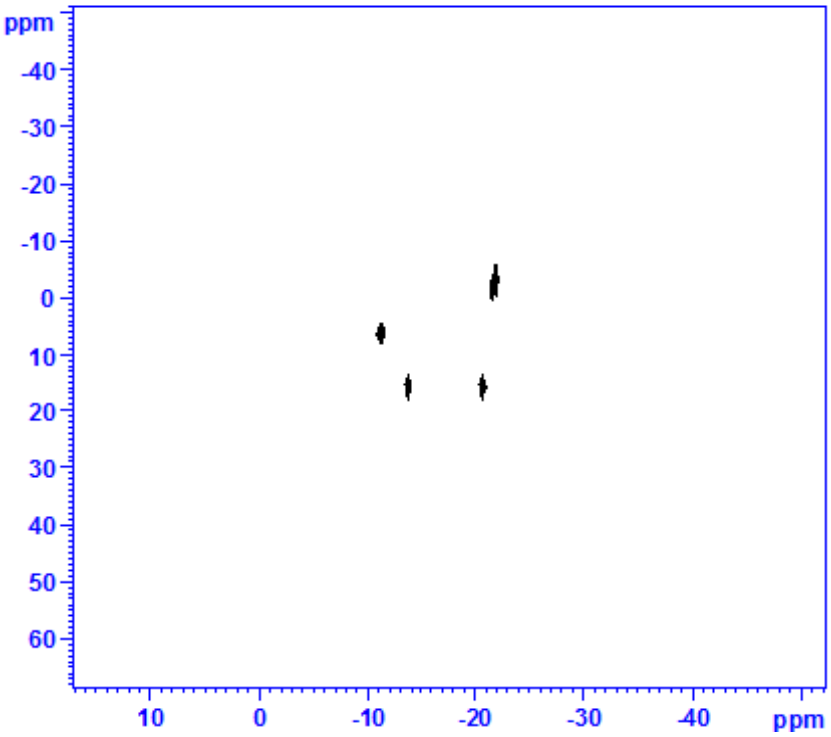

Figure C19: *^{1}H-^{31}P HMQC spectrum of complexes, 4c, and 4d, show the connection between the hydride resonances at, δ -12.15, δ -22.91 and δ -15.10, δ -20.85 along with ^{31}P signals resonating at δ 8.49, δ -1.95 and δ 14.47.*

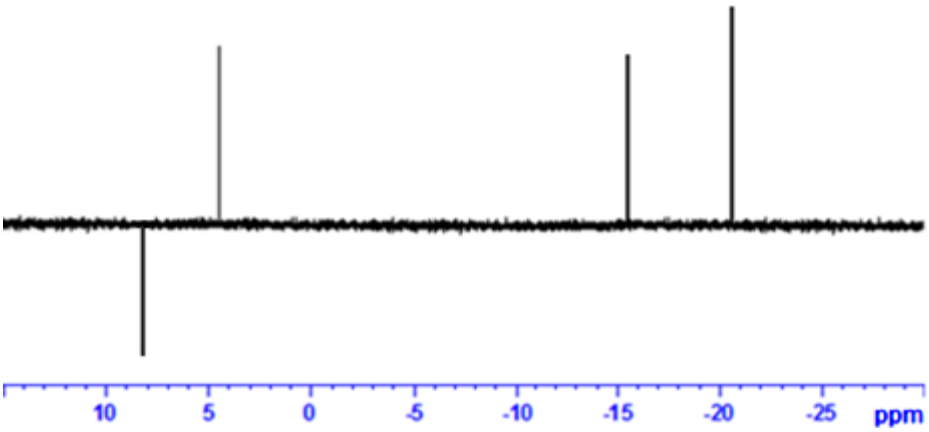

Figure C20: *1D EXSY spectrum obtained via selective irradiation of the hydride resonance at δ -20.85 in complex, 4d, at 298 K.*

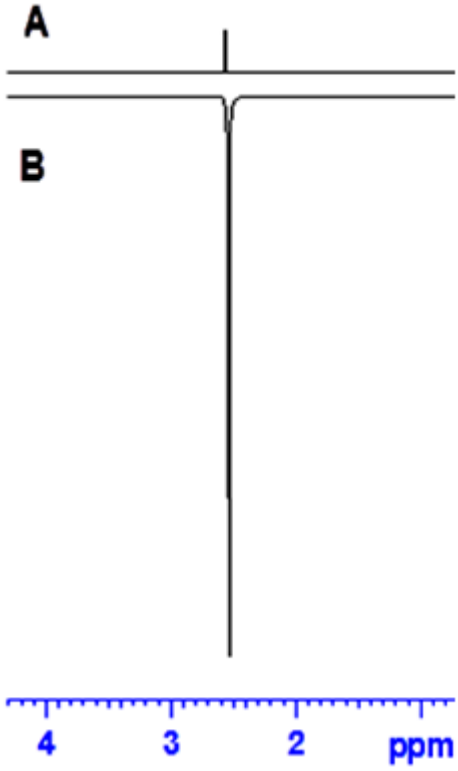

Figure C21: *(A) Single-scan ^{1}H NMR spectrum; (B) corresponding ^{1}H hyperpolarized NMR spectrum acquired in a magnetic field of 65 G exhibiting the enhanced proton signals for free DMSO.*

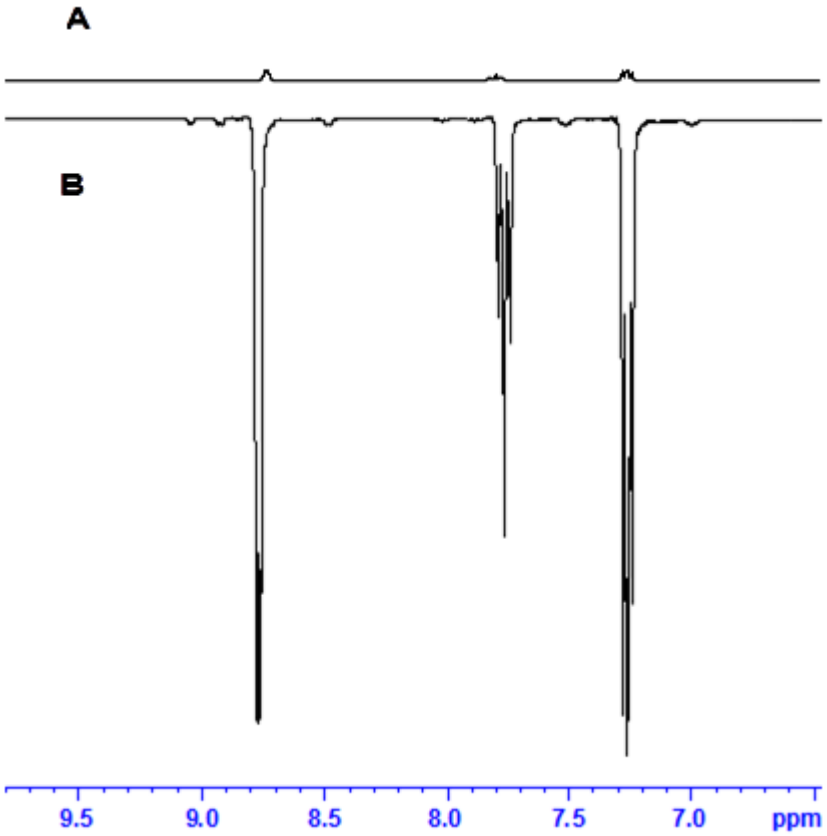

Figure C22: *(A) Single-scan ^{1}H NMR spectrum of the aromatic region showing resonances for free pyridine molecule that were obtained prior to polarization; (B) corresponding ^{1}H hyperpolarized NMR spectrum acquired immediately after polarization in a magnetic field of 65 G exhibiting the newly enhanced proton signals for free pyridine.*

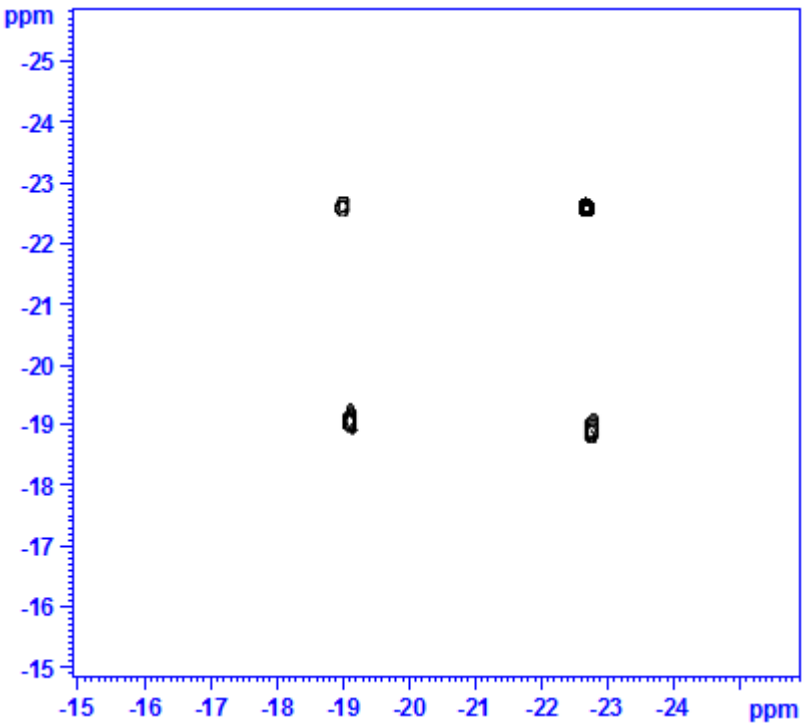

Figure C23: 2D COSY spectrum showing ^{1}H-^{1}H coupling between hydride signals resonating at δ -19.10 and δ -21.90 detected in the reaction of 4 with pyridine in the presence of p-H_2.

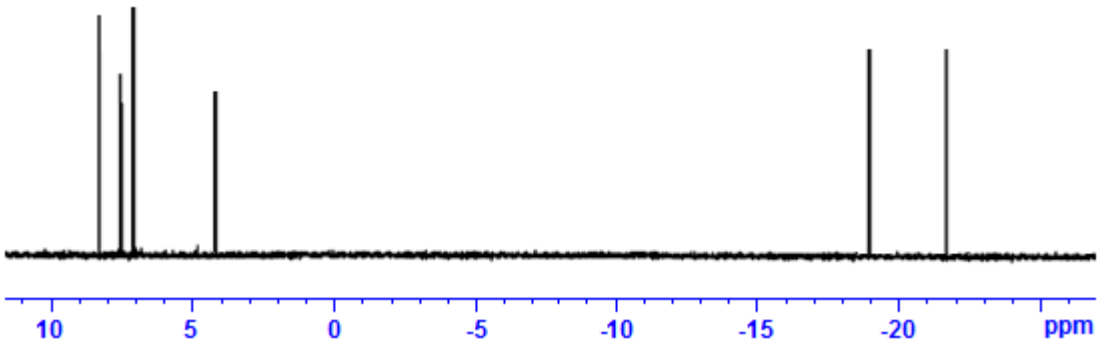

Figure C24: Depicts the dq-OPSY spectrum demonstrating the p-H_2 transfer in 4e to the hydride resonances in the high field region and also to the free pyridine in the low field region.

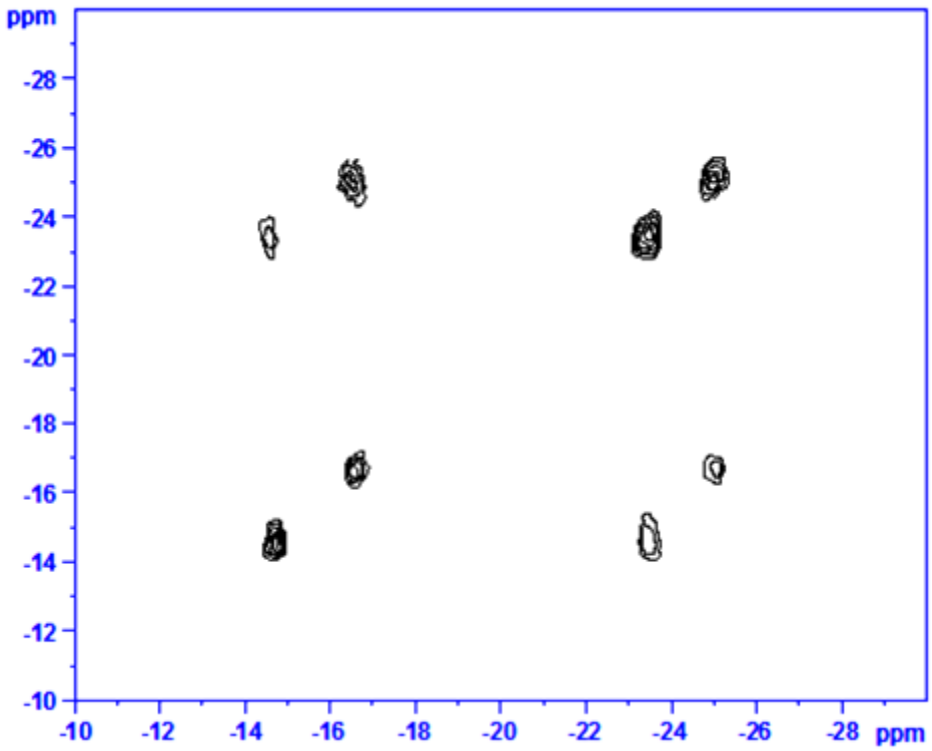

Figure C25: *2D COSY spectrum showing ^{1}H-^{1}H coupling between hydride signals resonating at δ -14.15, δ -23.70 and δ -16.05, δ -25.10 detected in the reaction of 4 with alanine in the presence of p-H_2.*

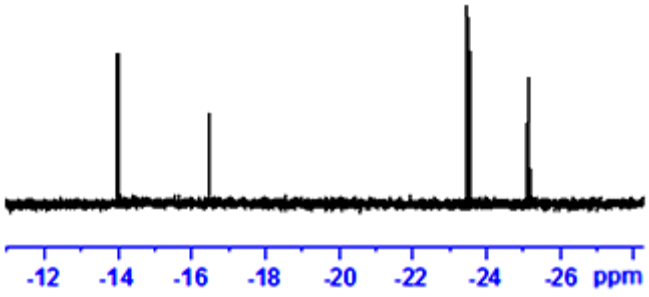

Figure C26: *dq-OPSY spectrum showing the p-H_2 derived resonances in 4f and 4g.*

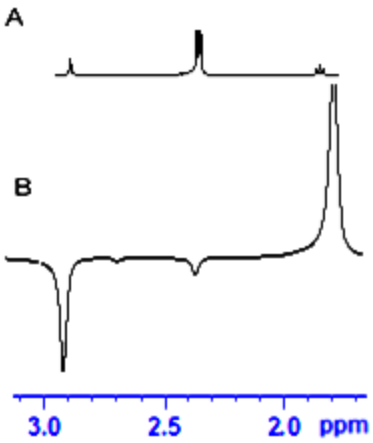

Figure C27: ***(A) Comparison between thermal; (B) corresponding hyperpolarized ^{1}H NMR spectrum shows the polarization transfer to the DMSO signal, CH_3 and CH protons of alanine in the low field region.***

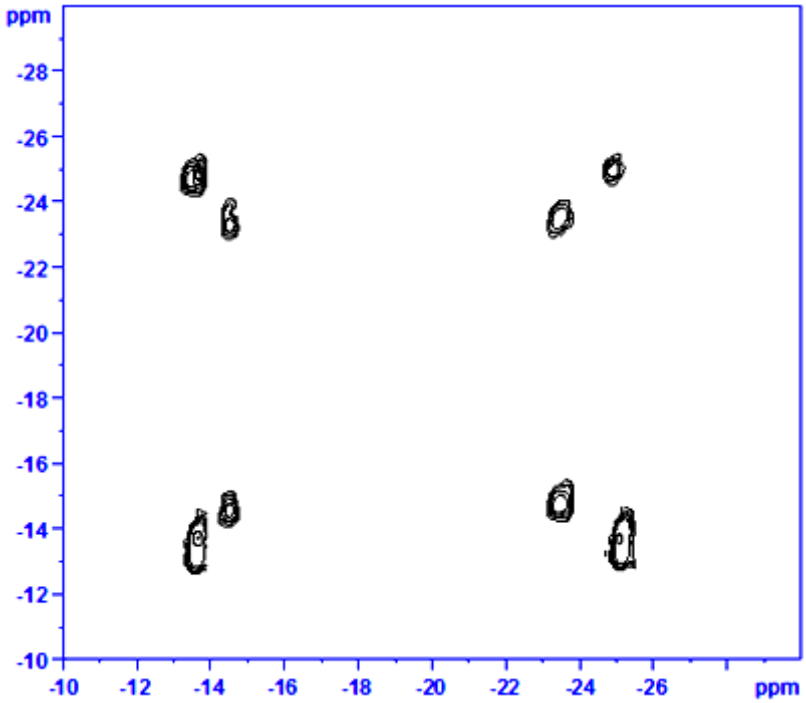

Figure C28: *2D COSY spectrum showing ^{1}H-^{1}H coupling between hydride signals resonating at δ -14.45, δ -23.79 and δ -13.10, δ -25.01 detected in the reaction of 4 with leucine in the presence of p-*H_2.

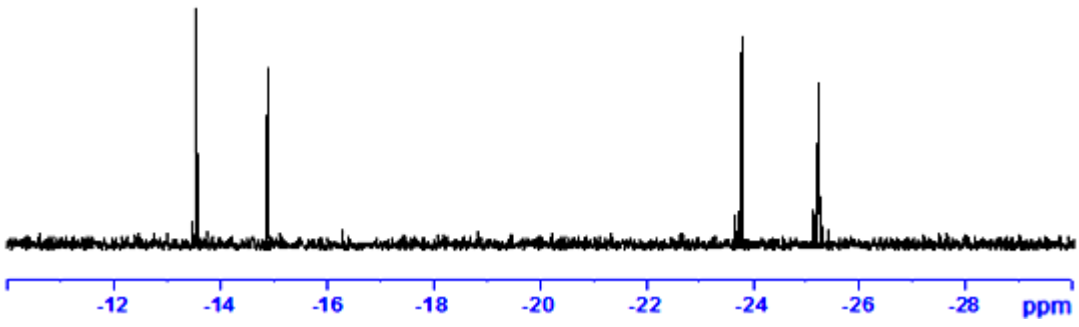

Figure C29: *dq-OPSY spectrum showing the p-*H_2 *derived resonances in case complexes,* ***4h****,* **and** ***4i****.*

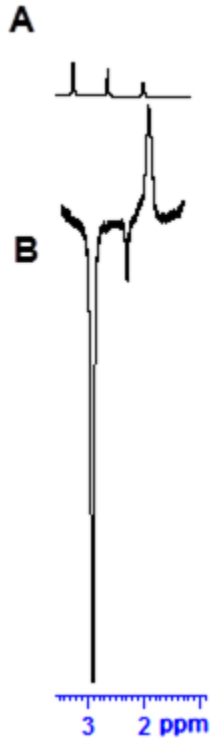

Figure C30: **(A)** *^{1}H NMR spectrum acquired under Boltzmann conditions; (B) corresponding hyperpolarized ^{1}H NMR spectrum shows the polarization transfer to the CH_3 protons of DMSO ligand, CH_2 and CH_3 protons of leucine in the low field region under non-Boltzmann conditions.*

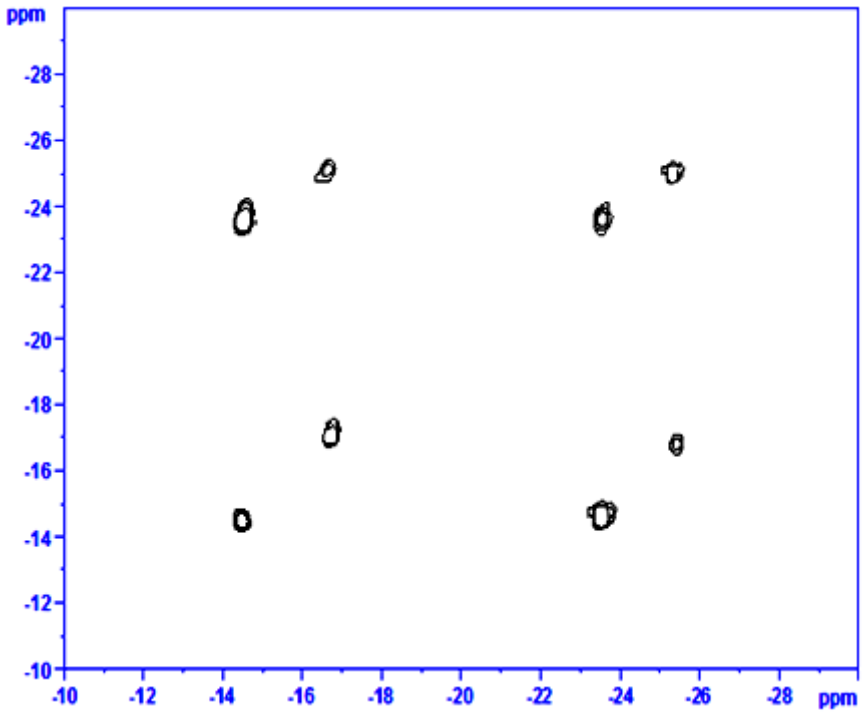

Figure C31: *2D COSY spectrum showing ^{1}H-^{1}H coupling between hydride signals resonating at δ -14.20, δ -23.90 and δ -16.80, δ -25.02 detected in the reaction of 4 with phenylalanine in the presence of p-H_2.*

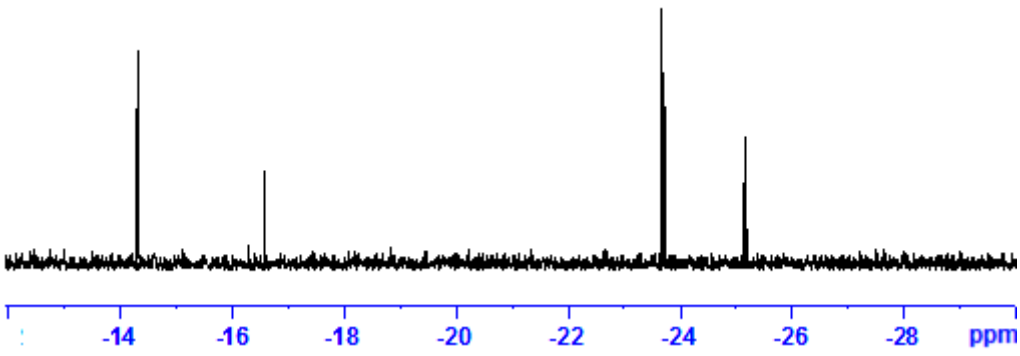

Figure C32: *dq-OPSY spectrum acquired in case of complexes, 4j, and 4k, indicating the p-H_2 derived resonances.*

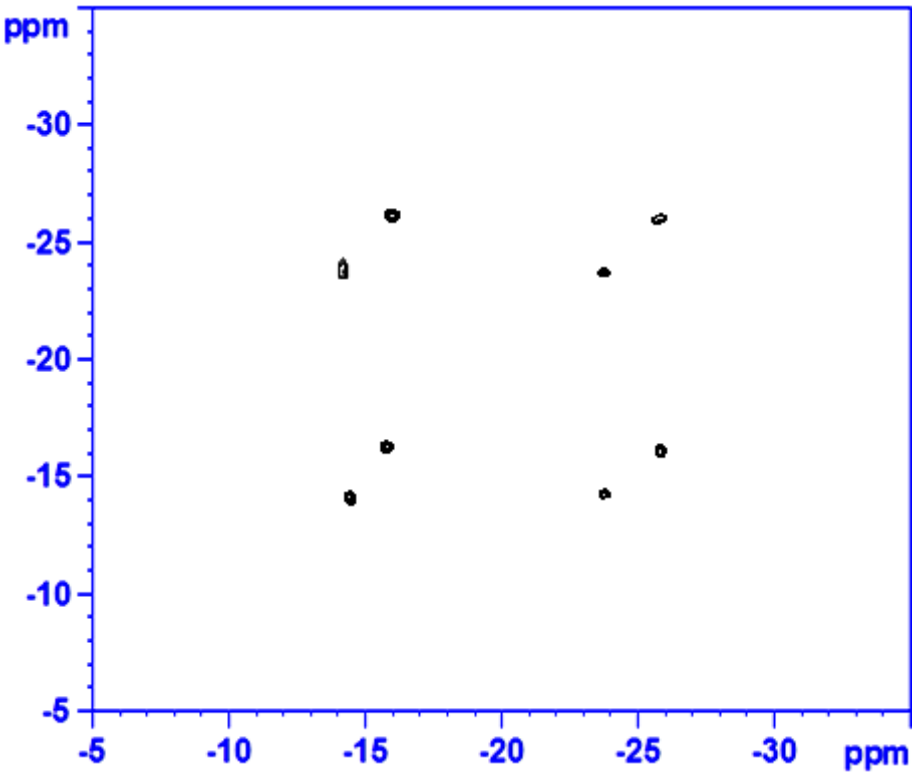

Figure C33: *2D COSY spectrum showing ^{1}H-^{1}H coupling between hydride signals resonating at δ -14.05., δ -24.10 and δ -16.01, δ -26.32 detected in the reaction of 4 with glycine in the presence of p-H_2.*

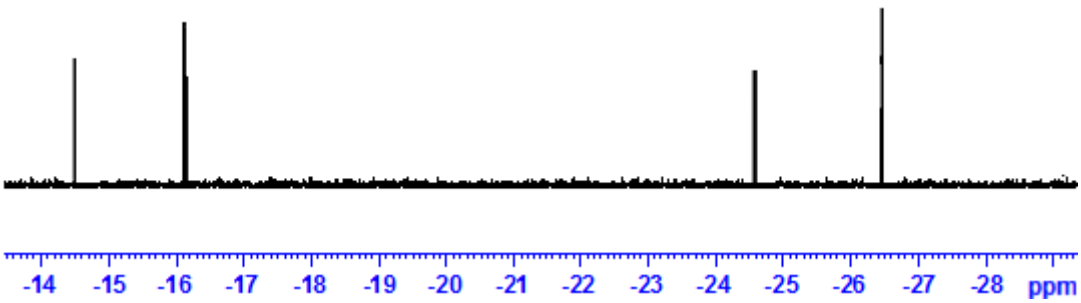

Figure C34: *dq-OPSY spectrum indicating that the complexes, 4l, and 4m are formed as a result of interaction with p-H_2.*

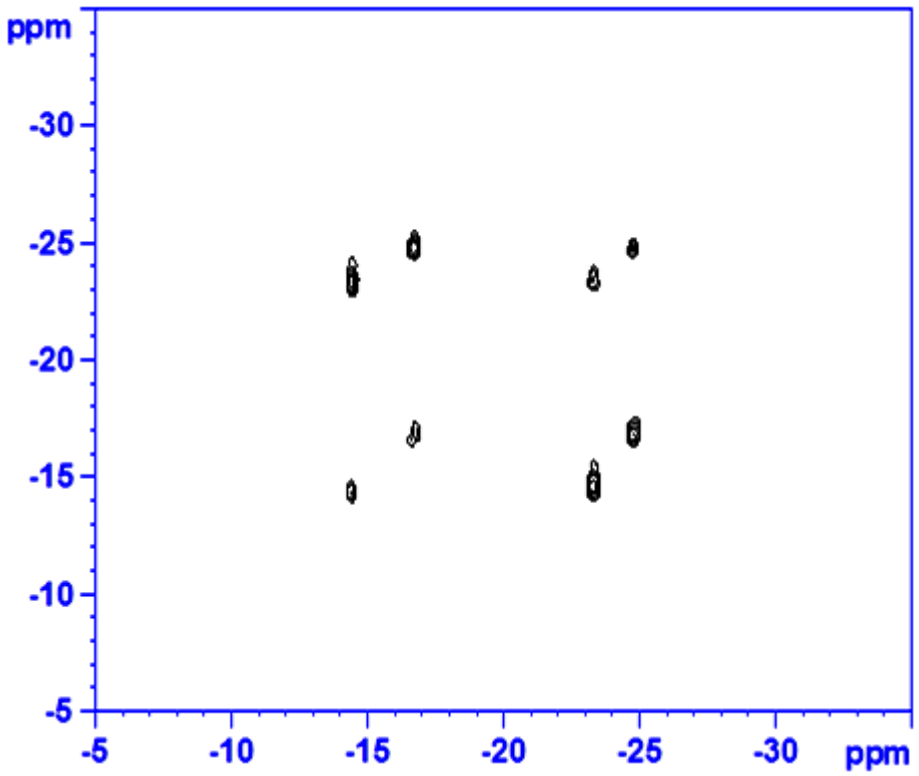

Figure C35: 2D COSY spectrum showing ^{1}H-^{1}H coupling between hydride signals resonating at δ -14.49, δ -23.16 and δ -16.18, δ -24.55 detected in the reaction of 4 with valine in the presence of p-H_2.

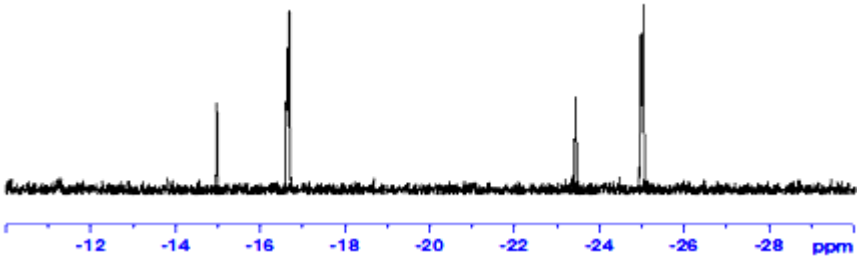

Figure C36: dq-OPSY spectrum indicating the resonances derived from p-H_2 in case of complexes, 4n, and 4o.

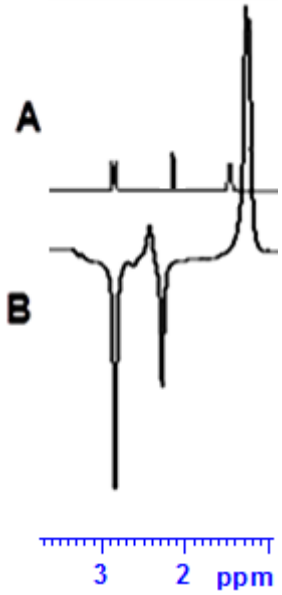

Figure C37: *(A) ^{1}H NMR thermal spectrum; (B) corresponding hyperpolarized ^{1}H NMR spectrum shows the polarization transfer to the methyl protons of the DMSO ligand , CH_3 and CH protons of valine in the low field region in at 65 G.*

Abbreviations

1D	One Dimensional
2D	Two Dimensional
δ	Chemical shift/ppm
{^{1}H}	Proton decoupled spectrum
{^{13}C}	Carbon decoupled spectrum
atm	Atmosphere
COD	Cyclooctadiene
COE	Cyclooctene
COSY	Correlated Spectroscopy
DMSO	Dimethyl sufoxide
COE	Cyclooctene
COSY	Correlated Spectroscopy
DMSO-	Dimethyl sufoxide
DNA	Deoxyribonucleic acid
DPFGSE	Double Pulsed Field Gradient Spin Echo
dppe	bis(diphenylphosphinoethane)
EXSY	Exchange Spectroscopy
Gly	Glycine
Phe	Phenylalanine
Ala	Alanine
Leu	Leucine
Hz	Hertz
HMQC	Heteronuclear Multiple Quantum Coherence
IR	Infrared Red spectroscopy
MRI	Magnetic Resonance Imaging

IMe	1, 3 –dimethylimidazole–2 –ylidene
IMes	1, 3-bis(2,4,6-trimethylphenyl)imidazoles-2-ylidine
IAd	1, 3-bis(1-adamantyl)imidazol-2-ylidene
I^{t}Bu	1, 3-di-*tert*-butylimidazole-2-ylidine
SIMes	1, 3-dimesityl-4, 5-dihydroimidazole-2-ylidine
OAc	Acetate ion
BF_4	Tetrafluoroborate ion
PCy_3	Tricyclohexlyphosphine
d_2-py	2-, 5-, d_2-pyridine
d_3-py	3-, 4-, 5, d_3-pyridine
pic	Picoline
Fpy	Fluoropyridine
Clpy	Chloropyridine
Brpy	Bromopyridine
Ipy	Iodopyridine
Nic	Nicotinic acid
Inic	Isonicotinic acid
Ina	Isonicotinamide
IN	Isoniazid
Pyz	Pyrazine
MN	Methyl nicotinate
pu	Purine
pym	Pyrimidine
N_2	Nitrogen
SABR	Signal amplification by reversible exchange
DNP	Dynamic nuclear polarization
Hz	Hertz

HMQC	Heteronuclear Multiple Quantum Coherence
IR	Infrared red spectroscopy
Pol	Polarization
p-H_2	*Para*hydrogen
PHIP	*Para*Hydrogen Induced Polarization
PPh_3	Triphenylphosphine
Vol	Volume
T	Tesla
G	Gauss
HP	Hyperpolarization
NHC	*N*-heterocyclic carbene

References

1) Purcell, E. M.; Torrey, H. C.; Pound, R. V. *Phys. Rev.* **1946**, 69, 37.

2) Bloch, F.; Hansen, W. W.; Packard, M. *Phys. Rev*. **1946**, 69, 127.

3) Martin, M. L.; Delpeuch, J. J.; Martin, G. J, Practical NMR Spectroscopy, Heydon, London, **1980**.

4) Harris, R. K.; Kowalewski, J.; Menezes, S. C. D. *Magn. Reson. Chem.*, **1998**, 36, 145-149.

5) Larive, C. K.; Rabenstein, D. L. *Magn. Reson. Chem.*, **1991**, 29, 409-417.

6) Harris, R. K. Nuclear Magnetic Resonance Spectroscopy, Longman, Harlow, **1986**.

7) Brunner, E.; Haake, M.; Kaiser, L.; Pines, A.; Reimer, J. A. *J. Magn. Reson***.** 138, 155–159.

8) Bowers, C, R.; Weitekamp, D, P. *Physical Review Letters*, **1986**, 57, 2645–2648**.**

9) Carravetta, M.; Levitt, M. H. *J. Phys. Chem*. 2005, **122**, 214505.

10) Adams, R.; Aguilar, J. A.; Atkinson, K. D.; Cowley, M. J.; Elliott, I. P.; Duckett, S. B.; Green, G. R.; Khazal, I. G.; Serrano, J. L.; Williamson, D. C. science. **2009**, 323, 1708-1711.

11) Atkinson, K. D.; Cowley, M. J.; Duckett, S. B.; Elliot, P. I. P.; Green, G. G. R.; Lopez-Serrano, J.; Khazal, I. G.; Whitwood, A. C. *Inorg. Chem.* **2009**, *48*, 663.

12) Abragam, A. The Principles of Nuclear Magnetism. Oxford University Press, **1961**.

13) Mecke, R. *Z. Phys*. **1925**, *31*, 709.

14) Sandler, Y. L. *J. Phys. Chem*. **1954**, *58*, 58.

15) Rasetti, F. *Phys. Rev*. **1929**, *34*, 367.

16) Hyman, H. H. *Phys*. *Rev*. **1930**, *36*, 187.

17) Canet, D.; Aroulanda. C.; Mutzzenhardt. P.; Aime. S.; Gobetto, R.; Reineri, F. *J. Magn. Reson.* **2006**, 28, 321-330.

18) Duckett, S. B.; Wood, N. J. **2008**, 252, 2278-2291

19) Blazina, D.; Duckett, S. B.; Dunne, J. P.; Godard, C. *Dalton*. *Trans*. **2004**, 2601.

20) Chapovsky, P. L.; Hermans, L. J. F. *Annu. Rev*. *Phys*. *Chem*. **1999**, 50, 315.

21) Bonhoeffer, K. F.; Hartect, P. *Z. Phys. Chem*. *B.* **1929**, *4*, 113.

22) Blazina, D.; Duckett, S. B.; Halstead, T. K.; Kozak, C. M.; Taylor, R. J. K.; Anwar, M. S.; Jones, J. A.; Carteret, H. A. *Magn*. *Reson*. *Chem*. **2005,** *43*, 200.

23) Bowers, C. R.; Weitekamp, D. P. *Phys*. *Rev*. *Lett*. **1986,** *57*, 2645.

24) Osborn, J. A.; Jardine, F. H. Joung. J. F and Wilkinson, G. *J*. *Chem*. Soc. **1966**, 1711.

25) Pravica, M. D.; Weitekamp, D. P. *Chem. Phys. Lett.* **1966**, 145, 255.

26) Bowers, C. R.; Weitekamp, D. P. *J. Am. Chem. Soc*. **1987,** 109, 5541.

27) Aime, S.; Gobetto, R.; Canet, D. *J*. *Am*. *Chem*. *Soc*. **1998**, *120*, 6770.

28) Eisenschmid, T. C.; Kirss, R. U.; Deutsch, P. A.; Hommeltoft, S. I.; Eisenberg, R.; Bargon, J.; Lawler, R. G.; Balch, A. L. *J. Am. Chem. Soc.* **1987**, 109, 5541

29) Levitt, M. H. "*Spin Dynamics Basics of Nuclear Magnetic Resonance"*,Wiley: Chichester, **2008**.

30) Aguilar, J. A.; Ralph, R. A.; Duckett, S. B.; Green, G. R.; Kandiah, R. *Magn*. *Reson*. *Chem*. **2011,** 43, 200.

31) Bax, P.G. Dejong, A.F. Mehlkopf, J. Smidt, , *Chem. Phys. Lett*.

1980, 69 567.

32) Eisenschmid, T.C.; McDonald, J.; Eisenberg, R.; Lawler, R.G. *J. Am. Chem. Soc.* **1980**, 111, 7267–7269.

33) (a) Barkemeyer, J.; Bargon, J.; Sengstschimd. H.; Freeman, R. *J. Magn. Reson*, Ser. A. **1996**, *120*, 129. (b) Sleigh, C. J. *D. Phil. Thesis*, University of York. **1999**.

34) Adams, R.; Aguilar, J. A.; Elliott, I. P.; Lopez-Serrano, J.; Duckett, S. B. Chem. Commun., **2007**, 1183–1185.

35) Stott, K.; Stonehouse, J.; Keeler, J.; Hwang, H. L.; Shaka, A. J. R. *J. Am. Chem. Soc.* **1995**, 117, 4199.

36) Sengschmid, H.; Freeman, R.; Barkemeyer, J. Bargon, J. *J. Magn. Reson. Ser. A*. **1996**, 120 249.

37) Messerle, B.A.; Sleigh, C. J.; Partridge, M, G.; Duckett, S. B. *Dalton Trans.* **1999**, 1429.

38) Hubler, P.; Bargon, J. Angew. Chem. Int. ED. 2000, 39, 3701.

39) Duckett, S. B.; Sleigh, C. J. *Prog. Nucl. Magn. Reson. Spectrosc.* **1999**, 34, 71.

40) Osborne, J. A.; Jardine, F. H.; Young, J. F.; Wilkinson, G. *J. Chem. Soc.* **1966,** 1711.

41) Duckett, S. B.; Field, L. D.; Messerle, B.A.; Shaw, W. J.; Soler, L. P. *Dalton Trans.* **2000**, 2251.

42) Permin, A.; Eisenberg, R. *J. Inorg. Chem.* **2002**, 41, 2451.

43) Morran, P. D.; Colebrook, S. A.; Duckett, S. B.; Lohman, J. A. B.; Eisenberg, R. J. *Chem. Soc., Dalton Trans.* **1998**, 3363.

44) Morran, P. D.; Colebrook, S. A.; Duckett, S. B.; McGrady, J. E.; Colebrook, S. A.; Eisenberg, R.; Partridge, M. G.; Lohman, J. A. B. *Dalton Trans.* **1999**, 3949.

45) Koch, A.; Bargon, J. *Inorg. Chem.* **2001**, 40, 553.

46) Chinn, M. S.; Eisenberg, R. *J. Am. Chem. Soc.* **1992**, 114, 1908.

47) Aime, S.; Gobetto, R.; Canet, D.; Dastru, W.; Viale, A. *J. Phys. Chem*. **2001**, 105, *6305*.

48) Harthun, A.; Selke, R.; Bargon, J. *Angew. Chem. Int. ED.* **1996**, 35, 2505.

49) Harthun, A.; Giernoth, R.; Elsevier, C. J.; Bargon, *J. Chem. Commun.* **1996**, 2483.

50) Hubler, P.; Giernoth, R.; Kummerle, G.; Bargon, J. *J. Am. Chem. Soc.* **1999**, 121, 5311.

51) Hubler, P.; Bargon, J. *Angew. Chem. Int. ED.* **2000**, 39, 3701.

52) Schott, D.; Sleigh, C.J.; Lowe, J.P.; Duckett, S. B.; Mawby, R.J.; Partridge, M. G. *Inorg. Chem.* **2002**, 41, 2960.

53) Ulrich, C.; Bargon, *J. Prog. Nucl. Magn. Reson. Spectrosc.* **2000**, 38, 33.

54) Giernoth, R.; Heinrich, H.; Adams, N.J.; Deeth, R. J.; Bargon, J.; Brown, J. M. *J. Am. Chem. Soc.* **2000**, 122, 12381.

55) Heinrich, H.; Giernoth, R.; Bargon, J. *Chem. Commun.* **2001**, 1296.

56) Wildshutz, S.; Heinrich, H.; Bargon, J. *Phys. Chem*. **2001**, 5, 328.

57) Golman, K.; Axelsson, O.; Johannesson, H.; Ma°nsson, S.; Olofsson, C.; Petersson, J. S. *Magn. Reson. Med*. **2001**, 46, 1-5.

58) Reineri, F.; Viale, A.; Ellena, S.; Alberti, D.; Boi, T.; Giovenzana, G, B.; Gobetto, R.; Premkumar, S. D.; Aime, S. *J. Am. Chem. Soc.* **2012**, 134, 11146-11152.

59) Richard, A. G.; Ralph, W. A.; Duckett, S. B.; Mewis, R. E.; Williamson, D. C.; Green, G. R. *J. Prog. NMR Spectrosc*., **2012**, 67,

1- 48.

60) Rosales, M.; Gonzalez , T.; Atencio, R.; Delgado, R, A, S. *Dalton. Trans*. **2004**, 2952.

61) Haake, M.; Natterer, J.; Bargon, J. *J. Am. Chem. Soc.* **1996**, 118, 8688–8691.

62) Cowley, M, J.; Adam, R. W.; Atkinson, K. D.; Cockett, M. C, R.; Duckett, S. B.; Green, G, R.; Lohman, R. J. A. B.; Kerssebaum, A.; Kilgour, D.; Mewis**,** R, E. *J. Am. Chem. Soc.*, **2011**, *133*, 6134–6137**.**

63) Lloyd, S.L.; Adams, R, W.; Bernstein, M.; Coombes, S.; Duckett, S, B.; Green, G, R.; Lewis, R, J.; Mewsi, R, E.; Sleigh, C, J. *J. Am. Chem. Soc.* **2012**, 134, 12904–12907.

64) Theis, T.; Ledbetter, M, P.; Kervern, G.; Blanchard, J, W.; Ganssle, P. J.; Butler, M, C.; Shin, H, D.; Budker, Dmitry.; Pines, A. *J. Am. Chem. Soc.* **2012**, 134, 3987–3990.

65) Carver, T. R.; Slichter, C.P. *Phys. Rev*., **1953**, 92, 212.

66) Jeffries, C. D. *Phys. Rev*., **1957**, 106, 164.

67) Erb, E., Motchane, J.L.; Uebersfeld, *C.R. Acad. Sci*., **1958**, 246, 2121.

68) Abragam, A.; Proctor, W.G. *C.R. Acad. Sci*., **1958**, 246, 2253.

69) Wind,R. A., Duijvestijn, M.J., van der Lugt, C. A.; Manenschijn.; Vriend, J. *Prog. NMR Spectrosc*. **1985**, 17, 33.

70) Bates, R.D. *Magn. Reson. Rev*. **1993**, 16, 237.

71) Wind, R.A. *Encyclopedia Magn. Reson*. **1996**, 3, 1798.

72) Wenckebach, W.T., Swanenburg, T. J. B.; Poulis, N. J. *Phys. Rep*. **1974**, 14, 181.

73) Provotorov, B. N., *Sov. Phys.– JETP (Engl. Transl.)*, **1962**, 14, 1126.

74) De Boer, W.; M, Borghini.; Morimoto, K.; Niinikoski, T.O.; Udo, T., *J. Low Temp. Phys*., **1974**, 15, 249.

75) Hall, D.A.; Maus, D.C. ; Gerfen, G.J.; Inati, S.J.; Becerra,L.R.; Dahlquist F.W.; Griffin, R. G. *Science*. **1997**, 276, 930.

76) Hu, J. Z.; Solum, M. S.; Wind, R. A.; Nilsson, B. L.; Peterson, M.A.; Pugmire, R. J.; Grant, D. M. *J. Phys. Chem. A*, **2000,** 104, 4413.

77) Bajaj, V.S.; Farrar, C.T.; Hornstein M.K.; Mastovsky I.; Vieregg, J.; Bryant , J.; Elena, B.; Kreischer, K.E.; Temkin, R.J.; Griffin, R.G.; *J. Magn. Reson*., **2003**, 160, 85.

78) Rosay, M.; Weis V.; Kreischer, K.E.; Temkin, R.J.; Griffin, R.G.; *J. Am. Chem. Soc*., **2002**, 124, 3214.

79) Bowers, C. R.; Weitekamp, D. P. *Phys. Rev. Lett*. **1986,** *57*, 2645.

80) Reynhardt, E. C.; High, G.L. *J. Chem. Phys*., **1998**, 109, 4090.

81) Reynhardt, E. C.; High, G.L. *J. Chem. Phys*., **1998**, 109, 4100.

82) Reynhardt, E. C.; High, G.L. *J. Chem. Phys*., **2000**, 113, 744.

83) Terblanche, C. L.; Reynhardt, E.C.; van Wyk, J.A. *Solid State Nucl. Magn. Reson*., **2001**, 20, 1.

84) Hautle, P.; Iinuma, M. *Nucl. Instrum. Methods Phys. Res. Sect. A*, **2000**, 440, 638.

85) Weis, V.; Bennati, M.; Rosay.; Bryant, M. J.A.; Griffin, R.G. *J. Magn. Reson*., **1999**, 140, 293.

86) Wenckebach, W.T., Swanenburg, T.J.B.; Poulis, N.J. *Phys. Rep*., **1974**, 14, 181.

87) C.T. Farrar, D.A. Hall, G.J. Gerfen, S.J. Inati and R.G. Griffin, *J. Chem. Phys*., **2001**, 114, 4922.

88) Hu, K.-N.; H. Yu H.; Swager, T.M.; Griffin, R.G. *J. Am. Chem.*

Soc., **2004**, 126, 10844.

89) Van der Wel, P.C.A.; Hu, K.-N.; Lewandowski, J.; Griffin, R.G. *J. Am. Chem. Soc*., **2006**, 128, 10840.

90) Song, C.; Hu, K.-N.; Joo, C.-G.; Swager, T.M.; Griffin, R.G. *J. Am. Chem. Soc*., **2006**, 128, 11385.

91) Hu, K.-N.; Bajaj, V.S.; Rosay M.; Griffin, R.G. *J. Chem. Phys*., **2007**, 126, 044512.

92) Odintsov, B.M.; Belford, R.L.; Ceroke, P. J.; Idiyatullin, Z. Sh.; Kashaev, R. S.; Kuriashkin, I.V.; Rukhlov, V. S.; Temnikov, A. N.; Clarkson, R. B. *J. Magn. Reson*., **1998**, 135, 435.

93) Wind, R. A.; Bai, S.; Hu, J. Z.; Solum, M. S.; Ellis, P. D.; Grant, D. M.; Pugmire, R. J.; Taylor, C. M. V.; Yonker, C. R. *J. Magn. Reson*., **2000**, 233.

94) Joo, C.-G.; Hu, K.-N.; Bryant, J.A.; Griffin, R. G. *J. Am. Chem. Soc*., **2006**, 128, 9428.

95) Ardenkjaer-Larsen, J. H.; Fridlund, B.; Gram, A.; Hansson, G.; Hansson, Lerche, L. M.; Servin, H. R.; Thaning M.; Golman, K. *Proc. Natl. Acad. Sci*., **2003**, 100, 10158.

96) Day, I. J.; Mitchell, J. C.; Snowden, M. J.; Davis, A. L. *J. Magn. Reson*., **2007**, 187, 216.

97) Frydman, L.; Blazina, D. *Nature Phys*., **2007**, 3, 415.

98) Shriver, Atkins "*Inorganic Chemistry*", 5th ed.; W.H Freeman and Company: New York, **2010**.

99) Crabtree, R. H.; Mingos D. M. P. "*Comprehensive organometallic chemistry III"*. Elsevier, Oxford, **2006**.

100) Adams, R.; Aguilar, J. A.; Atkinson, K. D.; Cowley, M. J.; Elliott, Paul. I. P.; Duckett, S. B.; Green, G, R.; Khazal, I, G.; López, S, J.; Williamson, D, C. *Science,* **2009**, 323, 1708-1711.

101) Atkinson, K. D.; Cowley, M. J.; Duckett, S. B.; Elliot, P. I. P.; Green, G. G. R.; Lopez-Serrano, J.; Khazal, I. G.; Whitwood, A. C. *Inorganic Chemistry* **2009**, *48*, 663.

102) (a) Zeng, Haifeng.; Xu, Jiadi.; Gillen, Joseph.; McMahon, J.; Artemov, Dmitri.; Tyburn, Jean-Max.; Lohman, Joost.; Mewis, R.E.; Duckett, S. B.; C. M, peter.; Zijl, Van. *J. Magn. Reson*., **2013**, 237, 73.

(b) Atkinson, K. D.; Cowley, M. J.; Elliot, P. I. P.; Duckett, S. B.; Green, G. G. R.; Lopez-Serrano, J.; Whitwood, A. C. *J. Chem. Soc*. **2009**, 131, 13362.

103) Cowley, M. J.; Adams, R. W.; Atkinson, K. D.; Cockett, M. C. R.; Duckett, S. B.; Green, G. G. R.; Lohman, J. A. B.; Kerssebaum, R.; Kilgour, D; Mewis, R. E. *J. Am. Chem. Soc*., **2011**, 133 (16), pp 6134–6137.

104) W.J. Evans, *Adv. Organomet. Chem.*, **1985**, 24, 131,

105) (a) C.J. Schaverien, *Adv. Organomet. Chem.*, **1994**, 36, 283. (b) W.J. Evans and B.L. Davis, *Chem. Rev.*, **2002**, 102, 2119.

106) Wanzlick, H.W.; Schonher, H.J. *Angewandte Chemie – International Edition*, **1968**, 7, 141.

107) Arduengo, A.J.; Harlow, R.L.; Kline, M. *J. Am. Chem. Soc.* **1991**, 1 113, 361.

108) Arduengo, A.J.; Harlow, R.L.; Kline, M. *J. Am. Chem. Soc.* **1992**, 114, 14, 5530-4

109) Huang, J.; Stevens, E. D.; Nolan, S. P.; Petersen, J. L. *J. Am.*

Chem. Soc. **1999**, *121*, 2674.

110) Herrmann, W. A.; Roesky, P. W.; Elison, M.; Artus, G.; O fele, K. *J. Organomet. Chem.* **1995**, *14*, 1085.

111) Hermann, W. A.; *Angew, Chem*. –*Int. Edit*. **2002**, 41, 1290-1309.

112) Ofele, K.; Hermann, W. A.; Mihalios, D.; Elison, M.; Herdtweck E.; Priermeier T.; Kiprof, P. *J. Organomet. Chem.* **1995**, 498, 1-14.

113) Ofele, K.; Hermann, W. A.; Mihalios, D.; Elison, M.; Herdtweck E.; Scherer, W.; Mink, *J. Am. Chem.* Soc. **1993**, 459, 177-1799.

114) Hermann, W. A.; Ellison, M.; Fisher, J.; Kocher.; C.; Artus, G. R. *J. Chem., - Eur,* J. **1996**, 2, 772-780.

115) Huang, J. K.; Stevens, E.D.; Nolan S. P.; Peterson, J. L. *J. Am. Chem.* Soc. **1999**, 121, 2674-2678.

116) Kuhl, O. "*Functionalised N-Heterocyclic carbene chemistry*", 5th ed.; John Wiley & Sons: Chichester, **2010**.

117) Herrmann, W. A.; K ö cher, C. *Angew. Chem*. **1997**, 109, 2256 .

118) Heinemann, C.; M ü ller, T.; Apeloig, Y.; Schwarz, H. *J. Am. Chem. Soc* . **1996**, 118, 2023.

119) Dixon, D. A.; Arduengo, A. J. *J. Phys. Chem* . **1991**, 95, 4180 .

120) Arduengo, A. J.; Harlow, R. L.; Kline, M. *J. Am. Chem. Soc* . **1991**, 113, 361.

121) Tafi polski, M.; Scherer , W.; Ö fele , K.; Artus, G.; Pedersen, B.; Herrmann, W. A.; McGrady, G. S. *J. Am. Chem. Soc.* **2002**, 124, 5865.

122) Cavallo, L.; Correa, A.; Costabile, C.; Jaocbsen, H. *J. Organomet. Chem.* **2005**, 690, 5407-5413.

123) M, Tafipolsky.; W, Scherer.; Ofele, K.; Artus, G.; Pedersen, B.; Herrmann, W. A.; McGrady, G. S. *J. Am. Chem. Soc.*, **2002**, 124, 5865.

124) Dorta, R.; Stevens, E. D.; Hoff, C. D.; Nolan, S. P.; *J. Am. Chem. Soc*. **2003,** 125, 10490-10491.

125) Becker, E.; Stingl, V.; Dazinger, G.; Puchberger, M.; Mereiter, K.; and K. Kirchner. *J. Am. Chem. Soc.* **2006**, 128, 6572-6573.

126) Jazzar, R. F. R.; Macgregor, S. A.; Mahon, M. F.; Richards S. P.; Whittlesey, M. K. *J. Am. Chem. Soc.* **2002**, 124, 4944-4945.

127) Hiller, A. C.; Sommer, W. J.; Yong, B. S.; Petersen, J.L.; Cavallo, L.; Nolan, S. P. *J. Chem. Organomet.* **2003**, 22, 4322-4326.

128) Termaten, A. T.; Schäkel, M.; Ehlers, A. W.; Lutz, M.; Spek A. L.; Lammertsma, K. *Chem.-Eur. J.* **2003**, 9, 3577-3582.

129) M. T. Lee and C. H. Hu, *J. Chem Organomet.* **2004**, 23, 976-983.

130) Hu, X. L.; Castro-Rodriguez I.; Meyer, K. *J. Am. Chem. Soc.* **2004**,126, 13464-13473.

131) Chianese, A. R.; Li, X. W.; M. C. Janzen, Faller, X W.; Crabtree, R. H. *J. Chem. Organomet*. **2003**, 22, 1663-1667.

132) Dorta, R.; Stevens, E. D.; Scott, N. M.; Costabile, C.; Cavallo, L.; Hoff, C. D.; Nolan, S. P.; *J. Am. Chem. Soc***. 2005**, 127, 2485-2495.

133) Tolman, C. *J. Am. Chem. Soc. Revs*, **1977**, 77, 313.

134) Nolan, S. P.; Nolan, "*N-Heterocyclic Carbenes in Synthesis*", Wiley-VCH, Weinheim, **2006**.

135) Dorta, R.; Stevens, E. D.; Scott, N. M.; Costabile, C.; Cavallo, L.; Hoff, C. D.; Nolan, S. P. *J. Am. Chem. Soc*. **2005**, 127, 2485.

136) Huang, J.; Schanz, H. - J.; Stevens, E. D.; Nolan, S. P. *J. Chem. Organomet.* **1999**, 18, 2370.

137) Müller , C.; Vogt, D. *Dalton Trans* . **2007** , 5505.

138) Cavallo, L.; Costabile A. C.; Jacobsen, C.H. *J. Organomet. Chem* . **2005**, 690, 5407.

139) Hillier, A. C.; Sommer, W. J.; Yong , B. S.; Petersen , J. L.; Cavallo, L.; Nolan , S. P. *J. Chem. Organomet,* **2003**, 22, 4322 .

140) (a)Hughes, E. D. *Q. Rev. Chem. Soc.*, **1948**, 2, 107-131; (b) Hughes, D. *Trans. Faraday SOC*., 1941, 37, 603; (c) Chem. Reviews, **1939**, 25, 204; (d) Ber., **1895**, 28, 1254.

141) (a) Pinter, B.; Fievez, T.; Matthias Bickelhaupt, A. F.; Geerlingsa, Paul.; Frank De Proft. *Phys. Chem. Chem. Phys*. **2012**, 14, 9846–9854. (b) R. W. Taft. "Steric Effects in Organic Chemistry", Wiley, New York, **1956**, p. 556.

142) Chang, R.; Overby, J. "THE ESSENTIAL CONCEPTS". McGraw-Hill, **2011**.

143) Silberberg, M. S. "PRINCIPLES OF GENERAL CHEMISTRY". McGraw-Hill, **2007**.

144) Zinner, S.C.; Rentzsch, C.F.; Herdtweck, E.; Hermann, W.A.; Kuln, F.E. *Dalton Trans.* **2009**, 7055-7062.

145) Kelly III, R. A.; Clavier , H.; Giudice, S.; Scott, N. M.; Stevens , E. D.; Bordner , J.; Samardjiev , I.; Hoff, C. D.; Cavallo, L.; Nolan, S. P. *J. Chem. Organometallics*. **2008**, 27, 202.

146) Voutchkova, A. M.; Feliz, M.; Clot, E.; Eisenstein, O.; Crabtree, R. H. *J. Am. Chem. Soc*. **2007**, 129, 12834-12846.

147) Perrin, C. L.; Dong, Y. *J. Am. Chem. Soc*. **2007**, 129, 4490-4497.

148) Wood, J. N.; Brannigan, J.A.; Duckett, S. B.; Heath, S. L.; Wagstaff, J. *J. Am. Chem. Soc.* **2007**, 129, 11012-11013.

149) Clavier, H.; Nolan, S. P. *Chem. Commun*., **2010**, 46, 841–861.

150) Hillier, A. C.; Sommer, W. J.; Yong, B. S. J.; Petersen, L.; Cavallo L.; Nolan, S. P. *Organometallics,* **2003**, 22, 4322-4326.

151) Cavallo, L.; Correa, A.; Costabille, C.; lez ,G.; Nolan, S. P. *Coord. Chem. Rev*., **2007**, 251, 874–883.

152) Poater, A.; Cosenza, B.; Correa, A.; Giudice, S.; Ragone,F.; Scarano V.; Cavallo, L. *Eur. J. Inorg. Chem*., **2009**, 1759–1766.

153) Kelly III, R. A.; Clavier, H.; Giudice, S.; Scott, N. M.; Stevens, E. D.; Bordner, J.; Samardjiev, I.; Hoff, C. D.; Cavallo L.; Nolan, S. P. *Organometallics*, **2008**, 27, 202–210

154) (a) Viciu, M. S.; Navarro, O.; Germaneau, R. F.; Kelly III, R. A.; Sommer, W.; Marion, N.; Stevens, E. D.; Cavallo L.; Nolan, S. P. *Organometallics*, **2004**, 23, 1629–1635; (b) Clavier, H.; Correa, A.; Cavallo, L.; Escudero, E. C.; Benet-Buchholz, J.; Slawin, A. M. Z.; and Nolan, S. P., *Eur. J. Inorg. Chem*., **2009**, 1767–1773

155) Bazinet, P.; Ong, T.-G.; O'Brien, J. S.; Lavoie, N.; Bell.; Yap, E. G.; Korobkov, I.; Richeson, D. S. *Organometallics,* **2007**, 26, 2885–2895.

156) Dorta, R.; Stevens, E. D. ; Scott, N. M.; Costabile, C.; Cavallo L.; Hoff, C. D.; and Nolan, S. P, *J. Am. Chem. Soc*., **2005**, 127, 2485-2495.

157) Gaillard, S.; Bantreil, X.; Nolan, S. P. *Dalton Trans*., **2009**, 6967-6971.

158) Wu¨rtz, S.; Lohre, C.; Fro¨hlich, R.; Bergander K.; and Glorius, F. *J. Am. Chem. Soc*., **2009**, 131, 8344-8345.

159) Torres, O.; Martı´n, M.; Sola, R. *Organometallics,* **2009,** *28,* 863-870.

160) Gutmann, T.; Ratajczyk, Tomasz.; Dillenberge, S.; Xu, Y.; Grunberg, A.; Breitzke, H.; Bommerich, U.; Trantzschel, T.; Bernarding, J.; Buntkowsky, G. *Solid State Nuclear Magnetic Resonance*. **2011**, 40, 88-90

161) Bruckert, E; Labreuche, J; Amarenco, P. *Atherosclerosis.* **2010**, 210, 353-361

162) (a) Grandberg, I. I.; Faizova, G. K.; Kost, A. N. *Chem. Heterocycl. Compd.* **1966**, *2*, 561; (b) pKa data compiled by Williams. R. (c) Brewer, G. A. "*Analytical profiles of drug substances and excipients"*, Vol. 6. *Academic. Press*, Inc, **1977**.

163) Primavera, G.; Berardesca, E. *Journal of Cosmetic Science*, **2005**, 27, 1-10

164) Joule, J. A.; Mills, K. "*Heterocyclic Chemistry"*, Wiley: New York, **2010**.

165) Riede, H. L. *Lancet*. **2009**, 373, 9670.

166) Rosemeyer, H. *Chemistry & Biodiversity*. **2004**, 1, 361.

167) Gilchrist, T. L. "*Heterocyclic chemistry"*. New York: Longman, **1977**.

168) Lagoja, I. M. *Chemistry and Biodiversity*. **2005**, **2**, 50.

169) Brown, D. J.; Evans, R. F.; Cowden, W. B.; Fenn, M. D. "*The Pyrimidines"*. Wiley: New York, **1994**.

170) David, N. L.; Cox, M. "*Principles of Biochemistry"*. W. H. Freeman and Company, **2008**.

171) Dorta, R.; Rozenberg, H.; Shimon, L.J.W.; Millestein, D. *J. Am. Chem. Soc*., **2002**, 124, 188.

172) (a) Dickson, R.S Organomettalic Chemistry of Rhodium and Iridium Academic Press, London, **1983**; (b) Collman, J.P;

Hegedus, L.S; Norton, J.R.; Finke, R.G. "*Principles and applications of organotransition Metal Chemistry*", University Science, Mlill Valley, **1987**.

173) Calligaris,M.; Carugo. O. Coord. Chem. Rev. **1996**, 153, 83.

174) Parshall, G.W.; little, S. D. "Homogenous Catalysis", 2nd ed, Wiley, New York, **1992**.

175) (a) Hamilton, D. J.; Wilkinson, G.; Nouv. J. Chim. **1977**, 1, 141; (b) T. Yoshida, T. Matsuda, T. Okono, S. Otsuka, *J. Am. Chem.Soc*. **1979**, 101, 2027.

176) Dotra, R.; Rozenberg, H.; Shimon, L.J.W.; Milstein. R. *Chem. Eur.J*. **2003**, 9, 5237.

177) B. R James. "*Comprehensive Organometallic Chemistry*", Paragon, New York, **1982**.

178) C.E Johnson, R. Eisenberg, *J. Am. Chem. Soc*. **1985**, 107, 3148.

179) Fotheringham, J. D.; Heath, G.A.; Lindsay, A.J.; Stephenson, T**.** *A. J. Chem. Research* (S), **1986**, 82**.**

180) Saillard, J. Y.; Hoffmann. R. *J. Am. Chem. Soc*. **1984**, *106*, 2006. (b) Kubas, G.J. *PNAS*. **2007,** 104, 17, 6901–6907**.**

181) (a) Fisher, B. J.; Eisenberg, R. *Organometallics*. **1983**, 2, 764; (b) Johnson, C.; Eisenberg, R. *J. Am. Chem. Soc*. **1985**, 107, 6531.

182) Longato, B.; Bresadola, S. Inorg. Chim. Acta. 1**979**, 33, 189.

183) Johnson, C. E.; Fisher, B. J.; Eisenberg, R. *J. Am. Chem. Soc*. **1983**, 105, 7772.

184) (a) Sargent, A. L.; Hall, M. B.; Guest, M. F. *J. Am. Chem. Soc*. **1992**, 114, 517.

185) (a) Sargent, A. L.; Hall, M. B.; Guest, M. F. *J. Am. Chem. Soc*. **1992**, 114, 517; (b) Halpern, *J. Acc. Chem. Res*. **1970**, 3, 386; (c) Drouin,

M.; Harrod, J. F. *Inorg. Chem.* **1983**, 22, 999; (d) Longato, B.; Morandini, F.; Bresadola, S. Ibid. **1976**, 15, 650. Bargon, D. G. Lawler, A. L. Balch, *J. Am. Chem. Soc.* **1987,** 109, 8089.

186) Heyes, D. M: *The Liquid State*, Wiley-VCH, Weinheim / Germany,**1997**.

187) Wicke, Angew. Chem. Int. Ed. Engl. **1966**, 5, 106

188) Luck, W. A. P. (Ed.): *Structure of Water and Aqueous Solutions*, Verlag Chemie, Weinheim, **1974.**

189) Frank, H. S.; Evans, M. W. *J. Phys. Chem.* **1945**, 13, 507.

190) Evans D. F.; Chen, S.-H.; Schriver, G. W.; Arnett, E. M.; *J. Am. Chem. Soc*. **1981**, 103, 481.

191) (a) Mirejovsky, D.; and Arnett, E. M. **1983**, 105, 1112 229-F; (b) A. Greco, *J. Phys. Chem.* **1984**, 88, 3132

192) Prabhu, N. K. Sharp: *Protein–Solvent Interactions*, *Chem. Rev*. **2006**, 106, 1616.

193) Burgess, J: Ions in Solution – *Basic Principles of Chemical Interaction*, 2nd ed., Harwood Publishing, Watergate/ U.K., **1999**.

194) Cox, B. G.; Waghorne, W. E. *Chem. Soc. Rev.* 9, 381 **(1980).**

195) Conway, B. E.: "*Ionic Hydration in Chemistry and Biophysics*", Elsevier, Amsterdam, **1981**.

196) Barthel, J. M. G.; Krienke, H.; Kunz, W.; *Physical Chemistry of Electrolyte Solutions* – Modern Aspects, Top, *Phys. Chem*. **1998**, 5, 1**.**

197) Bertini, I., J. A. Cowan, C. Luchinat, K. Natarajan, and M. Piccioli. **1997**. 36 (31):9332–39.

198) Lippard, S. J., and J. M. Berg. **1994**. *"Principles of Bioinorganic*

Chemistry". Mill Valley, CA: University Science Books.

199) Fenton, D. E. **1995**. "*Bio coordination Chemistry"*, Oxford Chemistry Primers, Oxford: Oxford University Press.

200) Gray, H. B. **2003**. Proc Natl Acad Sci, 100 (7): 3563–68.18.

201) Warder, S. E., M. Prorok, Z. Chen, L. Li, Y. Zhu, L. G. Pedersen, Ni, F.; Castellino F. J. **1998**. *J. Biol. Chem.* 273 (13):7512–22.

202) Rosenberg, B.; VanCamp, L.; Trosko, J.E.; Mansour,V.H. *Nature* 222. **1969**, 385- 386.

203) Sheldrick, W.S.; Heeb,S.; *Inorg. Chim. Acta,* 168. **1990**, 93-100.

204) Hay, R.W.; Morris, P. J. Metal Ions Biol. Syst. **1976**, 5 173-243.

205) Satchell, D.P.N. Annu. Rep. Prog. Chem., Sect. A: *Inorg. Chem.* **1978**, 75, 25-48.

206) Sigel, H.; Martin, R.B.; *Chem. Rev*. 82. **1982,** 385-426.34)

207) Herebian, D.; Sheldrick, W. S. *J. Chem. Soc*., *Dalton Trans*. **2002,** 966-974.

208) Crabtree, R. H. *"The Organometallic Chemistry of the Transition Metals", second ed., Wiley, New York,* **1994**.

209) (a) Grandberg, I. I.; Faizova, G. K.; Kost, A. N. "*Chem. Heterocycl. Compd".* **1966**, *2*, 561; (b) pKa data compiled by Williams. R.

210) *Nelson*, David L.; Cox, Michael M. **2005**, "*Principles of Biochemistry (4th ed.)*", New York: W. H. Freeman

211) Duckett, S. B.; Lowe, J, C.; Lowe, J, P.; Mawby, R, J. *Dalton. Trans.*, **2004**, 3788.

212) Herde, J. L.; Lambert, J. C.; Senoff, C. V. *Inorganic Synthesis*, **1974**, 15.